Arthritis & Rheumatology

An Official Journal of the American College of Rheumatology
www.arthritisrheum.org and wileyonlinelibrary.com

Cover design: Todd Machen

This journal is printed on acid-free paper.

Arthritis & Rheumatology

An Official Journal of the American College of Rheumatology
www.arthritisrheum.org and wileyonlinelibrary.com

VOLUME 77 • March 2025 • NO. 3

Cover image: The image on the cover (from Xiang Li et al) shows the hematoxylin and eosin staining of a cardiac mass resected from a patient with Erdheim–Chester disease. It is featured by the infiltration of "foamy" histocytes surrounded by multiple inflammatory cells, manifesting the typical sign of histiocytosis.

In this Issue

Highlights from this issue of *A&R* | By Lara C. Pullen, PhD

Urinary Biomarkers Reflect Histologic Findings in Lupus Nephritis

Researchers have previously reported that, in patients with active lupus nephritis (LN), some urinary proteins, such as vascular cell adhesion molecule 1 and activated leukocyte cell adhesion molecule, correlate with disease activity index. In this issue, Hiramoto et al (p. 298) report that an estimate of the urinary calgranulin B, monocyte chemotactic protein 1 (MCP-1), and insulin-like growth factor binding protein 5 (IGFBP-5) levels may help predict the presence and severity of histologic findings in LN. These renal histologic findings may thus reflect the different pathogenic pathways involved in each LN lesion. The work builds upon the previously reported protein analyses that compared patients with LN and healthy controls or those with active and inactive LN to identify distinguishing biomarkers.

p. 298

In the current study, the investigators used a scoring system that comprehensively included histologic findings based on the International Society of Nephrology/Renal Pathology Society classification and the National Institutes of Health index. They performed cluster analysis with each LN histologic finding and extracted five histologic subgroups. Pathway analyses revealed that each protein subgroup correlated with an LN histologic subgroup and had a distinct pathogenesis. The researchers then performed immunohistochemical staining to localize the proteins in each lesion and enzyme-linked immunosorbent assay validation to determine that levels of calgranulin B, MCP-1, and IGFBP-5 could specifically predict the presence and severity of active glomerular lesions, interstitial inflammation, and interstitial fibrosis, respectively.

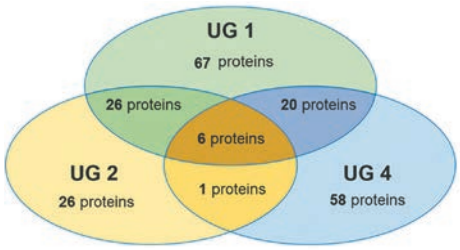

Figure 1. Venn diagram of urinary protein numbers in UG1, 2, and 4. UG: urinary protein subgroup.

The authors describe the precedence for each of these proteins playing a role in inflammation. Previous research has demonstrated that calgranulin B (S100A9) is pro-inflammatory in various autoimmune diseases. Likewise, MCP-1 contributes to monocyte activation and migration and has been established as a valuable biomarker for predicting disease activity and renal prognosis in patients with LN. IGFBP-5 regulates insulin-like growth factor signaling, and researchers have previously identified it as being involved in renal diseases. The authors concluded that extracting and identifying these urinary proteins may enhance clinical management and advance precision medicine.

Asymptomatic ANA Production Not a Genetic Risk for SLE

Researchers have demonstrated that asymptomatic antinuclear antibody (ANA) production can include a heterogeneous mixture of autoantibodies against nuclear antigens and represent an early event in the pathway to autoimmunity. In this issue, Hocaoglu et al (p. 356) report results from the first genome-wide association study (GWAS) of asymptomatic ANA production in multiple populations. They found that environmental factors primarily determine asymptomatic ANA production, and the presence of ANA is not associated with significant genetic risk for systemic lupus erythematosus (SLE).

p. 356

The investigators performed a GWAS of 1,955 asymptomatic ANA-positive and 3,634 asymptomatic ANA-negative individuals. They trained a random forest classifier to assign genetic similarity for each participant to one of the superpopulations of the 1000 Genomes Project: European (EUR), Admixed American (AMR), and African (AFR). The mean age and sex distribution between ANA-positive and ANA-negative individuals were similar across the genetic similarity groups.

While the multi-population meta-analysis revealed single-nucleotide polymorphisms with a suggestive association across 8 loci, the asymptomatic ANA-positive individuals were not enriched for SLE risk loci compared with ANA-negative individuals. The researchers then imputed human leukocyte antigen (HLA) classical alleles and examined genetic association by comparing asymptomatic individuals who were ANA-positive with asymptomatic individuals who were ANA-negative across the three genetic similarity groups, followed by a meta-analysis. The most significant suggestive genetic association revealed by this process was a gene variant upstream of *HLA-DQB1* previously reported in Japanese individuals.

The researchers estimated the heritability of asymptomatic ANA to be 24.9%. Calculating a total genetic risk for SLE in asymptomatic individuals who were ANA-positive compared with asymptomatic individuals who were ANA-negative and with patients with SLE, they found a statistically significant mean SLE genetic risk score between patients with SLE and both groups who were asymptomatic ANA-positive and asymptomatic ANA-negative across all three populations. The authors called for research to characterize the environmental determinants of ANA production and the role of gene–environment interactions in developing autoimmunity in ANA-positive individuals.

IgG Fc Glycosylation and Disease Dynamics in Primary SjD

Patients with Sjögren disease (SjD) have an enhanced risk of developing non-Hodgkin lymphoma (NHL). In this issue, Achten et al (p. 311) report that IgG Fc glycosylation in patients with SjD can be used to predict disease transition, monitor disease activity, and stratify the risk of NHL development. Theirs is the first study to investigate the role of IgG Fc glycosylation in an observational cohort of patients with suspected or confirmed SjD. Their findings suggest that Fc glycosylation could be a biomarker for predicting the transition to SjD.

p. 311

The study included patients representative of the entire disease spectrum within SjD, enabling the investigators to make comparisons across different patient groups and stages of disease. The researchers found that patients with SjD exhibited significantly lower sialylation and galactosylation levels compared to asymptomatic carriers of anti-SSA and patients with sicca.

Patients with lower sialylation and galactosylation levels also had increased B cell activation markers and distinct autoantibody profiles. Triple (anti-Ro52-60-SSB) reactivity had the lowest sialylation and galactosylation levels, and patients with anti-Ro52 who were double positive for the other antibodies had the second lowest sialylation and galactosylation levels. The investigators also noted a significant association between sialylation and galactosylation levels and histopathological salivary gland alterations, higher Hocevar scores, rheumatoid factor, and risk factors for NHL development. Conversely, patients with SjD who were mono-anti-Ro60 positive/anti-SSA negative had normal IgG Fc glycosylation. The authors called for rigorous multivariate analysis in larger cohorts to determine whether Fc glycosylation independently predicts NHL risk beyond established risk factors.

Journal Club

A monthly feature designed to facilitate discussion on research methods in rheumatology.

Weight Loss After Initiating Anti-Obesity Medications and Gout Among Overweight and Obese Individuals

Wei et al, *Arthritis Rheumatol.* 2025;77:335–345.

Overweight and obesity are key risk factors for gout, and weight loss has been conditionally recommended for gout patients who are overweight or obese. Anti-obesity medications, such as orlistat, may be an alternative to lifestyle interventions to achieve long-term weight loss. Wei et al emulated a hypothetical target trial using a "cloning, censoring, and weighting" approach to evaluate the effects of weight loss within one year of orlistat initiation on the risk of incident gout and gout flares.

Participants were "cloned" (i.e., replicated) into four groups, each assigned to one of four weight loss interventions: weight gain/stable (<2%), slow (2–5%), moderate (5–10%), or fast (≥10%) weight loss within one year after orlistat initiation. Cloning mimicked the randomization process of a hypothetical randomized controlled trial, ensuring that all confounders were evenly distributed among intervention groups. Follow-up began at the time of orlistat initiation, avoiding immortal time bias. "Censoring" ensured that replicates adhered to assigned strategies during the first year, with a one-year grace period allowed to achieve target weight. Specifically, replicates were censored if they deviated from their assigned group during the grace period.

Replicates who adhered to their assigned strategies and did not develop incident gout during the grace period were followed for an additional four years. Replicates who experienced gout, loss to follow-up, or death during the grace period were considered adherent across all assigned groups.

Inverse probability weighting (IPW) was used to address selection bias due to censoring. IPW up-weighted replicates who adhered to their assigned intervention, estimated through logistic regression, incorporating baseline and time-varying covariates from the index date to the censoring date. The study followed the protocol of a hypothetical clinical trial, including eligibility criteria, intervention strategies, intervention assignments, follow-up time, and outcome assessment. Results showed that faster weight loss within one year of orlistat initiation was associated with lower risks of incident gout and recurrent gout flares in overweight or obese individuals, adjusting for known confounders.

Questions

1. **What are challenges to intensive lifestyle intervention for weight loss in individuals with gout who are obese or overweight?**
2. **What was the purpose of cloning in the cloning, censoring, and weighting approach?**
3. **How did the study manage incident gout, loss to follow-up, or death during the grace period?**
4. **Why was IPW used in the study analysis? Can IPW eliminate selection bias from censoring?**

Clinical Connections

Evidence of Site-Specific Mucosal Autoantibody Secretion in Rheumatoid Arthritis

Derksen et al, *Arthritis Rheumatol.* 2025;77:272–282

CORRESPONDENCE
Diane van der Woude, MD, PhD: dvanderwoude@lumc.nl

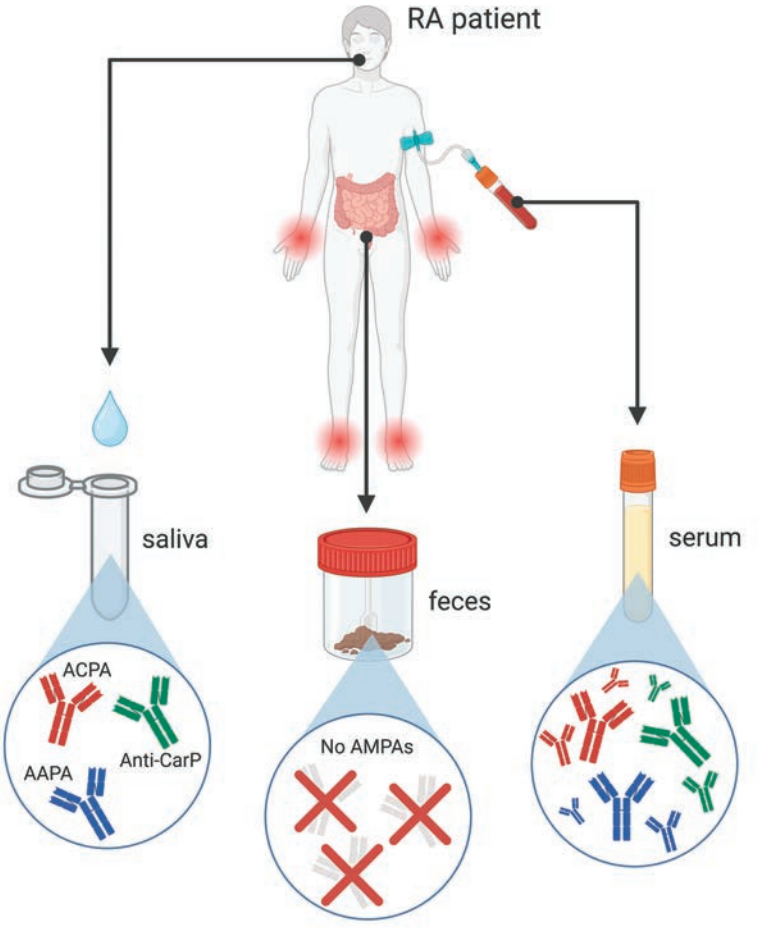

KEY POINTS

- ACPA, anti-CarP, and AAPA IgA were all detected in saliva of seropositive RA patients and were most likely produced locally in the oral mucosa.
- Salivary autoantibodies were only present in a small proportion of seropositive, established RA patients.
- No AMPAs were detected in ileal lavage fluid or feces of established RA patients. Thus, the lower intestinal tract seems unlikely to be a major site of AMPA secretion in established RA.

SUMMARY

A hallmark of seropositive rheumatoid arthritis (RA) is the presence of anti-modified protein antibodies (AMPA), of which antibodies against citrullinated (ACPA), carbamylated (anti-CarP) and acetylated (AAPA) proteins are generally considered to reflect the underlying autoimmune response. The mucosal immune system may be involved in the development of the AMPA response. ACPAs have been detected in sputum and saliva, indicating that (at least some) AMPAs can be produced at mucosal sites in RA patients. However, the body's largest mucosal compartment, the gut, has not yet been examined. To investigate intestinal involvement, Derksen et al collected material from feces / ileal wash, saliva, and serum of RA patients and healthy volunteers in three cohorts (MUCOSA, IntestRA, and Plants for Joints), and looked for the presence of AMPAs.

ACPA, anti-CarP, and AAPA IgA were all measurable in saliva of seropositive RA patients (prevalence 9-40%). However, in feces, no AMPAs could be detected in any of the cohorts, while total IgA and anti–*E. coli* IgA antibodies were detectable in feces. Results were confirmed in ileal wash samples collected by colonoscopy. These data suggest that mucosal autoantibody secretion may occur in the oral mucosa of RA patients, while no evidence could be found for this process in the lower gastrointestinal tract, thus indicating that the gut may be a less likely origin of the autoimmune response underlying RA.

Targeting Long Noncoding RNA H19 in Subchondral Bone Osteocytes and Alleviation of Cartilage Degradation in OA

Wang et al, *Arthritis Rheumatol.* 2025;77:283–297

CORRESPONDENCE
Wayne Yuk Wai Lee, PhD: waynelee@cuhk.edu.hk

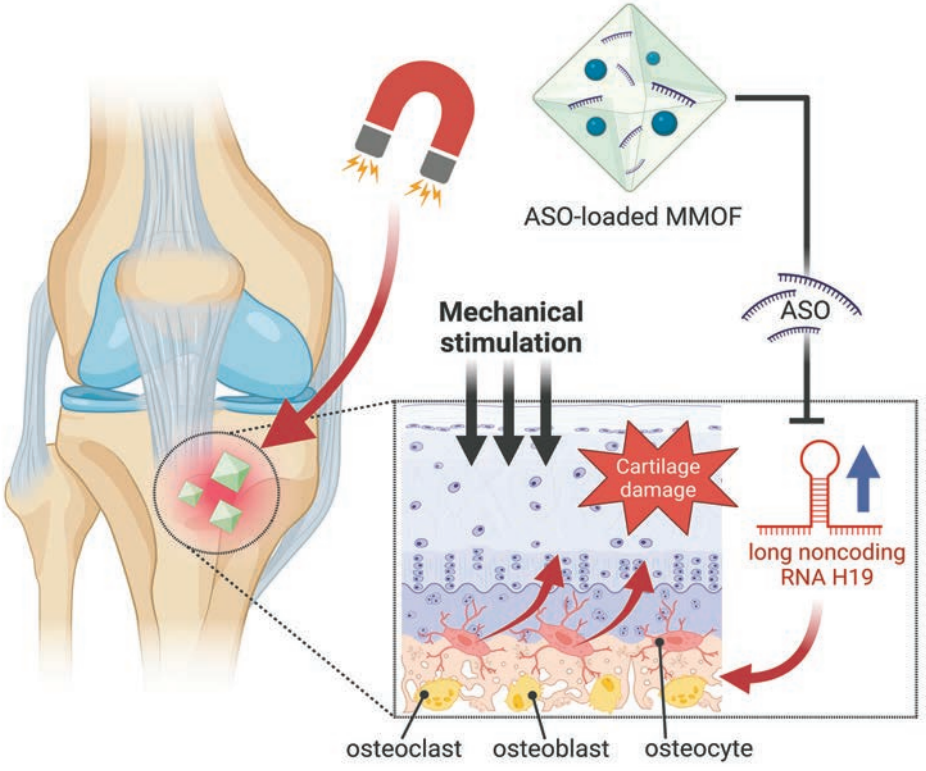

KEY POINTS

- Long noncoding RNA H19 expression is elevated in OA subchondral bone osteocytes in human OA samples and a DMM surgery-induced mouse model of OA.
- Osteocyte-specific H19 knockdown mitigates cartilage damage and subchondral bone sclerosis in a mouse OA model.
- H19 mediates osteocyte response to fluid shear stress mechanical stimulation by regulating protein phosphatase 2A and the PI3K/AKT/GSK3 axis.
- Inhibiting H19 expression in subchondral bone osteocytes through magnet-aided delivery of ASO against H19 alleviates OA progression in a mouse OA model.

SUMMARY

Subchondral bone remodeling is considered an aberrant mechanosensitive response to injury during osteoarthritis (OA) progression. Osteocytes play a major role in sensing and transmitting mechanical stimulation due to their wide distribution throughout the bone matrix, their complex interconnected lacunocanalicular network, and their secretion of various mechanoresponsive biomolecules. By investigating samples collected from OA patients undergoing knee replacement surgery and a destabilization of the medial meniscus (DMM)-induced mouse OA model, Wang et al demonstrated that long noncoding RNA H19 was highly expressed in subchondral bone osteocytes. In transgenic mice, H19 deficiency in osteocytes increased resistance to DMM-induced OA progression and subchondral bone remodeling. Furthermore, cellular experiments showed that H19 appears to enhance osteocyte cell response to mechanical stimulation through PI3K/AKT/GSK3 signal activation, which was partly attributed to protein phosphatase 2A inhibition.

To illustrate its translational potential, antisense oligonucleotide (ASO)-loaded magnetic metal–organic frameworks (MMOFs) were used to silence H19 in subchondral bone osteocytes in the mouse OA model. MMOFs were employed to facilitate more precise delivery of the anti-H19 ASO to the subchondral bone during treatment. This proof-of-concept approach effectively mitigated OA progression. The MMOF-based system could have significant translational potential for OA clinical applications by targeting subchondral bone osteocytes.

Arthritis & Rheumatology
Vol. 77, No. 3, March 2025, pp 241–243
DOI 10.1002/art.43026

American College of Rheumatology
Empowering Rheumatology Professionals

EDITORIAL

JAK Inhibitors Versus Biologic Disease-Modifying Antirheumatic Drugs: Which Is More Effective for Rheumatoid Arthritis Pain?

Abigail Weiland and Yvonne C. Lee

Pain is a near universal feature of patients with rheumatoid arthritis (RA). Although inflammation contributes to pain, it is not the only etiology, and pain often persists despite treatment of inflammation. Treatment with a disease-modifying antirheumatic drug (DMARD) is associated with improvements in pain intensity and pain interference in patients with RA, but improvements are often small in magnitude and may not be clinically meaningful.[1] The lack of resolution of pain may be due to multiple factors, including continued inflammation and abnormalities in central nervous system regulation of pain.[2] As a result, many patients with RA turn to other treatments, such as long-term opioids, which are not effective for chronic pain and are also associated with significant safety concerns.[3]

Given the unmet need for alleviating pain in patients with RA, there is considerable interest in identifying new treatment strategies. In recent years, JAK inhibitors have garnered attention for their potential in treating pain. Preclinical studies suggest that the JAK-STAT3 pathway is involved in nociceptive networks both peripherally (ie, at the joint level) and centrally (ie, in the spinal cord and brain). For example, in the collagen antibody-induced mouse model of arthritis (CAIA), inhibition of the JAK-STAT3 pathway was associated with decreased expression of colony-stimulating factor 1 in the dorsal root ganglion and inhibition of CAIA-induced microglial proliferation in the spinal dorsal horn, along with increases in paw withdrawal times (allodynia).[4]

In humans, data from phase 3 randomized controlled trials (RCTs) suggested that JAK inhibitors may be more effective for reducing pain than tumor necrosis factor (TNF) inhibitors. An early signal came from RA-BEAM, a phase 3 RCT of the JAK inhibitor baricitinib versus the TNF inhibitor adalimumab, which showed that patients randomized to receive baricitinib reported significantly less intense joint pain than those randomized to adalimumab.[5] This difference was evident two weeks after initiation of treatment. Similar results were seen in phase 3 RCTs of upadacitinib (SELECT-CHOICE, SELECT-COMPARE).[6,7] However, a secondary analysis of the ORAL Strategy trial showed no superiority for tofacitinib over adalimumab.[8] Similarly, a network meta-analysis of data from ORAL Strategy and ORAL Standard demonstrated no difference in the effect of tofacitinib versus adalimumab on residual pain (pain despite swollen joint count = 0 and C-reactive protein [CRP] < 6 mg/L).[9] In addition, there is a dearth of data on pain outcomes comparing JAK inhibitors to non-TNF DMARDs.

In this issue of *Arthritis & Rheumatology*, Eberhard and colleagues compared the treatment effect of JAK inhibitors and biologic DMARDs on pain among patients with RA using data from linked Swedish national registries.[10] At three months, patients initiating JAK inhibitors reported 4 mm (out of 100 mm) greater decreases in visual analog scale (VAS) pain scores, compared with patients initiating TNF inhibitors and rituximab in adjusted analyses. No increased benefit was noted compared to abatacept or interleukin-6 (IL-6) inhibitors. At 12 months, only 68% of patients remained on the drug that was initiated at baseline. Thus, the primary outcome at 12 months was designated as the proportion of patients who remained on the initiated drug and achieved low pain, defined as a VAS < 20. In adjusted analyses, a higher proportion of patients who initiated JAK inhibitors achieved low pain and remained on therapy, compared to those who initiated TNF and IL-6 inhibitors, but this did not reach statistical significance. Subgroup analyses suggested that patients who had been treated with at least two prior DMARDs had greater reductions in pain when treated with a JAK inhibitor versus a TNF inhibitor.

Notable strengths of this study are the use of data from the Swedish national registries, which yielded a large sample size of patients who are representative of routine clinical practice in Sweden. Limitations include potential confounding associated

Dr. Lee's work was supported by the NIH (grant K24-AR-080840).
[1]Abigail Weiland, MD, Yvonne C. Lee, MD, MMSc: Feinberg School of Medicine, Northwestern University, Chicago, Illinois.
Author disclosures are available at https://onlinelibrary.wiley.com/doi/10.1002/art.43026.

Address correspondence via email to Yvonne C. Lee, MD, MMSc, at yvonne.lee@northwestern.edu.
Submitted for publication August 13, 2024; accepted in revised form September 24, 2024.

with the observational design of the study, as well as a large amount of missing data. More than 50% of the patients were missing a VAS pain score at 12 months. In the primary analyses, these data were imputed using multiple imputation to minimize selection bias. However, there remains the potential for bias because of unmeasured factors. Thus, no definitive conclusions regarding the 12-month impact of JAK inhibitors on pain can be made.

What can we take away from this study? First, these data confirm that the initiation of a JAK inhibitor is associated with larger short-term (three month) reductions in pain compared with TNF inhibitors in the real-world setting. However, the magnitude of difference in pain reduction was small and did not meet published thresholds for clinically important differences (>1 cm or 15%).[11] Additionally, the small difference in pain reduction was found only in the adjusted analyses but not in the unadjusted analyses, calling to attention the potential issue of confounding. It should be emphasized that, in observational studies, the careful selection of covariates is key and may have a significant impact on results.

The particularly novel part of this study lies in the subgroup analyses in which Eberhard and colleagues examined relationships between the treatment and pain response in groups stratified by line of treatment. The superiority of JAK inhibitors over TNF inhibitors for reducing pain was only evident among patients starting second or later line DMARDs, not those starting first-line therapy after a conventional DMARD.[10] This observation could be consistent with these patients having noninflammatory pain mechanisms that are not targeted by first-line biologic DMARD treatment directed at inflammatory pathways. In line with this, Taylor, et al found that baricitinib had a greater effect on pain relief over placebo than adalimumab, and changes in objective markers of inflammation (measured by CRP, erythrocyte sedimentation rate, and swollen joint count) accounted for only 40% of the pain relief with baricitinib,[12] suggesting that 60% of pain improvement occurred via noninflammatory pathways.

In fact, several studies have reported that pain in patients with RA is likely multifactorial, including potential contributions of nociceptive pain from inflammation and active tissue destruction, neuropathic pain from peripheral nervous system processes (eg, carpal tunnel syndrome), and/or nociplastic pain from peripheral and/or central nervous system dysregulation.[13] Using data from the Accelerating Medicines Partnership RA/Systemic Lupus Erythematosus Network, Bai et al recently identified an 815-gene expression module that was associated with pain in patients with RA but minimal histologic evidence of inflammation on synovial biopsy.[14] This module includes *NTN4*, which encodes netrin-4, a secreted protein that increases branching of pain-sensitive dorsal root ganglion neurons into areas of synovial hypertrophy. These results support the existence of noninflammatory pathways of joint pain in RA. Future studies examining the effects of JAK inhibitors on these pain pathways would be of great interest.

Alternatively, the "noninflammatory" pathways through which JAK inhibitors work may not be noninflammatory at all. Instead, the findings could be a result of imperfect measures of inflammation. Typical measures of inflammation used in RCTs and clinical practice include swollen and tender joint counts, sedimentation rate, and CRP, but these measures may not provide a nuanced enough picture of local processes. The incorporation of synovial biopsies and/or musculoskeletal ultrasound in future studies would provide valuable information to help delineate different potential mechanisms of pain.

Ultimately, the holy grail is a precision-based medicine approach to managing pain in patients with RA. To move toward this goal, we provide a few high-level recommendations for investigators designing these research studies and clinicians caring for these patients. One, it is of critical importance to understand patient experiences and priorities when it comes to goals of treatment. Although some patients speak of inflammation, it is our experience that more patients report pain, and, when they do speak of inflammation, further probing often reveals pain to be the underlying symptom. However, not all pain is inflammatory. Two, given that patients with RA experience pain from many causes and can subsequently have differential responses to treatment, it is important to comprehensively phenotype pain, with the goal of identifying underlying etiological pathways. The unidimensional VAS pain rating, used in most of the existing literature, evaluates only the severity of pain but does not measure other domains such as pain quality or quality of life. We suggest that investigators use additional validated measurement tools, such as those recommended by the NIH HEAL Initiative's Common Data Elements Program,[15] as well other assessments, such as quantitative sensory testing, depending on the specific study question.

In conclusion, pain remains a critical problem for many patients with RA. This study by Eberhard and colleagues, in conjunction with existing clinical trial data, suggests that JAK inhibitors yield slightly better pain outcomes than TNF inhibitors.[10] The magnitude of these effects is unlikely to be clinically meaningful in unselected groups of patients with RA. However, this study showed that specific subgroups, such as those who have tried at least two DMARDs, may experience greater effects. To better delineate these subgroups, it is critically important to comprehensively phenotype pain in research studies and go beyond the simple VAS pain scale.

AUTHOR CONTRIBUTIONS

Drs Weiland and Lee drafted the article, revised it critically for important intellectual content, and approved the final version to be published.

REFERENCES

1. Wohlfahrt A, Bingham CO, 3rd, Marder W, et al. Responsiveness of patient-reported outcomes measurement information system measures in rheumatoid arthritis patients starting or switching a disease-modifying antirheumatic drug. Arthritis Care Res (Hoboken) 2019;71: 521–529.
2. Murphy AE, Minhas D, Clauw DJ, et al. Identifying and managing nociplastic pain in individuals with rheumatic diseases: a narrative review. Arthritis Care Res (Hoboken) 2023;75:2215–2222.
3. Lee YC, Lu B, Guan H, et al. Physician prescribing patterns and risk of future long-term opioid use among patients with rheumatoid arthritis: a prospective observational cohort study. Arthritis Rheumatol 2020; 72:1082–1090.
4. Makabe K, Okada H, Tachibana N, et al. Baricitinib ameliorates inflammatory and neuropathic pain in collagen antibody-induced arthritis mice by modulating the IL-6/JAK/STAT3 pathway and CSF-1 expression in dorsal root ganglion neurons. Arthritis Res Ther 2024;26:121.
5. Taylor PC, Keystone EC, van der Heijde D, et al. Baricitinib versus placebo or adalimumab in rheumatoid arthritis. N Engl J Med 2017;376: 652–662.
6. Fleischmann R, Pangan AL, Song IH, et al. Upadacitinib versus placebo or adalimumab in patients with rheumatoid arthritis and an inadequate response to methotrexate: results of a phase III, double-blind, randomized controlled trial. Arthritis Rheumatol 2019;71:1788–1800.
7. Bergman M, Tundia N, Martin N, et al. Patient-reported outcomes of upadacitinib versus abatacept in patients with rheumatoid arthritis and an inadequate response to biologic disease-modifying antirheumatic drugs: 12- and 24-week results of a phase 3 trial. Arthritis Res Ther 2022;24:155.
8. Strand V, Mysler E, Moots RJ, et al. Patient-reported outcomes for tofacitinib with and without methotrexate, or adalimumab with methotrexate, in rheumatoid arthritis: a phase IIIB/IV trial. RMD Open 2019; 5:e001040.
9. Dougados M, Taylor PC, Bingham CO, 3rd, et al. The effect of tofacitinib on residual pain in patients with rheumatoid arthritis and psoriatic arthritis. RMD Open 2022;8:e002478.
10. Eberhard A, Di Giuseppe D, Askling J, et al. Effectiveness of JAK inhibitors compared with biologic disease-modifying antirheumatic drugs on pain reduction in rheumatoid arthritis: Results from a nationwide swedish cohort study. Arthritis Rheumatol 2025;77(3):253–262.
11. Salaffi F, Stancati A, Silvestri CA, et al. Minimal clinically important changes in chronic musculoskeletal pain intensity measured on a numerical rating scale. Eur J Pain 2004;8:283–291.
12. Taylor PC, Lee YC, Fleischmann R, et al. Achieving pain control in rheumatoid arthritis with baricitinib or adalimumab plus methotrexate: results from the RA-BEAM trial. J Clin Med 2019;8:831.
13. Salaffi F, Giacobazzi G, Di Carlo M. Chronic pain in inflammatory arthritis: mechanisms, metrology, and emerging targets-a focus on the JAK-STAT pathway. Pain Res Manag 2018;2018:8564215.
14. Bai Z, Bartelo N, Aslam M, et al. Synovial fibroblast gene expression is associated with sensory nerve growth and pain in rheumatoid arthritis. Sci Transl Med 2024;16:eadk3506.
15. Wandner LD, Domenichiello AF, Beierlein J, et al. NIH's helping to end addiction long-term^{SM} initiative (NIH HEAL Initiative) clinical pain management common data element program. J Pain 2022;23:370–378.

American College of Rheumatology
Empowering Rheumatology Professionals

Arthritis & Rheumatology
Vol. 77, No. 3, March 2025, pp 244–246
DOI 10.1002/art.43020

EDITORIAL

Urinary Biomarkers: Toward a Liquid Biopsy for Lupus Nephritis

Andrea Fava

The suboptimal response rates in lupus nephritis (LN)[1,2] underscore the urgency for better management strategies. Among an ever-impressive pipeline of novel treatments on the horizon, we are still confronted with significant limitations in our ability to promptly diagnose, accurately classify, and adequately monitor treatment response in LN. LN is asymptomatic in most patients,[3] and thus, the current strategy relies on serial screening of patients with systemic lupus erythematosus, triggering a kidney biopsy when elevated proteinuria or unexplained decline of kidney function are detected.[4,5] However, proteinuria is an unreliable indicator; it cannot differentiate between histologic classes (including membranous vs proliferative[6]), correlates poorly with histologic activity, and may increase in cases of renal damage devoid of intrarenal inflammation.

Kidney biopsies remain the cornerstone for guiding LN treatment, providing insight into LN histologic class, presence of high-risk features, and the degree of inflammatory activity as well as chronicity (damage). Yet, treatment response is assessed mostly by proteinuria reduction,[4,5] an imperfect surrogate. Multiple studies on repeat biopsies revealed that up to half of patients who achieve remission-range proteinuria (<0.5 g/24 h) continue to exhibit histologic activity, and conversely, over half of those with complete histologic remission still have proteinuria exceeding 0.5 g/24 h.[7,8] Although the clinical impact of protocolized repeat biopsies is under formal investigation,[9] the urgency for frequent, accurate assessments of disease activity in LN—especially in the early months, when irreversible damage accrues[10]—is clear. As such, there is a pressing need for noninvasive biomarkers that can accurately reflect intrarenal disease activity within the heterogeneity of LN, enabling real-time therapeutic adjustments and preventing progression to renal fibrosis.

The recent study by Hiramoto et al, published in *Arthritis & Rheumatology*, tackles this challenge, focusing on urinary biomarkers that reflect histologic findings in LN.[11] The authors extended the evaluation beyond the 10 components of the NIH Activity and Chronicity Indices commonly used in practice, quantifying 20 histologic features and identifying four main clusters of co-correlated lesions based on location: extracapillary, endocapillary, mesangial/membranous, and tubulointerstitial. This clustering approach provides a nuanced view of LN pathology, offering a simpler potential framework for understanding disease heterogeneity.

Urine, by capturing the byproducts of intrarenal pathobiology in real time, serves as an ideal specimen for developing noninvasive biomarkers of LN and providing insight into disease pathogenesis. Hiramoto et al used a 1,305-plex urine proteomic assay to identify shared and distinct molecular signatures associated with each histologic cluster. A granulocyte signature was linked to multiple lesions, whereas fibrosis-related signatures were predominantly seen in tubulointerstitial lesions—consistent with the fact that this region is where most fibrosis and inflammation coalesce in LN.

Shifting the focus to biomarker discovery, the authors highlighted three key urinary proteins: calgranulin B (S100 calcium-binding protein A9), a clinically used biomarker for intestinal inflammation, which best correlated with intraglomerular inflammation; monocyte chemotactic protein 1, a well-established marker of active LN, which correlated with interstitial inflammation; and insulin-like growth factor binding protein 5 (IGFBP-5), a profibrotic molecule previously associated with chronic kidney disease, which correlated with interstitial fibrosis.

Although this study involved a relatively small sample size, it lays promising groundwork for the conceptualization of a liquid biopsy in LN. Biomarkers, by definition, provide a more convenient or noninvasive way to reflect biologic states or predict outcomes. In LN, kidney pathology remains the gold standard for assessing treatable inflammation and damage, but it is not yet clear how to optimally use this information to guide treatment. The framework proposed by this study, with its focus on principal histologic components and their relative biomarkers, might, if validated, refine the current prognostic limitations of renal biopsies

Andrea Fava, MD: Johns Hopkins University, Baltimore, Maryland.
Author disclosures are available at https://onlinelibrary.wiley.com/doi/10.1002/art.43020.

Address correspondence via email to Andrea Fava, MD, at afava1@jh.edu.
Submitted for publication September 9, 2024; accepted in revised form September 19, 2024.

by introducing a granular, longitudinal perspective through noninvasive biomarkers.

Histologic fibrosis, as quantified by the NIH Chronicity Index or interstitial fibrosis and tubular atrophy (IFTA), is one of the best predictors of nonresponse (based on proteinuria) and progression to end-stage kidney disease. But the degree of histologic activity in the diagnostic biopsy has not been shown to predict clinical response. The persistence of histologic activity, revealed through repeat biopsy, has demonstrated prognostic value. Therefore, a noninvasive biomarker capable of longitudinally tracking the evolution of specific lesions could provide critical insights into treatment efficacy, offering a much-needed tool for real-time therapeutic adjustments.

This exciting framework requires further validation. The novel histologic scoring and clustering systems introduced by Hiramoto et al must be tested in larger and more diverse cohorts and against meaningful outcomes to ensure clinical utility.[11] Moreover, the predictive power of these biomarkers in assessing long-term disease progression and treatment response needs confirmation through longitudinal studies.

This work contributes to the growing body of research on urinary biomarkers in LN[12–16] and underscores the power of multimodal analyses. We are now witnessing the early outcomes of large, ambitious collaborative projects that are dissecting the histologic, cellular, and molecular features of kidney disease with unprecedented depth, aiming to redefine the pathologically and clinically relevant features of these diseases.[17–19] The potential to integrate newly discovered pathologic, molecular, and clinically relevant endotypes through multiomic approaches and link them to noninvasive biomarkers is particularly exciting. With the current technological and computational explosive advancements, we are experiencing a 21st-century renaissance in the redefinition of anatomy—one that could revolutionize our understanding of disease groups, facilitate the identification of relevant biomarkers, and ultimately guide precise, individualized treatments.

However, the roadmap to the translation of candidate biomarkers to clinical application is long and winding (Figure 1). Biomarkers are often discovered through expensive and technically demanding platforms that are impractical for large-scale clinical use. The initial "discovery" phase involves selecting biomarkers and developing assays that are technologically feasible, reproducible, and scalable for clinical laboratories. This is followed by "validation," in which assays undergo technical and analytical testing to confirm they can replicate initial findings. In the subsequent "development" phase, external clinical validation and demonstration of clinical utility are essential.

Biomarkers are tested across diverse populations to ensure generalizability and, most importantly, must offer a meaningful improvement over the existing clinical standard. For instance, whereas a biomarker that predicts LN activity as defined by

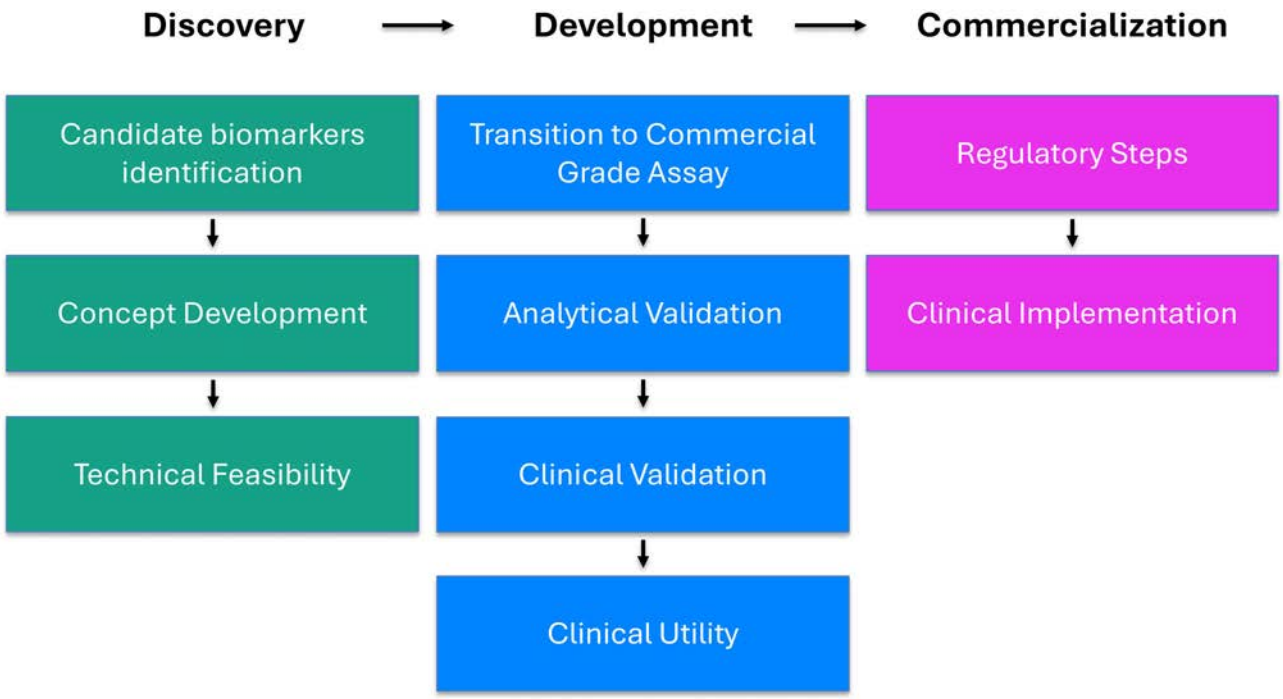

Figure 1. The pathway from biomarker discovery to clinical implementation: The process begins with identifying candidate biomarkers and developing the concept and feasibility for clinical assays ("Discovery"). The transition to commercial-grade assays and rigorous analytical and clinical validation steps ensures reproducibility and reliability. Most importantly, biomarkers must demonstrate clinical utility ("Development"). Each stage requires meticulous testing and validation across diverse cohorts to ensure efficacy and generalizability for each context of use. Finally, regulatory steps according to local guidelines are required to enable widespread clinical implementation ("Commercialization").

concurrent proteinuria offers little new value, one that noninvasively detects histologically active proliferative LN could revolutionize clinical practice by providing information currently accessible only through biopsy. To establish clinical utility, biomarkers need to be validated for specific contexts of use, such as predicting disease susceptibility, actionable histologic features, treatment response, or prognosis. Some may even redefine response criteria and primary outcomes in clinical trials. This phase of validation may require prospective trials, and regulatory approval is necessary for commercialization and reimbursement. Despite the challenges, several biomarkers are progressing through this pipeline, bringing us closer to personalized management of LN. As candidate urinary biomarkers for LN continue to undergo validation, the possibility of a reliable, noninvasive method for monitoring disease activity becomes increasingly tangible, offering the potential to transform management strategies and outcomes in LN.

AUTHOR CONTRIBUTIONS

All authors contributed to at least one of the following manuscript preparation roles: conceptualization AND/OR methodology, software, investigation, formal analysis, data curation, visualization, and validation AND drafting or reviewing/editing the final draft. As corresponding author, Dr Fava confirms that all authors have provided the final approval of the version to be published, and takes responsibility for the affirmations regarding article submission (eg, not under consideration by another journal), the integrity of the data presented, and the statements regarding compliance with institutional review board/Declaration of Helsinki requirements.

REFERENCES

1. Furie R, Rovin BH, Houssiau F, et al. Two-year, randomized, controlled trial of belimumab in lupus nephritis. N Engl J Med 2020; 383(12):1117–1128.
2. Rovin BH, Teng YKO, Ginzler EM, et al. Efficacy and safety of voclosporin versus placebo for lupus nephritis (AURORA 1): a double-blind, randomised, multicentre, placebo-controlled, phase 3 trial. Lancet 2021;397(10289):2070–2080.
3. Carlucci PM, Preisinger K, Deonaraine KK, et al. Extrarenal symptoms associate with worse quality of life in patients enrolled in the AMP RA/SLE Lupus Nephritis Network. Rheumatology (Oxford) Published online March 26, 2024. https://doi.org/10.1093/rheumatology/keae189
4. Kidney Disease: Improving Global Outcomes (KDIGO) Lupus Nephritis Work Group. KDIGO 2024 Clinical Practice Guideline for the management of lupus nephritis. Kidney Int 2024;105(1S):S1–S69.
5. Fanouriakis A, Kostopoulou M, Andersen J, et al. EULAR recommendations for the management of systemic lupus erythematosus: 2023 update. Ann Rheum Dis 2024;83(1):15–29.
6. Carlucci PM, Li J, Fava A, et al. High incidence of proliferative and membranous nephritis in SLE patients with low proteinuria in the Accelerating Medicines Partnership. Rheumatology (Oxford) 2022; 61(11):4335–4343.
7. Malvar A, Pirruccio P, Alberton V, et al. Histologic versus clinical remission in proliferative lupus nephritis. Nephrol Dial Transplant 2017; 32(8):1338–1344.
8. De Rosa M, Azzato F, Toblli JE, et al. A prospective observational cohort study highlights kidney biopsy findings of lupus nephritis patients in remission who flare following withdrawal of maintenance therapy. Kidney Int 2018;94(4):788–794.
9. Parodis I, Tamirou F, Houssiau FA. Treat-to-target in lupus nephritis. What is the role of the repeat kidney biopsy? Arch Immunol Ther Exp (Warsz) 2022;70(1):8.
10. Malvar A, Alberton V, Lococo B, et al. Remission of lupus nephritis: the trajectory of histological response in successfully treated patients. Lupus Sci Med 2023;10(1):e000932.
11. Hiramoto K, Saito S, Hanaoka H, et al. Urinary biomarkers associated with pathogenic pathways reflecting histological findings in lupus nephritis. Arthritis Rheumatol 2025;77(3):298–310.
12. Fava A, Buyon J, Magder L, et al; Accelerating Medicines Partnership in RA/SLE network. Urine proteomic signatures of histological class, activity, chronicity, and treatment response in lupus nephritis. JCI Insight 2024;9(2):e172569.
13. Mejia-Vilet JM, Zhang XL, Cruz C, et al. Urinary soluble CD163: a novel noninvasive biomarker of activity for lupus nephritis. J Am Soc Nephrol 2020;31(6):1335–1347.
14. Brunner HI, Bennett MR, Abulaban K, et al. Development of a novel renal activity index of lupus nephritis in children and young adults. Arthritis Care Res (Hoboken) 2016;68(7):1003–1011.
15. Vanarsa K, Soomro S, Zhang T, et al. Quantitative planar array screen of 1000 proteins uncovers novel urinary protein biomarkers of lupus nephritis. Ann Rheum Dis 2020;79(10):1349–1361.
16. Fava A, Rao DA, Mohan C, et al; Accelerating Medicines Partnership in Rheumatoid Arthritis and Systemic Lupus Erythematosus Network. Urine proteomics and renal single-cell transcriptomics implicate interleukin-16 in lupus nephritis. Arthritis Rheumatol 2022;74(5): 829–839.
17. Fava A, Raychaudhuri S, Rao DA. The power of systems biology: insights on lupus nephritis from the Accelerating Medicines Partnership. Rheum Dis Clin North Am 2021;47(3):335–350.
18. de Boer IH, Alpers CE, Azeloglu EU, et al; Kidney Precision Medicine Project. Rationale and design of the Kidney Precision Medicine Project. Kidney Int 2021;99(3):498–510.
19. Trachtman H, Desmond H, Williams AL, et al; NEPTUNE investigators. Rationale and design of the Nephrotic Syndrome Study Network (NEPTUNE) match in glomerular diseases: designing the right trial for the right patient, today. Kidney Int 2024;105(2):218–230.

Arthritis & Rheumatology
Vol. 77, No. 3, March 2025, pp 247–252
DOI 10.1002/art.43019

American College of Rheumatology
Empowering Rheumatology Professionals

REVIEW

Exploring the Role of Neutrophil Extracellular Traps in Systemic Lupus Erythematosus: A Clinical Case Study and Comprehensive Review

Mariana J. Kaplan

Introduction

Systemic lupus erythematosus (SLE) is a complex autoimmune syndrome characterized by a dysregulated immune response, leading to widespread inflammation and tissue damage. In recent years, research has highlighted the involvement of neutrophil extracellular traps (NETs) in the pathogenesis of lupus.[1] This case study aims to illustrate the clinical manifestations of lupus and explore the role of NETs in disease pathogenesis, diagnosis, and treatment.

Case presentation

The patient, a 31-year-old woman, presents to the rheumatology clinic with a 6-month history of fatigue, joint pain, intermittent fevers, and facial rash exacerbated by sun exposure. These symptoms were first noticed after the resolution of an upper respiratory tract infection. She also reports experiencing nonpainful recurrent oral ulcers, Raynaud phenomenon, and hair loss over the past 3 months. She has taken acetaminophen for the joint pain and has tried to stay away from the sun, but her symptoms have persisted. On physical examination, she displays an erythematous macular malar rash that spares the nasolabial folds, oral ulcers, and tenderness and swelling in multiple joints in hands and feet as well as in her knees. There is a maculopapular erythematous rash in her upper arms. Laboratory tests reveal leukopenia, lymphopenia, mild neutropenia, elevated erythrocyte sedimentation rate, normal C-reactive protein levels, increased levels of antinuclear antibodies (homogenous pattern), anti–double-stranded DNA (anti-dsDNA) and anti-Ro antibodies, and decreased C3 and C4 levels. Her renal function test results are normal and there is no proteinuria. The lipoprotein profile reveals low high-density lipoprotein (HDL) and elevated low-density lipoprotein and total cholesterol. A carotid ultrasound scan, done for research purposes as part of a lupus cardiovascular cohort assessment, reveals a significant increase in carotid intimal media thickness bilaterally. An evaluation of HDL function reveals impaired cholesterol efflux capacity. A plasma sample sent to a research laboratory reveals elevated myeloperoxidase (MPO):DNA remnants and citrullinated histone H3:DNA remnants consistent with NETs, and a flow cytometry analysis of peripheral blood mononuclear cells reveals the presence of low-density granulocytes (LDGs).

Given the clinical presentation and laboratory findings, the patient would be diagnosed as having SLE, preclinical atherosclerosis, and dyslipidemia and started on an antimalarial, a statin, and low-dose prednisone. The patient would also be advised regarding sun protection, vitamin D intake, warranted vaccinations, and other general preventive measures for SLE comorbidities.

SLE, neutrophil dysregulation, and NETs

The patient's case illustrates the classic presentation of SLE, characterized by a constellation of constitutional symptoms, mucocutaneous manifestations, and multisystem involvement, in association with evidence of cardiometabolic dysfunction. The pathogenesis of SLE involves a complex interplay between innate and adaptive immune responses. Although neutrophils have been proposed to play fundamental roles in the pathogenesis of SLE, including previous descriptions of aberrant clearance of apoptotic neutrophils and the LE cell phenomenon, recent discoveries over the past 15 years have highlighted and identified novel mechanisms by which these cells may play fundamental roles in the initiation and perpetuation of a variety of systemic autoimmune diseases, including SLE, antineutrophil cytoplasmic antibody–associated vasculitis, rheumatoid arthritis, and idiopathic inflammatory myopathies.[2–5]

Mariana J. Kaplan, MD: National Institute of Arthritis and Musculoskeletal and Skin Diseases, NIH, Bethesda, Maryland.

Author disclosures and graphical abstract are available at https://onlinelibrary.wiley.com/doi/10.1002/art.43019.

Address correspondence via email to Mariana J. Kaplan, MD, at mariana.kaplan@nih.gov.

Submitted for publication July 29, 2024; accepted in revised form September 10, 2024.

One of the neutrophil features that has been identified by various research groups as becoming dysregulated in autoimmunity is the formation of NETs.[6] These are web-like structures composed of DNA, RNA, histones, and various antimicrobial proteins, which are released to the extracellular space by activated neutrophils in response to a variety of microbial and sterile inflammatory stimuli. In SLE, dysregulated NET formation and impaired clearance of these structures have been reported to lead to their accumulation within tissues and to their extended half-life in circulation, potentially contributing to perpetuating autoantigen generation and modification, inflammation, and tissue damage.[6,7] NETs may contribute to the pathogenesis of lupus nephritis, lupus-associated skin disease, thrombosis, vascular damage, and tissue injury in various organs, including pregnancy complications such as preeclampsia.[6,8,9]

The aberrant exposure within NETs of modified autoantigens, including oxidized nucleic acids and posttranslationally modified histones,[10] may contribute to triggering the production of autoantibodies, including anti-dsDNA and antinucleosome antibodies, perpetuating the autoimmune responses in SLE. Furthermore, NETs promote the in vitro activation of plasmacytoid dendritic cells (DCs) and the production of type I interferons (IFNs), driving systemic inflammation and amplifying immune dysregulation in this disease.[6]

Mechanism of NET formation and triggers in SLE

NETosis is a unique form of cell death distinct from apoptosis and necrosis. It involves the release of neutrophil chromatin bound with various antimicrobial proteins, such as MPO and neutrophil elastase. NET formation can occur via several pathways. The classic pathway involves reactive oxygen species (ROS) generation by the NADPH oxidase pathway. This leads to the activation of protein-arginine deiminase 4 (PAD4), which catalyzes the conversion of arginine residues to citrulline in histones, resulting in chromatin decondensation. Subsequently, the nuclear envelope and granule membranes disintegrate, allowing the release of chromatin fibers decorated with antimicrobial proteins. The presence of citrullinated histones is a hallmark of NETs, distinguishing them from other extracellular DNA structures (reviewed in Wigerblad and Kaplan[1]).

In the context of SLE, several factors contribute to the enhanced formation and defective clearance of NETs. These include oxidative stress, autoantibodies, immune complexes, autoimmunity-inducing drugs, and proinflammatory cytokines.[10] Various genetic polymorphisms that confer risk for SLE, including *IRF-5, STAT-4*, and *PTPN22,* are also associated to enhanced NET formation.[11,12] As mentioned above, ROS play a crucial role in NET formation, and patients with lupus exhibit elevated levels of oxidative stress, which correlates with increased NETosis. Furthermore, lupus autoantibodies, particularly those targeting nuclear antigens, such as anti-RNP immune complexes, can directly induce NET formation.[3] These autoantibodies and immune complexes bind to neutrophil surface receptors, triggering intracellular signaling cascades that lead to NET release.

A putative link between infections and lupus flares has been reported.[13] It is possible that innate immune activation following some infections, including the formation of NETs, could link microbial exposure to disease flares. Furthermore, UV light (also linked with disease flares), has been associated with the formation of NETs.[14] As such, factors well-known to be associated with exacerbations of lupus symptoms may do so, in part, by inducing neutrophil dysregulation leading to NET formation and extrusion of autoantigens, alarmins, and other signals associated with innate and adaptive immune activation.

In the case of this patient, she had noticed that her symptoms had appeared and were exacerbated during sun exposure and following an upper respiratory tract infection. One can posit that these triggers may have promoted flares, at least in part, through the induction of NETs in skin, mucosal sites, and other organs. Furthermore, the mild neutropenia observed in this patient may be secondary to enhanced NET formation leading to neutrophil cell death; this is supported by the finding of elevated NET remnants in her plasma.

LDGs in SLE

LDGs have garnered significant attention in the context of SLE because of their distinctive characteristics and potential implications in disease pathogenesis. These cells, which are found in circulation at increased levels in a significant proportion of patients SLE and are typically purified from the mononuclear cell layer after density centrifugation (hence, their name because of having lower density than regular neutrophils), exhibit unique phenotypic and functional properties when compared with their higher-density counterparts.[15] These properties include altered cytokine production, enhanced ability to form NETs in the absence of added stimulation, exacerbated ability to synthesize ROS, and enhanced ability to damage the endothelium through matrix-metalloproteinases.[6,15] The increased prevalence of LDGs in patients with SLE, coupled with their potential to contribute to disease pathology through the release of inflammatory mediators and autoantigens, makes them a subject of interest for understanding disease mechanisms and progression in SLE.

Clinically, LDGs have emerged as potential biomarkers for SLE owing to their association with disease activity and flares.[16,17] Elevated levels of LDGs have been observed in patients with SLE during active disease phases, and their counts correlate with disease severity, coronary plaque severity, and vascular wall inflammation, as assessed by coronary computed tomography and fluorodeoxyglucose positron emission tomography, respectively.[16,17] Furthermore, LDGs have been associated with impaired lipoprotein (HDL) function, because they promote a loss of its atheroprotective function through oxidation during

NET formation.[18] As such, measuring LDG levels could provide valuable insights into disease activity, helping clinicians to monitor and potentially predict flares or response to therapy. These studies require large cohorts and further validation before deciding whether LDGs add additional value in the management of SLE. The identification of specific markers or functional characteristics of LDGs could facilitate more targeted therapeutic approaches, aiming to modulate the inflammatory responses mediated by these cells. Monitoring LDG levels could therefore provide insights into ongoing vascular damage and the efficacy of therapeutic interventions aimed at reducing inflammation and protecting vascular health.

In the case of this patient, there was evidence of accelerated vascular damage as assessed by carotid intima-media thickness, as well as dysregulated lipoprotein panel with impaired HDL function, elevated LDGs, and NET remnants in circulation. It is possible that these abnormalities were triggered, at least in part, by LDGs and associated NET formation, although such measurements were not readily available.

NETs and autoantigen exposure

One of the central pathogenic features of lupus is the generation of autoantibodies against nuclear components such as DNA, histones, and other chromatin-associated proteins. NETs expose these nuclear antigens to the immune system in an immunogenic context. During NET formation, neutrophils release various nuclear proteins, including modified histones, high-mobility group box 1, LL37, which can act as autoantigens, and DAMPs[6] (reviewed in Wigerblad and Kaplan[1]). The release of these nuclear proteins in the form of NETs provides a rich source of modified autoantigens that can stimulate the production of autoantibodies. This process is further amplified by the presence of DCs, macrophages, nonprofessional antigen-presenting cells, and various stromal cells that can take up NET components, process them, and present them to autoreactive T and B cells.[19,20] This phenomenon leads to a vicious cycle of autoantigen exposure and autoantibody production, perpetuating the autoimmune response. In addition, NET formation leads to enhanced oxidation of nucleic acids (genomic and mitochondrial DNA and RNA). The oxidation of nucleic acids enhances the half-life of these structures by making their degradation by nucleases more cumbersome. This increases the sensing by intracellular sensors of nucleic acids, including the cyclic GMP-AMP synthase (cGAS)-stimulator of interferon genes (STING) and endosomal toll-like receptor pathways, promoting the synthesis of type I IFN responses, a hallmark of lupus pathogenesis.[10,21]

Impaired NET clearance

In healthy individuals, NETs are rapidly cleared by nucleases such as DNases, which degrade the extracellular DNA. However, patients with lupus often exhibit defects in NET clearance. This impaired clearance can be attributed to several factors, including the above-mentioned nucleic acid oxidation, genetically driven reduced DNase activity, presence of DNase inhibitors, and other factors that contribute to the formation of DNase-resistant NETs. Persistent NETs in the circulation or those deposited in tissues can serve as a continuous source of autoantigens and proinflammatory stimuli.[7,10] Various studies have shown that a significant proportion of patients with lupus have elevated levels of circulating NETs and that these NETs are often resistant to degradation.

NETs and inflammation

NETs are not only a source of autoantigens but also potent inducers of inflammation (Figure 1). The components of NETs, including histones, proteases, and antimicrobial peptides, can act as DAMPs that trigger the release of proinflammatory cytokines and chemokines. These inflammatory mediators recruit and activate other immune cells, amplifying the inflammatory response.

In lupus, the chronic presence of NETs can lead to sustained inflammation in various tissues, including the skin, kidneys, placenta, and blood vessels.[6,8] This persistent inflammation is a hallmark of lupus and may contribute to the clinical manifestations of the disease, such as nephritis, vasculitis, and skin rash. Moreover, the inflammatory milieu created and exacerbated by NETs can promote further NETosis, creating a feedback loop that exacerbates tissue damage and autoimmunity.

NETs and organ damage

The deposition of NETs in tissues is associated with organ damage in lupus. In the kidneys, for example, NETs can accumulate in the glomeruli and tubular-interstitial compartment, contributing to the pathogenesis of lupus glomerulonephritis, a common and severe manifestation of SLE.[6] The presence of NETs in the kidneys can induce local inflammation and complement fibroblast activation and endothelial cell damage, contributing to the pathology of lupus nephritis.[22] NETs have also been found in lupus skin, where they are detected in areas of clinical disease.[6] It has been posited that this local NET production may contribute to activating other cells in the skin, as well as to local type I IFN synthesis. In turn, type I IFNs may prime neutrophils to synthesize more NETs.[3]

Similarly, in blood vessels, NETs can contribute to the development of vasculitis and atherosclerosis. NETs can activate and damage endothelial cells and promote the recruitment of inflammatory cells to the vessel wall.[3,23] This NET-mediated process can lead to endothelial dysfunction, increased vascular permeability, and thrombosis. Patients with lupus have a higher risk of cardiovascular disease, and NETs are believed to play a role in this increased risk by promoting vascular inflammation and injury.[24]

This patient had evidence of increased carotid intimal media thickness at a young age, which is unusual and likely related to vascular damage associated with SLE. She also has evidence of

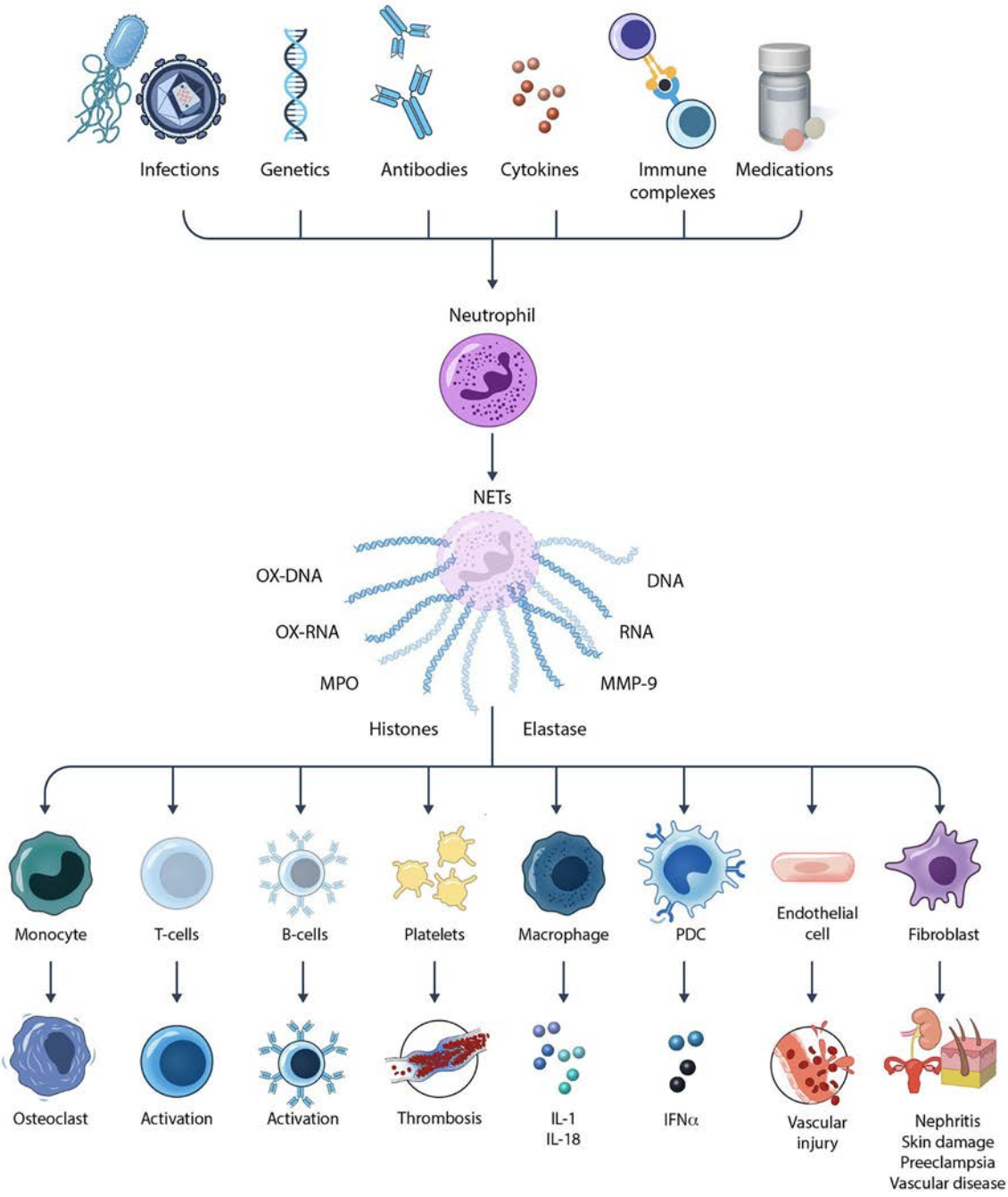

Figure 1. Mechanisms by which NETs promote autoimmunity and organ damage in systemic lupus erythematosus. A variety of stimuli (microbial and sterile inflammatory) can induce NET formation. NETs externalize several alarmins, native and oxidized nucleic acids, and modified histones that can activate many immune and stromal cells to promote inflammation and tissue damage. If NET formation is enhanced or clearance mechanisms of these structures are impaired, the enhanced half-life of the NETs can exacerbate the deleterious role of these structures regarding immunogenicity and inflammatory potential. IFN, interferon; IL, interleukin; MMP-9, matrix metalloproteinase-9; MPO, myeloperoxidase; NET, neutrophil extracellular trap; OX, oxidized; PDC, plasmacytoid dendritic cells.

dyslipidemia with aberrant HDL levels and function. These abnormalities have been previously linked to dysregulated NET formation and to increased LDG levels in circulation. As such, it is possible that neutrophil dysregulation has played a prominent role in vascular damage, which has likely preceded SLE diagnosis.

NETs as biomarkers

Measurement of circulating NET and LDG markers may aid in the diagnosis and monitoring of disease activity in patients with lupus, providing valuable insights into disease progression and treatment response. NETs can be detected in blood and tissue

samples using various techniques, such as immunofluorescence microscopy, enzyme-linked immunosorbent assay, and semiautomated live-cell analysis.[10] Markers used to identify NETs include citrullinated histone:DNA complexes, DNA-MPO or DNA-neutrophil and elastase complexes.[25] The use of cell-free DNA is not a specific marker of NET formation and should be avoided as a sole marker. Several studies have demonstrated a correlation among elevated NET levels, LDGs, and increased disease activity in patients with SLE.[17,24] High levels of NETs are associated with active disease, renal involvement, and increased risk of flares. It is possible that, once properly validated, monitoring NET levels could provide valuable information for assessing disease progression and treatment response. It is possible that NETs could be used to identify patients at risk of relapse and guide preemptive therapeutic interventions. Furthermore, anti-NET antibodies targeting NET components, such as citrullinated histones and MPO, have emerged as potential biomarkers for lupus diagnosis and stratification but require further validation. Finally, previous studies have linked levels of LDGs to vascular damage as mentioned above.

Although NETs and LDGs are not currently used as clinical biomarkers of vascular risk, it is possible that they will be incorporated in the future in the clinical decision-making of patients with SLE. In the case of this patient, her active disease was associated with the presence of elevated LDGs and NETs. It is possible that these NETs have contributed to her active skin and joint disease, although tissue biopsies would have been needed to document their involvement.

Therapeutic implications

Understanding the role of NETs in the pathogenesis of lupus opens new therapeutic avenues. Targeting NET formation, promoting NET clearance, or neutralizing NET components could potentially mitigate the harmful effects of NETs in lupus. Several strategies are being explored in this regard. Current therapies for SLE include immunosuppressive drugs, such as corticosteroids, antimalarials, and biologics targeting B cells and cytokines. Some of these therapies, such as hydroxychloroquine, JAK inhibitors (tofacitinib),[12] some anti–B cell therapies,[26] and the type I IFN receptor blocker anifrolumab,[24] have been reported to reduce NET formation and/or LDG numbers and the deleterious effects of NETs. However, there is a need for more targeted therapies specifically designed to inhibit NETosis and LDGs, to suppress their deleterious effects in a more specific manner (reviewed in Wigerblad and Kaplan[1]).

Several potential therapeutic agents targeting NETs are under investigation, including the following. (1) PAD4 inhibitors, which can prevent histone citrullination and NET formation, but their clinical applicability remains to be determined. (2) NADPH oxidase inhibitors and/or inhibitors of mitochondrial ROS, which can reduce ROS production and inhibit NETosis; however, clinical strategies for this pathway remain to be systematically studied. Of note, the antioxidant N-acetyl-cysteine, a compound that can inhibit NET formation in vitro, has shown potential efficacy in SLE.[27,28] (3) DNase therapy, specifically with DNase I and DNase1L3, can degrade DNA in NETs, reducing their proinflammatory effects.[29] (4) Anti-IFN therapy targeting type I IFNs can reduce NET-induced inflammation and autoimmunity, and the role of this approach in inhibiting vascular disease in SLE is currently being tested (NCT05440422).

In the patient's case, antimalarial use may have multiprong beneficial effects, including resolution/control of clinical symptoms and cardiovascular prevention and direct effects on the dysregulation of NET formation. Whether adding other drugs or biologics will further prevent damage mediated by innate immune dysregulation will have to be determined by the patient's response to treatment.

Future research should focus on identifying additional targets for NET inhibition and developing combination therapies to enhance treatment efficacy. Overall, accumulating evidence indicates that NETs play a significant role in the pathogenesis of SLE by promoting autoimmunity and inflammation. It remains to be further characterized whether they serve as valuable biomarkers for disease activity and flares and whether targeting NET formation may be a promising therapeutic strategy. In this clinical case, it is possible that in the future, measurements of NETs and LDGs will add clinical information regarding diagnosis, prognosis, and disease severity and contribute to further understanding mechanisms of flares following infections and UV light exposure.

Conclusions

This case study underscores the critical role of NETs in the pathogenesis of SLE and highlights the clinical implications of NET biomarkers in disease diagnosis and management. By elucidating the mechanisms underlying NET-mediated inflammation, clinicians can develop targeted therapies to mitigate disease activity and improve outcomes in patients with lupus. Further research is needed to validate the diagnostic and therapeutic utility of NET-targeted interventions and optimize their integration into clinical practice.

AUTHOR CONTRIBUTIONS

Dr Kaplan contributed to at least one of the following manuscript preparation roles: conceptualization AND/OR methodology, software, investigation, formal analysis, data curation, visualization, and validation AND drafting or reviewing/editing the final draft. As corresponding author, Dr Kaplan provided the final approval of the version to be published, and takes responsibility for the affirmations regarding article submission (eg, not under consideration by another journal), the integrity of the data presented, and the statements regarding compliance with institutional review board/Declaration of Helsinki requirements.

REFERENCES

1. Wigerblad G, Kaplan MJ. Neutrophil extracellular traps in systemic autoimmune and autoinflammatory diseases. Nat Rev Immunol 2023;23(5):274–288.
2. Liu Y, Kaplan MJ. Neutrophil dysregulation in the pathogenesis of systemic lupus erythematosus. Rheum Dis Clin North Am 2021; 47(3):317–333.
3. Nakabo S, Romo-Tena J, Kaplan MJ. Neutrophils as drivers of immune dysregulation in autoimmune diseases with skin manifestations. J Invest Dermatol 2022;142(3)(3 Pt B):823–833.
4. Khandpur R, Carmona-Rivera C, Vivekanandan-Giri A, et al. NETs are a source of citrullinated autoantigens and stimulate inflammatory responses in rheumatoid arthritis. Sci Transl Med 2013;5(178): 178ra40.
5. Seto N, Torres-Ruiz JJ, Carmona-Rivera C, et al. Neutrophil dysregulation is pathogenic in idiopathic inflammatory myopathies. JCI Insight 2020;5(3):e134189.
6. Villanueva E, Yalavarthi S, Berthier CC, et al. Netting neutrophils induce endothelial damage, infiltrate tissues, and expose immunostimulatory molecules in systemic lupus erythematosus. J Immunol 2011;187(1):538–552.
7. Hakkim A, Fürnrohr BG, Amann K, et al. Impairment of neutrophil extracellular trap degradation is associated with lupus nephritis. Proc Natl Acad Sci U S A 2010;107(21):9813–9818.
8. Marder W, Knight JS, Kaplan MJ, et al. Placental histology and neutrophil extracellular traps in lupus and pre-eclampsia pregnancies. Lupus Sci Med 2016;3(1):e000134.
9. Knight JS, Subramanian V, O'Dell AA, et al. Peptidylarginine deiminase inhibition disrupts NET formation and protects against kidney, skin and vascular disease in lupus-prone MRL/lpr mice. Ann Rheum Dis 2015;74(12):2199–2206.
10. Lood C, Blanco LP, Purmalek MM, et al. Neutrophil extracellular traps enriched in oxidized mitochondrial DNA are interferogenic and contribute to lupus-like disease. Nat Med 2016;22(2):146–153.
11. Li D, Matta B, Song S, et al. IRF5 genetic risk variants drive myeloid-specific IRF5 hyperactivation and presymptomatic SLE. JCI Insight 2020;5(2):e124020.
12. Hasni SA, Gupta S, Davis M, et al. Phase 1 double-blind randomized safety trial of the Janus kinase inhibitor tofacitinib in systemic lupus erythematosus. Nat Commun 2021;12(1):3391.
13. Fernandez D, Kirou KA. What causes lupus flares? Curr Rheumatol Rep 2016;18(3):14.
14. Zawrotniak M, Bartnicka D, Rapala-Kozik M. UVA and UVB radiation induce the formation of neutrophil extracellular traps by human polymorphonuclear cells. J Photochem Photobiol B 2019;196:111511.
15. Denny MF, Yalavarthi S, Zhao W, et al. A distinct subset of proinflammatory neutrophils isolated from patients with systemic lupus erythematosus induces vascular damage and synthesizes type I IFNs. J Immunol 2010;184(6):3284–3297.
16. Carlucci PM, Purmalek MM, Dey AK, et al. Neutrophil subsets and their gene signature associate with vascular inflammation and coronary atherosclerosis in lupus. JCI Insight 2018;3(8):e99276.
17. Mistry P, Nakabo S, O'Neil L, et al. Transcriptomic, epigenetic, and functional analyses implicate neutrophil diversity in the pathogenesis of systemic lupus erythematosus. Proc Natl Acad Sci U S A. 2019; 116(50):25222–25228.
18. Smith CK, Vivekanandan-Giri A, Tang C, et al. Neutrophil extracellular trap-derived enzymes oxidize high-density lipoprotein: an additional proatherogenic mechanism in systemic lupus erythematosus. Arthritis Rheumatol 2014;66(9):2532–2544.
19. Kahlenberg JM, Carmona-Rivera C, Smith CK, et al. Neutrophil extracellular trap-associated protein activation of the NLRP3 inflammasome is enhanced in lupus macrophages. J Immunol 2013;190(3): 1217–1226.
20. Carmona-Rivera C, Carlucci PM, Moore E, et al. Synovial fibroblast-neutrophil interactions promote pathogenic adaptive immunity in rheumatoid arthritis. Sci Immunol 2017;2(10):eaag3358.
21. Blanco LP, Wang X, Carlucci PM, et al. RNA externalized by neutrophil extracellular traps promotes inflammatory pathways in endothelial cells. Arthritis Rheumatol 2021;73(12):2282–2292.
22. Frangou E, Chrysanthopoulou A, Mitsios A, et al. REDD1/autophagy pathway promotes thromboinflammation and fibrosis in human systemic lupus erythematosus (SLE) through NETs decorated with tissue factor (TF) and interleukin-17A (IL-17A). Ann Rheum Dis 2019; 78(2):238–248.
23. Carmona-Rivera C, Zhao W, Yalavarthi S, et al. Neutrophil extracellular traps induce endothelial dysfunction in systemic lupus erythematosus through the activation of matrix metalloproteinase-2. Ann Rheum Dis 2015;74(7):1417–1424.
24. Casey KA, Smith MA, Sinibaldi D, et al. Modulation of cardiometabolic disease markers by type I interferon inhibition in systemic lupus erythematosus. Arthritis Rheumatol 2021;73(3):459–471.
25. Whittall-Garcia LP, Naderinabi F, Gladman DD, et al. Circulating neutrophil extracellular trap remnants as a biomarker to predict outcomes in lupus nephritis. Lupus Sci Med 2024;11(1):e001038.
26. Kraaij T, Kamerling SWA, de Rooij ENM, et al. The NET-effect of combining rituximab with belimumab in severe systemic lupus erythematosus. J Autoimmun 2018;91:45–54.
27. Lai ZW, Hanczko R, Bonilla E, et al. N-acetylcysteine reduces disease activity by blocking mammalian target of rapamycin in T cells from systemic lupus erythematosus patients: a randomized, double-blind, placebo-controlled trial. Arthritis Rheum 2012;64(9):2937–2946.
28. Muñoz-Sánchez G, Godínez-Méndez LA, Fafutis-Morris M, et al. Effect of antioxidant supplementation on NET formation induced by LPS in vitro; the roles of vitamins E and C, glutathione, and N-acetyl cysteine. Int J Mol Sci 2023;24(17):13162.
29. Stabach PR, Sims D, Gomez-Bañuelos E, et al. A dual-acting DNASE1/DNASE1L3 biologic prevents autoimmunity and death in genetic and induced lupus models. JCI Insight 2024;9(14):e177003.

Arthritis & Rheumatology
Vol. 77, No. 3, March 2025, pp 253–262
DOI 10.1002/art.43014

American College of Rheumatology
Empowering Rheumatology Professionals

Effectiveness of JAK Inhibitors Compared With Biologic Disease-Modifying Antirheumatic Drugs on Pain Reduction in Rheumatoid Arthritis: Results From a Nationwide Swedish Cohort Study

Anna Eberhard,[1] Daniela Di Giuseppe,[2] Johan Askling,[2] Stefan Bergman,[3] Hannah Bower,[2] Katerina Chatzidionysiou,[4] Helena Forsblad-d'Elia,[5] Alf Kastbom,[6] Tor Olofsson,[7] Thomas Frisell,[2] and Carl Turesson[1]

Objective. To compare the effectiveness of JAK inhibitors (JAKis) and biologic disease-modifying antirheumatic drugs (bDMARDs) on pain in patients with rheumatoid arthritis.

Methods. In this retrospective study, we investigated patients with a diagnosis of rheumatoid arthritis, starting treatment with a JAKi (n = 1,827), a tumor necrosis factor inhibitor (TNFi; n = 6,422), an interleukin-6 inhibitor (n = 887), abatacept (n = 1,102), or rituximab (n = 1,149) in 2017 to 2019, using data from several linked Swedish national registers. Differences in change in pain, assessed with a visual analog scale (0–100 mm), from baseline to 3 months, as well as proportions of patients remaining on initial treatment with low pain (visual analog scale pain <20) at 12 months, were compared between treatments. Comparisons of treatment responses between JAKis and bDMARDs were evaluated using multivariable linear regression, adjusted for patient characteristics, comorbidities, current comedication, and previous treatment.

Results. JAKi treatment was associated with a greater decrease in pain at 3 months compared with TNFi treatment (adjusted mean additional decrease 4.0 mm; 95% confidence interval 1.6–6.3), with similar trends in comparisons with non-TNFi bDMARDs. More patients achieved low pain at 12 months on JAKis compared with TNFis, in particular among those previously treated with at least two bDMARDs (adjusted change contrast 5.3 percentage points; 95% confidence interval 1.0–9.6).

Conclusion. JAKis had a slightly better effect on pain outcomes at 3 and 12 months compared with TNFis, with significantly greater differences in patients previously treated with at least two bDMARDs. The effect of JAKis on pain reduction was at least similar to that of non-TNFi bDMARDs.

INTRODUCTION

JAK inhibitors (JAKis) have been used for treating rheumatoid arthritis (RA) in the European Union since 2017. Several randomized clinical trials (RCTs) have compared the efficacy of biologic disease-modifying antirheumatic drugs (bDMARDs) and targeted synthetic (ts)DMARDs (ie, JAKis) as add-on treatments after inadequate response to methotrexate (MTX). Better or equivalent effect on disease activity was found for the JAKis baricitinib and upadacitinib compared with the tumor necrosis factor inhibitor (TNFi) adalimumab,[1–3] whereas tofacitinib and filgotinib were reported as noninferior to adalimumab.[4,5] In particular, it has been reported that JAKis may have a special impact on pain.[6] Specifically, in the RA-BEAM and SELECT-COMPARE trials,

Supported by The Swedish Research Council (grant 2015-02228), The Swedish Rheumatism Association (grant R-664091), and Lund University (grant ALFSKANE-446501).

[1]Anna Eberhard, MD, Carl Turesson, MD, PhD: Lund University, Malmö, Sweden; [2]Daniela Di Giuseppe, PhD, Johan Askling, MD, PhD, Hannah Bower, PhD, Thomas Frisell, PhD: Karolinska Institutet, Stockholm, Sweden; [3]Stefan Bergman, MD, PhD: Institute of Medicine, Sahlgrenska Academy, University of Gothenburg, Gothenburg, Sweden; [4]Katerina Chatzidionysiou, MD, PhD: Karolinska Institutet and Karolinska University Hospital, Stockholm, Sweden; [5]Helena Forsblad-d'Elia, MD, PhD: Sahlgrenska Academy, University of Gothenburg, Gothenburg, Sweden; [6]Alf Kastbom, MD, PhD: Linköping University, Linköping, Sweden; [7]Tor Olofsson, MD, PhD: Lund University, Lund, Sweden.

Drs Eberhard and Di Giuseppe are co-first authors and contributed equally to this work. Drs Frisell and Turesson are co-last authors and contributed equally to this work.

Additional supplementary information cited in this article can be found online in the Supporting Information section (http://onlinelibrary.wiley.com/doi/10.1002/art.43014).

Author disclosures are available at https://onlinelibrary.wiley.com/doi/10.1002/art.43014.

Address correspondence via email to Anna Eberhard, MD, at anna.eberhard@med.lu.se.

Submitted for publication April 15, 2024; accepted in revised form August 30, 2024.

treatment with baricitinib and upadacitinib, respectively, resulted in greater pain reduction compared with adalimumab.[2,7] In a systematic review and meta-analysis of clinical trials, the authors concluded that pain reduction was significantly greater for JAKis compared with bDMARDs.[8] Furthermore, baricitinib has been associated with a greater pain improvement compared with adalimumab also in a subanalysis of patients with well-controlled RA.[9] This suggests that JAKis may have direct analgesic effects beyond its antiinflammatory properties.

In a previous Swedish study, one-third of patients with RA had unacceptably high pain levels (visual analog scale [VAS] pain >40) up to 2 years after diagnosis.[10] Pain has also been shown to persist in patients with well-controlled disease. Several studies have supported that noninflammatory pain, presumably because of central sensitization, is a cause for remaining pain in RA.[11–13] Furthermore, pain relief has been identified as the most important goal for a substantial proportion of patients.[14,15] This taken together points to a need for improvement in pain management in RA.

So far, only limited results are available from observational studies comparing the effectiveness of JAKis and bDMARDs on pain reduction in clinical practice, especially when it comes to non-TNFi bDMARDs. In one large observational cohort study from the United States, no difference in mean pain at 6 months were observed between patients initiating treatment with third/fourth line of TNFi combination therapy and third/fourth line of tofacitinib combination therapy.[16] However, the reduction in pain from baseline was not evaluated. Furthermore, although the study[16] used propensity score matching to ensure comparable groups, it did not consider differences in patient characteristics such as comorbidities and previous conventional treatments. The aim of this study was therefore to compare the effect of JAKis and each class of bDMARDs on pain in patients with RA seen in clinical practice, treated according to standard of care.

MATERIALS AND METHODS

Patients. The present cohort study, using Swedish national register data, is similar in design (but not in outcome) to a previous report.[17] Patients with a diagnosis of RA, starting treatment in 2017 to 2019 with a TNFi, rituximab, abatacept, interleukin-6 inhibitor (IL-6i), or a JAKi, regardless of previous treatment, with data in the Swedish Rheumatology Quality Register (SRQ), were included in this study. The SRQ is a national clinical register of patients with rheumatic disorders, where data have been prospectively registered by the treating physician at visits in standard clinical care. The register has an estimated national coverage of 95% for patients with RA treated with bDMARD.[18] The study was approved by the Ethical Review Board in Stockholm (DNR: 2016/1986-32).

Data sources and data assessment. Data on patient characteristics, disease activity measures, and patient-reported outcomes (PROs) were retrieved from the SRQ at baseline, and at 3 and 12 months following treatment start, with time-windows defined as 90 days before to 30 days after treatment start for baseline measurements, 60 days to 183 days after treatment start for 3-month measurements, and 275 to 455 days after treatment start for the 12-month measurements, consistent with those used previously.[17] If there were more than one visit in each window, the measurement closest to the selected follow-up time point (0, 3, and 12 months) was used. Data retrieved from the SRQ included the patient's assessment of pain using a VAS (0–100 mm), Health Assessment Questionnaire Disability Index (HAQ-DI), Disease Activity Score in 28 joints (DAS28) measured with erythrocyte sedimentation rate, Clinical Disease Activity Index (CDAI), and serologic status (rheumatoid factor [RF] and anticitrullinated peptide antibodies).

Dates of initiation and discontinuation of bDMARD or JAKi therapy were also extracted from the SRQ. One patient could participate with more than one treatment episode, including several episodes of the same drug and class. If a patient restarted the same drug within 90 days (or 270 days for rituximab) of a previous stop, the two episodes were counted as one. Data on cotreatment with conventional synthetic (cs)DMARDs, glucocorticosteroids, and nonsteroidal anti-inflammatory drugs (NSAIDs), as well as previous csDMARD treatment and other prescribed drugs were retrieved from the SRQ and/or from the Prescribed Drug Register— a national register covering dispensations from community pharmacies. Cotreatment with a csDMARD was defined as at least one prescription from 180 days before to 30 days after treatment start of the b/tsDMARD.

History of joint surgeries and days of hospitalization were retrieved from the National Patient Register, covering all inpatient care and a vast majority of specialized outpatient care since 2001. Data on demographics were obtained from registers at Statistics Sweden. Comorbidity data were retrieved from the National Patient Register, the Swedish Cancer Register, and/or from the Prescribed Drug Register, and was defined based on International Classification of Diseases tenth revision, and/or Anatomic Theraputic Chemical (ATC) classification system-codes.

Outcomes. Pain responses were evaluated at 3 and 12 months from treatment initiation. Drug survival was assessed throughout the follow-up. Start of a new bDMARD or tsDMARD was counted as discontinuation, if earlier than a recorded stop. A switch between originator and biosimilar was not considered discontinuation. Patients discontinuing therapy because of remission were considered on therapy until the start of another b/tsDMARD. Patients were excluded in the case of death, emigration from Sweden, or discontinuation because of pregnancy.

Treatment response at 3 months. The change in pain from baseline was evaluated at 3 months, assuming that the

proportion who discontinued therapy because of lack of effectiveness before the follow-up visit was low. Treatment episodes that were discontinued before the defined window for the evaluation visit were excluded.

Treatment response at 12 months. The response measure at 12 months was the proportion of patients attaining low pain, defined as VAS pain less than 20 mm, in accordance with the cutoff used in definitions of minimal disease activity in RA.[19,20] However, because excluding patients who discontinued therapy before the evaluation visit could lead to a selection bias, the response measure at 12 months was defined as the proportion attaining low pain and remaining on therapy (LUNDEX corrected response).[21]

Additional analyses. In addition, treatment responses at 3 months and at 12 months were evaluated in patients stratified by monotherapy or combination therapy with csDMARDs, and by line of treatment with b/tsDMARDs (first line, second line, and third line or later, respectively). In exploratory analyses, we calculated the proportions of patients in each treatment group that, at 12 months, were in remission, low disease activity, and moderate/high disease activity, based on their CDAI (ie, CDAI ≤2.8, CDAI >2.8 and ≤10 and CDAI >10, respectively), among those with 12-month VAS pain less than 20 mm.

Covariates. Confounders accounted for in the models were selected as in previous studies, taking into account factors that have been described to influence treatment in Swedish patients with RA.[22] The baseline covariates included demographics (ie, age, sex, health care region, year of treatment start, smoking, education level, and country of origin), disease history (days of hospitalization during the last 5 years, number of drug classes prescribed during the last year, and comorbidities), previous and current RA treatment (line of treatment with b/tsDMARD, cotreatment with csDMARDs, glucocorticosteroids, or NSAIDs, previous treatment with csDMARDs and b/tsDMARDs, and average daily dose of glucocorticosteroid use), and RA characteristics (symptom duration, RF, joint surgeries, baseline DAS28, CDAI, HAQ-DI, and VAS pain). All baseline covariate definitions can be found in Supplementary Table 1. Among the comorbidities that were adjusted for, we included disorders that may have a special impact on pain (ie, pain-related and psychiatric comorbidities) (Supplementary Table 2).

Statistics. Comparisons between treatment arms for differences in mean change in pain at 3 months and in proportions attaining low pain at 12 months were evaluated with crude and adjusted linear regression models with Huber-White standard errors. All models were adjusted for potential baseline confounders. Multiple imputation with the fully conditional specification method[23] was used to account for missing data for covariates and pain at baseline, and for the outcome measures at 3 and 12 months, with 25 imputed datasets, to ensure that results were not biased by nonrandom missingness linked to measured variables. Imputation models included all variables included in the analysis models. Nonresponder imputation for the 12-month outcome was applied after multiple imputation. Treatment outcome at 3 and 12 months and corresponding standard errors were calculated from each imputed data set and pooled using Rubin's rules. Separate imputation models were used for analyses stratified by monotherapy or combination therapy, and by line of treatment. In supplementary analyses, outcomes among patients on drug at 12 months were evaluated (without LUNDEX corrected response), and separate analyses were performed, including only complete cases (without multiple imputation for missing data).

The individual patient data comes entirely from national Swedish registers. According to Swedish law, access to national register data is granted on a restrictive basis and may not be shared without additional specific permissions from the Swedish register-holding authorities.

RESULTS

Patients. A total of 8,430 patients were included in this study, with a total of 11,387 treatment episodes (1,102 with abatacept, 887 with an IL-6i, 1,827 with a JAKi [82% baricitinib], 1,149 with rituximab, and 6,422 with a TNFi) (Table 1). The distribution of treatment starts with different IL-6is, JAKis and TNFis are listed in Supplementary Table 3. TNFis and rituximab were more frequently used as first or second line of b/tsDMARD treatment, whereas abatacept, IL-6is, and JAKis were primarily used as third/fourth line of treatment. Demographics were similar between treatment groups. Disease duration and disease activity/severity measures at baseline (ie, DAS28, HAQ-DI, CDAI, and pain) were slightly lower in patients starting treatment with a TNFi compared with patients starting treatment with any other b/tsDMARD, and combination therapy with a csDMARD was somewhat more frequent among those starting TNFi. The proportion of patients initiating treatment as monotherapy but who started csDMARD treatment within 12 months were as follows: 13% for abatacept, 8% for IL-6is, 9% for JAKis, 21% for rituximab, and 16% for TNFis. Conversely, the proportion of patients starting treatment at baseline as combination therapy but who discontinued csDMARD treatment during the 12-month follow-up were 21% for abatacept, 35% for IL-6is, 21% for JAKis, 16% for rituximab, and 20% for TNFis. Pain values were missing for about 30% of the patients at baseline and for 50% to 60% at 12 months (amount of missing data are shown in Supplementary Table 4). Sixty-seven percent of the patients initiating a JAKi were still on this treatment at 12 months from baseline; for other treatments, this proportion ranged from 58% for IL-6is to 80% for rituximab (Supplementary Table 5).

Crude and adjusted differences in Δ pain between baseline and 3 months. Overall, pain scores improved from

Table 1. Patient characteristics at baseline between treatment arms*

Variable	Abatacept	IL-6 inhibitor	JAK inhibitor	Rituximab	TNF inhibitor
n	1,102	887	1,827	1,149	6,422
Sex, female, n (%)	873 (79.2)	722 (81.4)	1,496 (81.9)	869 (75.6)	5,013 (78.1)
Age	63 (53–72)	59 (49–70)	61 (52–71)	64 (54–73)	59 (47–69)
RA characteristics					
Symptom duration, years	12.8 (5.4–22.1)	10.3 (4.7–18.5)	13.2 (6.8–22.7)	12.8 (6.2–22.3)	8.1 (2.9–16.3)
RF seropositivity, n (%)	835 (77.9)	649 (74.4)	1,353 (75.6)	968 (86.0)	4,429 (70.3)
MTX, n (%)	546 (49.5)	401 (45.2)	792 (43.3)	585 (50.9)	4,092 (63.7)
Non-MTX csDMARD n (%)	220 (20.0)	152 (17.1)	356 (19.5)	277 (24.1)	1,572 (24.5)
Glucocorticoids, n (%)	775 (70.3)	631 (71.1)	1,282 (70.2)	879 (76.5)	4,104 (63.9)
NSAID, n (%)	204 (24.6)	193 (26.9)	447 (30.9)	213 (24.3)	1,037 (20.6)
Joint surgeries, n (%)	187 (17.0)	135 (15.2)	344 (18.8)	191 (16.6)	677 (10.5)
Treatment line	3 (2–4)	3 (2–5)	4 (2–5)	2 (1–4)	1 (1–2)
DAS28	4.8 (3.9–5.6)	4.9 (4.0–5.7)	4.7 (3.8–5.6)	4.8 (3.9–5.6)	4.4 (3.4–5.2)
SJC	4 (2–7)	4 (2–7)	4 (2–7)	4 (2–7)	3 (1–6)
TJC	5 (2–9)	6 (3–10)	5 (2–10)	5 (2–9)	4 (2–8)
CDAI	21 (15–28)	22 (15–29.5)	20 (14–28)	21 (14–28.5)	18 (12–25)
HAQ-DI	1.1 (0.8–1.6)	1.1 (0.8–1.6)	1.3 (0.8–1.6)	1.1 (0.8–1.6)	0.9 (0.5–1.4)
VAS pain	63 (42–77)	65 (44–80)	61 (40–76)	60.5 (38–76)	56 (34–73)
General health					
Never smoker, n (%)	325 (37.3)	313 (42.6)	601 (39.8)	334 (35.6)	2,041 (42.9)
Previous smoker, n (%)	458 (52.6)	339 (46.1)	736 (48.8)	488 (52.0)	2,141 (45.0)
Current smoker, n (%)	88 (10.1)	83 (11.3)	172 (11.4)	117 (12.5)	572 (12.0)
Days in hospital	3 (0–11)	1 (0–7)	2 (0–8)	3 (0–10)	0 (0–5)
Education level, years, n (%)					
≤9	248 (22.6)	165 (18.8)	363 (19.9)	251 (22.1)	1,173 (18.4)
10–12	507 (46.2)	447 (51.0)	885 (48.5)	548 (48.2)	2,977 (46.7)
>12	342 (31.2)	265 (30.2)	575 (31.5)	337 (29.7)	2,219 (34.8)
Country of birth, n (%)					
Swedish	953 (86.5)	754 (85.0)	1,573 (86.1)	954 (83.0)	5,474 (85.2)
Scandinavian, non-Swedish	60 (5.4)	48 (5.4)	82 (4.5)	67 (5.8)	282 (4.4)
Other	89 (8.1)	85 (9.6)	172 (9.4)	128 (11.1)	666 (10.4)
Comorbidities, n (%)					
Cancer	105 (9.5)	53 (6.0)	134 (7.3)	192 (16.7)	396 (6.2)
Acute coronary syndrome	35 (3.2)	12 (1.4)	41 (2.2)	30 (2.6)	92 (1.4)
Congestive heart failure	43 (3.9)	14 (1.6)	38 (2.1)	40 (3.5)	73 (1.1)
Stroke	39 (3.5)	20 (2.3)	33 (1.8)	27 (2.3)	118 (1.8)
Diabetes	145 (13.2)	87 (9.8)	187 (10.2)	130 (11.3)	585 (9.1)
Liver disease	17 (1.5)	14 (1.6)	22 (1.2)	23 (2.0)	67 (1.0)
Kidney disease	24 (2.2)	16 (1.8)	28 (1.5)	23 (2.0)	82 (1.3)
Obstructive pulmonary disease	83 (7.5)	33 (3.7)	91 (5.0)	67 (5.8)	186 (2.9)
Interstitial lung disease	52 (4.7)	21 (2.4)	40 (2.2)	77 (6.7)	44 (0.7)
Severe infection	103 (9.3)	23 (2.6)	95 (5.2)	73 (6.4)	178 (2.8)
Herpes	49 (4.4)	37 (4.2)	64 (3.5)	46 (4.0)	203 (3.2)
Venous thromboembolism	35 (3.2)	21 (2.4)	58 (3.2)	38 (3.3)	102 (1.6)
Pain-related comorbidities	522 (47.4)	418 (47.1)	892 (48.8)	520 (45.3)	2,508 (39.1)
Psychiatric comorbidities	334 (30.3)	250 (28.2)	550 (30.1)	365 (31.8)	1,683 (26.2)

* Values are median (interquartile range) unless otherwise indicated. Only observed values are shown (not imputed values). CDAI, clinical disease activity index; csDMARD, conventional synthetic disease-modifying antirheumatic drug; DAS28, disease activity score in 28 joints; HAQ-DI, Health Assessment Questionnaire Disability Index; IL-6, interleukin-6; MTX, methotrexate; NSAID, nonsteroidal antiinflammatory drug; RA, rheumatoid arthritis; RF, rheumatoid factor; SJC, swollen joint count; TJC, tender joint count; TNF, tumor necrosis factor; VAS, visual analog scale.

baseline to 3 months in all treatment arms—with mean changes ranging from –20.1 mm (95% confidence interval [95% CI] –23.1 to –17.2) for IL-6is to –16.6 mm (95% CI –19.1 to –14.0) for rituximab (Table 2). In patients treated with a JAKi, the mean change in pain at 3 months was –18.3 mm (95% CI –20.2 to –16.5). The distribution of changes in pain per treatment arm is presented in Supplementary Figure 1. In all groups, pain was reduced for most patients, but a small subset experienced increased pain. In analysis of differences in change in pain between JAKis and bDMARDs adjusted for demographics, RA characteristics and for current comedication and previous b/tsDMARD treatment, JAKis decreased pain scores by 4.0 mm (95% CI 1.7–6.3) more than TNFis, and by 3.9 mm (95% CI 0.9–6.9) more than rituximab, at 3 months (Table 2). Further adjustment for comorbidities did not have a major impact on the results (Figure 1). There was no statistically significant difference in change in VAS pain at 3 months when comparing JAKis with abatacept or IL-6is (Table 2, Figure 1).

Table 2. Differences in mean change in pain from baseline to 3-months follow-up*

Treatment initiation	n	Baseline mean	Mean change	Crude change contrast	Adj. change contrast
Abatacept	1,040	58.7 (56.7–60.7)	−18.3 (−20.5 to −16.1)	0.0 (−2.9 to 3.0)	2.2 (−0.5 to 4.8)
IL-6 inhibitor	821	60.8 (58.9–62.8)	−20.1 (−23.1 to −17.2)	−1.8 (−5.4 to 1.8)	1.2 (−2.1 to 4.5)
Rituximab	1,101	56.4 (54.6–58.1)	−16.6 (−19.1 to −14.0)	1.8 (−1.4 to 4.9)	3.9 (0.9–6.9)
TNF inhibitor	6,118	53.2 (52.4–54.0)	−18.1 (−19.2 to −17.1)	0.20 (−2.1 to 2.5)	4.0 (1.7–6.3)
JAK inhibitor	1,699	57.6 (56.2–59.0)	−18.3 (−20.2 to −16.5)	Ref	Ref

* Values are estimates (95% confidence interval) unless otherwise indicated. Univariate and multivariate linear regression with JAK inhibitor as reference. Adj. for demographics, RA characteristics and previous and current RA treatment. Adj., adjusted; IL-6, interleukin-6; RA, rheumatoid arthritis; Ref, reference; TNF, tumor necrosis factor.

The proportion of patients who discontinued treatment before the 3-month time frame, and therefore were excluded from this analysis, were 6% for abatacept, 7% for IL-6is, 4% for rituximab, 5% for TNFis, and 7% for JAKis. The mean change in pain from baseline to 3 months was missing for 57% of patients treated with a JAKi. For bDMARDs, this ranged from 56% for IL-6is to 67% for rituximab (Supplementary Table 4).

Proportions remaining on drug and in low pain at 12 months. Twenty percent of patients treated with a JAKi remained on drug and reached low pain at 12 months from baseline (the corresponding proportions for the bDMARDs ranged from 17% for IL-6is to 26% for rituximab) (Table 3). Adjusted proportions remaining on drug and with low pain were numerically higher for patients treated with a JAKi compared with patients treated with a TNFi or an IL-6i, although the differences did not reach statistical significance (Figure 2). Among those with low pain at 12 months, the proportion in remission was lower and the fraction with active disease higher in patients treated with JAKi compared with the TNFi group (Supplementary Table 6).

VAS pain at 12 months was missing for 62% of patients treated with a JAKi. For bDMARDs this proportion ranged from 54% for abatacept to 62% for TNFis (Supplementary Table 4).

Pain responses by line of treatment with b/tsDMARD. Analyses restricted to individuals who started their first ever b/tsDMARD were affected by the small sample size as only a limited number of patients were treated with a JAKi as first b/tsDMARD treatment. In this analysis, the reduction in pain at 3 months was significantly greater for IL-6is compared with JAKis (Figure 3). By contrast, in the analysis restricted to those starting their second ever b/tsDMARD, JAKis decreased pain significantly more at 3 months after full adjustment compared with both TNFis and rituximab. The same was found when comparing JAKis with TNFis among patients starting their third or more b/tsDMARD (Figure 3).

In the analysis of pain response at 12 months (attaining VAS pain <20) restricted to first line of treatment, the results were pointing toward higher proportions with low pain for bDMARDs compared with JAKis, especially for IL-6is and abatacept in which differences were statistically significant (Supplementary Figure 2). In the analysis restricted to second line of treatment, there were no significant differences in fractions reaching low pain at 12 months between treatments. However, in patients treated with a JAKi as third line of b/tsDMARD or later, proportions with low pain at 12 months were significantly higher compared with TNFis and IL-6is, with a similar trend in the comparison with abatacept (Supplementary Figure 2).

Pain responses by monotherapy or combination therapy with csDMARDs. When stratifying the b/tsDMARD initiator cohorts by monotherapy versus combination therapy with csDMARDs, differences in mean change in pain at 3 months between JAKis and bDMARDs were similar to the main analysis, but were in general more prominent when comparing monotherapies, with adjusted mean differences for JAKi monotherapy of

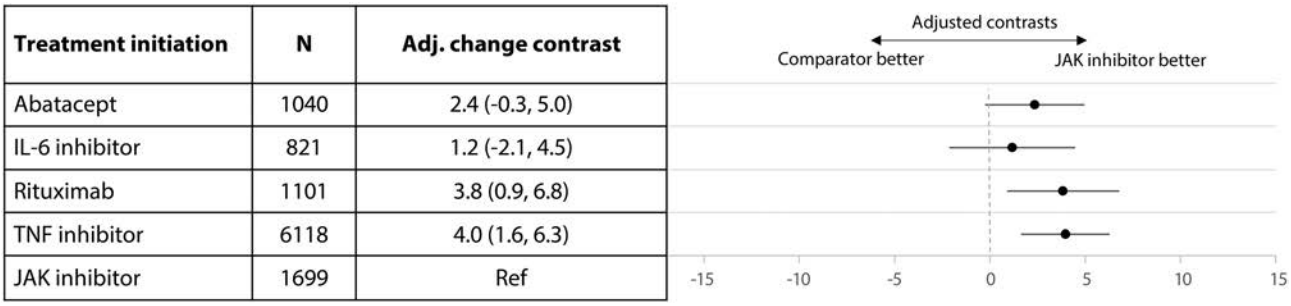

Figure 1. Fully adjusted differences in mean change in pain from baseline to 3-months follow-up. Multivariate linear regression with JAK inhibitor as reference. Adj. for demographics, RA characteristics, current and previous RA treatment, and further for comorbidities. Adj., adjusted; IL-6, interleukin-6; RA, rheumatoid arthritis; TNF, tumor necrosis factor.

Table 3. Differences in proportions attaining low pain score at 12 months*

Treatment initiation	n	Crude proportion	Crude contrast	Adj. contrast
Abatacept	1,102	20.3 (17.0–23.6)	0.8 (–3.2 to 4.8)	–0.3 (–4.4 to 3.8)
IL-6 inhibitor	887	17.0 (13.8–20.1)	–2.6 (–6.8 to 1.7)	–3.3 (–7.4 to 0.8)
Rituximab	1,149	26.3 (21.9–30.6)	6.7 (1.8–11.7)	3.7 (–1.7 to 8.1)
TNF inhibitor	6,422	25.7 (24.1–27.3)	6.2 (2.7–9.7)	–3.4 (–7.2 to 0.3)
JAK inhibitor	1,827	19.5 (16.7–22.3)	Ref	Ref

* Values are estimates (95% confidence interval) unless otherwise indicated. Univariate and multivariate linear regression with JAK inhibitor as reference. Adj. for demographics, RA characteristics and previous and current RA treatment. Low pain: visual analog scale pain <20. Adj., adjusted; IL-6, interleukin-6; RA, rheumatoid arthritis; TNF, tumor necrosis factor.

5.4 mm (95% CI 2.9–8.8) compared with TNFi monotherapy, and 9.7 mm (95% CI 4.1–15.3) compared with rituximab monotherapy. In those receiving combination therapy, only the difference between JAKis and TNFis remained statistically significant (Supplementary Figure 3).

Pain response at 12 months stratified by monotherapy or combination therapy were also similar to the main analysis, but fully adjusted differences were again more pronounced in the analysis restricted to patients on monotherapy, with a 5.5% (95% CI 0.1–10.8) higher response rate for JAKi monotherapy compared with TNFi monotherapy. Statistically significant differences in proportions reaching low pain were also found for JAKi monotherapy compared with IL-6i monotherapy, but not to rituximab or abatacept monotherapy (Supplementary Figure 4). There were no statistically significant differences between JAKi combination therapy and bDMARD combination therapy in proportions with low pain at 12 months.

Supplementary analyses. *Restriction to patients on drug at 12 months.* When restricting the analysis to patients still on drug at 12 months, crude proportions for low pain at 12 months increased for all treatment groups, which could be anticipated as the nonresponder imputation was not applied. In this analysis, there were no differences in treatment responses at 12 months between JAKis and bDMARDs (Supplementary Figure 5).

Complete case analysis. In the complete case analysis, the difference in the reduction of pain at 3 months were similar to the main analysis, although slightly more pronounced (Supplementary Figure 6). Pain response at 12 months, including only complete cases, also supported the main analysis results (Supplementary Figure 7).

DISCUSSION

In this observational retrospective study, comparing the effectiveness of JAKis and bDMARDs while taking patient characteristics and treatment history into account, JAKis had a significantly better effect on the 3-month pain outcome. Although there were major improvements in pain with all treatments, only a minority of patients achieved a pain score of less than 20 at 12 months. The effect of JAKis was numerically better also regarding the pain outcome at 12 months compared with TNFis. The superior effect of JAKis was more pronounced for monotherapy and when used as third line of treatment with b/tsDMARD or later. Moreover, the effect of JAKis on pain was at least similar compared with non-TNFi bDMARDs.

Superior effectiveness of JAKis on pain compared with TNFis has also been found in clinical trials. In the RA-BEAM study, significantly greater improvements in pain were seen for patients treated with baricitinib compared with adalimumab, already at weeks 2 to 4.[1] In the SELECT-COMPARE trial, upadacitinib was superior to adalimumab regarding pain improvement from baseline to week 12, and also at the 3-year follow-up.[24,25] However, results from ORAL Strategy showed similar efficacy in pain

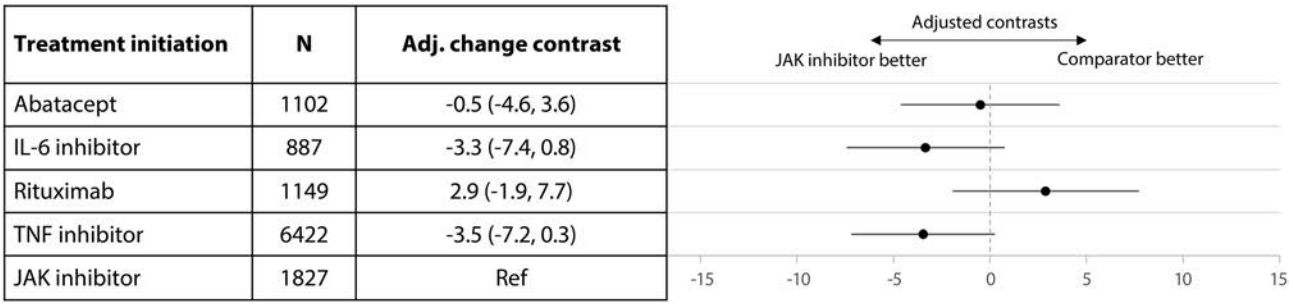

Figure 2. Fully adjusted differences in proportions attaining low pain score at 12 months. Multivariate linear regression with JAK inhibitor as reference. Adj. for demographics, RA characteristics, current and previous RA treatment, and further for comorbidities. Low pain: visual analog scale pain <20. Adj., adjusted; IL-6, interleukin-6; RA, rheumatoid arthritis; TNF, tumor necrosis factor.

First line b/tsDMARD					
Treatment initiation	**N**	**Baseline mean**	**Mean change**	**Crude change contrast**	**Adj. change contrast**
Abatacept	179	53.9 (49.4, 58.3)	-23.5 (-29.2, -17.7)	-3.6 (-10.8, 3.6)	-1.6 (-7.7, 4.5)
IL-6 inhibitor	106	58.1 (52.3, 63.8)	-34.1 (-42.7, -25.5)	-14.2 (-24.2, -4.2)	-11.1 (-19.8, -2.4)
Rituximab	317	52.1 (48.7, 55.5)	-19.0 (-24.04, -14.0)	0.9 (-6.1, 7.9)	0.7 (-6.2, 7.7)
TNF inhibitor	3466	52.3 (51.3, 53.3)	-21.7 (-22.9, -20.4)	-1.8 (-7.1, 3.6)	-1.0 (-5.8, 3.9)
JAK inhibitor	229	51.5 (47.1, 55.9)	-19.9 (-25.2, -14.6)	Ref	Ref

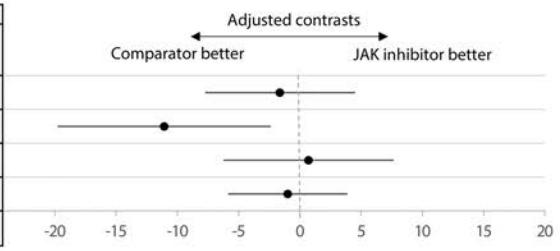

Second line b/tsDMARD					
Treatment initiation	**N**	**Baseline mean**	**Mean change**	**Crude change contrast**	**Adj. change contrast**
Abatacept	254	55.1 (51.2, 59.0)	-16.5 (-21.4, -11.5)	3.2 (-4.0, 10.4)	5.6 (-1.1, 12.4)
IL-6 inhibitor	187	57.3 (53.2, 61.3)	-16.8 (-22.3, -11.2)	2.9 (-4.2, 10.0)	6.6 (-0.1, 13.4)
Rituximab	260	54.4 (50.9, 58.0)	-12.4 (-19.5, -5.3)	7.3 (-1.3, 15.8)	10.9 (2.6, 19.2)
TNF inhibitor	1443	52.6 (50.9, 54.4)	-14.1 (-16.4, -11.9)	5.6 (0.6, 10.5)	7.3 (2.8, 11.8)
JAK inhibitor	284	51.6 (48.2, 54.9)	-19.7 (-24.1, -15.3)	Ref	Ref

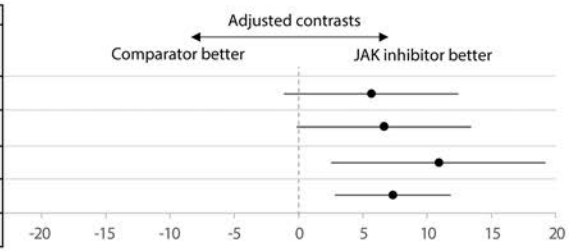

Third or later line b/tsDMARD					
Treatment initiation	**N**	**Baseline mean**	**Mean change**	**Crude change contrast**	**Adj. change contrast**
Abatacept	607	61.7 (59.5, 64.0)	-17.5 (-21.1, -14.0)	0.1 (-3.8, 4.1)	2.6 (-1.0, 6.2)
IL-6 inhibitor	528	62.5 (59.9, 65.1)	-18.7 (-22.5, -15.0)	-1.1 (-5.6, 3.4)	1.3 (-2.8, 5.5)
Rituximab	524	60.2 (57.8, 62.7)	-17.1 (-21.4, -12.8)	0.6 (-4.3, 5.4)	1.6 (-3.3, 6.6)
TNF inhibitor	1209	55.5 (53.8, 57.2)	-12.3 (-14.8, -9.9)	5.3 (1.6, 9.0)	4.8 (1.4, 8.2)
JAK inhibitor	1186	60.2 (58.7, 61.8)	-17.7 (-19.7, -15.6)	Ref	Ref

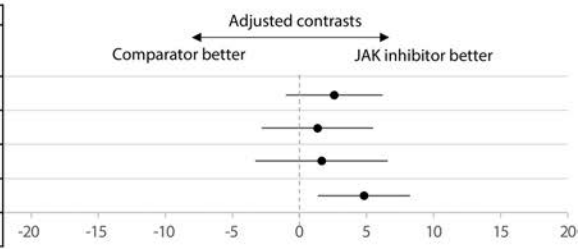

Figure 3. Differences in mean change in pain from baseline to 3 months, stratified by line of treatment. Univariate and multivariate linear regression with JAK inhibitor as reference. Adjustment for demographics, RA characteristics, current and previous RA treatment, and further for comorbidities. Adj., adjusted; b/tsDMARD, biologic/targeted synthetic disease-modifying antirheumatic drug; IL-6, interleukin-6; RA, rheumatoid arthritis; Ref, reference; TNF, tumor necrosis factor.

improvement at 12 weeks for tofacitinib and adalimumab, and similar proportions with low pain at 12 months.[26] In our study, the adjusted mean difference in VAS pain from baseline to 3 months between JAKis and TNFis was 4.0 mm, which is slightly lower than that found in SELECT-COMPARE (mean difference 6.5 mm for upadacitinib compared with adalimumab) at 12 weeks, and to RA-BEAM (mean pain reduction at week 12: –31.5 mm and –26.4 mm for baricitinib and adalimumab, respectively).[1,24]

Because baricitinib and upadacitinib were found to be superior to adalimumab in the RA-BEAM and SELECT-COMPARE trials respectively, although no such superiority was found for tofacitinib vs adalimumab in ORAL Strategy, it is possible that the effect on pain reduction differs between the different classes of JAKis. In the present study, more than 80% of the patients were treated with baricitinib, and the remainder with tofacitinib.

Although statistically significant differences in pain reduction at 3 months between JAKis and TNFis were found in our study, and in the above mentioned RCTs, it could be debated whether the estimated difference is of clinical relevance. The minimal clinically important difference for improvement or worsening of pain has been reported as somewhere between 5 and 11 mm,[20] or a 15% relative change.[27] Yet, with a mean difference in pain of 3 to 4 mm for JAKis compared with TNFis in the whole cohort, it is plausible that JAKis could entail a clinically relevant advantage regarding pain in certain subgroups.

The line of treatment with b/tsDMARD had a considerable impact on the results in this study. As first line treatment, all therapies were numerically better regarding pain reduction compared with being given as a later treatment line, with no superiority for JAKis, suggesting that the first advanced therapy is clinically effective in most patients. By contrast, in the stratified analysis, pain improvement at 3 months and fraction of patients with low pain at 12 months were significantly greater for JAKis compared with TNFis when given as third line with b/tsDMARD or later. This is compatible with the known efficacy of JAKis in bDMARD refractory patients.[28,29] It could also imply that JAKis are particularly effective in reducing pain in patients that are more resistant to therapy. It has been reported that JAKis may have analgesic effects beyond antiinflammatory properties,[9] which could possibly explain the better effect of JAKis compared with TNFis in the more treatment refractory patients observed in this study, because a higher share of patients with pain causes other than nociceptive could be expected in this group. In an experimental rat model, JAK/signal transducer and activator of transcription signaling has been suggested to increase mechanical pain sensitivity, and subsequent blocking of that pathway, to reduce

mechanical allodynia, suggesting a role for JAKis in modulating central pain processing pathways.[30,31] The higher proportion with low pain on JAKi despite active disease in this study is in line with this concept.

In this study, we found better pain responses at 3 and 12 months with JAKi monotherapy than with TNFi monotherapy, with numerically greater differences in pain responses for JAKi monotherapy vs TNFi monotherapy compared with JAKi combination therapy vs TNFi combination therapy. This is compatible with previous studies that found JAKi monotherapy to be effective in reducing signs and symptoms of RA, including pain.[32,33] Furthermore, JAKi monotherapy appears to be more effective than MTX in reducing PROs.[34] As TNFis in monotherapy were shown to have similar effects as MTX on PROs,[35,36] it could be expected that when it comes to monotherapy, JAKis are more efficient for reducing pain than TNFis. Greater pain reduction for baricitinib monotherapy than with adalimumab monotherapy was also found in a matching-adjusted indirect comparison from a prior systematic literature review.[37]

Only a limited number of studies have compared the overall effectiveness of JAKis and non-TNFi bDMARDs. In a previous analysis of a partly overlapping sample, we found overall equivalent or better treatment responses with baricitinib compared with both TNFis and non-TNFi bDMARDs when analyzing the outcome measures HAQ-DI, CDAI, and DAS28 at 3 and 12 months.[17] In the SELECT-CHOICE trial, in which patients with inadequate response to TNFi treatment were randomized to either upadacitinib or abatacept, greater improvements in pain at 12 weeks were observed in the upadacitinib-treated patients,[38] while at the same time, there were no differences in the number of swollen joints between the treatment groups.[39] Taken together, this suggests that the observed superior effect of JAKis on composite outcomes[17] is partly driven by a greater reduction in pain.

Regarding comparisons with non-TNFi bDMARDs, the proportion of patients with low pain at 12 months in the current study were numerically higher for JAKis compared with abatacept when initiated as third treatment line or later, but the difference was not statistically significant. However, when compared with IL-6i monotherapy, a significantly larger fraction of patients treated with JAKi monotherapy achieved low pain at 12 months. In line with this, greater improvements in pain at 6 months were observed for patients treated with baricitinib compared with tocilizumab in indirect comparisons based on a systematic literature review.[37] In the present study, the share of patients with low pain at 12 months was also greater for JAKis compared with IL-6is when comparing patients receiving treatment as third line or later with b/tsDMARD. Overall, JAKis were at least as effective as non-TNFi bDMARDs for pain outcomes at 3 and 12 months.

Several limitations of this study should be mentioned. The majority of patients were treated with baricitinib, potentially limiting generalizability to other JAKis. Although we adjusted for multiple relevant patient characteristics, residual confounding cannot be excluded. Because of a significant amount of missing data, in particular for the follow-up evaluations, we used multiple imputation to avoid selection bias from potential factors influencing missingness. However, additional bias is possible if factors not accounted for in the model correlated with missingness, and if data were complete, one cannot exclude that the results could have been somewhat different. Nevertheless, the analysis restricted to complete cases supported the main results.

We defined all patients discontinuing treatment as nonresponders in regard to reaching low pain at 12 months, irrespective of the cause of termination, presumably leading to an underestimation of the proportion of responders. However, restricting the analysis to patients on drug would have favored treatments with high discontinuation rates. Notably, the sensitivity analysis, including only patients on drug at 12 months, favored abatacept and IL-6is, which had somewhat higher discontinuation rates, whereas rituximab was disadvantaged.

Finally, the classifications of monotherapy and combination therapy with csDMARD may not always be correct, as some patients could have stopped csDMARD treatment during the first year. Nevertheless, between 65% and 80% of the patients in the different treatment groups that were classified as comedicating were still on csDMARD treatment at 12 months, and 79% to 92% of patients starting treatment as monotherapy had no registered concurrent csDMARD at 12 months.

The strengths of this study include the real-world setting for the evaluation of the effectiveness of JAKis on pain compared with various bDMARDs, through the use of a nationwide register in which patients have been observed and treated according to usual care, and hence corresponding to patients seen in daily clinical practice. The main novelty that emerged from this study is the structured estimation of the efficacy of JAKis on pain in patients with RA treated in usual clinical care.

In conclusion, although differences were modest, JAKis had a slightly better effect on pain outcomes at 3 and 12 months in this study compared with TNFis, particularly in patients previously treated with at least two bDMARDs and when given as monotherapy. In addition, JAKis were at least as effective in reducing pain as non-TNFi bDMARDs.

ACKNOWLEDGMENTS

The authors would like to thank Andrei Barbulescu for his contributions to the statistical analysis plan and his comments on the study.

AUTHOR CONTRIBUTIONS

All authors were involved in drafting the article or revising it critically for important intellectual content, and all authors approved the final version to be published. Dr Eberhard and Dr Di Giuseppe had full access to all of the data in the study and takes responsibility for the integrity of the data and the accuracy of the data analysis.

Study conception and design. Eberhard, Askling, Frisell, Turesson.

Acquisition of data. Di Giuseppe, Chatzidionysiou, Forsblad-d'Elia, Kastbom, Olofsson, Turesson.
Analysis and interpretation of data. Eberhard, Di Giuseppe, Askling, Bergman, Bower, Chatzidionysiou, Forsblad-d'Elia, Kastbom, Olofsson, Frisell, Turesson.

REFERENCES

1. Taylor PC, Keystone EC, van der Heijde D, et al. Baricitinib versus placebo or adalimumab in rheumatoid arthritis. N Engl J Med 2017;376: 652–662.
2. Fleischmann RM, Genovese MC, Enejosa JV, et al. Safety and effectiveness of upadacitinib or adalimumab plus methotrexate in patients with rheumatoid arthritis over 48 weeks with switch to alternate therapy in patients with insufficient response. Ann Rheum Dis 2019;78: 1454–1462.
3. Lee YH, Song GG. Relative efficacy and safety of tofacitinib, baricitinib, upadacitinib, and filgotinib in comparison to adalimumab in patients with active rheumatoid arthritis. Z Rheumatol 2020;79: 785–796.
4. Fleischmann R, Mysler E, Hall S, et al; ORAL Strategy investigators. Efficacy and safety of tofacitinib monotherapy, tofacitinib with methotrexate, and adalimumab with methotrexate in patients with rheumatoid arthritis (ORAL Strategy): a phase 3b/4, double-blind, head-to-head, randomised controlled trial. Lancet 2017;390: 457–468.
5. Combe B, Kivitz A, Tanaka Y, et al. Filgotinib versus placebo or adalimumab in patients with rheumatoid arthritis and inadequate response to methotrexate: a phase III randomised clinical trial. Ann Rheum Dis 2021;80:848–858.
6. Harrington R, Al Nokhatha SA, Conway R. JAK inhibitors in rheumatoid arthritis: an evidence-based review on the emerging clinical data. J Inflamm Res 2020;13:519–531.
7. Taylor PC, Lee YC, Fleischmann R, et al. Achieving pain control in rheumatoid arthritis with baricitinib or adalimumab plus methotrexate: results from the RA-BEAM Trial. J Clin Med 2019;8:831.
8. Toth L, Juhasz MF, Szabo L, et al. Janus kinase inhibitors improve disease activity and patient-reported outcomes in rheumatoid arthritis: a systematic review and meta-analysis of 24,135 patients. Int J Mol Sci 2022;23:1246.
9. Fautrel B, Kirkham B, Pope JE, et al. Effect of baricitinib and adalimumab in reducing pain and improving function in patients with rheumatoid arthritis in low disease activity: exploratory analyses from RA-BEAM. J Clin Med 2019;8:1394.
10. Eberhard A, Bergman S, Mandl T, et al. Joint tenderness at 3 months follow-up better predicts long-term pain than baseline characteristics in early rheumatoid arthritis patients. Rheumatology (Oxford) 2024; 63(3):734–741.
11. Altawil R, Saevarsdottir S, Wedren S, et al. Remaining pain in early rheumatoid arthritis patients treated with methotrexate. Arthritis Care Res (Hoboken) 2016;68:1061–1068.
12. Olofsson T, Wallman JK, Joud A, et al. Pain over two years after start of biologic versus conventional combination treatment in early rheumatoid arthritis: results from a Swedish Randomized Controlled Trial. Arthritis Care Res (Hoboken) 2021;73:1312–1321.
13. Heisler A, Song J, Muhammad L, et al. Association between changes in pain sensitization and changes in disease activity after 12 weeks of diease modifying anti-rheumatic drug therapy in rheumatoid arthritis [abstract]. Arthritis Rheumatol 2020;72(suppl 10).
14. Taylor P, Manger B, Alvaro-Gracia J, et al. Patient perceptions concerning pain management in the treatment of rheumatoid arthritis. J Int Med Res 2010;38:1213–1224.
15. ten Klooster PM, Veehof MM, Taal E, van Riel PL, van de Laar MA. Changes in priorities for improvement in patients with rheumatoid arthritis during 1 year of anti-tumour necrosis factor treatment. Ann Rheum Dis 2007;66:1485–1490.
16. Reed GW, Gerber RA, Shan Y, et al. Real-world comparative effectiveness of tofacitinib and tumor necrosis factor inhibitors as monotherapy and combination therapy for treatment of rheumatoid arthritis. Rheumatol Ther 2019;6:573–586.
17. Barbulescu A, Askling J, Chatzidionysiou K, et al. Effectiveness of baricitinib and tofacitinib compared with bDMARDs in RA: results from a cohort study using nationwide Swedish register data. Rheumatology (Oxford) 2022;61:3952–3962.
18. Wadström H, Eriksson JK, Neovius M, et al. ARTIS Study Group. How good is the coverage and how accurate are exposure data in the Swedish Biologics Register (ARTIS)? Scand J Rheumatol 2015;44: 22–28.
19. Wells GA, Boers M, Shea B, et al. Minimal disease activity for rheumatoid arthritis: a preliminary definition. J Rheumatol 2005;32:2016–2024.
20. Wolfe F, Michaud K. Assessment of pain in rheumatoid arthritis: minimal clinically significant difference, predictors, and the effect of antitumor necrosis factor therapy. J Rheumatol 2007;34:1674–1683.
21. Kristensen LE, Saxne T, Geborek P. The LUNDEX, a new index of drug efficacy in clinical practice: results of a five-year observational study of treatment with infliximab and etanercept among rheumatoid arthritis patients in southern Sweden. Arthritis Rheum 2006;54: 600–606.
22. Frisell T, Baecklund E, Bengtsson K, et al. Patient characteristics influence the choice of biological drug in RA, and will make non-TNFi biologics appear more harmful than TNFi biologics. Ann Rheum Dis 2018;77:650–657.
23. Lydersen S. Multiple imputation of missing data. Tidsskr Nor Laegeforen 2022;142.
24. Fleischmann R, Pangan AL, Song IH, et al. Upadacitinib versus placebo or adalimumab in patients with rheumatoid arthritis and an inadequate response to methotrexate: results of a phase III, double-blind, randomized controlled trial. Arthritis Rheumatol 2019;71:1788–1800.
25. Fleischmann R, Mysler E, Bessette L, et al. Long-term safety and efficacy of upadacitinib or adalimumab in patients with rheumatoid arthritis: results through 3 years from the SELECT-COMPARE study. RMD Open 2022;8:e002012.
26. Strand V, Mysler E, Moots RJ, et al. Patient-reported outcomes for tofacitinib with and without methotrexate, or adalimumab with methotrexate, in rheumatoid arthritis: a phase IIIB/IV trial. RMD Open 2019; 5:e001040.
27. Salaffi F, Stancati A, Silvestri CA, et al. Minimal clinically important changes in chronic musculoskeletal pain intensity measured on a numerical rating scale. Eur J Pain 2004;8:283–291.
28. Tanaka Y, Fautrel B, Keystone EC, et al. Clinical outcomes in patients switched from adalimumab to baricitinib due to non-response and/or study design: phase III data in patients with rheumatoid arthritis. Ann Rheum Dis 2019;78:890–898.
29. Fleischmann R, Blanco R, Van den Bosch F, et al. Long-term efficacy and safety following switch between upadacitinib and adalimumab in patients with rheumatoid arthritis: 5-year data from SELECT-COMPARE. Rheumatol Ther 2024;11:599–615.
30. Busch-Dienstfertig M, González-Rodríguez S. IL-4, JAK-STAT signaling, and pain. JAKSTAT 2013;2:e27638.
31. Dominguez E, Mauborgne A, Mallet J, et al. SOCS3-mediated blockade of JAK/STAT3 signaling pathway reveals its major contribution to spinal cord neuroinflammation and mechanical allodynia after peripheral nerve injury. J Neurosci 2010;30:5754–5766.

32. Genovese M, Westhovens R, Meuleners L, et al. Effect of filgotinib, a selective JAK 1 inhibitor, with and without methotrexate in patients with rheumatoid arthritis: patient-reported outcomes. Arthritis Res Ther 2018;20:57.
33. Lee EB, Fleischmann R, Hall S, et al. ORAL Start Investigators. Tofacitinib versus methotrexate in rheumatoid arthritis. N Engl J Med 2014; 370:2377–2386.
34. Schiff M, Takeuchi T, Fleischmann R, et al. Patient-reported outcomes of baricitinib in patients with rheumatoid arthritis and no or limited prior disease-modifying antirheumatic drug treatment. Arthritis Res Ther 2017;19:208.
35. van der Heijde D, Klareskog L, Singh A, et al. Patient reported outcomes in a trial of combination therapy with etanercept and methotrexate for rheumatoid arthritis: the TEMPO trial. Ann Rheum Dis 2006;65:328–334.
36. Singh JA, Hossain A, Mudano AS, et al. Biologics or tofacitinib for people with rheumatoid arthritis naive to methotrexate: a systematic review and network meta-analysis. Cochrane Database Syst Rev 2017;5:CD012657.
37. Fautrel B, Zhu B, Taylor PC, et al. Comparative effectiveness of improvement in pain and physical function for baricitinib versus adalimumab, tocilizumab and tofacitinib monotherapies in rheumatoid arthritis patients who are naive to treatment with biologic or conventional synthetic disease-modifying antirheumatic drugs: a matching-adjusted indirect comparison. RMD Open 2020;6(1).
38. Bergman M, Tundia N, Martin N, et al. Patient-reported outcomes of upadacitinib versus abatacept in patients with rheumatoid arthritis and an inadequate response to biologic disease-modifying antirheumatic drugs: 12- and 24-week results of a phase 3 trial. Arthritis Res Ther 2022;24:155.
39. Rubbert-Roth A, Enejosa J, Pangan AL, et al. Trial of upadacitinib or abatacept in rheumatoid arthritis. N Engl J Med 2020;383:1511–1521.

Arthritis & Rheumatology
Vol. 77, No. 3, March 2025, pp 263–271
DOI 10.1002/art.43034

American College of Rheumatology
Empowering Rheumatology Professionals

Metabolic Syndrome, Adipokines, and Response to Advanced Therapies in Rheumatoid Arthritis

Joshua F. Baker,[1] George Reed,[2] Ted R. Mikuls,[3] Geoffrey M. Thiele,[3] Dimitrios A. Pappas,[4] Christina Charles-Schoeman,[5] Monica Guma,[6] Leslie R. Harrold,[7] Jeffrey R. Curtis,[8] and Joel M. Kremer[9]

Objective. We determined if metabolic syndrome, its components, and adipokines (adiponectin, leptin, and fibroblast growth factor-21) were associated with response to advanced therapies among patients with rheumatoid arthritis (RA).

Methods. This study included participants with RA initiating either tumor necrosis factor inhibitor (TNFi) or non-TNFi biologic therapies from the Comparative Effectiveness Registry to study Therapies for Arthritis and Inflammatory Conditions (CERTAIN) cohort within the CorEvitas registry. Metabolic syndrome was defined according to the National Cholesterol Education Program Adult Treatment Panel III definition. Adipokines were assessed on stored samples from a subsample of responders and nonresponders (n = 200). The primary outcome was the achievement of a change as large as the minimal clinically important difference (MCID) for the Clinical Disease Activity Index (CDAI) at 6 months.

Results. Among 2,368 participants, 687 (29%) had metabolic syndrome. Metabolic syndrome was associated with lower odds of achieving CDAI MCID (odds ratio [OR] 0.69, 95% confidence interval [CI] 0.56–0.86, $P = 0.001$) with a dose-dependent decrease in response rate according to the number of components present. Model fit was superior for metabolic syndrome compared with body mass index. Associations between metabolic syndrome and MCID achievement were similar between patients receiving TNFi (OR 0.65, 95% CI 0.49–0.87, $P = 0.003$) versus non-TNF therapies (OR 0.76, 95% CI 0.55–1.04, $P = 0.08$ [P for interaction = 0.49]). Adipokines were not associated with MCID achievement.

Conclusion. Metabolic syndrome is associated with lower response rates with the initiation of an advanced therapy in RA, with similar effects for both TNFi and non-TNFi agents. Adipokines were strongly associated with metabolic syndrome but were not associated with clinical response.

INTRODUCTION

In current practice in rheumatoid arthritis (RA), it is difficult for physicians to predict who will have refractory disease and demonstrate a poor response to the initiation of therapy. We recently demonstrated that patients with abnormally low weight (body mass index [BMI] < 18.5) as well as patients with obesity and RA were less likely to achieve a meaningful clinical response to biologic disease-modifying therapies from the CorEvitas clinical registry.[1] In fact, a number of prior studies have identified reduced response rates among patients with BMI in the obese range.[2–4]

The opinions or assertions presented herein are the private views and opinions of the authors and do not represent the views of the Department of the Veterans Affairs.

Supported by the Corrona Research Foundation and by a Department of Veterans Affairs Clinical Science Research and Development Merit award (grant I01-CX-001703). Dr Baker's work is supported by a Rehabilitation Research and Development Merit award (I01-RX-003644) and a Veterans Affairs Clinical Science Research and Development Merit award (IK2-CX-001703). Dr. Mikuls' work is supported by the US Department of Defense (PR200793), the National Institute of General Medical Sciences (U54-GM-115458), and the Department of Veterans Affairs Biomedical Laboratory Research and Development (BX006049 and BX005413). Dr Curtis's work is supported by the National Institute of Arthritis and Musculoskeletal and Skin Diseases, NIH (grant P30-AR-072583).

[1]Joshua F. Baker, MD, MSCE: Corporal Michael J. Crescenz Department of Veterans Affairs Medical Center and the University of Pennsylvania, Philadelphia; [2]George Reed, PhD: University of Massachusetts Chan Medical School, Worcester; [3]Ted R. Mikuls, MD, MSPH, Geoffrey M. Thiele, PhD: Department of Veterans Affairs Nebraska-Western Iowa Health Care System and the University of Nebraska Medical Center, Omaha; [4]Dimitrios A. Pappas, MD, MPH: Corrona Research Foundation, Albany, and Columbia University, New York City, New York; [5]Christina Charles-Schoeman, MD: University of California, Los Angeles; [6]Monica Guma, MD, PhD: University of California San Diego; [7]Leslie R. Harrold, MD, MPH: University of Massachusetts Chan Medical School, Worcester, and Corrona Research Foundation, Albany, New York; [8]Jeffrey R. Curtis, MD, MS, MPH: University of Alabama at Birmingham; [9]Joel M. Kremer, MD: Corrona Research Foundation and Albany Medical College, Emeritus, New York.

Additional supplementary information cited in this article can be found online in the Supporting Information section (https://acrjournals.onlinelibrary.wiley.com/doi/10.1002/art.43034).

Author disclosures are available at https://onlinelibrary.wiley.com/doi/10.1002/art.43034.

Address correspondence via email to Joshua F. Baker, MD, MSCE, at Joshua.Baker@pennmedicine.upenn.edu.

Submitted for publication June 27, 2024; accepted in revised form October 8, 2024.

Although obesity and underweight have been associated with poor response to advanced therapies, our prior study found that BMI did not distinguish those that were more likely to benefit from a tumor necrosis factor inhibitor (TNFi) versus a non-TNFi advanced therapy. In other words, there was no evidence that one treatment would work better than the other in the context of obesity or underweight BMI ranges. In contrast, we recently showed that a low or normal BMI was associated with greater response to TNFi compared with conventional therapies, specifically "triple therapy,"[5] suggesting that BMI may be informative as part of a precision medicine approach because it may differentially predict responses among different therapies in RA. Although BMI has been associated with clinical response to therapy in several studies, it is not a comprehensive measure of the metabolic consequences of obesity, and few RA studies to our knowledge have evaluated metabolic syndrome itself (central adiposity, hypertension, lipid abnormalities, and insulin resistance), its individual components, and their independent effects on disease activity.[6–9]

Adipokines are produced in adipose tissue and serve as metabolic regulators that are strongly associated with obesity and its metabolic complications. The systemic and immune effects of adipokines are not completely understood, but they have been shown to significantly influence the metabolic activities of tissues, including regulating insulin sensitivity.[10] In addition, adipokines have been shown to play a role in regulating adaptive and innate immune cells and have been postulated to mediate the inflammatory features of obesity along with circulating cytokines, such as TNF and interleukin-6.[11]

In a previous study we showed that high levels of adiponectin and leptin predicted a lower likelihood of achieving low disease activity (LDA) over time in a clinical registry independent of BMI.[12] Adipokines also differentiated those that were most likely to benefit from a TNFi over triple therapy in one study,[5] although we are not aware of studies evaluating adipokines as predictors of response to one advanced therapy over another. These prior observations suggest that adipokines are informative of disease phenotype, although whether these associations are independent of metabolic syndrome is not known.

In this study, we aimed to determine if metabolic syndrome, and high levels of adiponectin, leptin, and fibroblast growth factor (FGF) 21 are associated with a lower likelihood of achieving a clinical response to therapy among patients with RA from the Comparative Effectiveness Registry to study Therapies for Arthritis and Inflammatory Conditions (CERTAIN) cohort. We also aimed to evaluate whether metabolic syndrome and adipokines can identify patients who are more likely to respond to a TNFi over a non-TNFi biologic.

PATIENTS AND METHODS

We used data from the CERTAIN comparative effectiveness study, which was a prospective, protocolized 12-month observational cohort study of adult patients and was conducted as an ancillary study and nested within the CorEvitas (formerly known as Corrona) RA registry.[13,14] Data were collected using structured case report forms that include medication use and dose, height, weight, RA clinical disease activity, function, comorbid illnesses, and adverse events.[15] CERTAIN initiations occurred between November 2010 and April 2014. We included participants with a diagnosis of RA initiating either TNFi or non-TNFi biologic therapies within CERTAIN (JAK inhibitors were not included in CERTAIN).

CERTAIN used the CorEvitas network of participating private and academic sites to recruit patients fulfilling the 1987 American College of Rheumatology criteria that had at least moderate disease activity.[16] Patients starting or switching biologic agents, either a TNFi or a non-TNFi biologic, were eligible for enrollment. Patient visits and all laboratory blood work, performed centrally in all patients, were mandated every 3 months for 1 year or until discontinuation of the initiated drug. Safety data were collected through 1 year and beyond.

This study was conducted in accordance with the Declaration of Helsinki, and all patients were required to provide written informed consent and authorization before participating. All participating investigators were required to obtain full institutional review board (IRB) approval for conducting noninterventional research involving human subjects. Sponsor approval and continuing review was obtained through a central IRB (the New England Independent Review Board, NEIRB No. 120160610). For academic investigative sites that did not receive a waiver to use the central IRB, full approval was obtained from the respective governing IRBs and documentation was submitted to CorEvitas, LLC, before initiating any study procedures. Patients were not involved in the design, conduct, reporting, or dissemination plans of this research. Data from the CorEvitas RA Registry are available from CorEvitas, LLC, through a commercial subscription agreement and are not publicly available.

Definition of metabolic syndrome. Waist circumference and blood pressure were measured as part of a standard clinical protocol at participating sites. Standard laboratory assessments (glucose and lipid profiles) were performed centrally on stored samples from enrollment (stored for <1 week). Metabolic syndrome was defined according to the National Cholesterol Education Program Adult Treatment Panel III definition, which requires that three of the following criteria be met: (1) waist circumference >40 inches (men) or >35 inches (women), (2) blood pressure >130/85 mm Hg or a diagnosis of hypertension, (3) fasting triglyceride level >150 mg/dl, (4) nonfasting high-density lipoprotein cholesterol level <40 mg/dL (men) or <50 mg/dL (women), and (5) fasting blood glucose level >100 mg/dL or a history of diabetes. Because the fasting glucose level was not available, we used a threshold of 140 mg/dL.[17] For analyses that dichotomized metabolic syndrome, we included participants with

missing data for one or more of the above if the missing data would not be expected to change the categorization (eg, they met the criteria already with only four of the components available). For BMI, we used the World Health Organization guidelines to categorize BMI as underweight (<18.5 kg/m^2), normal weight (≥18.5–25 kg/m^2), overweight (≥25–30 kg/m^2), obese (≥30–35 kg/m^2), and severely obese (≥35 kg/m^2).

Adipokine assessments. Adipokines (adiponectin, leptin, and FGF-21) were measured on stored samples in 100 biologic-naive TNFi and 100 biologic-experienced non-TNFi users (powered to detect a moderate effect size [d] of 0.40 between responders and nonresponders). For each therapy, the best 50 responders and worst 50 nonresponders (based on the change in Clinical Disease Activity Index [CDAI]) of those who had remained on therapy at 6 months and had sufficient blood samples were selected. The CDAI minimal clinically important difference (MCID) was used to categorize initiators as responders or nonresponders. The relative decrease (or increase) was used to rank patients within responder/nonresponder groups. Samples were collected at enrollment, using a multianalyte panel from Meso Scale Discovery (Rockville, MD). Adipokine values were log-transformed and standardized so that a 1-unit difference in the value represented a 1 SD difference for all individual analytes. An adipokine score was also generated to reflect the number of adipokines above/below the median in a pattern consistent with metabolic obesity as previously described.[5] Thus, the range is from 1 to 4, wherein 1 is the lowest score possible with one additional point given for each of the following: an adiponectin level below the median, a leptin level above the median, and/or an FGF-21 level above the median.

Response outcomes. The primary clinical outcome was the achievement of a change at least as large as the MCID for the CDAI at 6 months.[18] The MCID cut points for improvement have been previously described as 12 for patients starting with a high CDAI, 6 for those in moderate CDAI, and 1 for those with low CDAI. The main secondary outcome was the achievement of LDA (CDAI ≤ 10). We also explored associations with the achievement of low individual components of disease activity including pain, patient global scores, evaluator global scores, tender joint counts, and swollen joint counts as defined by Boolean 2.0 criteria.[19]

For the primary analysis, we imputed or replaced the outcome as nonresponse for binary outcomes if the initiator switched to an alternative therapy before 6 months. This approach assumes that those who did not continue the therapy did not have a meaningful clinical response. If the initiator discontinued therapy but did not start another biologic therapy by 6 months, we used the actual response at 6 months.

Covariable assessments. Several covariables were collected at each visit. We evaluated factors prehypothesized to represent important predictors of response to therapy and included age; sex; race; comorbidities including an adapted Charlson Comorbidity Index, smoking, and CDAI; and the use of other RA therapies, including prednisone, prior biologic experience, and disease duration. Levels of C-reactive protein, anticitrullinated protein antibody (ACPA), and rheumatoid factor were available at baseline.

Statistical analysis. Characteristics of participants stratified by metabolic syndrome status were described and standardized differences presented to assess group differences. The primary analysis used mixed effect logistic regression models to evaluate the association between metabolic syndrome at baseline and the odds of achieving the primary outcome of a change at least as large as the MCID for CDAI. Random effects were used for patients who could contribute more than one initiation and for patients nested within provider. For initial models, we adjusted for prehypothesized factors (age, sex, race, baseline disease activity, and prior biologic experience) as well as characteristics that were significantly different at enrollment between those with and without metabolic syndrome and were not considered likely to be in the causal pathway (comorbidity score).

Secondary analyses evaluated individual components of the metabolic syndrome, evaluated the number of components of metabolic syndrome (to assess dose dependency), and explored model fit compared with BMI alone. Model fit was explored using the Akaike Information Criterion (AIC) and the Bayesian Information Criterion and by testing for additive effects through likelihood ratio testing.

To determine if the effect of metabolic syndrome on clinical response varied by therapeutic mechanism of action, the significance of multiplicative interaction terms between treatment (TNFi vs non-TNFi) and metabolic syndrome was evaluated in regression models. We also tested for interaction by sex and ACPA/rheumatoid factor status.

Associations between adipokines and clinical response were assessed in multivariable logistic regression models adjusting for age, sex, BMI, metabolic syndrome, TNFi (biologic naive) versus non-TNFi (biologic experienced), combination versus monotherapy use, ACPA serostatus, and baseline CDAI. We also explored testing the significance of multiplicative interactions terms between each adipokine and type of therapy (TNFi versus non-TNFi) within these models to assess whether adipokine levels were associated with a superior response to one therapy over another. Because all TNFi initiators were biologic naive and all non-TNFi initiators were bio-experienced within the adipokine subcohort, it was not possible to include both line of therapy and type of therapy in regression models because of collinearity. Analyses were performed using STATA version 18 (College Station, TX).

RESULTS

A total of 2,368 participants in CERTAIN were eligible for the analysis (Supplementary Figure 1; Table 1). Among these, 687 (29%) had metabolic syndrome at enrollment. The components that were most frequently present were a high waist circumference (53%) and high blood pressure (56%) (Supplementary Table 1). Among those with metabolic syndrome, most had three components (61%) (Supplementary Table 2).

Several covariates were significantly different between groups ($P < 0.05$). Participants with metabolic syndrome were slightly older, were more likely to have obesity, had higher overall comorbidity, had higher rates of diabetes and cardiovascular disease, had higher CDAI, had higher C-reactive protein levels, and were somewhat more likely to have previously received an advanced therapy (biologic experienced) (Table 1). Patients receiving a TNFi were also more likely to be using the therapy as a first-line advanced therapy (55%) compared with those receiving a non-TNFi (13%). Non-TNFi biologics included tocilizumab (38%), rituximab (15%), and abatacept (47%).

Metabolic syndrome was associated with a lower rate of MCID achievement as well as a lower rate of achieving LDA in all models (Table 2). For example, in the fully adjusted model, the odds ratio (OR) for MCID achievement was 0.70 (95% confidence interval [CI] 0.56–0.87) for those with metabolic syndrome. The unadjusted rates of achieving MCID at 6 months were 56% for those without and 48% for those with metabolic syndrome. In addition, the OR for LDA achievement was 0.56 (95% CI 0.43–0.74) for those with metabolic syndrome.

When the individual components of metabolic syndrome were explored separately in regression models, each was associated with lower response (all $P < 0.05$) with the exception of a diagnosis of hypertension (OR 0.92, 95% CI 0.76–1.13) (Table 2). When all components were included in a single model, high waist circumference (OR 0.80, 95% CI 0.64–0.98) and low high-density lipoprotein were independently associated (OR 0.75, 95% CI 0.58–0.97) (Supplementary Table 3). There was a dose-dependent relationship such that the odds of response were lower when a greater number of components of metabolic syndrome were present (Figure 1).

A regression model including the metabolic syndrome variable had better model fit compared with a model that included BMI category (AIC 3,127 vs AIC 3,135; Bayesian Information Criterion 3,202 vs 3,222). Further, the addition of metabolic syndrome to a regression model that included BMI category significantly improved model fit (likelihood ratio test $P = 0.008$).

Table 1. Patient characteristics at initiation of therapy*

Characteristic	Metabolic syndrome		Standardized difference
	No	Yes	
N	1,681	687	–
Age, mean (SD), years	56.0 (0.33)	57.4 (0.44)	−0.11
Female, n (%)	1,348 (80)	325 (77)	0.07
White, n (%)	1,386 (82)	561 (82)	0.02
BMI, mean (SD), kg/m^2	28.6 (0.16)	34.5 (0.28)	−0.85
BMI categories, n (%)			0.91
Underweight	16 (1.0)	2 (0.3)	–
Normal	509 (30.3)	41 (6.0)	–
Overweight	607 (36.1)	163 (23.7)	–
Obese I	287 (17.1)	191 (27.8)	–
Obese II	262 (15.6)	290 (42.2)	–
Smoking, n (%)	16 (1.0)	–	–
Never	792 (48)	313 (46)	0.06
Past	530 (32)	239 (35)	–
Current	325 (20)	127 (19)	–
Comorbidity score, mean (SD)[a]	1.18 (0.01)	1.48 (0.03)	−0.51
Cancer, n (%)	97 (6)	51 (7.4)	−0.07
Diabetes, n (%)	90 (5)	292 (43)	−0.97
Cardiovascular disease, n (%)	129 (8)	98 (14)	−0.21
Disease duration, mean (SD), years	8.33 (0.21)	9.15 (0.37)	−0.09
ACPA or RF positive, n (%)	1,207 (72)	487 (71)	0.02
CDAI, mean (SD)	29.2 (0.32)	30.3 (0.48)	−0.09
Log(CRP), mean (SD)	0.55 (0.63)	0.70 (0.55)	−0.25
CRP, mean (SD)	10.1 (19.0)	10.4 (15.2)	−0.02
Biologic experienced, n (%)	1,034 (62)	453 (66)	−0.09
TNFi initiation, n (%)	986 (59)	383 (56)	0.06
Non-TNFi initiation, n (%)	695 (41)	304 (44)	–

* ACPA, anticitrullinated peptide antibody; BMI, body mass index; CDAI, Clinical Disease Activity Index; CRP, C-reactive protein; RF, rheumatoid factor; TNFi, tumor necrosis factor inhibitor.
[a] Modified Charlson Comorbidity score.

Table 2. Adjusted OR for achieving CDAI MCID at 6 months for metabolic syndrome and its individual components. Each variable is evaluated in a separate model adjusting for the covariates below*

	CDAI MCID		CDAI LDA	
	OR (95% CI)	*P*	OR (95% CI)	*P*
Metabolic syndrome	0.70 (0.56–0.87)	0.001	0.56 (0.43–0.74)	<0.001
Components				
Hypertension	0.92 (0.76–1.13)	0.43	0.74 (0.57–0.94)	0.02
Diabetes	0.76 (0.59–0.99)	0.04	0.66 (0.48–0.92)	0.01
High triglycerides	0.80 (0.66–0.97)	0.03	0.74 (0.58–0.94)	0.01
Low HDL	0.71 (0.56–0.90)	0.004	0.66 (0.49–0.88)	0.004
High waist circumference	0.75 (0.61–0.92)	0.006	0.59 (0.46–0.77)	<0.001

* Adjusted for age, sex, CDAI, biologic naive versus experienced, tumor necrosis factor inhibitor versus non–tumor necrosis factor inhibitor, anticitrullinated peptide antibody/rheumatoid factor serostatus, disease duration, and baseline C-reactive protein level. CDAI, Clinical Disease Activity Index; CI, confidence interval; HDL, high-density lipoprotein; LDA, low disease activity; MCID, minimal clinically important difference; OR, odds ratio.

In this model, underweight BMI was independently associated with a lower odds of response compared with normal BMI (OR 0.24, 95% CI 0.075–0.77; $P = 0.02$) whereas obesity categories showed lower efficacy although these differences did not achieve significance with the exception of severe obesity (BMI ≥ 35: OR 0.72, 95% CI 0.53–0.98) (Table 3).

The association between metabolic syndrome and MCID was similar between those patients receiving TNFi and non-TNFi advanced therapies (P for interaction = 0.49) (Figure 2). Similarly, there was no difference in the effect of metabolic syndrome on achieving LDA among those receiving TNFi or non-TNFi advanced therapies (P for interaction = 0.26). In stratified analyses, metabolic syndrome was only significantly associated with response among the larger seropositive subgroup, although the association between metabolic syndrome and response was not statistically different in seropositive and seronegative patients (Supplementary Table 4).

Metabolic syndrome was associated with a lower likelihood of achieving low individual components of disease activity, including a lower odds of achieving a low patient global score, low evaluator global score, low swollen joint count, and low pain score (Supplementary Table 5). Although the odds of achieving a low tender joint count was lower among those with metabolic syndrome, this was not statistically significant (OR 0.81, 95% CI 0.61–1.06).

Adipokines and response. Compared with individuals without metabolic syndrome, those with metabolic syndrome also had lower levels of adiponectin (median 14.2, interquartile range [IQR] 10.0–20.0 vs median 24.1, IQR 14.2–37.5 ug/mL; $P < 0.001$), higher levels of leptin (median 10,014, IQR 4,585–25,435 vs median 5,725, IQR 1,656–11,808 pg/mL; $P = 0.01$), and higher levels of FGF-21 (median 262, IQR 83–1,162.1 vs median 138 IQR 64–350 pg/mL; $P = 0.009$)

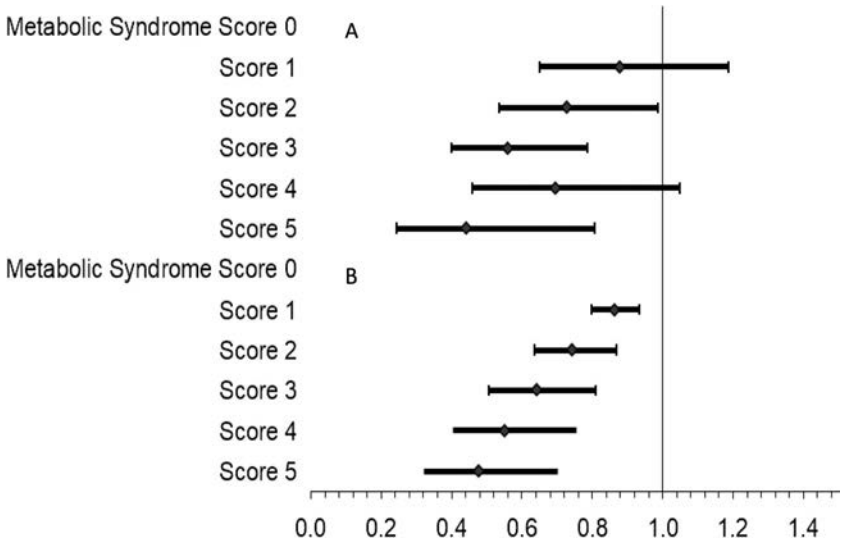

Figure 1. Odds of response by the number of components of metabolic syndrome present. (A) The results of a model with the variable included as a categorical variable, whereas (B) shows it included as an ordinal variable (assuming linearity of effect).

Table 3. Independent associations between BMI and metabolic syndrome with MCID responder status (all tested within the same model)*

	Odds of CDAI MCID	
	OR (95% CI)	*P*
Metabolic syndrome	0.74 (0.59–0.93)	0.009
BMI category		
Underweight	0.25 (0.08–0.79)	0.02
Normal weight	1 (reference)	–
Overweight	0.82 (0.63–1.07)	0.14
Obese	0.80 (0.53–1.08)	0.14
Severely obese	0.72 (0.53–0.98)	0.04

* BMI, body mass index; CDAI, Clinical Disease Activity Index; CI, confidence interval; MCID, minimal clinically important difference; OR, odds ratio.

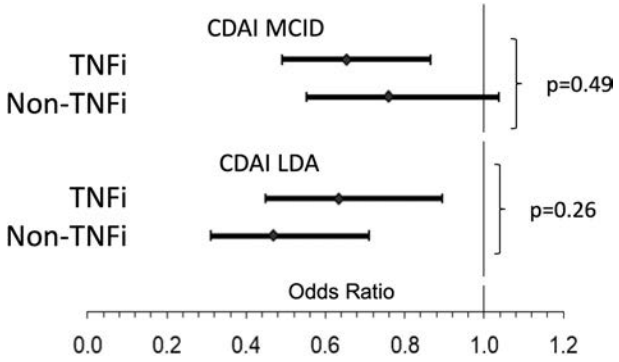

Figure 2. Odds of response for patients with metabolic syndrome compared with those without, stratified by initiators of either TNFi or non-TNFi biologics. CDAI, Clinical Disease Activity Index; LDA, low disease activity; MCID, minimal clinically important difference; TNFi, tumor necrosis factor inhibitor.

(Supplementary Table 6). Similarly, higher BMI was correlated with lower adiponectin levels ($\rho = -0.28$, $P < 0.001$), higher leptin levels ($\rho = 0.43$, $P < 0.001$), and higher FGF-21 levels ($\rho = 0.15$, $P = 0.04$).

In multivariable models, there was not an association between any of the adipokines and achievement of the MCID for CDAI independent of other clinical measures, such as BMI and metabolic syndrome (Table 4). In these models, those with metabolic syndrome had lower response rates, but this was not statistically significant (OR range 0.53–0.61; *P* range 0.09–0.19). There was no significant interaction by therapeutic mechanism of action (TNFi-naive vs biologic-experienced non-TNFi; all $P > 0.05$) (Supplementary Table S2). Those with higher adiponectin levels had a numerically greater likelihood of response among patients who were seronegative (hazard ratio [HR] 2.07, 95% CI 0.82–5.19; $P = 0.12$), a finding that was significantly different from that observed in seropositive patients (HR 0.95, 95% CI 0.67–1.36; $P = 0.78$) (P for interaction = 0.04). There was not a significant association between leptin and FGF-21 levels among seronegative patients (Supplementary Table 4).

DISCUSSION

This study demonstrated a strong association between the presence of metabolic syndrome and lower responses to advanced therapies among patients with RA. On the whole, the rate of response was 56% among those without metabolic syndrome, but this was reduced to 48% among those with metabolic syndrome. Model fit was better for metabolic syndrome than that of BMI alone, suggesting that metabolic syndrome is more informative to clinical response than a simple assessment of weight or BMI. Importantly, there was no difference in the association observed according to whether the participants received a TNFi or non-TNFi biologic therapy, suggesting that the observation is common to multiple treatment pathways and not specific to those receiving TNFi therapies. The primary takeaway from this study is to further our understanding of prior work that has suggested an association between obesity and treatment response and to suggest that metabolic factors play an important role.

We observed no significant associations between adipokines and clinical response, although adipokines were associated with metabolic syndrome. In a prior observational study, high adipokine levels were associated with lower rates of remission and LDA over time in a longitudinal cohort.[12] In contrast to the current report, the prior study was performed in a larger sample of >1,200 older adults, was conducted over a longer period of follow-up, and was not limited to initiators of new therapies. The current study does not support the hypothesis that adipokines play a causal role in affecting response to therapy that is independent of metabolic syndrome itself. In the current study, we also found that adipokines did not differentiate the likely responders to TNFi versus non-TNFi in this subsample. Although we are not aware of prior studies evaluating adipokines as predictors of response to two different classes of advanced therapies, prior work has shown that BMI and adipokines can help identify those who are most likely to respond to the initiation of a TNFi over conventional therapies (ie, triple therapy).[5] A comparison with conventional therapies, as previously studied, was not possible within the CERTAIN data.

A number of prior studies have evaluated obesity and clinical response, summarized in several reviews and meta-analyses.[2–4] Our study confirms prior studies and advances the literature by illustrating that this effect is stronger when considering the metabolic implications of obesity, including changes in lipids, blood pressure, insulin resistance, and fat distribution. Few studies have evaluated the impact of metabolic syndrome on disease outcomes in RA, although some observational studies have observed an association between higher disease activity scores and features of metabolic obesity.[6,7]

The mechanisms by which metabolic syndrome lowers the likelihood of clinical response are unknown. Some have suggested that obesity (and metabolic syndrome) may drive

Table 4. Association between adipokines (log-adjusted) and Clinical Disease Activity Index minimal clinically important difference achievement at 6 months*

	Unadjusted (n = 190)		Adjusted (n = 190)	
	OR (95% CI)	*P*	OR (95% CI)	*P*
Adiponectin (per 1 SD)	1.04 (0.78–1.47)	0.81	1.08 (0.76–1.52)	0.67
Leptin (per 1 SD)	0.92 (0.69–1.23)	0.58	1.09 (0.77–1.55)	0.62
FGF-21 (per 1 SD)	0.86 (0.78–1.39)	0.30	0.89 (0.65–1.23)	0.49
Adipokine score (v. 1)				
2	0.57 (0.25–1.31)	0.19	0.60 (0.24–1.46)	0.26
3	0.63 (0.27–1.49)	0.29	0.82 (0.31–2.15)	0.68
4	0.49 (0.20–1.24)	0.13	0.55 (0.19–1.63)	0.28

* Each exposure (on the left) is evaluated in its own model adjusted for the below covariates. Two patients were missing data on anticitrullinated peptide antibody/rheumatoid factor serostatus and one was missing disease duration. Adjusted for treatment (tumor necrosis factor inhibitor vs non–tumor necrosis factor inhibitor), age, sex, baseline Clinical Disease Activity Index, metabolic syndrome, body mass index, anticitrullinated peptide antibody/rheumatoid factor serostatus, C-reactive protein level, and disease duration. CI, confidence interval; FGF, fibroblast growth factor; OR, odds ratio.

inflammatory processes that may lead to more resistant disease. However, studies have also shown reduced rates of inflammation detected with advanced imaging and lower rates of radiographic damage among those with obese BMI and, in some studies, among those with greater visceral fat.[20–23] Metabolic syndrome is also strongly associated with osteoarthritis, sleep disturbance, and chronic pain syndromes.[24–26] Thus, poor response among patients with metabolic syndrome may represent refractory symptoms because of competing comorbid conditions like osteoarthritis that would be unlikely to improve with RA therapies. Indeed, one study showed that low clinical response rates in patients with obesity were not mirrored by similarly poor response rates on imaging,[27] suggesting that lower response rates in the context of obesity are driven by factors other than refractory articular inflammation. Although this prior work puts the current observations in context, it is difficult to establish from the current analysis alone whether persistence of subjective symptoms or refractory joint inflammation drive the observed associations, particularly because all components of disease activity appeared to be affected by the presence of metabolic syndrome. Differences in response among those with metabolic syndrome may also reflect differences in disease phenotype. For example, the link between metabolic obesity and psoriatic disease is well established.[28] Thus, further study is needed to understand the biologic mechanisms at play.

We are aware of one prior study evaluating the effect of obesity on clinical response across advanced therapies with different mechanisms of action. In that study, also from the CorEvitas registry, the lower response rates for patients with obesity were similarly observed for both TNFi and non-TNFi biologics, suggesting that low response rates for obesity were not specific to drugs with a particular mechanism of action.[1] In the current study, there was again no clear benefit of one class of biologic over another in the context of metabolic syndrome or among those with higher/lower levels of adipokines. This observation perhaps supports the concept that comorbidity and chronic pain, rather than more aggressive RA-related inflammation, drive the reduction in response, because such an effect would not be likely to vary across treatments.

This study also confirmed a prior study in the CorEvitas registry that having an underweight BMI is associated with poor clinical response at 6 months.[1] It is perhaps not surprising that the current study continues to observe this relationship independent of the presence of metabolic syndrome because metabolic syndrome would be highly unlikely to be observed in this group. Although the effects of obesity on clinical response seem to be at least partially explained by metabolic syndrome, the lower response seen among those with low BMI is not. Patients with RA who have a low BMI are observed to have greater synovitis and osteitis and adverse long-term outcomes, such as radiographic progression.[22,29,30] Low BMI likely develops over time in the context of more severe and refractory inflammatory disease (ie, cachexia). Thus, low BMI and poor response to therapy may be associated with each other through their shared etiology (ie, an association with a severe disease phenotype).

The primary limitation of the current study is the potential for residual confounding from other exposures that are correlated with metabolic syndrome. Although we assessed and adjusted for a number of potential confounders, unmeasured confounding may be present. Although we used a validated outcome for clinical response, our study did not have imaging outcomes to directly assess the extent of inflammatory arthritis at the articular level. The presence of comorbid diseases in patients with metabolic syndrome might also affect response rates. Patients with metabolic syndrome are more likely to have other comorbidities, including noninflammatory joint conditions. Finally, the subsample evaluating adipokines was smaller, and we may have been underpowered to identify small effects of adipokines on clinical response. Although the cohort was smaller, it was selected

carefully from the best and worst responders, suggesting that we might expect a larger effect size in this subcohort. Thus, the lack of association may not be adequately explained by somewhat diminished study power alone.

In conclusion, metabolic syndrome and its components are associated with lower clinical response rates in patients with RA after the initiation of a new advanced therapy; an association that is independent of BMI and increased with the number of components present for the syndrome. Although adipokines were strongly associated with metabolic syndrome, the lack of an independent association with clinical response suggests that they do not drive the relationship between metabolic syndrome and poor response. These observations have implications for clinical practice as well as clinical trial design. Future study may help to determine whether low response rates are caused by refractory inflammatory arthritis versus poor improvement in symptoms because of chronic pain and comorbidity.

ACKNOWLEDGMENTS

The authors would like to thank all the participating providers and patients in the CorEvitas Rheumatoid Arthritis Registry who contributed data for this study.

AUTHOR CONTRIBUTIONS

All authors contributed to at least one of the following manuscript preparation roles: conceptualization AND/OR methodology, software, investigation, formal analysis, data curation, visualization, and validation AND drafting or reviewing/editing the final draft. As corresponding author, Dr Baker confirms that all authors have provided the final approval of the version to be published, and takes responsibility for the affirmations regarding article submission (eg, not under consideration by another journal), the integrity of the data presented, and the statements regarding compliance with institutional review board/Declaration of Helsinki requirements.

REFERENCES

1. Baker JF, Reed G, Poudel DR, et al. Obesity and response to advanced therapies in rheumatoid arthritis. Arthritis Care Res (Hoboken) 2022;74(11):1909–1916.
2. Shan J, Zhang J. Impact of obesity on the efficacy of different biologic agents in inflammatory diseases: a systematic review and meta-analysis. Joint Bone Spine 2019;86(2):173–183.
3. Liu Y, Hazlewood GS, Kaplan GG, et al. Impact of obesity on remission and disease activity in rheumatoid arthritis: a systematic review and meta-analysis. Arthritis Care Res (Hoboken) 2017;69(2): 157–165.
4. Poudel D, George MD, Baker JF. The impact of obesity on disease activity and treatment response in rheumatoid arthritis. Curr Rheumatol Rep 2020;22(9):56.
5. Baker JF, ODell JR, England BR, et al. Lower body mass and lower adiposity are associated with differential responses to two treatment strategies for rheumatoid arthritis. Ann Rheum Dis 2024;83(4): 429–436.
6. Parra-Salcedo F, Contreras-Yanez I, Elias-Lopez D, et al. Prevalence, incidence and characteristics of the metabolic syndrome (MetS) in a cohort of Mexican Mestizo early rheumatoid arthritis patients treated with conventional disease modifying anti-rheumatic drugs: the complex relationship between MetS and disease activity. Arthritis Res Ther 2015;17(1):34.
7. Grzechnik K, Targonska-Stepniak B. Metabolic syndrome and rheumatoid arthritis activity: an analysis of clinical, laboratory, and ultrasound parameters. Nutrients 2023;15(22):4756.
8. Baker JF, Curtis JR, Chernoff D, et al. Evaluation of the impact of age and adiposity on a multi-biomarker disease activity score before and after adjustment. Clin Rheumatol 2021;40(6):2419–2426.
9. Curtis JR, Greenberg JD, Harrold LR, et al. Influence of obesity, age, and comorbidities on the multi-biomarker disease activity test in rheumatoid arthritis. Semin Arthritis Rheum 2018;47(4):472–477.
10. Kahn CR, Wang G, Lee KY. Altered adipose tissue and adipocyte function in the pathogenesis of metabolic syndrome. J Clin Invest 2019;129(10):3990–4000.
11. Taylor EB. The complex role of adipokines in obesity, inflammation, and autoimmunity. Clin Sci (Lond) 2021;135(6):731–752.
12. Baker JF, England BR, George MD, et al. Adipocytokines and achievement of low disease activity in rheumatoid arthritis. Semin Arthritis Rheum 2022;55:152003.
13. Pappas DA, Kremer JM, Reed G, et al. Design characteristics of the Corrona CERTAIN study: a comparative effectiveness study of biologic agents for rheumatoid arthritis patients. BMC Musculoskelet Disord 2014;15(1):113.
14. Kremer JM. The Corrona US registry of rheumatic and autoimmune diseases. Clin Exp Rheumatol 2016;34(5 Suppl 101):S96–S99.
15. Kremer JM. The Corrona database. Autoimmun Rev 2006;5(1):46–54.
16. Arnett FC, Edworthy SM, Bloch DA, et al. The American Rheumatism Association 1987 revised criteria for the classification of rheumatoid arthritis. Arthritis Rheum 1988;31(3):315–24.
17. Grundy SM, Brewer HB Jr, Cleeman JI, et al; American Heart Association; National Heart, Lung, and Blood Institute. Definition of metabolic syndrome: report of the National Heart, Lung, and Blood Institute/American Heart Association conference on scientific issues related to definition. Circulation 2004;109(3):433–438.
18. Curtis JR, Yang S, Chen L, et al. Determining the minimally important difference in the Clinical Disease Activity Index for improvement and worsening in early rheumatoid arthritis patients. Arthritis Care Res (Hoboken) 2015;67(10):1345–1353.
19. Studenic P, Aletaha D, de Wit M, et al. American College of Rheumatology/EULAR remission criteria for rheumatoid arthritis: 2022 revision. Ann Rheum Dis 2023;82(1):74–80.
20. Giles JT, Allison M, Bingham CO III, et al. Adiponectin is a mediator of the inverse association of adiposity with radiographic damage in rheumatoid arthritis. Arthritis Care Res 2009;61(9):1248–1256.
21. Baker JF, George M, Baker DG, et al. Associations between body mass, radiographic joint damage, adipokines, and risk factors for bone loss in rheumatoid arthritis. Rheumatology (Oxford) 2011; 50(11):2100–2107.
22. Baker JF, Ostergaard M, George M, et al. Greater body mass independently predicts less radiographic progression on x-ray and MRI over 1-2 years. Ann Rheum Dis 2014;73(11):1923–1928.
23. Westhoff G, Rau R, Zink A. Radiographic joint damage in early rheumatoid arthritis is highly dependent on body mass index. Arthritis Rheum 2007;56(11):3575–3582.
24. Cakit O, Gumustepe A, Duyur Cakit B, et al. Coexistence of fibromyalgia and metabolic syndrome in females: the effects on fatigue, clinical features, pain sensitivity, urinary cortisol and norepinephrine levels: a cross-sectional study. Arch Rheumatol 2021;36(1):26–37.

25. Baker JF, Wipfler K, Olave M, et al. Obesity, adipokines, and chronic and persistent pain in rheumatoid arthritis. J Pain 2023;24(10):1813–1819.
26. Kim DH, Kim B, Han K, et al. The relationship between metabolic syndrome and obstructive sleep apnea syndrome: a nationwide population-based study. Sci Rep 2021;11(1):8751.
27. George MD, Ostergaard M, Conaghan PG, et al. Obesity and rates of clinical remission and low MRI inflammation in rheumatoid arthritis. Ann Rheum Dis 2017;76(10):1743–1746.
28. Branisteanu DE, Pirvulescu RA, Spinu AE, et al. Metabolic comorbidities of psoriasis. Exp Ther Med 2022;23(2):179.
29. Baker JF, Billig E, Michaud K, et al. Weight loss, the obesity paradox, and the risk of death in rheumatoid arthritis. Arthritis Rheumatol 2015;67(7):1711–1717.
30. England BR, Baker JF, Sayles H, et al. Body mass index, weight loss, and cause-specific mortality in rheumatoid arthritis. Arthritis Care Res (Hoboken). 2018;70(1):11–18.

Arthritis & Rheumatology
Vol. 77, No. 3, March 2025, pp 272–282
DOI 10.1002/art.43036

American College of Rheumatology
Empowering Rheumatology Professionals

Evidence of Site-Specific Mucosal Autoantibody Secretion in Rheumatoid Arthritis

Veerle F. A. M. Derksen,[1] Klara Martinsson,[2] Anouk G. van Mourik,[1] Carlijn A. Wagenaar,[3] René E. M. Toes,[1] Wendy Walrabenstein,[4] Daniel Sjöberg,[5] Dirkjan van Schaardenburg,[3] Tom W. J. Huizinga,[1] Alf Kastbom,[2] Anna Svärd,[6] and Diane van der Woude[1]

Objective. Anti–citrullinated protein antibodies (ACPA) have been detected in sputum and saliva, indicating that anti–modified protein antibodies (AMPA) can be produced at mucosal sites in patients with rheumatoid arthritis (RA). However, the body's largest mucosal compartment, the gut, has not yet been examined. We therefore investigated the presence of several AMPA (ACPA, anti–carbamylated protein antibodies [anti-CarP], and anti–acetylated protein antibodies [AAPA]) at different mucosal sites, including the intestinal tract.

Methods. Paired fecal/ileal wash, saliva, and serum samples of patients with RA and healthy volunteers were collected in two independent cohorts. Data involving feces were replicated in a third cohort. In these secretions, AMPA were analyzed using in-house enzyme-linked immunosorbent assay with unmodified peptides as control. In fecal samples, total IgA and anti–*Escherichia coli* IgA were measured.

Results. ACPA, anti-CarP, and AAPA IgA were measurable in saliva of seropositive patients with RA (prevalence 9%–40%). No AMPA could be detected in feces. IgA was present because total IgA and anti–*E. coli* IgA were detectable in feces of ACPA-positive patients with RA and healthy donors. Results were confirmed in another cohort using colonoscopically collected ileal wash samples.

Conclusion. Our study shows the presence of ACPA, anti-CarP, and AAPA IgA in saliva of ACPA-seropositive patients with RA. However, no AMPA could be detected in feces/ileal wash samples of these patients, although our assays were able to measure other antigen-specific antibodies. These data suggest that mucosal autoantibody secretion may occur in the oral mucosa of patients with RA, whereas no evidence could be found for this process in the lower gastrointestinal tract.

INTRODUCTION

The presence of anti–modified protein antibodies (AMPA) directed against post-translational modified proteins (PTMs) is a hallmark of seropositive rheumatoid arthritis (RA). The most well-known and clinically important AMPA are anti–citrullinated protein antibodies (ACPA), whereas other AMPA recognize anti–carbamylated protein antibodies (anti-CarP) or anti–acetylated protein antibodies (AAPA). The processes leading to the break of tolerance against PTMs, to the maturation of the AMPA response, and eventually to the development of seropositive RA are not fully understood. One of the hypotheses gaining increased attention is that mucosal surfaces play a role in AMPA formation.[1–3] Inflammation at mucosal surfaces, triggered by environmental factors and microbiome–host interactions in combination with the local

The Plants for Joints trial was supported by Reade, Reade Foundation, Stichting Vermeer 14 (private foundation, The Netherlands), and W. M. de Hoop Stichting (private foundation, The Netherlands). Dr Wagenaar's work was supported by The Netherlands Organization for Health Research and Development. Dr Svärd's work was supported by a grant from the Center for Clinical Research Dalarna, Uppsala University. Dr van der Woude's work was supported by a Vidi grant from the Dutch Research Council.

[1]Veerle F. A. M. Derksen, MD, Anouk G. van Mourik, MSc, René E. M. Toes, PhD, Tom W. J. Huizinga, MD, PhD, Diane van der Woude, MD, PhD: Leiden University Medical Center, Leiden, The Netherlands; [2]Klara Martinsson, PhD, Alf Kastbom, MD, PhD: Linköping University, Linköping, Sweden; [3]Carlijn A. Wagenaar, MD, Dirkjan van Schaardenburg, MD, PhD: Reade and Amsterdam University Medical Center, Amsterdam, The Netherlands; [4]Wendy Walrabenstein, PhD: Amsterdam Rheumatology and Immunology Center, Reade, Amsterdam, The Netherlands; [5]Daniel Sjöberg, MD, PhD: Uppsala University, Uppsala, Sweden, and Falun Hospital, Falun, Sweden; [6]Anna Svärd, MD, PhD: Linköping University, Linköping, Sweden, and Uppsala University, Uppsala, Sweden.

Drs Svärd and van der Woude contributed equally to this work.

Additional supplementary information cited in this article can be found online in the Supporting Information section (https://acrjournals.onlinelibrary.wiley.com/doi/10.1002/art.43036).

Author disclosures are available at https://onlinelibrary.wiley.com/doi/10.1002/art.43036.

Address correspondence via email to Diane van der Woude, MD, PhD, at dvanderwoude@lumc.nl.

Submitted for publication November 21, 2023; accepted in revised form September 17, 2024.

presence of PTMs, might create conditions in which tolerance to PTMs is broken.[1,2,4,5]

There is accumulating evidence that the airway mucosa is involved in seropositive RA. Smoking, along with exposure to silica dust and other inhalants, is a major risk factor for the development of seropositive RA and the concurrent presence of multiple RA-associated antibodies.[6–8] It is hypothesized that these environmental factors induce airway inflammation, which can contribute to autoantibody formation.[9] However, the lungs are not the only mucosal sites that may be involved in RA development. The epidemiologic association between RA and periodontitis was already reported years ago.[10] Oral and intestinal microbiome disturbances have been described in patients with RA and people at risk of developing RA.[11–14] Novel research shows that patients with RA with ongoing periodontitis experience repeated bacteremia with oral bacteria. Bacteria can be citrullinated, and citrullinated bacterial epitopes can be recognized by ACPAs. These findings provide an interesting potential link between physiologic antibacterial responses and autoimmunity in RA.[15] The association between the lung and oral mucosa and RA is further substantiated by the discovery that ACPA can be present in sputum, bronchoalveolar fluid, and saliva of patients with RA.[16–18] Rheumatoid factor can also be present in the saliva of those patients.[19]

However, the largest mucosal site in the body, the intestine, has received less attention over the years compared to the lung and mouth. Lately, this has changed with the finding that monoclonals derived from circulating plasmablasts in individuals at risk of RA can bind both RA-associated citrullinated autoantigens and bacteria in feces.[20] These findings suggest that the intestinal mucosa might also be involved in the pathophysiology of RA. The presence of other AMPA (besides ACPA) at mucosal sites has not yet been investigated, although this could provide new information on the development of the AMPA response in RA, especially in the gut. AAPA might provide an interesting angle when it comes to mucosal microbial exposures as a potential trigger for autoimmunity because various bacterial species use acetylation of self-proteins to regulate cell processes.[21,22] Anti-CarP responses may also have an intestinal origin because carbamylation has been shown to occur in the human gastrointestinal tract.[23] It therefore appears plausible that anti-CarP and AAPA could be produced at mucosal sites and that local availability of specific post-translational modifications, as a product of microbiome, food constituents, and host cell interactions, might diversify and broaden the AMPA response in RA. Nevertheless, whether AMPAs are secreted in the intestinal tract is currently unknown.

Hence, we investigated whether ACPA, anti-CarP, and AAPA can all be detected in mucosal secretions, with emphasis on material derived from the intestinal tract of patients with RA. To this end, we collected paired serum, saliva, and feces of patients with RA and healthy donors and tested these samples for the presence of ACPA, anti-CarP, and AAPA. Two other independent cohorts were used to replicate our findings.

PATIENTS AND METHODS

Cohorts. In the Dutch MUCosal Origin of Serum Autoantibodies in rheumatoid arthritis (MUCOSA) study, paired serum, saliva, and feces samples were collected cross-sectionally from 47 patients with RA visiting the outpatient clinic (of whom 36 were ACPA seropositive) and from 21 healthy controls. Saliva was collected by passive drooling, and feces were collected by participants themselves and immediately frozen. One patient had severe hyposalivation precluding the collection of saliva. Details are provided in Supplementary Data 1.

To substantiate our findings, we made use of samples from another independent study. The Swedish IntestRA study included 20 ACPA-seropositive patients with RA, 10 healthy donors, and 9 patients with inflammatory bowel disease (IBD) as additional controls. Serum and saliva samples were collected in a similar method. However, to investigate the presence of autoantibodies in the gut, ileal wash fluid was collected via colonoscopy instead. Details are provided in Supplementary Data 2.

Feces samples from a third cohort, the Dutch Plants for Joints (PFJ) trial,[24,25] were examined to corroborate the results regarding AMPA in feces. Baseline feces samples of 42 ACPA-seropositive patients with RA and 10 patients with osteoarthritis as control were investigated. Feces were collected by participants themselves at home and sent by mail, after which samples were stored at –80°C.

In all three studies, all patients fulfilled the 2010 American College of Rheumatology/EULAR criteria for RA, and most had longstanding disease. Throughout this manuscript, ACPA seropositive refers to ACPA IgG seropositivity. All studies were performed in concordance with the Declaration of Helsinki, approved by the relevant local medical ethical committees, and all participants provided written informed consent.

Measurements. The presence of AMPAs and rheumatoid factor (RF) in serum, saliva, and feces in the MUCOSA study was tested by in-house enzyme-linked immunosorbent assay (ELISA) using peptides containing different modifications on a Cyclic Citrullinated Peptide 2 backbone. Measurements in the PFJ trial were performed in accordance with the protocols used for feces samples in the MUCOSA study. In the IntestRA study, modified commercial anti-CCP assays (CCPlus Immunoscan, Svar Life Science) were used to measure ACPA IgA in ileal wash and saliva samples. Autoantibody analyses in the IntestRA study focused on ACPA only. Total IgA levels and anti–*Escherichia coli* antibodies were also measured in mucosal secretions by ELISA. For anti–*E. coli*, ELISA plates were coated with *E. coli* lysates. After blocking and adding undiluted fecal extracts, horseradish peroxidase-labeled detection antibodies were used stepwise before visualization with ABTS (Supplementary Data 1). Furthermore, analysis of markers of inflammation in saliva (total protein and matrix metalloproteinase-8 [MMP-8] levels) and feces (calprotectin)

was performed in the MUCOSA study using ELISA kits (Total MMP-8 ELISA kit, R&D systems, DMP800B; and Calprotectin ELISA kit, Orgentec, ORG580) according to manufacturer's instruction.

Saliva samples were homogenized and centrifugated before use to remove any debris. To be able to detect autoantibodies in fecal matter, protein fractions were prepared by diluting the feces 1:5 in feces dilution buffer (phosphate-buffered saline + 0.05 M ethylenediaminetetraacetic acid + 1.66 mM phenylmethylsulfonyl fluoride + 0.1 mg/mL soybean trypsin inhibitor [Sigma]). Samples were mixed vigorously for 10 to 20 minutes until homogeneous and spun down. Ileal wash samples were centrifuged and frozen within one hour after collection.

When testing for AMPA positivity, all samples were also measured simultaneously on the unmodified control peptide to investigate whether binding was specific for the post-translational modification. In the MUCOSA study and PFJ trial, a sample was considered AMPA positive when both of the following criteria were met: 1) The value measured on the modified peptide was higher than the cut-off based on the mean plus two times the SD of the signal of healthy controls on that peptide, and 2) the optical density (OD) of the signal measured on the modified peptide was >2 times higher than the OD of the same sample measured on the unmodified peptide. In the IntestRA study, OD signals on the arginine control were first subtracted from the ACPA OD values. Thereafter, a cut-off was calculated in a similar manner.

More information about sample processing and autoantibody detection can be found in Supplementary Data 1 (MUCOSA and PFJ) and 2 (IntestRA). Mann-Whitney U tests, chi-square tests, or Fisher's exact tests, as appropriate depending on the kind of data, were performed to compare antibody positivity and markers of inflammation among groups.

RESULTS

AMPAs in saliva. Mucosal autoantibodies were investigated in three independent cohorts, of which the clinical characteristics are listed in Table 1. First, autoantibodies were measured in serum and saliva of participants in the MUCOSA study. Seventeen percent of ACPA-seropositive patients with RA in the MUCOSA study had detectable ACPA IgA in saliva, whereas ACPA could not be detected in the saliva of patients who were ACPA seronegative or healthy donors (Figure 1A) (not significant [ns]). In the Swedish IntestRA study, ACPA IgA was found in saliva of 40% of the patients who were ACPA seropositive (Figure 1B), whereas none of the patients with IBD or healthy controls were positive ($P = 0.03$ compared with healthy controls). However, the presence of AMPA was not limited to ACPA IgA. Also, anti-CarP IgA and AAPA IgA could be detected in saliva of seropositive patients with RA in the MUCOSA study (Figure 1C and D), although the number of patients positive for salivary autoantibodies was low (9%) for both autoantibodies. RF IgA could be found in saliva 46% of ACPA-seropositive patients with RA (Figure 1E) ($P = 0.001$ compared with healthy controls) and was present more frequently compared with salivary ACPA IgA.

Table 1. Patient characteristics of all cohorts*

	MUCOSA		IntestRA			Plants for Joints	
Characteristics	RA, n = 47	Healthy, n = 21	RA, n = 20	Healthy, n = 10	IBD, n = 9	RA, n = 42	OA, n = 10
Age, y, mean ± SD	59 ± 13	48 ± 16	61 ± 9	62 ± 9	30 ± 8	55 ± 12	62 ± 6
Female, n (%)	37 (79)	13 (62)	15 (75)	7 (70)	6 (67)	36 (86)	10 (100)
Disease duration, years, median (IQR)	14 (8–16)	–	0.7 (0–12)	–	–	6.5 (3–15)	–
Smoking ever, n (%)	26 (55)	6 (29)	12 (60)	4 (44) (n = 9)	3 (33)	–	–
ESR, mm/h, median (IQR)	9 (2–34)	–	13 (8–20)	6 (4–24)	8 (4–15)	15 (8–32)	–
DAS28, median (IQR)	2.6 (1.7–3.6) (n = 45)	–	3.0 (2.0–4.0) (n = 10)	–	–	3.9 (3.2–4.5)	–
Serum antibody positivity[a]							
ACPA IgG, n (%)	36 (77)	0 (0)	20 (100)	0 (0)	0 (0)	42 (100)	–
Anti-CarP IgG, n (%)	21 (45)	0 (0)	–	–	–	–	–
AAPA IgG, n (%)	21 (45)	0 (0)	–	–	–	–	–
ACPA IgA, n (%)	18 (38)	0 (0)	20 (100)	0 (0)	0 (0)	–	–
Anti-CarP IgA, n (%)	4 (9)	0 (0)	–	–	–	–	–
AAPA IgA, n (%)	5 (11)	0 (0)	–	–	–	–	–
RF IgM n (%)	34 (72)	3 (14)	–	–	–	–	–
RF IgA, n (%)	21 (45)	1 (5)	–	–	–	–	–

* Characteristics of all cohorts at inclusion. AAPA, anti–acetylated protein antibodies; ACPA, anti–citrullinated protein antibodies; CarP, carbamylated protein antibodies; DAS28, Disease Activity Score in 28 joints; ELISA, enzyme-linked immunosorbent assay; ESR, erythrocyte sedimentation rate; IBD, inflammatory bowel disease; IQR, interquartile range; OA, osteoarthritis; RA, rheumatoid arthritis; RF, rheumatoid factor.
[a] All serum autoantibody measurements in the MUCOSA study are done with in-house ELISAs.

Notably, when examining reactivity to the modified peptides (citrulline, homocitrulline, and acetylated lysine) and unmodified peptides (arginine and lysine, respectively) in saliva in more detail, a substantial number of seropositive patients with RA, but not seronegative patients or healthy controls, had high reactivity to the modified peptide but also showed a similarly high degree of reactivity to the unmodified peptide (Figure 2A–C). When the reactivity to the modified and unmodified peptide was similar, antibody binding was not specific for the PTM, and samples were considered AMPA negative. The high signal measured on the unmodified peptide in saliva samples is markedly different from serum, where background signals are usually very low (Figure 2D–F). In the IntestRA study, unmodified peptide signals were more equally distributed between patients with RA and controls (Figure 2G) (ns).

Next, we investigated whether the presence of autoantibodies in saliva was related to the amount of total IgA in these samples, as salivary IgA levels can differ among individuals and over time.[27] There was no significant difference in salivary total IgA between seropositive patients with RA who were positive for AMPA in their saliva and those who were negative (Supplementary Figure 1). Therefore, it seems that prevalence of IgA AMPA in saliva cannot solely be attributed to differences in salivary total IgA levels, but may rather point to inherent differences among patients.

AMPA profile in saliva and serum. Different types of AMPA in saliva tend to co-occur. Among the seven patients with AMPA-positive saliva in the MUCOSA study, two were triple positive for ACPA, anti-CarP, and AAPA, and one patient was anti-CarP and AAPA double positive (Figure 3). Furthermore, six patients with AMPA-positive saliva were also saliva RF IgA positive. The presence of an AMPA in saliva always coincided with the presence of that specific AMPA in serum, although the isotype

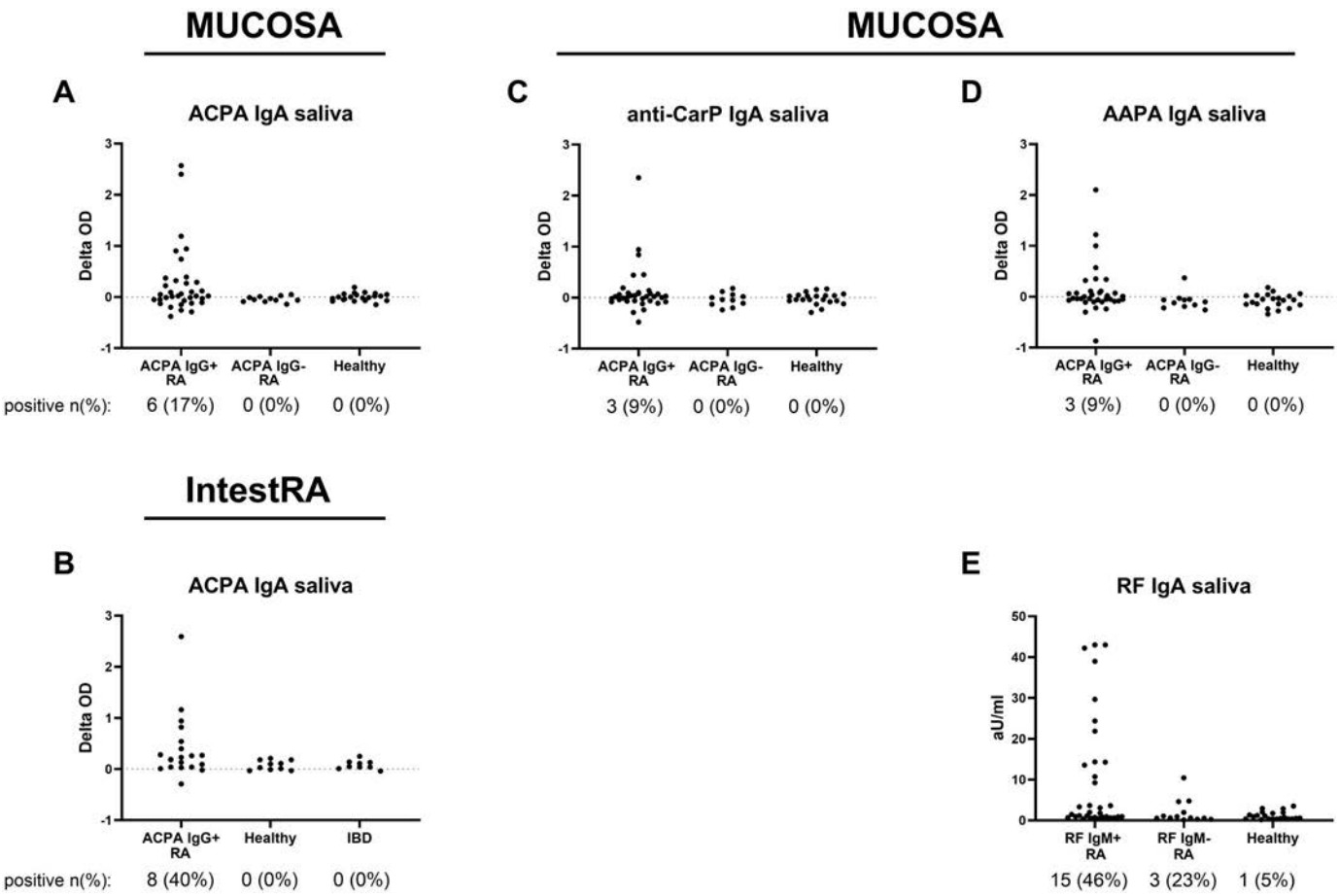

Figure 1. Autoantibody measurements in saliva. (A) ACPA IgA in saliva in the MUCOSA study, (B) ACPA IgA in saliva in the IntestRA study, and (C) anti-CarP IgA, (D) AAPA IgA, and (E) RF IgA in saliva in the MUCOSA study are shown. Delta OD (difference in OD between modified peptide and unmodified peptide) for AMPAs and aU/mL (arbitrary units per milliliter) for RF are depicted. Groups on *x* axis are based on diagnosis and seropositivity (panel E uses RF IgM seropositivity to define groups). The number (%) of positive patients for that specific autoantibody is given. AAPA, anti–acetylated protein antibody; ACPA, anti–citrullinated protein antibody; AMPA, anti–modified protein antibody; CarP, carbamylated protein; IBD, inflammatory bowel disease; MUCOSA, MUCosal Origin of Serum Autoantibodies in rheumatoid arthritis; OD, optical density; RA, rheumatoid arthritis; RF, rheumatoid factor.

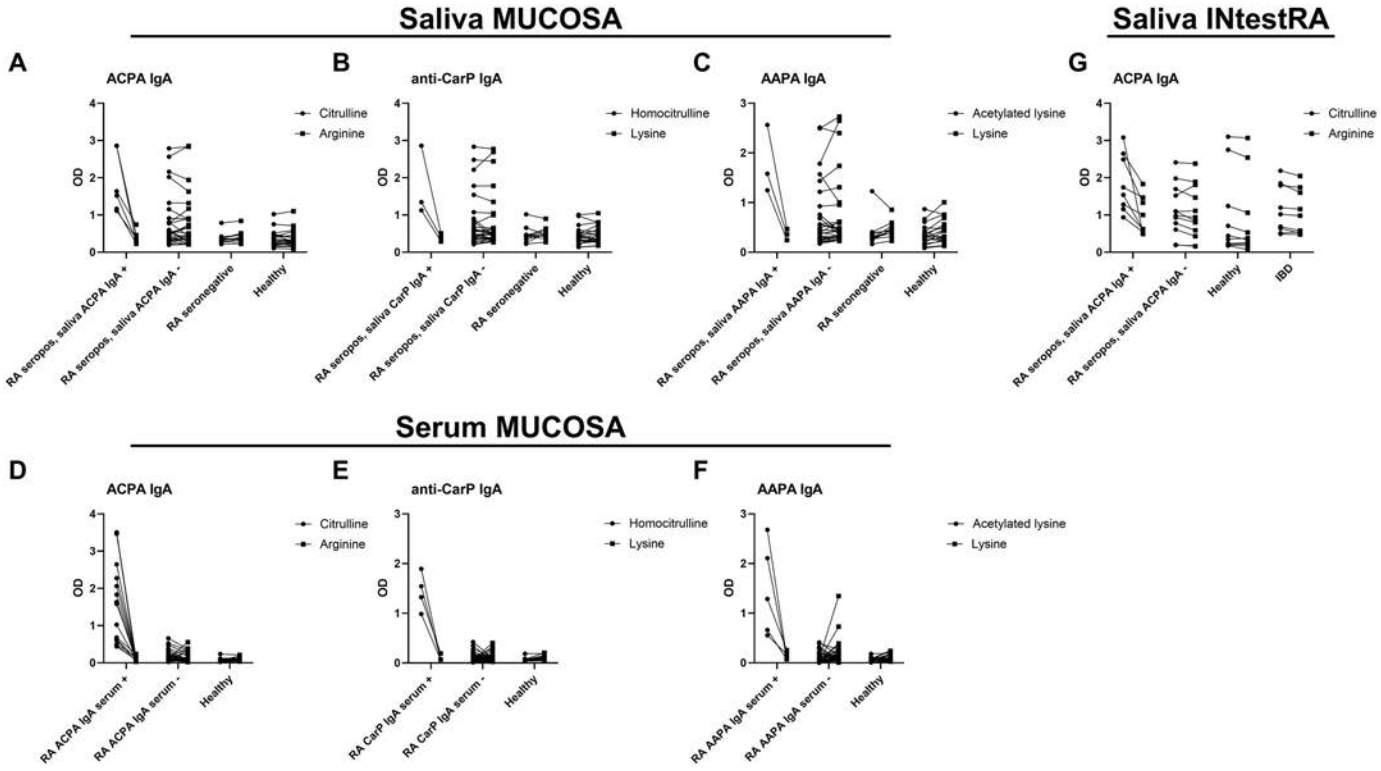

Figure 2. Paired OD values on the modified and unmodified peptide for each AMPA in saliva (A–C) and serum (D–F) of patients and healthy donors in the MUCOSA study and in saliva (G) of patients and controls in the IntestRA study. (A–C) First group of each graph shows all seropositive patients with RA who tested positive for that specific AMPA in saliva, and the second group depicts all seropositive patients with RA who tested negative for that specific AMPA in saliva. (D–F) First group shows patients who were positive for that specific AMPA IgA in serum, and the second group shows patients negative for that specific AMPA IgA in serum. AAPA, anti–acetylated protein antibody; ACPA, anti–citrullinated protein antibody; AMPA, anti–modified protein antibody; CarP, carbamylated protein; IBD, inflammatory bowel disorder; MUCOSA, MUCosal Origin of Serum Autoantibodies in rheumatoid arthritis; OD, optical density; RA, rheumatoid arthritis.

could differ (Figure 3). For example, one patient was positive for AAPA IgA in saliva, whereas AAPA IgG, but no AAPA IgA, could be detected in serum. Similar findings were made for RF. However, three patients with RA who tested positive for RF IgA in saliva tested negative for both RF IgM and IgA in serum. This suggests a local origin and subsequent secretion of

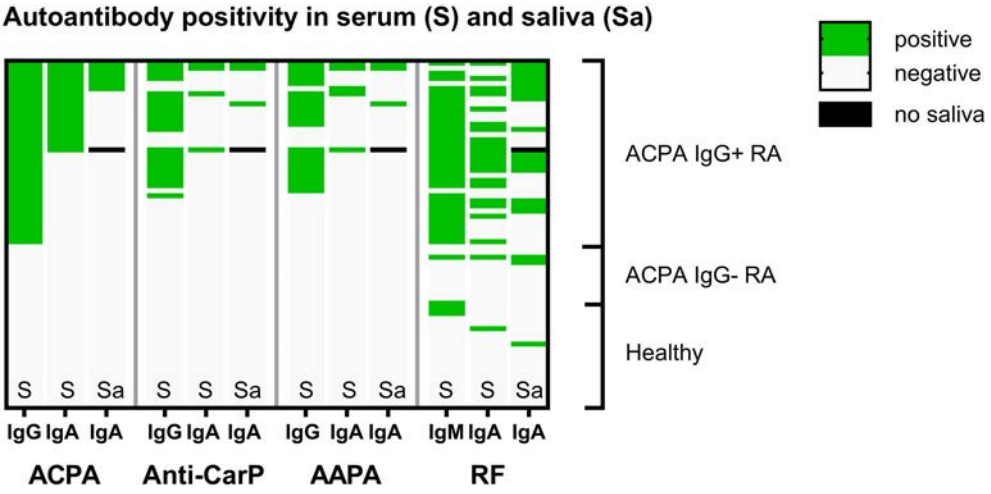

Figure 3. Autoantibody profile in serum (S) and saliva (Sa) in the MUCOSA study. Positivity for autoantibodies in serum and saliva is shown. Each row depicts a study participant. Black field indicates no saliva available due to hyposalivation. AAPA, anti–acetylated protein antibody; ACPA, anti–citrullinated protein antibody; CarP, carbamylated protein; MUCOSA, MUCosal Origin of Serum Autoantibodies in rheumatoid arthritis; RA, rheumatoid arthritis; RF, rheumatoid factor.

autoantibodies rather than leakage from serum antibodies to the saliva. Furthermore, the amount of IgG measured in these saliva samples is, on average ± SD, 9 ± 8 μg/mL, a thousandfold lower than serum IgG (reference levels 7–16 g/L), making contamination of saliva samples with serum autoantibodies in measurable amounts less likely. Thus, the saliva autoantibody profile displays similarity to, but does not necessarily originate from, the serum autoantibody profile.

Saliva AMPAs and local inflammation. Next, we investigated whether the presence of salivary autoantibodies was associated with oral inflammation. Total protein content, MMP-8 levels, and total IgA levels in saliva have been determined as markers of local inflammation.[27,28] In the MUCOSA study, patients with RA in general had slightly lower total IgA levels in saliva compared to healthy donors, whereas there was a nonsignificant trend toward higher MMP-8 and total protein values in patients with RA. There were no significant differences in all three salivary markers of inflammation between patients with RA who were positive for ACPA in their saliva (median [interquartile range, IQR]: total protein 1,380 μg/mL [1,057–1,747], total IgA 343 μg/mL [253–562], MMP-8 123 ng/mL [33–150]) and those who were not (median [IQR]: total protein 1,411 μg/mL [1,040–1,621], total IgA 259 μg/mL [169–386], MMP-8 83 ng/mL [26–138]) (Supplementary Figure 2A–C). Because the number of patients who were ACPA saliva positive is small, salivary markers of inflammation were also compared among ACPA-seropositive patients with RA, ACPA-seronegative patients with RA, and healthy donors (Supplementary Figure 2D–F), which showed similar results. Because smoking directly affects the oral mucosa, the relation between autoantibody positivity in saliva and smoking was examined. No significant relation between smoking and the presence of autoantibodies was seen in saliva (Supplementary Table 1), despite the significant association between RF IgM seropositivity and smoking in the MUCOSA study (P = 0.04) and a similar trend for ACPA seropositivity (Supplementary Table 1).

AMPA in the intestinal tract. In the MUCOSA study, no ACPA, anti-CarP, or AAPA were found in feces samples of patients with RA or healthy controls (Figure 4A–C), as there was almost no difference between the signals on the modified and unmodified peptides. Also, in the PFJ trial, no AMPA were found in feces (Figure 4D–F). Like in saliva, reactivity to the modified and unmodified peptides was evaluated separately in feces as well. Multiple ACPA-seropositive patients with RA, ACPA-seronegative patients with RA, and controls showed an OD >1 to the citrullinated peptide in their stool but also to unmodified arginine-containing peptide, which was thus considered as nonspecific binding/AMPA negative (Figure 5A and D). Similar results were found for anti-CarP and AAPA (Figure 5B,C,E,F) in both cohorts. The high OD signals on the unmodified peptides in feces are in contrast to saliva, for which only seropositive patients with RA showed a high background (Supplementary Figure 3).

To determine whether the fecal supernatants contained sufficient amounts of Ig to fall within the detection range of our ELISAs, total IgA levels were measured. Fecal supernatants in the MUCOSA study contained a median of 48 μg/mL total IgA, with no significant differences among seropositive patients with RA, seronegative patients with RA, and healthy donors (Figure 4G). Similar results were found in the PFJ trial (Figure 4I). These total IgA levels are roughly comparable with the amount of total IgA in the diluted saliva samples used for AMPA ELISA. Furthermore, anti–*E. coli* IgA was used as an additional (antigen-specific) control. High anti–*E. coli* signals could both be detected in patients with RA and healthy donors. Interestingly, anti–*E. coli* reactivity was significantly higher in seropositive patients with RA compared with healthy donors in the MUCOSA study (P = 0.04) (Figure 4H), although the numbers are small. In the PFJ trial, no significant difference was observed (Figure 4J). These data indicate that the methods used are able to detect the presence of (antigen-specific) antibodies in feces samples in general and that the lack of AMPA signal is not due to the absence of total IgA in these samples.

To substantiate our findings regarding the intestines, we also investigated ileal wash samples, collected via colonoscopy in the independent IntestRA cohort. Antibodies in such samples might be less prone to degradation compared with feces. However, also in the ileal wash samples, no ACPA IgA was detected (Figure 4K), whereas total IgA (median 20.5 μg/mL) (Figure 4L) and anti–*E. coli* IgA (Figure 4M) were detectable. ODs for both the modified and unmodified peptides were overall low (Figure 5G). Total IgA levels and anti–*E. coli* antibody signals were also slightly lower compared with the feces samples, possibly due to dilution by the lavage fluid instilled in the ileum used to collect these samples.

Calprotectin in feces of patients with RA. Because previous reports have suggested that RA might be characterized by a leaky intestinal barrier, gut dysbiosis, and inflammation,[3,11,29,30] intestinal inflammation was investigated in the MUCOSA study. Calprotectin was measured in feces of both patients with RA and healthy donors by commercial ELISA (Orgentec) (Supplementary Figure 4A). Values above 200 μg/g are considered significantly elevated and reflect active inflammatory intestinal disease. Six out of 47 patients with RA and 1 out of 21 healthy controls had calprotectin values >200 μg/g, and an additional 7 patients had slightly elevated calprotectin levels between 100 and 200 μg/g. However, five of seven participants with strongly elevated calprotectin levels and four out of seven participants with slightly elevated calprotectin levels reported regular nonsteroidal anti-inflammatory drug (NSAID) treatment (Supplementary Figure 4B) (ns, P = 0.07). NSAIDs are known to cause gastrointestinal mucosal damage,[31] and it has been

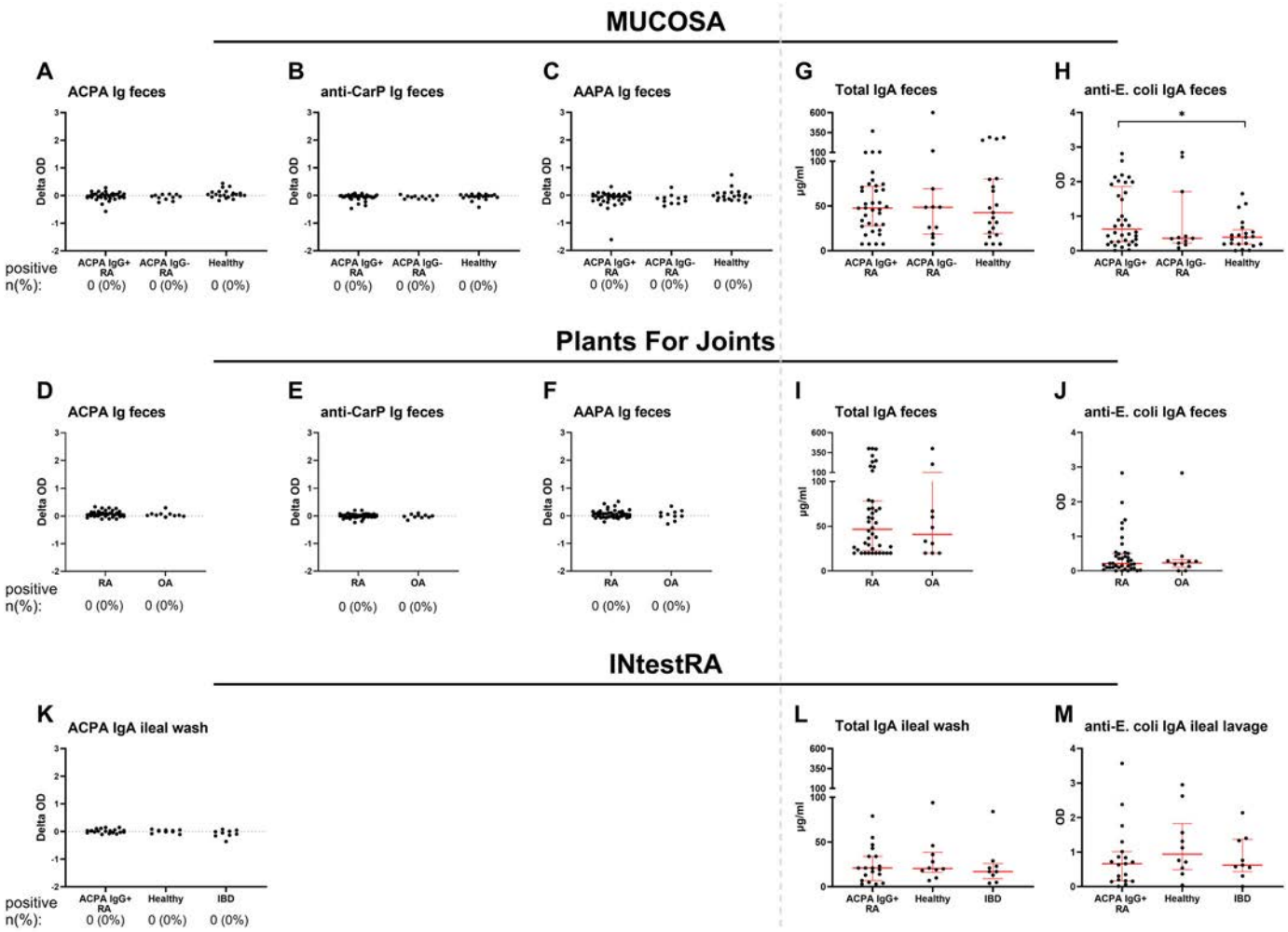

Figure 4. AMPA Ig in feces and ileal lavage of patients with RA. (A–C) ACPA, anti-CarP, and AAPA Ig, respectively, in feces from patients and healthy donors in the MUCOSA study are shown. Groups on *x* axis are based on diagnosis and seropositivity. (D–F) AMPA Ig in feces of the Plants for Joints cohort is shown. (G–J) Total IgA levels in µg/mL (G and I) and OD (H and J) on the anti–*E. coli* IgA ELISA in the same feces samples. (K) ACPA IgA in ileal lavage samples from the IntestRA study is shown. (L) Total IgA levels and (M) anti–*E. coli* IgA OD in the same ileal lavage samples are shown. For AMPAs, the number (%) of positive patients is given. For AMPAs, the *y* axis depicts difference in OD (delta OD) between the modified and unmodified peptide. Red bars show the median and interquartile range. *$P < 0.05$. AAPA, anti–acetylated protein antibody; ACPA, anti–citrullinated protein antibody; AMPA, anti–modified protein antibody; CarP, carbamylated protein; ELISA, enzyme-linked immunosorbent assay; IBD, inflammatory bowel disease; MUCOSA, MUCosal Origin of Serum Autoantibodies in rheumatoid arthritis; OA, osteoarthritis; OD, optical density; RA, rheumatoid arthritis. Color figure can be viewed in the online issue, which is available at http://onlinelibrary.wiley.com/doi/10.1002/art.43036/abstract.

reported that two weeks of NSAID treatment in healthy individuals can lead to significantly elevated fecal calprotectin levels.[32]

DISCUSSION

This study aimed to examine the RA-associated autoantibody profile in various mucosal compartments. In the saliva of patients with established seropositive RA, we found that ACPA, anti-CarP, and AAPA IgA antibodies can all be present, although in modest quantities compared with serum. Differences in the percentage of patients with ACPA-positive saliva (17%–40% in ACPA IgG-seropositive RA) among cohorts might reflect the inclusion of only patients with moderate to high ACPA serum levels in the IntestRA study. When salivary AMPA are present, the breadth of the response is similar to the AMPA serum profile. In contrast, no AMPA were found in feces of the same patients with RA, although the fecal supernatants did contain total IgA and anti–*E. coli* IgA antibodies. These findings were confirmed in feces and in ileal lavage samples from two independent cohorts of patients with RA. Our findings suggest that secretion of AMPA is limited to certain mucosal sites, with local secretion of all AMPA taking place in the oral cavity, but not to a detectable degree in the lower intestinal tract.

These observations are in line with previous studies showing the presence of salivary ACPA IgA in patients with RA.[17] ACPA IgA and IgG were also previously found in sputum of seropositive

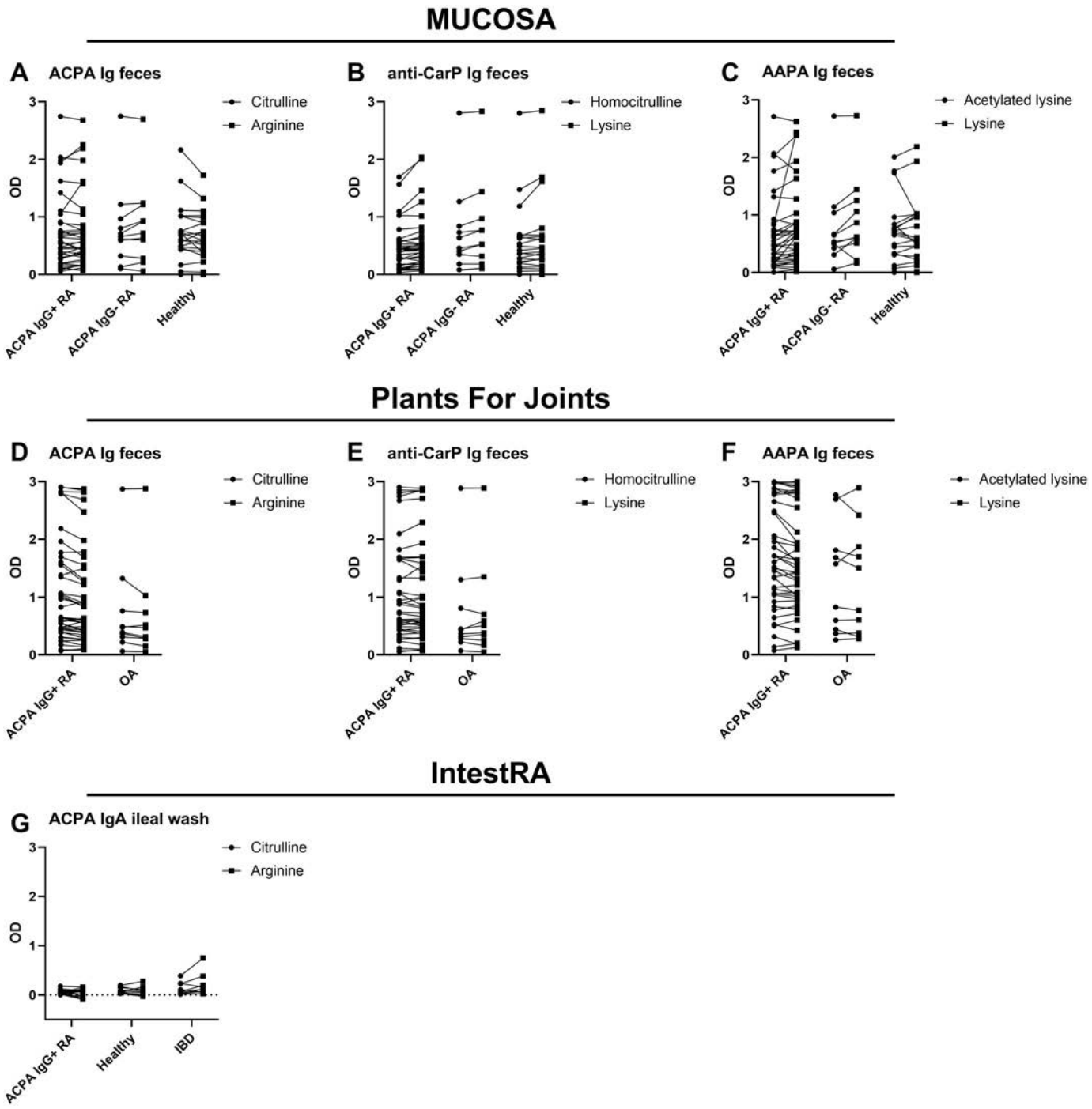

Figure 5. (A–G) Paired OD values on the modified and unmodified peptide for each AMPA Ig in feces of patients and controls in the MUCOSA study (A, C, E) and in the Plants for Joints trial (B, D, F) and ACPA IgA in ileal wash in patients and controls in the IntestRA study (G). AAPA, anti–acetylated protein antibody; ACPA, anti–citrullinated protein antibody; AMPA, anti–modified protein antibody; CarP, carbamylated protein; IBD, inflammatory bowel disease; MUCOSA, MUCosal Origin of Serum Autoantibodies in rheumatoid arthritis; OA, osteoarthritis; OD, optical density; RA, rheumatoid arthritis.

patients with RA and first-degree relatives (FDRs) of patients with RA.[16] Some of the FDRs who were positive for ACPA in their sputum were serum ACPA negative, indicating that sputum ACPAs are produced locally and can precede or occur independently of a serological ACPA response. Our findings provide further evidence that autoantibodies found in mucosal secretions can be secreted locally at mucosal sites because the AMPA isotype present in saliva was not always measurable in serum. The low amount of IgG present in the saliva samples may further support that both the detected AMPAs and RF originated from the

mucosal lining of the oral cavity instead of leaking from serum because leakage would have led to a higher quantity of IgG as the most abundant isotype present in serum. Furthermore, monomeric IgA from serum cannot be actively transported over the mucosal epithelium by the polymeric immunoglobulin receptor, whereas mucosal-derived dimeric IgA can.

These findings raise the question of where the initial activation of autoreactive B cells in RA can take place and which triggers elicit these anti–modified protein responses. Activated B cells re-enter the tissue where they were activated based on homing marker expression, although there probably is some crossover to other, often anatomically closely related tissues.[26] This suggests that the cells secreting AMPA in the oral mucosa are probably derived from B cells activated in local lymphoid tissue. Our study shows that the salivary AMPA response not only includes ACPA, but also antibody responses against carbamylated and acetylated proteins, suggesting the local presence of these antigens. Interestingly, bacteria can acetylate self-proteins[21,22] and thus might evoke an anti–acetylated bacterial protein response, which could be cross-reactive to acetylated self-proteins. It is hypothesized that, via this mechanism, the antibody responses against acetylated bacterial content can contribute to diversification and epitope spreading of the AMPA response in RA. Furthermore, in the MUCOSA study, seropositive patients with RA tended to have a higher reactivity in saliva toward the unmodified peptides compared with seronegative patients with RA and healthy donors, although this was not as clear in the IntestRA cohort. This higher reactivity toward unmodified peptides in seropositive patients with RA could also point to activated humoral immune responses in general in these patients, for example, due to decreased barrier function or local inflammation.

Our study did not include a dental examination to determine the presence of periodontitis (inflammation of the gums), which can be caused by bacterial infection. To gather some information on oral inflammation nonetheless, total protein content, MMP-8 levels, and total IgA were measured in saliva. No association between these markers of inflammation and ACPA positivity in saliva was seen. This could be explained in several ways: The sensitivity of these markers might be more limited than a dental examination, and gingivitis or periodontitis could have been missed. Alternatively, a true lack of association could suggest that oral production of autoantibodies is independent of simultaneously occurring mucosal inflammation and would either not require inflammation at all or could be related to barrier dysfunction and inflammation in the past.

Not only the oral mucosa, but also the gut could represent a large source of citrullinated, carbamylated, and acetylated (microbial) proteins. From an immunologic point of view, it appears conceivable that a T cell response against post-translationally modified bacteria (as foreign/nonself) may provide the required T cell help to activate self-reactive AMPA-directed B cells. Reactivity to intestinal bacteria was found to be a normal property of the human CD4+ T cell repertoire in healthy individuals.[33] Moreover, it has been described that monoclonal ACPA derived from individuals at risk for RA can bind bacterial isolates from human feces.[20] Based on these findings, one would have expected to find AMPAs in intestinal secretions as well, but we did not find ACPA, anti-CarP, or AAPA in feces or ileal wash samples. This suggests that there is no substantial ACPA production in the lower intestinal tract. Anti–*E. coli* IgA and total IgA were measurable in these intestinal samples, indicating that the methodology is adequate to detect (antigen-specific) antibodies.

Our results suggest that mucosal AMPA production is site specific, with local secretion of AMPA taking place in the oral mucosa, but not substantially in the gut. In addition, earlier studies provide evidence for AMPA responses in the airways.[16,18] This spatial variation might be due to differences in the local microenvironment, such as antigen availability, and local inflammatory processes, such as NETosis (release of Neutrophil Extracellular Traps). However, there are several other reasons why AMPA might not be detectable in the gut, for example, due to strong binding to their antigen, degradation of antibodies by digestive enzymes, or the amount of AMPA being under the detection limit of our assays. The facts that total IgA and anti–*E. coli* IgA were detectable in feces and that ACPA were also not present in ileal lavage samples, which might be less prone to degradation, make it more likely that the gut is not a major site of secretion for AMPA. Nevertheless, further research on barrier dysfunction and presence of PTMs in the intestinal tract of seropositive patients with RA is warranted because there are other potential mechanisms via which the intestinal mucosal compartment could contribute to the systemic AMPA response that are beyond the scope of our study, such as microbiome dysbiosis, decreased intestinal barrier function, and trafficking of immune cells primed in the intestine to the systemic circulation. For example, in one cohort, there was a difference in fecal anti–*E. coli* reactivity between seropositive patients with RA and healthy donors, which could point to increased interactions between gut bacteria and the immune system in RA.

Our study provides new insights in the autoantibody profile at mucosal surfaces, but it comes with some limitations. Most patients had longstanding RA and used various immunosuppressive therapies, which could have influenced the results. Previous studies investigating the effect of antirheumatic treatment on serologic AMPA responses have revealed that the presence of AMPA in serum is quite stable under treatment,[34] but it is unknown whether mucosal AMPA responses originate from antibody-secreting cells with similar (long-lived) characteristics. Positivity for secretory ACPA in serum declined more strongly compared with ACPA IgG after initiation of therapy.[35] Furthermore, despite the use of three independent cohorts to verify our findings, the number of patients included is limited. Because of the COVID-19 pandemic, we were prohibited from collecting paired sputum samples in the MUCOSA study, as originally

planned. Therefore, whether anti-CarP and AAPA are also present in sputum of patients with RA remains unknown.

To the best of our knowledge, our study nonetheless represents the most extensive investigation to date of a large variety of autoantibodies in a diverse array of bodily fluids. Our results show that ACPA, anti-CarP, and AAPA can be secreted locally in the oral mucosa. This suggests that local immune responses against PTMs, for example, in the context of an antibacterial response, might contribute to the development and diversification of the AMPA response in patients with RA. No support for local AMPA secretion in the lower intestinal tract was found. This study, therefore, for the first time sheds light on one of the possible roles (or potential lack thereof) of the intestinal mucosa in the onset of the AMPA responses in RA.

ACKNOWLEDGMENTS

We thank Dani Yoganathan for his work on the laboratory experiments for the MUCOSA study during his internship. We also thank Holger Bang, Orgentec Diagnostica, for supplying the calprotectin ELISAs free of charge.

AUTHOR CONTRIBUTIONS

All authors contributed to at least one of the following manuscript preparation roles: conceptualization AND/OR methodology, software, investigation, formal analysis, data curation, visualization, and validation AND drafting or reviewing/editing the final draft. As corresponding author, Dr van der Woude confirms that all authors have provided the final approval of the version to be published, and takes responsibility for the affirmations regarding article submission (eg, not under consideration by another journal), the integrity of the data presented, and the statements regarding compliance with institutional review board/Declaration of Helsinki requirements.

REFERENCES

1. Gravallese EM, Firestein GS. Rheumatoid arthritis - common origins, divergent mechanisms. N Engl J Med 2023;388:529–542.
2. Holers VM, Demoruelle MK, Kuhn KA, et al. Rheumatoid arthritis and the mucosal origins hypothesis: protection turns to destruction. Nat Rev Rheumatol 2018;14:542–557.
3. Zaiss MM, Joyce Wu HJ, Mauro D, et al. The gut-joint axis in rheumatoid arthritis. Nat Rev Rheumatol 2021;17:224–237.
4. Ayyappan P, Harms RZ, Seifert JA, et al. Heightened levels of antimicrobial response factors in patients with rheumatoid arthritis. Front Immunol 2020;11:427.
5. Kampstra ASB, Dekkers JS, Volkov M, et al. Different classes of anti-modified protein antibodies are induced on exposure to antigens expressing only one type of modification. Ann Rheum Dis 2019;78:908–916.
6. Kronzer VL, Sparks JA. Occupational inhalants, genetics and the respiratory mucosal paradigm for ACPA-positive rheumatoid arthritis. Ann Rheum Dis 2023;82:303–305.
7. Tang B, Liu Q, Ilar A, et al. Occupational inhalable agents constitute major risk factors for rheumatoid arthritis, particularly in the context of genetic predisposition and smoking. Ann Rheum Dis 2023;82:316–323.
8. van Wesemael TJ, Ajeganova S, Humphreys J, et al. Smoking is associated with the concurrent presence of multiple autoantibodies in rheumatoid arthritis rather than with anti-citrullinated protein antibodies per se: a multicenter cohort study. Arthritis Res Ther 2016;18:285.
9. Demoruelle MK, Wilson TM, Deane KD. Lung inflammation in the pathogenesis of rheumatoid arthritis. Immunol Rev 2020;294:124–132.
10. Perricone C, Ceccarelli F, Saccucci M, et al. Porphyromonas gingivalis and rheumatoid arthritis. Curr Opin Rheumatol 2019;31:517–524.
11. Zhang X, Zhang D, Jia H, et al. The oral and gut microbiomes are perturbed in rheumatoid arthritis and partly normalized after treatment. Nat Med 2015;21:895–905.
12. Kroese JM, Brandt BW, Buijs MJ, et al. Differences in the oral microbiome in patients with early rheumatoid arthritis and individuals at risk of rheumatoid arthritis compared to healthy individuals. Arthritis Rheumatol 2021;73:1986–1993.
13. Rooney CM, Mankia K, Mitra S, et al. Perturbations of the gut microbiome in anti-CCP positive individuals at risk of developing rheumatoid arthritis. Rheumatology (Oxford) 2021;60:3380–3387.
14. He J, Chu Y, Li J, et al. Intestinal butyrate-metabolizing species contribute to autoantibody production and bone erosion in rheumatoid arthritis. Sci Adv 2022;8:eabm1511.
15. Brewer RC, Lanz TV, Hale CR, et al. Oral mucosal breaks trigger anti-citrullinated bacterial and human protein antibody responses in rheumatoid arthritis. Sci Transl Med 2023;15:eabq8476.
16. Demoruelle MK, Harrall KK, Ho L, et al. Anti-citrullinated protein antibodies are associated with neutrophil extracellular traps in the sputum in relatives of rheumatoid arthritis patients. Arthritis Rheumatol 2017;69:1165–1175.
17. Svard A, Kastbom A, Sommarin Y, et al. Salivary IgA antibodies to cyclic citrullinated peptides (CCP) in rheumatoid arthritis. Immunobiology 2013;218:232–237.
18. Roos Ljungberg K, Joshua V, Skogh T, et al. Secretory anti-citrullinated protein antibodies in serum associate with lung involvement in early rheumatoid arthritis. Rheumatology (Oxford) 2020;59:852–859.
19. Otten HG, Daha MR, van der Maarl MGJ, et al. IgA rheumatoid factor in mucosal fluids and serum of patients with rheumatoid arthritis: immunological aspects and clinical significance. Clin Exp Immunol 1992;90:256–259.
20. Chriswell ME, Lefferts AR, Clay MR, et al. Clonal IgA and IgG autoantibodies from individuals at risk for rheumatoid arthritis identify an arthritogenic strain of *Subdoligranulum*. Sci Transl Med 2022;14:eabn5166.
21. Kuhn ML, Zemaitaitis B, Hu LI, et al. Structural, kinetic and proteomic characterization of acetyl phosphate-dependent bacterial protein acetylation. PLoS One 2014;9:e94816.
22. Macek B, Forchhammer K, Hardouin J, et al. Protein post-translational modifications in bacteria. Nat Rev Microbiol 2019;17:651–664.
23. Di Iorio BR, Marzocco S, Bellasi A, et al. Nutritional therapy reduces protein carbamylation through urea lowering in chronic kidney disease. Nephrol Dial Transplant 2018;33:804–813.
24. Walrabenstein W, van der Leeden M, Weijs P, et al. The effect of a multidisciplinary lifestyle program for patients with rheumatoid arthritis, an increased risk for rheumatoid arthritis or with metabolic syndrome-associated osteoarthritis: the "Plants for Joints" randomized controlled trial protocol. Trials 2021;22:715.
25. Walrabenstein W, Wagenaar CA, van der Leeden M, et al. A multidisciplinary lifestyle program for rheumatoid arthritis: the 'Plants for Joints' randomized controlled trial. Rheumatology (Oxford) 2023;62:2683–2691.

26. Aletaha D, Neogi T, Silman AJ, et al. Rheumatoid arthritis classification criteria: An american college of rheumatology/european league against rheumatism collaborative initiative. *Arthritis Rheum* 2010;62: 2569–2581.
27. Brandtzaeg P. Do salivary antibodies reliably reflect both mucosal and systemic immunity? Ann N Y Acad Sci 2007;1098:288–311.
28. Bostanci N, Mitsakakis K, Afacan B, et al. Validation and verification of predictive salivary biomarkers for oral health. Sci Rep 2021;11: 6406.
29. Nissinen R, Leirisalo-Repo M, Nieminen AM, et al. Immune activation in the small intestine in patients with rheumatoid arthritis. Ann Rheum Dis 2004;63:1327–1330.
30. Tajik N, Frech M, Schulz O, et al. Targeting zonulin and intestinal epithelial barrier function to prevent onset of arthritis. Nat Commun 2020;11:1995.
31. Rendek Z, Falk M, Grodzinsky E, et al. Oral omeprazole and diclofenac intake is associated with increased faecal calprotectin levels: a randomised open-label clinical trial. Eur J Gastroenterol Hepatol 2023;35:52–58.
32. Rendek Z, Falk M, Grodzinsky E, et al. Effect of oral diclofenac intake on faecal calprotectin. Scand J Gastroenterol 2016;51:28–32.
33. Hegazy AN, West NR, Stubbington MJT, et al. Circulating and tissue-resident CD4(+) T cells with reactivity to intestinal microbiota are abundant in healthy individuals and function is altered during inflammation. Gastroenterology 2017;153:1320–1337.e16.
34. de Moel EC, Derksen VFAM, Trouw LA, et al. In rheumatoid arthritis, changes in autoantibody levels reflect intensity of immunosuppression, not subsequent treatment response. Arthritis Res Ther 2019; 21:28.
35. Kastbom A, Roos Ljungberg K, Ziegelasch M, et al. Changes in anti-citrullinated protein antibody isotype levels in relation to disease activity and response to treatment in early rheumatoid arthritis. Clin Exp Immunol 2018;194:391–399.

Arthritis & Rheumatology
Vol. 77, No. 3, March 2025, pp 283–297
DOI 10.1002/art.43028

American College of Rheumatology
Empowering Rheumatology Professionals

Targeting Long Noncoding RNA H19 in Subchondral Bone Osteocytes and the Alleviation of Cartilage Degradation in Osteoarthritis

Rongliang Wang,[1] Babak Mehrjou,[2] Dorsa Dehghan-Banian,[3] Belle Yu Hsuan Wang,[4] Qiangqiang Li,[1] Shuai Deng,[5] Chuanhai Liu,[6] Zhe Zhang,[7] Yanlun Zhu,[6] Haixing Wang,[3] Dan Li,[2] Xiaomin Lu,[3] Jack Chun Yiu Cheng,[8] Michael Tim Yun Ong,[9] Hon Fai Chan,[6] Gang Li,[3] Paul K. Chu,[2] and Wayne Yuk Wai Lee[10]

Objective. Emerging evidence suggests long noncoding RNA H19 is associated with osteoarthritis (OA) pathology. However, how H19 contributes to OA has not been reported. This study aims to investigate the biologic function of H19 in OA subchondral bone remodeling and OA progression.

Methods. Clinical joint samples and OA animal models induced by surgical destabilization of the medial meniscus (DMM) were used to verify the causal relationship between osteocyte H19 and OA subchondral bone and cartilage changes. MLO-Y4 osteocyte cells subjected to fluid shear stress were used to verify the mechanism underlying H19-mediated mechanoresponse. Finally, the antisense oligonucleotide (ASO) against H19 was delivered to mice knee joints by magnetic metal–organic framework (MMOF) nanoparticles to develop a site-specific delivery method for targeting osteocyte H19 for OA treatment.

Results. Both clinical OA subchondral bone and wildtype mice with DMM-induced OA exhibit aberrant higher subchondral bone mass, with more H19 mice expressing osteocytes. On the contrary, mice with osteocyte-specific deletion of H19 are less vulnerable to DMM-induced OA phenotype. In MLO-Y4 cells, H19-mediated osteocyte mechanoresponse through PI3K/AKT/GSK3 signal activation by EZH2-induced H3K27me3 regulation on protein phosphatase 2A inhibition. Targeted inhibition of H19 (using ASO-loaded MMOF) substantially alleviates subchondral bone remodeling and OA phenotype.

Conclusion. In summary, our results provide new evidence that the elevated H19 expression in osteocytes may contribute to aberrant subchondral bone remodeling and OA progression. H19 appears to be required for the osteocyte response to mechanical stimulation, and targeting H19 represents a new promising approach for OA treatment.

INTRODUCTION

Osteoarthritis (OA) is a common joint disease characterized by the degradation of articular cartilage, synovial inflammation, and bone remodeling.[1] Many risk factors are reported to incur or exacerbate OA development, such as aging, sex, obesity, and inherent genetic alterations; however, its etiology and pathogenesis remain elusive, and there is yet no disease-modifying drug

This work was mainly supported by the General Research Fund (reference 24121622), University Grants Committee, Hong Kong SAR; and partly by Area of Excellence (reference AoE/M-402/20) and Matching Grant Scheme, University Grants Committee, Hong Kong SAR; the "Start-up Fund" of The Chinese University of Hong Kong; a Rising Star Award provided by the American Society for Bone and Mineral Research; the Center for Neuromusculoskeletal Restorative Medicine (reference CT1.1), Health@InnoHK program, Innovation Technology Commission, Hong Kong SAR.

[1]Rongliang Wang, PhD, Qiangqiang Li, PhD: Department of Orthopaedics and Traumatology, Faculty of Medicine, Prince of Wales Hospital, The Chinese University of Hong Kong, Shatin, Hong Kong SAR, China; Li Ka Shing Institute of Health Sciences, The Chinese University of Hong Kong, Shatin, Hong Kong SAR, China; SH Ho Scoliosis Research Laboratory, Joint Scoliosis Research Center of the Chinese University of Hong Kong and Nanjing University, The Chinese University of Hong Kong, Shatin, Hong Kong SAR, China; and State Key Laboratory of Pharmaceutical Biotechnology, Division of Sports Medicine and Adult Reconstructive Surgery, Nanjing Drum Tower Hospital, The Affiliated Hospital of Nanjing University Medical School, Nanjing, China; [2]Babak Mehrjou, PhD, Dan Li, PhD, Paul K. Chu, PhD: Department of Physics, Department of Materials Science and Engineering, Department of Biomedical Engineering, City University of Hong Kong, Tat Chee Avenue, Kowloon, Hong Kong SAR, China; [3]Dorsa Dehghan-Banian, PhD, Haixing Wang, PhD, Xiaomin Lu, MSc, Gang Li, MBBS, D. Phil: Department of Orthopaedics and Traumatology, Faculty of Medicine, Prince of Wales Hospital, The Chinese University of Hong Kong, Shatin, Hong Kong SAR, China, and Li Ka Shing Institute of Health Sciences, The Chinese University of Hong Kong, Shatin, Hong Kong SAR, China; [4]Belle Yu Hsuan Wang, PhD: Department of Orthopaedics and Traumatology, Faculty of Medicine, Prince of Wales Hospital, The Chinese University of Hong Kong, Shatin, Hong Kong SAR, China; Li Ka Shing Institute of Health Sciences, The Chinese University of Hong Kong, Shatin, Hong Kong SAR, China; and Center for Neuromusculoskeletal Restorative Medicine, CUHK InnoHK Centres, Hong Kong Science Park, Hong Kong SAR, China; [5]Shuai Deng, PhD: Institute for Tissue Engineering and Regenerative Medicine, The Chinese University of Hong Kong, Shatin, Hong Kong SAR, China,

available to slow or reverse OA progression.[2] As one of the critical factors, mechanical loading was reported to exert anticatabolic and anabolic effects on cartilage, resulting in abnormal subchondral bone remodeling.[3] Therefore, reducing loading and/or blocking mechanotransduction in responsive joint tissues has been postulated to modify OA progression.

Subchondral bone remodeling is an important feature of OA pathology that is regarded as an aberrant mechanosensitive response upon injury during OA progression. Such alteration plays a vital role in cartilage degradation.[4] The resultant stiffer subchondral bone in late-stage OA could transmit more shear stresses to overlying cartilage, leading to cartilage splitting and fibrillation.[5] As a result, the disintegration of the subchondral bone physical boundary along OA progression results in more risk exposure in the cartilage environment, including vasculature, oxygen, nutrients, and cytokines.[1] Osteocytes constitute 90% to 95% of the total bone cells and play a major role in sensing and transmitting mechanical stimulation owing to their wide distribution throughout the bone matrix and their complex interconnected lacunocanalicular network.[6] Hence, osteocytes can respond to mechanical signals and secret soluble factors to regulate both osteoclast and osteoblast activities.[7] The intercellular communication required for such a feat is achieved by the production of biomolecules such as prostaglandins (produced by cyclooxygenase 2 [COX-2]), osteoprotegerin (OPG), RANKL, and dentin matrix protein 1 (DMP1).[8] Although some of these biomarkers have been reported to be associated with OA progression,[9–11] the role of osteocytes in OA subchondral bone remains elusive.

Long noncoding RNAs (lncRNAs) is a type of transcript having more than 200 nucleotides without protein encoding function.[12] Several lncRNAs have been found to be associated with OA severity and influence the functions of cells derived from OA joint tissues in vitro. The plausible roles of lncRNAs in various OA phenotypic changes, such as cartilage degradation, synovial inflammation, dysfunction of subchondral bone homeostasis, and meniscus injury, are yet to be elucidated.[13] lncRNA H19 (H19) is the first reported mammalian lncRNA and has been widely studied in different human diseases. Recent evidence primarily indicates an association between H19 and the cartilage and synovium changes in OA without a clear relationship.[14,15] In addition, H19 is involved in maintaining bone quality through regulation of osteoblast differentiation, bone regeneration, and bone metabolism.[16] Notably, H19 has been shown to influence the osteogenic differentiation capacity of bone marrow–derived mesenchymal stromal cells under tensile stimulation.[17] With these, it is reasonable for us to hypothesize that H19 may be able to influence subchondral bone remodeling in OA, particularly in response to altered mechanical alignment, thus potentially contributing to the progression of cartilage erosion and other pathologic changes.

Nanoparticles have been extensively used to deliver drugs and genes to tissue sites of interest for various purposes with no exemption in the OA research field.[18] Recently, the metal–organic frameworks (MOFs) have emerged as a promising tool for gene delivery with high loading capacity, good protection against biologic degradation, and excellent biocompatibility.[19] Furthermore, the modification of physiochemical properties on MOFs, for example, conjugation with the metallic nodes, organic linkers, and other compounds, enables their response to exogenous stimuli, such as a magnetic field for target delivery, thus facilitating localization at specific sites of interest and prolonged release applications.[20] In this study, to explore the translational value of targeting H19 for OA treatment, we developed a specific gene-delivery system by combining Fe_3O_4 nanoparticles and MOFs to form magnetic MOFs (MMOFs) and to transport anti-H19 antisense oligonucleotides (ASOs) to subchondral bone osteocytes in the presence of an external magnetic field for in vivo functional evaluation.

and Key Laboratory for Regenerative Medicine, Ministry of Education, School of Biomedical Sciences, Faculty of Medicine, The Chinese University of Hong Kong, Hong Kong SAR, China; [6]Chuanhai Liu, MD, Yanlun Zhu, PhD, Hon Fai Chan, PhD: Center for Neuromusculoskeletal Restorative Medicine, CUHK InnoHK Centres, Hong Kong Science Park, Hong Kong SAR, China; Institute for Tissue Engineering and Regenerative Medicine, The Chinese University of Hong Kong, Shatin, Hong Kong SAR, China; and Key Laboratory for Regenerative Medicine, Ministry of Education, School of Biomedical Sciences, Faculty of Medicine, The Chinese University of Hong Kong, Hong Kong SAR, China; [7]Zhe Zhang, PhD: Department of Orthopaedics and Traumatology, Faculty of Medicine, Prince of Wales Hospital, The Chinese University of Hong Kong, Shatin, Hong Kong SAR, China; Li Ka Shing Institute of Health Sciences, The Chinese University of Hong Kong, Shatin, Hong Kong SAR, China; and SH Ho Scoliosis Research Laboratory, Joint Scoliosis Research Center of the Chinese University of Hong Kong and Nanjing University, The Chinese University of Hong Kong, Shatin, Hong Kong SAR, China; [8]Jack Chun Yiu Cheng, MBBS, MD, Department of Orthopaedics and Traumatology, Faculty of Medicine, Prince of Wales Hospital, The Chinese University of Hong Kong, Shatin, Hong Kong SAR, China, and SH Ho Scoliosis Research Laboratory, Joint Scoliosis Research Center of the Chinese University of Hong Kong and Nanjing University, The Chinese University of Hong Kong, Shatin, Hong Kong SAR, China; [9]Michael Tim Yun Ong, MBChB, MSc: Department of Orthopaedics and Traumatology, Faculty of Medicine, Prince of Wales Hospital, The Chinese University of Hong Kong, Shatin, Hong Kong SAR, China; [10]Wayne Yuk Wai Lee, PhD: Department of Orthopaedics and Traumatology, Faculty of Medicine, Prince of Wales Hospital, The Chinese University of Hong Kong, Shatin, Hong Kong SAR, China; Li Ka Shing Institute of Health Sciences, The Chinese University of Hong Kong, Shatin, Hong Kong SAR, China; SH Ho Scoliosis Research Laboratory, Joint Scoliosis Research Center of the Chinese University of Hong Kong and Nanjing University, The Chinese University of Hong Kong, Shatin, Hong Kong SAR, China; and Center for Neuromusculoskeletal Restorative Medicine, CUHK InnoHK Centres, Hong Kong Science Park, Hong Kong SAR, China.

Drs R. Wang and Mehrjou contributed equally to this work.

Additional supplementary information cited in this article can be found online in the Supporting Information section (http://onlinelibrary.wiley.com/doi/10.1002/art.43028).

Author disclosures and graphical abstract are available at https://onlinelibrary.wiley.com/doi/10.1002/art.43028.

Address correspondence via email to Wayne Yuk Wai Lee, PhD, at waynelee@cuhk.edu.hk; to Paul K. Chu, PhD, at paul.chu@cityu.edu.hk; or to Gang Li, MBBS, D. Phil, at gangli@cuhk.edu.hk

Submitted for publication October 13, 2023; accepted in revised form September 13, 2024.

MATERIALS AND METHODS

A detailed description of the procedures and specific materials used for micro–computed tomography (micro-CT) analysis, histology and immunohistochemistry, fluorescence in situ hybridization (FISH), MLO-Y4 cell culture, fluid shear stress (FSS), RNA sequencing and analysis, real-time quantitative reverse transcription polymerase chain reaction, Western blot, synthesis of MMOF, in vitro ASO release assay, and in vivo biodistribution is provided in the Supplementary Methods.

Collection of clinical samples. Recruitment of patients was under strict guidance of clinical ethics approval from the Joint Chinese University of Hong Kong-New Territories East Cluster Clinical Research Ethics Committee (CREC-2013.248) and in compliance with the Declaration of Helsinki. Informed consent was obtained before surgery from all patients and their guardians. The subchondral bone tissue samples used in the study were collected from patients with knee OA undergoing joint replacement surgery (five women and seven men with an average ± SD age of 72.75 ± 5.817 years). Then the regions of interest were divided into different parts with a saw blade and subjected to different processing procedures to preserve the sample quality for RNA extraction and histologic and micro-CT analyses. Exclusion criteria were as follows: (1) patients with a history of surgical treatments or severe OA lesions of the lateral compartment or patellofemoral compartment, metabolic arthritis, joint infections, or mechanical pain caused by meniscal tears; (2) patients with malignancy, diabetes, or other severe diseases in the previous five years; and (3) patients with pathologic fractures, concomitant polytrauma or high-energy mechanism of injury.

Animals. The animal use and the experimental protocols were reviewed and approved by the Animal Experimentation Ethics Committee of The Chinese University of Hong Kong (ethical approval number 20-268-MIS). Osteocyte-specific deletion of H19 was obtained by crossing $H19^{fl/fl}$ mice (project number XM200616, Nanjing Biomedical Research Institute of Nanjing University) with transgenic mice expressing Cre recombinase under the control of the Dmp1 gene promoter (strain #: 023047, Jackson Laboratory). Dmp1-Cre^{+} $H19^{fl/fl}$ mice (referred to as conditional knockout [cKO] mice) and control Dmp1-Cre^{-} $H19^{fl/fl}$ (referred to as Flox mice) were used in the subsequent experiments. All mice were on a 100% C57BL/6 background. The primers for genotyping are listed in Supplementary Table 1.

Male C57BL/6 mice and Flox and cKO mice of around 12 weeks old were subjected to destabilization of the medial meniscus (DMM) surgery. From day 1 to day 3 post operation, the mice received buprenorphine (0.3 mg/kg of body weight) daily. The mice were allowed free to food, water, and cage activities after the operation.

In vivo therapeutic efficacy. After one week of DMM surgery, the C57BL/6 mice were randomly divided into six groups. Over a period of seven consecutive weeks, the mice received different treatments: ASO, MMOF, ASO-loaded MMOF at a dosage of 5 mg/kg, or phosphate buffered saline as vehicle control with concurrent six-hour magnetic field exposure once a week. Another group with ASO-loaded MMOF administration without magnetic field exposure served as the control group for magnetic cotreatment. Mice with a sham operation served as the positive control. To apply the external magnetic field, a 5 × 2 × 1–cm magnet was placed beside the targeted knee joint. Before magnetic field exposure, the mice were anesthetized using a mixture of ketamine and xylazine and maintained under isoflurane anesthesia throughout the six-hour period to ensure immobility. Three days after the last administration, the mice were killed to collect their knee joints and major organs for analysis.

Statistical analysis and data availability statement. All data are presented as mean ± SD, and n represents the number of tissue preparations, cells, or animals. In vitro experiments were performed in triplicates. Paired two-tailed Student's *t*-test was used for comparison between injured and uninjured groups of human bone samples. Unpaired two-tailed Student's *t*-test was used for comparison between two groups when data were normally distributed. One-way analysis of variance with relevant post hoc tests was used for multigroup comparisons. A *P* value of 0.05 was considered to be statistically significant using the GraphPad Prism software. The raw data that support the findings of this study will be openly available on publication in the GEO database (GSE254053).

RESULTS

Identification of H19 in subchondral bone alteration of OA. Subchondral bone tissues were collected from patients with OA undergoing total knee replacement surgery. The medial condyle side with severe cartilage erosion was labeled as injured, and the lateral condyle side with relatively intact cartilage was labeled as uninjured for internal control comparison (Figure 1A). Micro-CT showed a remarkable increase in the bone volume fraction in subchondral bone underneath the injured cartilage (Figure 1B, Supplementary Figure 1A and B). Notably, the expression level of the mechanical responsive proteins COX-2, OPG, and DMP1 in subchondral bone osteocytes was upregulated in the injured group (Figure 1B and C). In addition, FISH staining of H19 indicated a significantly higher ratio of H19-positive osteocytes in the subchondral bone of the injured group than that in the uninjured group (Figure 1B and C), which was further confirmed with a high expression level of *H19* observed in the subchondral bone of the injured group (Figure 1D). In the OA mouse model, OA phenotype was successfully developed in the knee joint with the meniscus

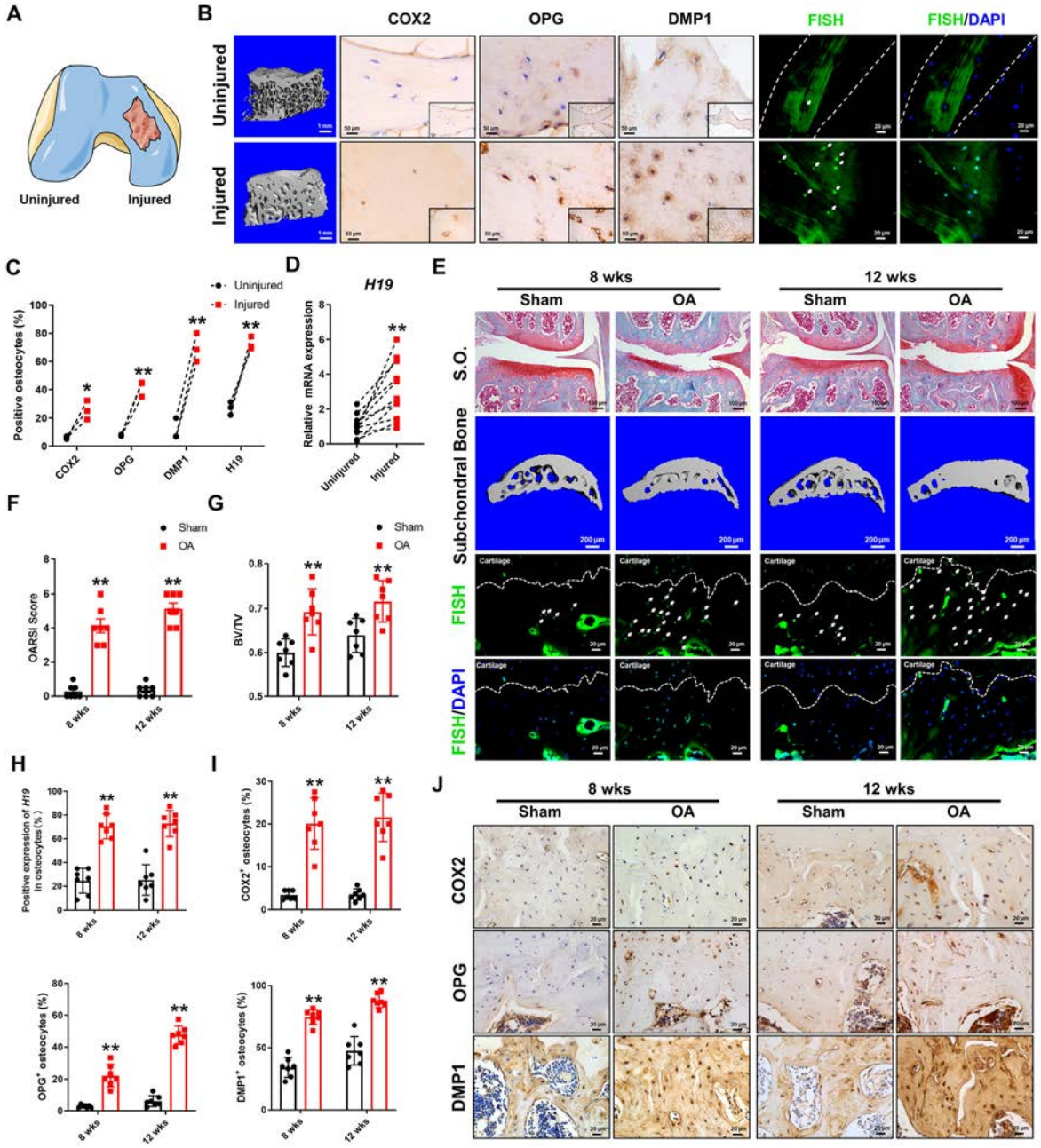

Figure 1. Elevated osteocyte H19 in subchondral bone during OA development. (A) Schematic illustration of the subchondral bone source from human OA samples. (B) Representative micro-CT 3D reconstruction of human OA subchondral bone; IHC staining for COX-2, OPG, and DMP1; and FISH staining of osteocytes counterstained with DAPI in human OA subchondral bone from the uninjured and injured groups (scale bar = 20 μm). (C) Quantification of the number for COX-2, OPG, DMP1, and H19-positive osteocytes in human OA subchondral bone. n = 3 in each group. (D) The expression of *H19* in human OA subchondral bone from the uninjured and injured groups was assessed by qPCR. n = 12 in each group. (E) Representative S.O. staining of knee joints (scale bar = 100 μm), micro-CT 3D reconstruction of subchondral bone (scale bar = 200 μm), FISH staining of osteocytes counterstained with DAPI (scale bar = 20 μm) in subchondral bone from C57BL/6 mice subjected to sham or DMM operation for 8 and 12 weeks. Quantitation of OA severity by (F) OARSI scores, (G) subchondral bone parameter (BV/TV), and (H) the percentage number for H19-positive osteocytes in subchondral bone for C57BL/6 mice subjected to sham or DMM operation for 8 and 12 weeks. n = 7 in each group. (I) The percentage number for COX-2-, OPG-, and DMP1-positive osteocytes in subchondral bone for C57BL/6 mice subjected to sham or DMM operation for 8 and 12 weeks. n = 7 in each group. (J) Representative IHC staining of subchondral bone for COX-2, OPG, and DMP1 in osteocytes from C57BL/6 mice subjected to sham or DMM operation for 8 and 12 weeks. n = 7 in each group (scale bar = 20 μm). *$P < 0.05$; **$P < 0.01$. 3D, three-dimensional; BV/TV, bone volume fraction; COX-2, cyclooxygenase 2; DMM, destabilization of the medial meniscus; DMP1, dentin matrix protein 1; FISH, fluorescence in situ hybridization; IHC, immunohistochemistry; micro-CT, micro–computed tomography; OA, osteoarthritis; OARSI, Osteoarthritis Research Society International; OPG, osteoprotegerin; qPCR, quantitative reverse transcription polymerase chain reaction; S.O., safranin O/fast green.

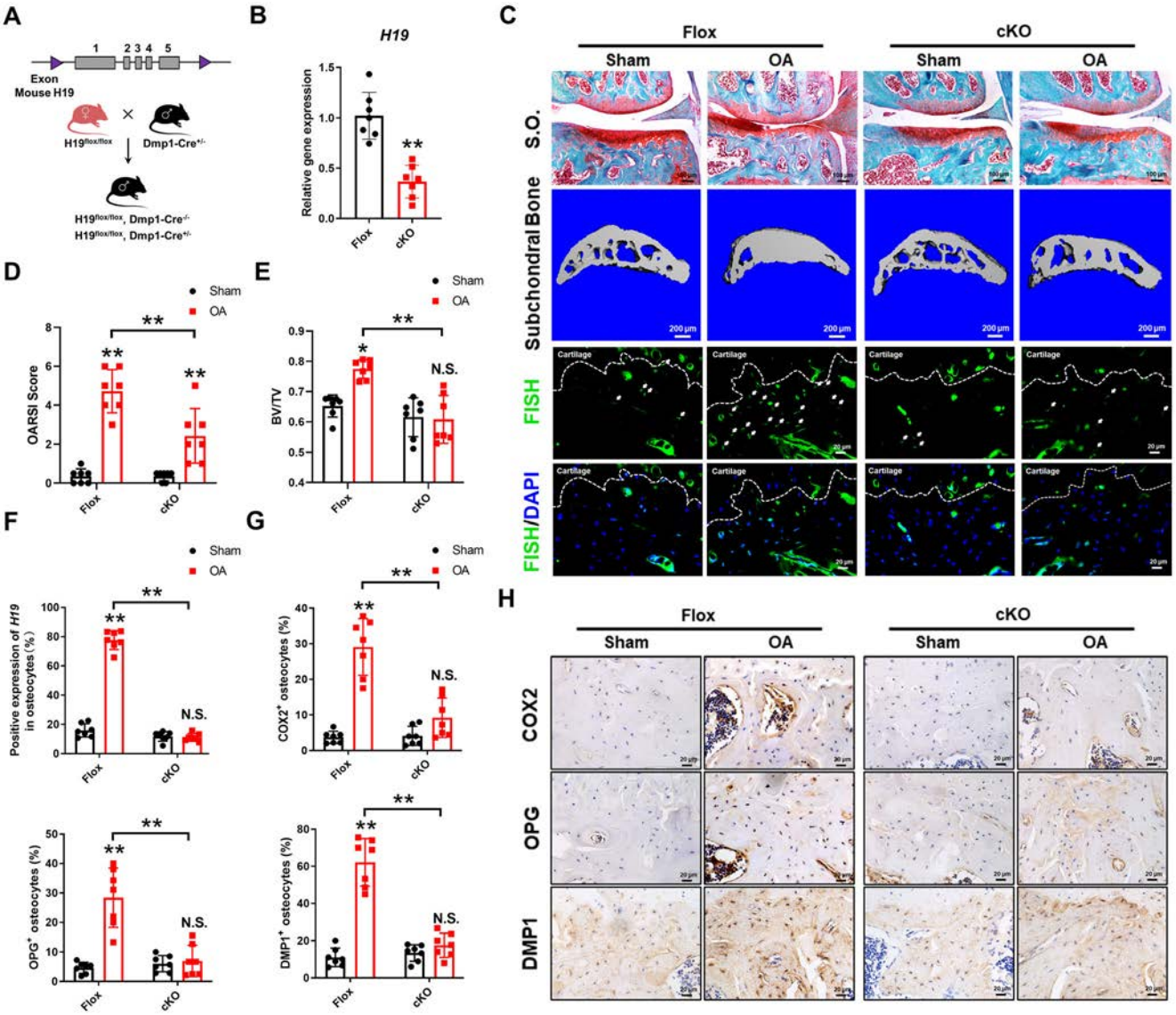

Figure 2. Mice with H19 deficiency are resistant to OA progression and subchondral bone remodeling. (A) Breeding strategy for generation of the osteocyte-specific H19 cKO mice. (B) The expression of *H19* in osteocyte-rich bone tissues of three-month-old male Flox and cKO mice was assessed by qPCR. n = 7 in each group. (C) Representative S.O. staining of knee joints (scale bar = 100 μm), micro-CT 3D reconstruction of subchondral bone (scale bar = 200 μm), and FISH staining of osteocytes counterstained with DAPI (scale bar = 20 μm) in subchondral bone from Flox and cKO mice subjected to sham or DMM operation for eight weeks. (D) Quantitation of OA severity by OARSI scores for three-month-old male Flox and cKO mice subjected to sham or DMM operation for eight weeks. n = 7 in each group. (E) Quantitation subchondral bone parameter (BV/TV) for three-month-old male Flox and cKO mice subjected to sham or DMM operation for eight weeks. n = 7 in each group. (F) Quantitation of the percentage number for H19-positive osteocytes in subchondral bone from Flox and cKO mice subjected to sham or DMM operation for eight weeks. n = 7 in each group. (G) The percentage number for COX-2-, OPG-, and DMP1-positive osteocytes in subchondral bone for three-month-old male Flox and cKO mice subjected to sham or DMM operation for eight weeks. n = 7 in each group. (H) Representative IHC staining of subchondral bone for COX-2, OPG, and DMP1, in osteocytes from Flox and cKO mice subjected to sham or DMM operation for eight weeks (scale bar = 20 μm). **P* < 0.05; ***P* < 0.01. 3D, three-dimensional; BV/TV, bone volume fraction; cKO, conditional knockout; COX-2, cyclooxygenase 2; DMM, destabilization of the medial meniscus; DMP1, dentin matrix protein 1; FISH, fluorescence in situ hybridization; IHC, immunohistochemistry; micro-CT, micro–computed tomography; N.S., no significance; OA, osteoarthritis; OARSI, Osteoarthritis Research Society International; OPG, osteoprotegerin; qPCR, quantitative reverse transcription polymerase chain reaction; S.O., safranin O/fast green. Color figure can be viewed in the online issue, which is available at http://onlinelibrary.wiley.com/doi/10.1002/art.43028/abstract.

removed as shown by extensive lesion of articular cartilage and increased thickness of the subchondral bone at 8 and 12 weeks after DMM surgery (Figure 1E–G and Supplementary Figure 1C). Similar to human OA specimens, the expression of H19, COX-2, OPG, and DMP1 was found to be significantly up-regulated in mice OA joint, particularly in the osteocytes of the subchondral bone region (Figure 1H–J and Supplementary Figure 1D and E). These results suggest that osteocyte H19

expression is up-regulated and associated with abnormal structural changes in response to mechanical stress in OA subchondral bone.

cKO of osteocyte H19 in osteocytes mitigates cartilage damage and subchondral bone sclerosis in OA mouse model. To investigate the effect of osteocyte H19 on OA, we generated osteocyte H19 cKO mice by crossing the $H19^{fl/fl}$ mice (Flox) with the Dmp1-Cre transgenic mice (Figure 2A), which had significantly lower *H19* expression in osteocyte-enriched bone tissues (Figure 2B). At 12 weeks old, the H19 cKO mice were comparable to control Flox mice in terms of size, body weight, and bone quality (Supplementary Figure 2A–D). The knockout efficiency was verified by FISH staining in the trabecular and cortical bone tissues (Supplementary Figure 2E). The Flox mice showed degenerative cartilage damage and subchondral bone sclerosis at eight weeks post DMM surgery, whereas the cKO mice were found nearly invulnerable to DMM-induced cartilage and subchondral bone changes (Figure 2C and 2D and 2E and Supplementary Figure 2F). As expected, the degree of H19 up-regulation in subchondral bone osteocytes diminished in cKO mice (Figure 2C and F), associated with notable decreased protein expression of COX-2, OPG, and DMP1 in the subchondral bone osteocytes (Figure 2G and H). These results provide supporting evidence that H19 up-regulation in subchondral bone osteocytes can promote OA development and subchondral bone alteration.

H19-mediated mechanoresponse in MLO-Y4 cells. To explore the molecular mechanism underlying H19-mediated osteocyte mechanotransduction in OA, we first employed FSS stimulation on MLO-Y4 cells to mimic the mechanical stimulations that osteocytes experience in vivo[21] (Figure 3A). In line with previous studies, the application of FSS on MLO-Y4 cells resulted in the up-regulation of *Ptgs2*, *Tnfrsf11b*, the *Opg/Rankl* ratio, and *Dmp1* Figure 3B. Of note, prior H19 overexpression enhanced the response of MLO-Y4 cells toward FSS-induced up-regulations of these mechanoresponsive genes Figure 3B and Supplementary Figure 3A.[22] In contrast, knockdown of H19 by ASO reduced the mechanoresponse of MLO-Y4 cells to FSS-mediated up-regulation of *Ptgs2*, *Tnfrsf11b*, the *Opg/Rankl* ratio, and *Dmp1* (Figure 3C and Supplementary Figure 3B and C). Then bulk RNA sequencing analysis was conducted to compare ASO-treated and control MLO-Y4 cells upon FSS stimulation to determine the potential underlying mechanism. In brief, the 451 differentially expressed genes were found with expression level change more than 1.5 times in ASO-treated cells upon FSS stimulation. Twenty-six percent of genes were associated with environment information processing according to Kyoto Encyclopedia of Genes and Genomes (KEGG) pathway classification (Figure 3E). Of note, signal transduction was the most enriched one (53.8%), and a gene set enrichment analysis identified that most of the up-regulated genes were related to phosphatidylinositol 3-kinase (PI3K)/protein kinase B (AKT) signaling (Figure 3D and F and Supplementary Figure 3D). Consistent with previous results and RNA sequencing data in which PI3K/AKT signaling activation was involved in osteocyte-mediated intracellular mechanotransduction,[23] phosphorylation of AKT and glycogen synthase kinase 3 (GSK3) increased significantly upon concurrent FSS stimulation and H19 overexpression (Figure 3G). With H19 knockdown, FSS stimulation failed to activate the AKT/GSK3 signaling pathway in MLO-Y4 cells (Figure 3H and Supplementary Figure 3E). The pretreatment of LY290042, a PI3K inhibitor, prevented the up-regulation of H19 on AKT/GSK3 pathway activation and targeted expression of mechanotransduction (Figure 3I and Supplementary Figure 3F). Our data suggest that H19 participates as an enhancer of the PI3K/AKT/GSK3 signaling pathway in the mechanoresponse of osteocytes.

H19-mediated mechanoresponse and mechanotransduction via protein phosphatase 2A regulation. To further investigate the downstream target of H19 on mechanotransduction in osteocytes, we compared the differentially expressed genes related to the PI3K/AKT/GSK3 signaling pathway in ASO-treated and control MLO-Y4 cells upon FSS stimulation. Among the candidate signaling genes dysregulated by H19 reduction, *Ppp2r1a* and *Ppp2r5d* belong to the subunit genes of protein phosphatase 2A (PP2A) complex enzymes (Figure 4A), which is reported to be an important and ubiquitously expressed phosphatase for dephosphorylating AKT.[24] H19 overexpression or depletion, independent of FSS stimulation, influenced *Ppp2r1a* and *Ppp2r5d* expression in osteocytes (Figure 4B and C and Supplementary Figure 3G). To elucidate the role of PP2A in H19-mediated osteocyte mechanotransduction, the cells were pretreated with either DT-601 (PP2A activator) or okadaic acid (OKA; PP2A inhibitor) to interfere with PP2A before FSS stimulation. In the presence of DT-601, the up-regulated expression of *Ptgs2*, *Tnfrsf11b*, the *Opg/Rankl* ratio, and *Dmp1* in response to FSS stimulation and H19 overexpression was abolished (Figure 4D), whereas OKA restored the down-regulated expression of these marker genes caused by H19 knockdown despite the FSS stimulation (Figure 4E and Supplementary Figure 3H). In addition, the AKT/GSK3 signaling pathway activated by H19 overexpression was suppressed by DT-601 (Figure 4F). In contrast, OKA treatment promoted activation of the AKT/GSK3 signaling pathway even in H19 deficiency (Figure 4G and Supplementary Figure 3I). These results indicate that the regulatory effect of H19 on osteocyte mechanotransduction via the AKT/GSK3 signaling pathway can be mediated by PP2A.

To explore the interactions between H19 and PP2A, we first determined the protein expression level of PPP2R1A and PPP2R5D in osteocytes after overexpression or knockdown of

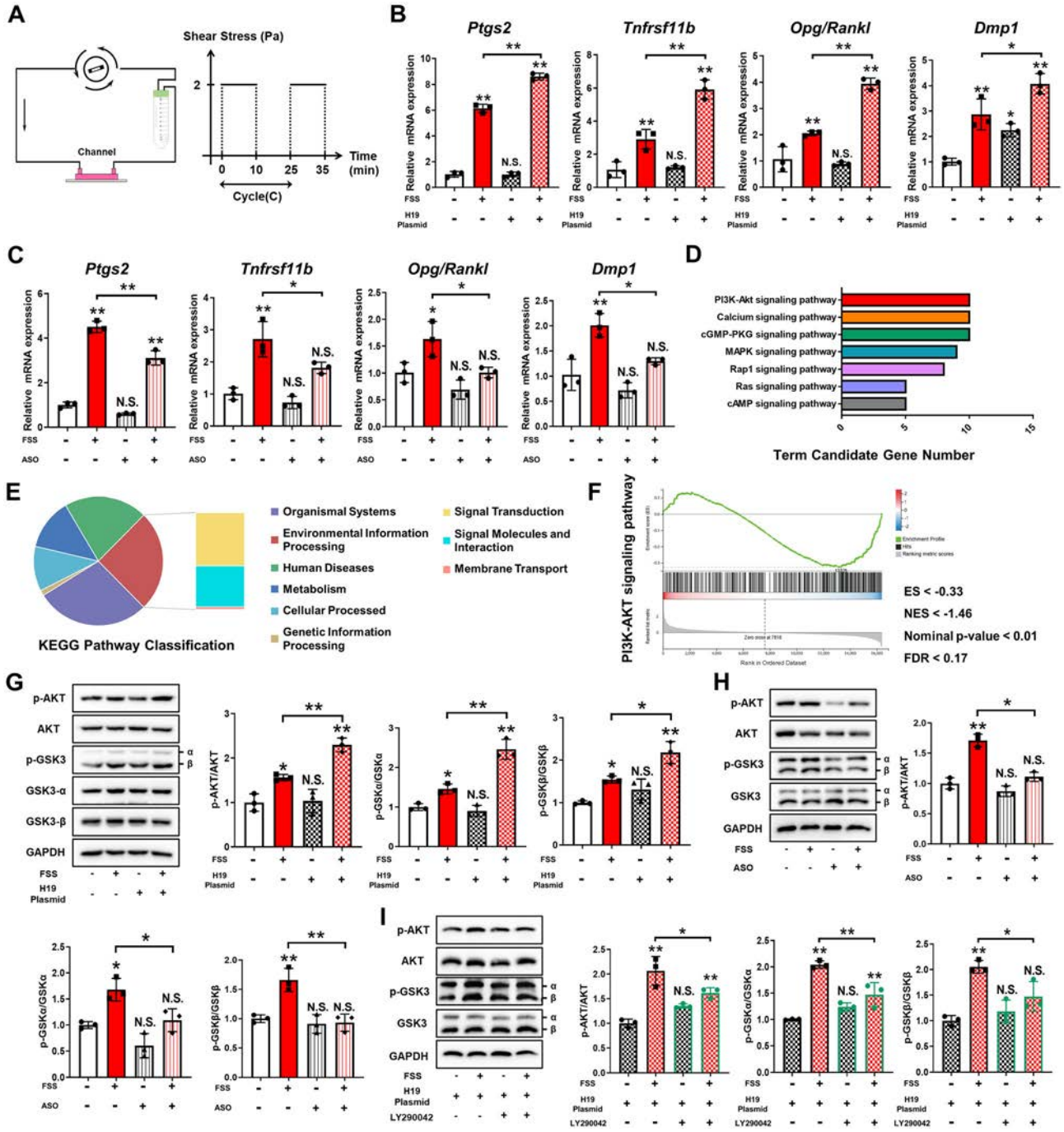

Figure 3. H19-mediated osteocyte mechanoresponse via PI3K/AKT/GSK3 signaling. (A) Schematic illustration showing the in vitro FSS mode. (B) The expression of *Ptgs2*, *Tnfrsf11b*, the *Opg/Rankl* ratio, and *Dmp1* was assessed by qPCR in control or H19-overexpressed MLO-Y4 cells under FSS conditions. n = 3 per group. (C) The expression of *Ptgs2*, *Tnfrsf11b*, the *Opg/Rankl* ratio, and *Dmp1* was assessed by qPCR in control or H19-silenced MLO-Y4 cells under FSS conditions. n = 3 per group. (D) KEGG analysis of the pathway candidate gene number and (E) classification from DEGs in MLO-Y4 cells transfected with control and ASO after FSS stimulation. n = 4 per group. (F) GSEA showing the enrichment of PI3K/AKT signaling pathways in MLO-Y4 cells transfected with control and ASO after FSS stimulation. n = 4 per group. (G) The protein levels of AKT/GSK3 signaling in control or H19-overexpressed MLO-Y4 cells were analyzed by Western blot under FSS conditions. n = 3 per group. (H) The protein levels of AKT/GSK3 signaling in control or H19-silenced MLO-Y4 cells were analyzed by Western blot under FSS conditions. n = 3 per group. (I) The protein levels of AKT/GSK3 signaling in H19-overexpressed MLO-Y4 cells were analyzed by Western blot under FSS conditions with or without pretreatment of LY290042 (10 μM) for 30 minutes. n = 3 per group. $^{*}P < 0.05$; $^{**}P < 0.01$. AKT, protein kinase B; ASO, antisense oligonucleotide; DEG, differentially expressed gene; ES, enrichment score; FDR, false discovery rate; FSS, fluid shear stress; GSEA, gene set enrichment analysis; GSK3, glycogen synthase kinase 3; KEGG, Kyoto Encyclopedia of Genes and Genomes; mRNA, messenger RNA; NES, normalized enrichment score; N.S., no significance; PI3K, phosphatidylinositol 3-kinase; qPCR, quantitative reverse transcription polymerase chain reaction. Color figure can be viewed in the online issue, which is available at http://onlinelibrary.wiley.com/doi/10.1002/art.43028/abstract.

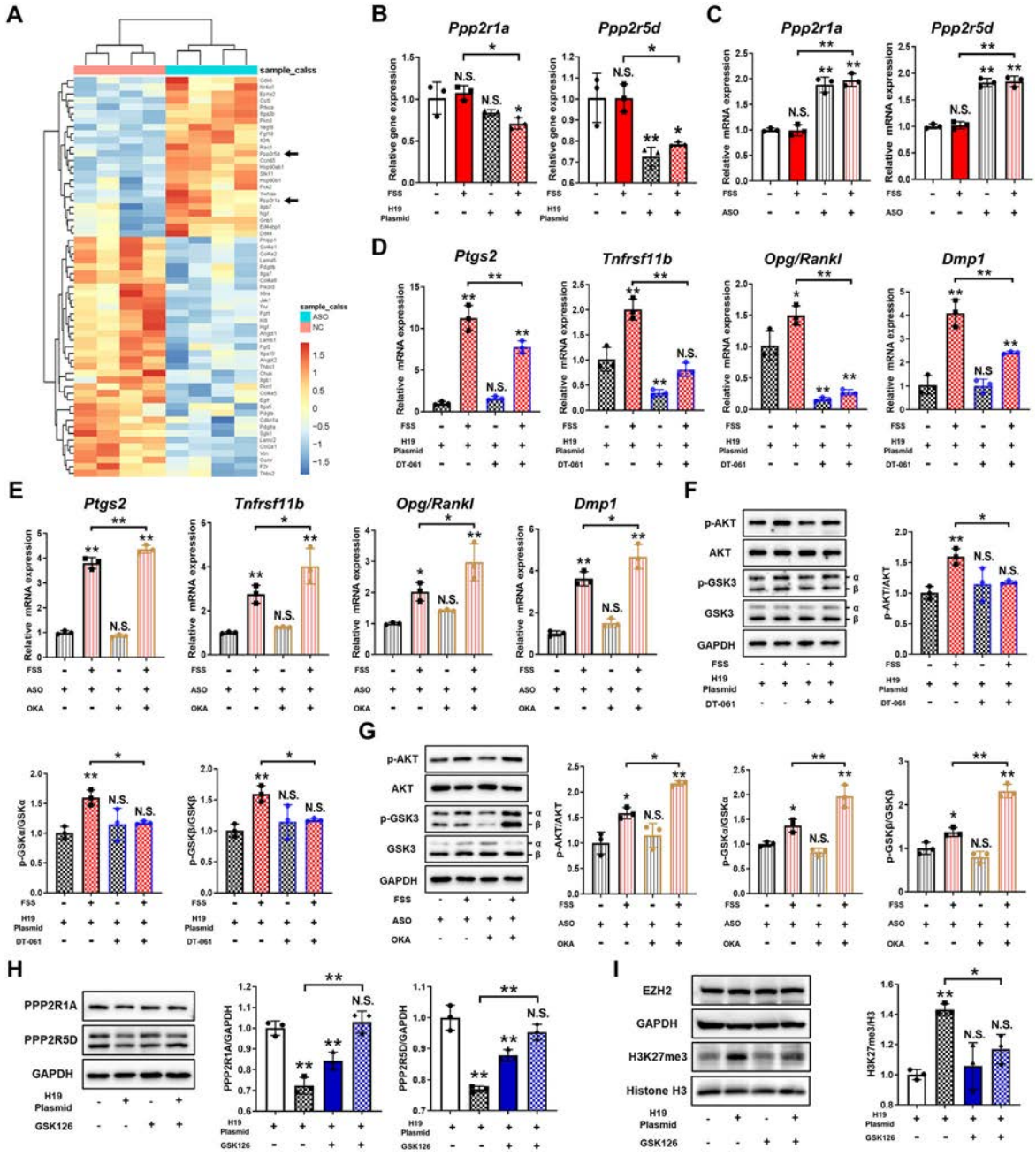

Figure 4. H19-mediated osteocyte mechanoresponse and mechanotransduction via PP2A regulation. (A) Heatmap representing DEGs of PI3K/AKT signaling pathways in MLO-Y4 cells transfected with control and ASO after FSS stimulation. n = 4 per group. The expression of *Ppp2r1a* and *Ppp2r5d* in (B) H19-overexpressed and (C) H19-silenced MLO-Y4 cells was assessed by qPCR under FSS conditions. n = 3 per group. (D) The expression of *Ptgs2*, *Tnfrsf11b*, the *Opg/Rankl* ratio, and *Dmp1* in H19-overexpressed MLO-Y4 cells was assessed by qPCR under FSS conditions with or without pretreatment of DT-061 (10 μM) for 30 minutes. n = 3 per group. (E) The expression of *Ptgs2*, *Tnfrsf11b*, the *Opg/Rankl* ratio, and *Dmp1* in H19-silenced MLO-Y4 cells was assessed by qPCR under FSS conditions with or without pretreatment of OKA (10 n*M*) for 30 minutes. n = 3 per group. (F) The protein levels of AKT/GSK3 signaling in H19-overexpressed MLO-Y4 cells were analyzed by Western blot under FSS conditions with or without pretreatment of DT-061 (10 μM) for 30 minutes. n = 3 per group. (G) The protein levels of AKT/GSK3 signaling in H19-silenced MLO-Y4 cells were analyzed by Western blot under FSS conditions with or without pretreatment of OKA (10 nM) for 30 minutes. n = 3 per group. (H) The protein levels of EZH2 and H3K27me3 were analyzed by Western blot in control or H19-overexpressed MLO-Y4 cells with or without GSK126 (6 μM) treatment for 24 hours. n = 3 per group. (I) The protein levels of PPP2R1A and PPP2R5D were analyzed by Western blot in control or H19-overexpressed MLO-Y4 cells with or without GSK126 (6 μM) treatment for 24 hours. n = 3 per group. $^{*}P < 0.05$; $^{**}P < 0.01$. AKT, protein kinase B; ASO, antisense oligonucleotide; DEG, differentially expressed gene; FSS, fluid shear stress; GSK3, glycogen synthase kinase 3; mRNA, messenger RNA; N.S., no significance; OKA, okadaic acid; PI3K, phosphatidylinositol 3-kinase; PP2A, protein phosphatase 2A; qPCR, quantitative reverse transcription polymerase chain reaction. Color figure can be viewed in the online issue, which is available at http://onlinelibrary.wiley.com/doi/10.1002/art.43028/abstract.

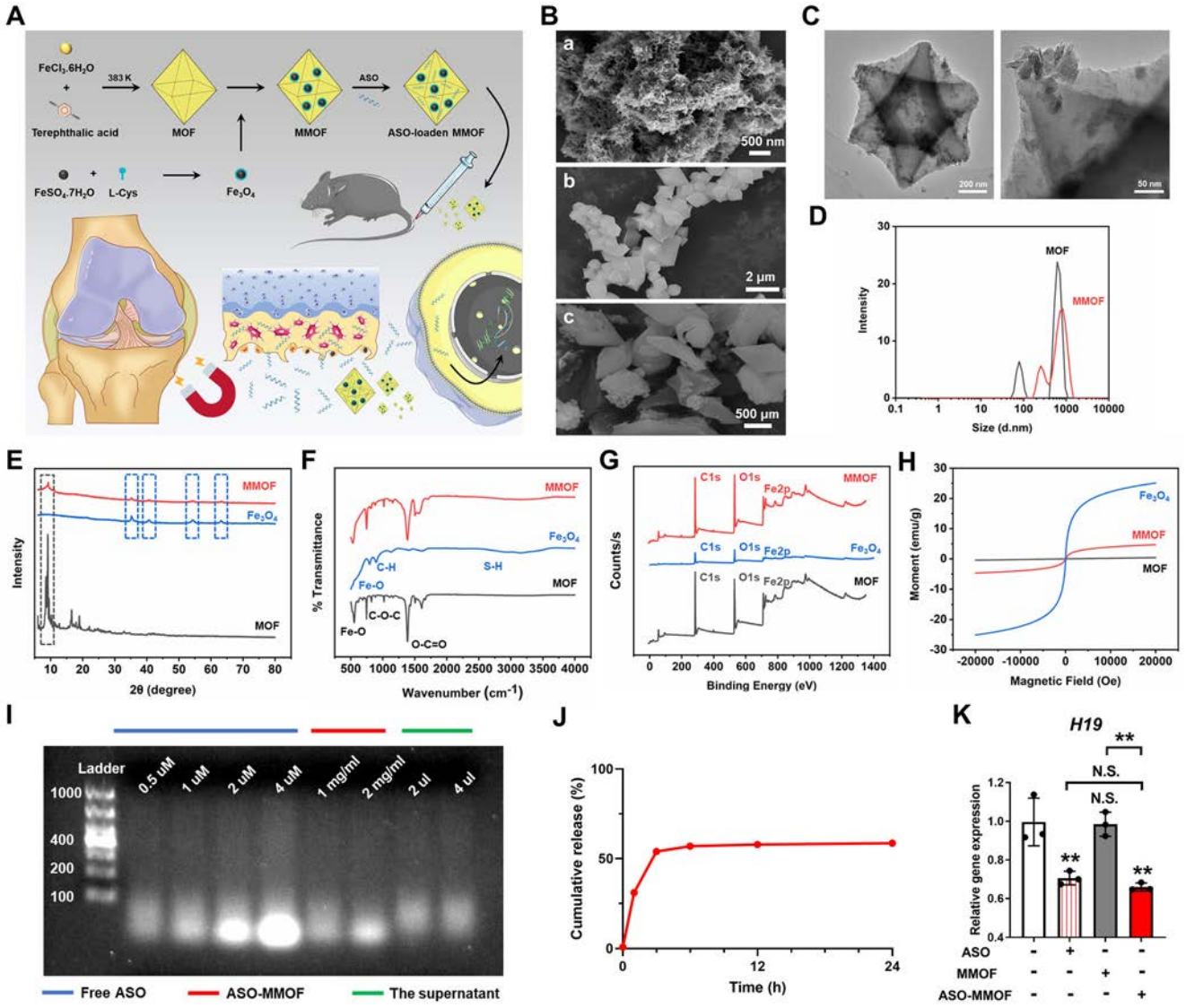

Figure 5. Characterization of MMOF. (A) Schematic illustration for MMOF synthesis. (B) Representative SEM images of (a) Fe_3O_4 (scale bar = 500 nm), (b) MOF (scale bar = 2 μm), and (c) MMOF (scale bar = 500 μm). (C) Representative TEM images of MMOF (scale bar = 200 nm and 50 nm). (D) DLS of MOF and MMOF. The size ranges of MOF with two polydispersity indexes were not affected by the addition of Fe_3O_4. (E) XRD spectra of Fe_3O_4, MOF, and MMOF. Characteristic peaks ascribed to Fe_3O_4 or MOF were marked with blue or black boxes, respectively. (F) FTIR spectra of Fe_3O_4, MOF, and MMOF. Characteristic absorption peaks of chemical bonds to Fe_3O_4 or MOF were marked in blue or black, respectively. (G) Full XPS spectra of Fe_3O_4, MOF, and MMOF. Characteristic spectra of O1s, C1s, and Fe2p of the Fe3O4, MOF, and MMOF were marked in blue, black, or red, respectively. (H) The hysteresis loop of Fe_3O_4, MOF, and MMOF. MOF exhibited magnetic behavior by the addition of Fe_3O_4. (I) DNA gel electrophoresis of ASO-loaded MMOF. The signal of ASO from MMOF (2 mg/mL) was comparable with that from the free ASO (1 μM). (J) Cumulative in vitro ASO release profile of MMOF. (K) The expression of *H19* was assessed by qPCR in MLO-Y4 cells treated with control, ASO, MMOF, and ASO-loaded MMOF. n = 3 per group. $^*P < 0.05$; $^{**}P < 0.01$. ASO, antisense oligonucleotide; DLS, dynamic light scattering; FTIR, Fourier transform infrared spectroscopy; MOF, metal–organic framework; MMOF, magnetic metal–organic framework; N.S., no significance; qPCR, quantitative reverse transcription polymerase chain reaction; SEM, scanning electron microscope; TEM, transmission electron microscopetransmission electron microscope; XPS, x-ray photoelectron spectroscopy; XRD, X-ray diffraction. Color figure can be viewed in the online issue, which is available at http://onlinelibrary.wiley.com/doi/10.1002/art.43028/abstract.

H19. H19 overexpression reduced the protein level of PPP2R1A and PPP2R5D, whereas H19 knockdown induced their protein levels (Supplementary Figure 4A and B), indicating that H19 might be able to negatively regulate the expression of PP2A. Given that H19 was found predominantly in the nuclei of osteocytes (Supplementary Figure 4C) and it was previously reported that EZH2, commonly known as a methyltransferase, could be recruited by H19 and induce trimethylation of lysine (K) at position 27 of histone H3 (H3K27me3),[25] we speculated that EZH2 inhibition might be involved in H19-mediated suppression of PP2A. The inducement of H3K27me3 was confirmed in MLO-Y4 cells by H19 overexpression, which could be significantly inhibited by GSK126 (a selective EZH2 methyltransferase inhibitor) (Figure 4H). Intriguingly, our findings show that EZH2

methyltransferase inhibition increased PPP2R1A and PPP2R5D expressions in a concentration-dependent manner (Supplementary Figure 4D). Furthermore, inhibiting EZH2 could suppress the inhibitory effect of H19 on PPP2R1A and PPP2R5D expressions (Figure 4I). Collectively, our findings suggest the plausible regulatory role of EZH2 via the PP2A-associated signaling pathway on H19-mediated osteocyte mechanotransduction.

Targeting H19 by MMOF nanoparticles. To confirm the H19 potential as a therapeutic target for OA treatment through modulation of subchondral bone remodeling, we designed an MMOF nanoplatform (Figure 5A) to deliver anti-H19 ASO in a controlled manner to the target and to augment its effectiveness when compared with that of systemic injection of ASO alone. Scanning Electron Microscope (SEM) and Transmission Electron Microscope (TEM) were employed to observe the morphology of the synthesized nanoparticles, and the distribution of Fe_3O_4 nanoparticles on the MOF surface was observed (Figure 5B and C). The addition of Fe_3O_4 did not significantly affect the size range of MOF nanoparticles (Figure 5D). The synthesized MOF had Brunauer Emmett Teller (BET) and Langmuir surface areas of around 282 m^2/g and 635 m^2/g, respectively, with a 0.394-cm^3/g pore volume, whereas the presence of iron oxide in MMOF decreased the BET and Langmuir surface area and pore volume to 25.8 m^2/g, 220 m^2/g, and 0.098 cm^3/g, respectively (Supplementary Figure 5J and K). Furthermore, the zeta potential of MMOF was lower (9.7 mV) than that of MOF (around 17 mV) because of the presence of Fe_3O_4 (–6.21 mV) on its surface. After introducing ASO, the zeta potential shifted to a negative value (–3.95 mV) because the synthesized oligonucleotides normally had negative charge,[26,27] and this result proved that ASO was successfully loaded into the particles. The chemical structure of the synthesized powders was studied by X-ray diffraction (XRD) and Fourier transform infrared spectroscopy, which indicated successful synthesizing of Fe_3O_4, MOF, and MMOF (Figure 5E and F). To further analyze their chemical states, the full spectra; the corresponding atomic percentage of Fe, C, and O; and high-resolution spectra of O1s, C1s, and Fe2p of the Fe_3O_4, MOF, and MMOF were acquired by x-ray photoelectron spectroscopy (Figure 5G, Supplementary Table 4, and Supplementary Figure 5A–I). From the full spectra and corresponding atomic contents, it was concluded that because of conjugation of Fe_3O_4 to MOF, the contents of Fe and O increased compared to that of MOF (Supplementary Information). Upon proving the successful synthesis of MMOF, its saturation magnetization value was measured to be 4.69 emu/g, whereas this value for MOF was 0.43 emu/g (Figure 5H), thus making the administrated MMOF able to be guided by the external magnetic field exposure (Supplementary Figure 5L). Taken together, MMOF was successfully made for subsequent experiments.

Next, the presence of the loaded ASO was verified by DNA gel electrophoresis on the supernatant and precipitate of the ASO-loaded MMOF. The precipitate exhibited the characteristic markers of free ASO, whereas free ASO was barely detected from the supernatant, indicating that the ASO was successfully conjugated to the MMOF (Figure 5I) with a loading ratio of 2.185% (weight/weight%) (Supplementary Figure 6A). The ASO release profile indicated that 54% of the ASO released within the first three hours whereas the release percentage reached its maximum (57%) after six hours upon incubation in the releasing medium (Figure 5J). Furthermore, efficient inhibition of *H19* expression in osteocytes upon the in vitro supplementation of MMOF revealed the capability of MMOF in the delivery of the ASO to the cells with suitable bioavailability (Figure 5K).

In vivo treatment of MMOF. In vivo fluorescence imaging was employed to verify the efficient MMOF accumulation in the knee joints under magnetic field exposure. The fluorescence intensity of Indocyanine Green (ICG)-labeled MMOF was predominately accumulated in the target knee joint exposed to the external magnetic field, whereas the contralateral side without magnetic field exposure showed a weak fluorescence signal (Figure 6A and B). The efficient knee joint accumulation of ASO-loaded MMOF upon magnetic field exposure six hours post injection was confirmed because the fluorescence signals in these samples were significantly higher in the knee joint when compared to those without magnetic stimulation across the studied period (Figure 6C and Supplementary Figure 6B). Because MMOF can be retained in the joint for a longer time once exposed to the magnetic field, they have a delayed circulation to other organs upon exposure to the magnetic field. Ex vivo images of the excised organs and knee joints after 24 hours of MMOF injection showed a remarkable fluorescence signal in the liver and kidney, indicating a possible toxicity accumulation for other organs in the subsequent treatment (Figure 6D and Supplementary Figure 6C).

The therapeutic effectiveness of ASO-loaded MMOF was evaluated with a DMM-induced OA mouse model. After eight weeks of treatment, cartilage degradation and subchondral bone sclerosis were significantly alleviated in mice receiving magnet-guided, ASO-loaded MMOF treatment. In the absence of a magnetic field, there was subtle improvement of Osteoarthritis Research Society International scores and subchondral bone sclerosis (Figure 6E–G and Supplementary Figure 6D). The FISH staining results confirmed that ASO-loaded MMOF treatment alone slightly decreased the distribution of osteocyte H19 in the subchondral bone region, whereas considerable inhibition of H19-positive osteocytes was observed once combined with a magnetic field (Figure 6E and H). Upon exposure to a magnetic field, MMOF injection significantly reduced the expression of COX-2, OPG, and DMP1 in OA subchondral bone osteocytes (Supplementary Figure 6E and F). Histologic analysis of the major

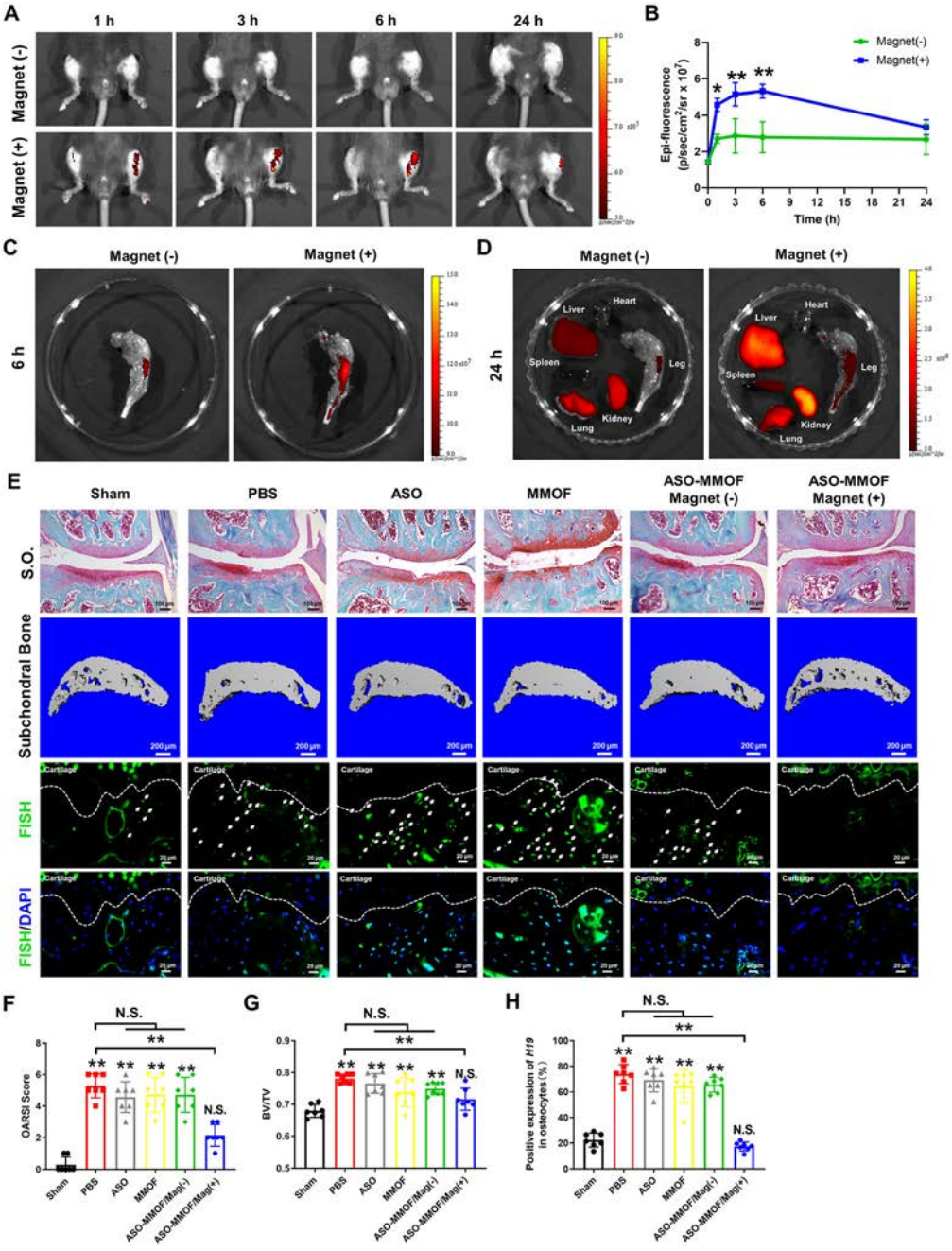

Figure 6. In vivo treatment of MMOF. (A) Fluorescence imaging and (B) fluorescence quantitative assessment in C57BL/6 mice post IV injection of ICG-labeled MMOF with or without six-hour external magnetic field exposure. n = 3 in each group. (C) Fluorescent images of isolated knee joints from C57BL/6 mice at six hours post IV injection of ICG-labeled MMOF with or without six-hour external magnetic field exposure. (D) Fluorescence images of isolated major organs and knee joints from C57BL/6 mice at 24 hours post IV injection of ICG-labeled MMOF with or without six-hour external magnetic field exposure. (E) Representative S.O. staining of knee joints (scale bar = 100 μm), micro-CT 3D reconstruction of subchondral bone (scale bar = 200 μm), and FISH staining of osteocytes counterstained with DAPI (scale bar = 20 μm) in subchondral bone from C57BL/6 mice following the indicated treatments. The mice received different treatments: ASO, MMOF, ASO-loaded MMOF at a dosage of 5 mg/kg or PBS as vehicle control with concurrent six-hour magnetic field exposure once a week. Another group with ASO-loaded MMOF administration without magnetic field exposure served as the control group for magnetic cotreatment. Mice with sham operation served as the positive control. Quantitation of OA severity by (F) OARSI scores, (G) subchondral bone parameter (BV/TV), and (H) the percentage number for H19-positive osteocytes in subchondral bone for C57BL/6 mice following the indicated treatments for seven consecutive weeks. n = 7 in each group. *$P < 0.05$; **$P < 0.01$. 3D, three-dimensional; ASO, antisense oligonucleotide; BV/TV, bone volume fraction; FISH, fluorescence in situ hybridization; ICG, Indocyanine Green; IV, intravenous; micro-CT, micro–computed tomography; MMOF, magnetic metal–organic framework; N.S., no significance; OA, osteoarthritis; OARSI, Osteoarthritis Research Society International; PBS, phosphate buffered saline; qPCR, quantitative reverse transcription polymerase chain reaction; S.O., safranin O/fast green. Color figure can be viewed in the online issue, which is available at http://onlinelibrary.wiley.com/doi/10.1002/art.43028/abstract.

organs showed no pathologic change, suggesting a highly acceptable MMOF biocompatibility in vivo (Supplementary Figure 7A).

DISCUSSION

Subchondral bone is the bone tissue underneath the calcified cartilage and tidemark. Altered subchondral bone remodeling in OA represents abnormal bone formation and bone resorption. Several bone anabolic or catabolic agents targeting osteoclasts and osteoblasts have been under intensive investigation to modulate subchondral bone abnormal remodeling in OA, including bisphosphonates, calcitonin, and strontium ranelate.[28] Apart from osteoblasts and osteoclasts, growing evidence indicates that matrix-embedded osteocytes also play important roles in arthritic subchondral bone remodeling. The causative role of elevated COX-2 expression has been reported in subchondral bone osteocytes in both spontaneous OA and rheumatoid arthritis.[9] COX-2 is one of the factors released by osteocytes upon mechanical stimulation, which modulates bone remodeling.[29] Interestingly, in line with this previous finding, we have found that COX-2 messenger RNA expression (*Ptgs2*) could be positively regulated by H19 during cellular and animal functional experiments. Although our clinical samples did not show a significant correlation between H19 and *Ptgs2*, *Tnfrsf11b*, and *Dmp1* levels (Supplementary Figure 1F), it is important to consider the diverse etiologies of human OA, involving a range of internal and external factors that also influence the expression level[9] of COX-2. In addition, spatial expression patterns of H19 and the target genes in clinical OA samples should be taken into consideration in correlation analysis. Therefore, the complementary role between H19 and COX-2 as well as other mechanoresponsive genes in OA development is warranted for further investigation.

The mechanosensitivity response of osteocytes on abnormal subchondral bone remodeling and OA development is further evidenced by another study ablating osteocyte transforming growth factor β (TGFβ) type II receptor.[30] In addition to the response to mechanical stimulation, the altered osteocyte function, such as matrix metalloproteinase 13–dependent perilacunar/canalicular remodeling in OA subchondral bone, has been reported.[31] This emerging evidence supports the notion of targeting osteocytes for OA treatment. Along this line, we provide fresh evidence on the novel biologic function of H19 in terms of regulating osteocyte mechanoresponse, modulating subchondral bone alteration, and maintaining cartilage homeostasis during OA progression. H19 mediates the mechanotransduction of osteocytes in response to FSS stimulation by repressing PP2A through PI3K/AKT/GSK3 signaling pathway activation. A previous in silico study suggests that H19 is a potential noncoding RNA candidate mediating mechanoresponsive signaling pathways.[32] However, the clinical implication of its mechanoresponse function in OA has not been elucidated. In this study, we identified the PI3K/AKT/GSK3 signaling pathway as one of the key downstream pathways of H19-mediated osteocyte mechanotransduction, which may regulate the downstream Wnt/β-catenin pathway to induce mechanoresponse in osteocytes[33] and lead to a series of consequences, including the release of bioactive factors and interaction with osteoblasts and osteoclasts molecules, resulting in aberrant bone formation in OA subchondral bone.[34] By using MMOF for site-specific anti-H19 ASO delivery, we demonstrated that reducing the H19 level in OA subchondral bone osteocytes is a new therapeutic target for alleviating the progression of cartilage degeneration and subchondral bone sclerosis.

PP2A is one of the major phosphatases and is ubiquitously expressed in all mammalian cells.[35] PP2A is composed of the scaffold subunit (A subunit), the catalytic subunit (C subunit), and the regulatory subunit (B subunit).[36] The PP2A scaffold subunit is encoded by *PPP2R1A*, and *PPP2R5D* encodes the regulatory subunit of PP2A. Both of their mutants have been reported to trigger the hyperphosphorylation of the AKT/GSK3 singling pathway.[37,38] Previous studies showed that inhibition of PP2A could induce apoptosis of chondrocytes through mediating TGFβ1 signaling transduction.[39] In osteocytes, PP2A can participant in 26S proteosome complex formation to maintain a low level of intracellular β-catenin, which is implicated in osteocyte function, such as transmitting signals of mechanical loading.[40] However, how PP2A is involved in osteocyte mechanical signaling transduction in the context of OA has not been reported. Our findings show that PP2A is the downstream target of H19, participating in the regulation of PI3K/AKT/GSK3 pathway activation, which is in line with a previous study showing the link between increased phosphorylation of AKT and aberrant bone formation in subchondral bone remodeling during OA progression.[41] The biologic roles of lncRNAs in epigenetics have been extensively investigated, and DNA methylation is closely linked to the changes in the nucleosome DNA scaffold by recruiting methyltransferases that coordinate individual cellular gene expression.[42] EZH2, the catalytic subunit of polycomb repressive complex 2, is closely associated with gene silencing by trimethylating lysine 27 on histone 3 (H3K27).[43] EZH2-dependent H3K27me3 was reported to influence the expression of PP2A in breast cancer.[44] In the nuclei, the interaction between H19 and EZH2 has drawn researchers' interest.[45] For instance, lncRNA H19 could accelerate bladder cancer metastasis by recruiting EZH2 and enhancing H3K27me3 interaction with target gene transcription.[46] In liver fibrosis, H19 could directly bind to EZH2 to reprogram H3K27me3 profiles and promote excess formation of the extracellular matrix from activated hepatic stellate cells.[47] By using EZH2 methyltransferase inhibitor, our findings suggest that EZH2 might participate as a negative transcriptional regulation of PP2A, thus affecting H19-mediated PP2A expression in

osteocytes. However, further in-depth mechanistic investigation is warranted to elucidate their interaction and impact on osteocytes activity.

This is the first study to investigate the potential therapeutic effect of targeted inhibition of lncRNA H19 in subchondral bone for OA treatment. Growing evidence suggests that lncRNAs can be potential drug targets by using ASOs[48]; however, undesired off-target effects and unspecific biodistribution remain technical hindrances in ASO-based treatment.[49] In recent years, the use of MOF carriers for nucleic acid delivery has emerged as an effective therapeutic strategy because of their ease of preparation, high drug-loading capacity, and good biocompatibility.[50] In addition, MOF as a carrier can be modified to be magnetic responsive,[51] providing a feasible platform to enhance the accumulation at the target site upon external magnetic field exposure, thereby promoting the delivery efficiency of the drug.[52] As far as we known, this study represents the initial endeavor to design and fabricate an MMOF carrier to deliver ASO for H19 silencing in the knee subchondral bone of an OA mouse model, which holds promise for ameliorating cartilage degradation and subchondral sclerosis in OA through a site-specific drug delivery system. The gradual releasing profile of ASO from MMOF further reduces its rapid clearance from the blood stream; thus, persistent effective concentration of ASO at the site of interest could be achieved without the requirement of multiple injections of pure ASO at high dosages.[53] However, it is important to note that our developed ASO-loaded MMOF treatment approach does not exclusively target osteocytes and may also affect other cell types, such as chondrocytes, synoviocytes, vascular cells, and osteoclasts and osteoblasts in OA subchondral bone. Therefore, more investigation is needed to assess the long-term efficacy and side effects of MMOF treatment. Future development of MMOF as a drug delivery carrier in the clinical setting should consider the specificity of site delivery mediated by the magnetic field in view of the complex geometry of the knee joint and the balance of wearing comfort and magnetic field intensity; thus, it is more reasonable to place the magnetic device adjacent to the affected side of the joints of patients.

The findings of the present study have generated additional research questions for future investigation. Firstly, although we have demonstrated that reducing the H19 expression level in subchondral bone osteocytes could ameliorate OA progression, the complicated pathologic changes caused by DMM surgery should be acknowledged, and further investigation on the effect of H19 on other joint compartment tissues during OA progression is warranted. Hence, a noninvasive loading model, such as the ulnar axial loading system and the tibial loading model, could be considered to explore the role and response of H19 in the context of the mechanical stimulation. Secondly, the epigenetic regulation of H19 is unique and complex in osteocyte mechanotransduction, which will further define the role of H19 on influencing target gene expression as an epigenetic modifier. For instance, the direct interaction between the promoter region of PP2A and histone H3K27me3 may provide a new perspective for the mechanism of H19 on PP2A expression. Finally, the biomedical safety of ASO-loaded MOFs remains unexplored, particularly in the assessment of their biologic activity, toxicity to tissue diseases, and drug damage.

ACKNOWLEDGMENTS

This work was mainly supported by the General Research Fund (Ref. No. 24121622), and partly by Area of Excellence (Ref. No. AoE/M-402/20) and Matching Grant Scheme, University Grants Committee, Hong Kong SAR, China; Start-up Fund, The Chinese University of Hong Kong, Hong Kong SAR, China; Rising Star Award provided by American Society for Bone and Mineral Research; Research fund to the Center for Neuromusculoskeletal Restorative Medicine from Health@InnoHK program launched by Innovation Technology Commission, Hong Kong SAR, China. We gratefully acknowledged the support from Nanobiotechnology Laboratory (S106b) of the Biomedical Engineering Department of the Hong Kong Polytechnic University for providing facility for DLS analysis.

AUTHOR CONTRIBUTIONS

All authors contributed to at least one of the following manuscript preparation roles: conceptualization AND/OR methodology, software, investigation, formal analysis, data curation, visualization, and validation AND drafting or reviewing/editing the final draft. As corresponding author, Drs G. Li, Chu, and Lee confirm that all authors have provided the final approval of the version to be published and take responsibility for the affirmations regarding article submission (eg, not under consideration by another journal), the integrity of the data presented, and the statements regarding compliance with institutional review board/Declaration of Helsinki requirements.

DATA AVAILABILITY STATEMENT

RNA seq source data for Figure 3E–F, Figure 4A, Supplements Figure 3D, and Supplementary Data file 1. The raw data that support the findings of this study will be openly available on publication in GEO database (GSE254053).

REFERENCES

1. Goldring SR, Goldring MB. Changes in the osteochondral unit during osteoarthritis: structure, function and cartilage-bone crosstalk. Nat Rev Rheumatol 2016;12(11):632–644.
2. Glyn-Jones S, Palmer AJ, Agricola R, et al. Osteoarthritis. Lancet 2015;386(9991):376–387.
3. Chang SH, Mori D, Kobayashi H, et al. Excessive mechanical loading promotes osteoarthritis through the gremlin-1-NF-κB pathway. Nat Commun 2019;10(1):1442.
4. Hu Y, Chen X, Wang S, et al. Subchondral bone microenvironment in osteoarthritis and pain. Bone Res 2021;9(1):20.
5. Burr DB, Gallant MA. Bone remodelling in osteoarthritis. Nat Rev Rheumatol 2012;8(11):665–673.
6. Tatsumi S, Ishii K, Amizuka N, et al. Targeted ablation of osteocytes induces osteoporosis with defective mechanotransduction. Cell Metab 2007;5(6):464–475.

7. Bonewald LF. The amazing osteocyte. J Bone Miner Res 2011;26(2): 229–238.
8. Klein-Nulend J, Bakker AD, Bacabac RG, et al. Mechanosensation and transduction in osteocytes. Bone 2013;54(2):182–190.
9. Tu M, Yang M, Yu N, et al. Inhibition of cyclooxygenase-2 activity in subchondral bone modifies a subtype of osteoarthritis. Bone Res 2019;7(1):29.
10. Kovács B, Vajda E, Nagy EE. Regulatory effects and interactions of the Wnt and OPG-RANKL-RANK Signaling at the bone-cartilage interface in osteoarthritis. Int J Mol Sci 2019;20(18):4653.
11. Zhang Q, Lin S, Liu Y, et al. *Dmp1* null mice develop a unique osteoarthritis-like phenotype. Int J Biol Sci 2016;12(10): 1203–1212.
12. Kapranov P, Cheng J, Dike S, et al. RNA maps reveal new RNA classes and a possible function for pervasive transcription. Science 2007; 316(5830):1484–1488.
13. Wang R, Shiu HT, Lee WYW. Emerging role of lncRNAs in osteoarthritis: an updated review. Front Immunol 2022;13:982773.
14. Steck E, Boeuf S, Gabler J, et al. Regulation of H19 and its encoded microRNA-675 in osteoarthritis and under anabolic and catabolic in vitro conditions. J Mol Med (Berl) 2012;90(10): 1185–1195.
15. Stuhlmüller B, Kunisch E, Franz J, et al. Detection of oncofetal h19 RNA in rheumatoid arthritis synovial tissue. Am J Pathol 2003; 163(3):901–911.
16. Chen S, Liu D, Zhou Z, et al. Role of long non-coding RNA H19 in the development of osteoporosis. Mol Med 2021;27(1):122.
17. Wu J, Zhao J, Sun L, et al. Long non-coding RNA H19 mediates mechanical tension-induced osteogenesis of bone marrow mesenchymal stem cells via FAK by sponging miR-138. Bone 2018;108: 62–70.
18. Eichaker LR, Cho H, Duvall CL, et al. Future nanomedicine for the diagnosis and treatment of osteoarthritis. Nanomedicine (Lond) 2014;9(14):2203–2215.
19. Guo L, Zhong S, Liu P, et al. Radicals scavenging MOFs enabling targeting delivery of siRNA for rheumatoid arthritis therapy. Small 2022; 18(27):e2202604.
20. Riccò R, Liang W, Li S, et al. Metal-organic frameworks for cell and virus biology: a perspective. ACS Nano 2018;12(1):13–23.
21. Bonewald LF. Mechanosensation and transduction in osteocytes. Bonekey Osteovision 2006;3(10):7–15.
22. Li X, Han L, Nookaew I, et al. Stimulation of Piezo1 by mechanical signals promotes bone anabolism. eLife 2019;8:8.
23. Riquelme MA, Gu S, Hua R, et al. Mechanotransduction via the coordinated actions of integrins, PI3K signaling and Connexin hemichannels. Bone Res 2021;9(1):8.
24. Seshacharyulu P, Pandey P, Datta K, et al. Phosphatase: PP2A structural importance, regulation and its aberrant expression in cancer. Cancer Lett 2013;335(1):9–18.
25. Du Z, Shi X, Guan A. lncRNA H19 facilitates the proliferation and differentiation of human dental pulp stem cells via EZH2-dependent LATS1 methylation. Mol Ther Nucleic Acids 2021;25:116–126.
26. Di Fusco D, Dinallo V, Marafini I, et al. Antisense oligonucleotide: basic concepts and therapeutic application in inflammatory bowel disease. Front Pharmacol 2019;10:305.
27. Sharma VK, Watts JK. Oligonucleotide therapeutics: chemistry, delivery and clinical progress. Future Med Chem 2015;7(16):2221–2242.
28. Zhu X, Chan YT, Yung PSH, et al. Subchondral bone remodeling: a therapeutic target for osteoarthritis. Front Cell Dev Biol 2021;8: 607764.
29. Choi JUA, Kijas AW, Lauko J, et al. The mechanosensory role of osteocytes and implications for bone health and disease states. Front Cell Dev Biol 2022;9:770143.
30. Bailey KN, Nguyen J, Yee CS, et al. Mechanosensitive control of articular cartilage and subchondral bone homeostasis in mice requires osteocytic transforming growth factor β signaling. Arthritis Rheumatol 2021;73(3):414–425.
31. Mazur CM, Woo JJ, Yee CS, et al. Osteocyte dysfunction promotes osteoarthritis through MMP13-dependent suppression of subchondral bone homeostasis. Bone Res 2019;7(1):34.
32. Cai J, Li C, Li S, et al. A quartet network analysis identifying mechanically responsive long noncoding RNAs in bone remodeling. Front Bioeng Biotechnol 2022;10:780211.
33. Kitase Y, Barragan L, Qing H, et al. Mechanical induction of PGE2 in osteocytes blocks glucocorticoid-induced apoptosis through both the β-catenin and PKA pathways. J Bone Miner Res 2010;25(12): 2657–2668.
34. Lin C, Shao Y, Zeng C, et al. Blocking PI3K/AKT signaling inhibits bone sclerosis in subchondral bone and attenuates post-traumatic osteoarthritis. J Cell Physiol 2018;233(8):6135–6147.
35. Shi Y. Serine/threonine phosphatases: mechanism through structure. Cell 2009;139(3):468–484.
36. Xu Y, Xing Y, Chen Y, et al. Structure of the protein phosphatase 2A holoenzyme. Cell 2006;127(6):1239–1251.
37. Haesen D, Abbasi Asbagh L, Derua R, et al. Recurrent PPP2R1A mutations in uterine cancer act through a dominant-negative mechanism to promote malignant cell growth. Cancer Res 2016;76(19): 5719–5731.
38. Papke CM, Smolen KA, Swingle MR, et al. A disorder-related variant (E420K) of a PP2A-regulatory subunit (PPP2R5D) causes constitutively active AKT-mTOR signaling and uncoordinated cell growth. J Biol Chem 2021;296:100313.
39. López-Armada MJ, Caramés B, Cillero-Pastor B, et al. Phosphatase-1 and -2A inhibition modulates apoptosis in human osteoarthritis chondrocytes independently of nitric oxide production. Ann Rheum Dis 2005;64(7):1079–1082.
40. Bonewald LF, Johnson ML. Osteocytes, mechanosensing and Wnt signaling. Bone 2008;42(4):606–615.
41. Sun K, Luo J, Guo J, et al. The PI3K/AKT/mTOR signaling pathway in osteoarthritis: a narrative review. Osteoarthritis Cartilage 2020;28(4): 400–409.
42. Houseman EA, Accomando WP, Koestler DC, et al. DNA methylation arrays as surrogate measures of cell mixture distribution. BMC Bioinformatics 2012;13(1):86.
43. Eich ML, Athar M, Ferguson JE III, et al. EZH2-targeted therapies in cancer: hype or a reality. Cancer Res 2020;80(24):5449–5458.
44. Bao Y, Oguz G, Lee WC, et al. EZH2-mediated PP2A inactivation confers resistance to HER2-targeted breast cancer therapy. Nat Commun 2020;11(1):5878.
45. Guo CJ, Xu G, Chen LL. Mechanisms of long noncoding RNA nuclear retention. Trends Biochem Sci 2020;45(11):947–960.
46. Luo M, Li Z, Wang W, et al. Long non-coding RNA H19 increases bladder cancer metastasis by associating with EZH2 and inhibiting E-cadherin expression. Cancer Lett 2013;333(2):213–221.
47. Li XJ, Zhou F, Li YJ, et al. LncRNA H19-EZH2 interaction promotes liver fibrosis via reprogramming H3K27me3 profiles. Acta Pharmacol Sin 2023;44(12):2479–2491.
48. Chen Y, Li Z, Chen X, et al. Long non-coding RNAs: from disease code to drug role. Acta Pharm Sin B 2021;11(2):340–354.
49. Nakamura A, Ali SA, Kapoor M. Antisense oligonucleotide-based therapies for the treatment of osteoarthritis: opportunities and roadblocks. Bone 2020;138:115461.

50. Cai W, Wang J, Chu C, et al. Metal-organic framework-based stimuli-responsive systems for drug delivery. Adv Sci (Weinh) 2018;6(1): 1801526.
51. Chung CW, Liao BW, Huang SW, et al. Magnetic responsive release of nitric oxide from an MOF-derived Fe_3O_4@PLGA microsphere for the treatment of bacteria-infected cutaneous wound. ACS Appl Mater Interfaces 2022;14(5):6343–6357.
52. Zhang M, Hu W, Cai C, et al. Advanced application of stimuli-responsive drug delivery system for inflammatory arthritis treatment. Mater Today Bio 2022;14:100223.
53. Miao YB, Pan WY, Chen KH, et al. Engineering a nanoscale Al-MOF-armored antigen carried by a "trojan horse"-like platform for oral vaccination to induce potent and long-lasting immunity. Adv Funct Mater 2019;29(43):1904828.

Arthritis & Rheumatology
Vol. 77, No. 3, March 2025, pp 298–310
DOI 10.1002/art.43017

American College of Rheumatology
Empowering Rheumatology Professionals

Urinary Biomarkers Associated With Pathogenic Pathways Reflecting Histologic Findings in Lupus Nephritis

Kazuoto Hiramoto,[1] Shuntaro Saito,[1] Hironari Hanaoka,[1] Jun Kikuchi,[1] Hiroyuki Fukui,[1] Akinori Hashiguchi,[1] Katsuya Suzuki,[1] Tsutomu Takeuchi,[2] and Yuko Kaneko[1]

Objective. There is a pressing need to understand the pathogenesis of histologic findings and identify the biomarkers for predicting the histologic severity in lupus nephritis (LN). This study aimed to identify the pathogenic signal pathway and elucidate urinary biomarkers for predicting the presence or severity of histologic findings in LN.

Methods. Urine samples from patients with biopsy-proven active LN were screened for 1,305 proteins using an aptamer-based proteomic assay. The diversity and expansion of individual renal histologic features in LN were quantified to identify the urinary proteins associated with the histologic findings found in each score. Candidate urinary proteins were validated in a validation cohort. Immunohistochemical staining of the renal tissues was performed to clarify the localization of the candidate proteins.

Results. Cluster analysis extracted five histologic subgroups according to their correlations with each histologic finding in LN. Protein groups that correlated with each histologic subgroup revealed a distinct pathogenesis in LN using pathway analyses. Enzyme-linked immunosorbent assay validation revealed that urinary calgranulin B (S100A9), monocyte chemotactic protein 1 (MCP-1), and insulin-like growth factor binding protein 5 (IGFBP-5) levels could specifically predict the presence and severity of active glomerular lesions, interstitial inflammation, and interstitial fibrosis, respectively. Immunohistochemical staining revealed the localization of these proteins in each lesion.

Conclusion. Renal histologic findings may reflect the different pathogeneses involved in each lesion, and estimating the urinary calgranulin B, MCP-1, and IGFBP-5 levels may be useful in predicting the presence and severity of histologic findings in LN.

INTRODUCTION

Systemic lupus erythematosus (SLE) is a common autoimmune disease that affects young female patients and causes a variety of organ disorders.[1] Half of the patients with SLE develop lupus nephritis (LN), and 10% to 15% of patients with LN develop end-stage renal disease.[2,3] LN has six classifications according to its glomerular lesions based on the International Society of Nephrology/Renal Pathology Society (ISN/RPS) classification. However, this classification is not precise enough to evaluate and quantify the accurate progression or expansion of lesions, which leads to the necessity to add activity and chronicity indices defined by the National Institutes of Health (NIH) to ISN/RPS classification.[4] In addition, it is important to evaluate chronic tubulointerstitial lesions, which better reflect renal prognosis.[5–7] Therefore, renal biopsy is still the gold standard for the definitive diagnosis and classification of LN, and its severity is determined by various pathologic parameters.[8] However, renal biopsy is an invasive procedure that accompanies bleeding in various degrees and is not feasible in cases with associated complications and risk factors. Therefore, the development of noninvasive predictive biomarkers for renal histopathological findings is a great unmet need in clinical practice.

The role of urinary biomarkers in diagnosing LN and predicting relapse has been recognized, and many candidate proteins have been reported for this purpose.[9] Recently, proteomic

Supported by Mitsubishi Tanabe Pharma Corporation.
[1]Kazuoto Hiramoto, MD, Shuntaro Saito, MD, PhD, Hironari Hanaoka, MD, PhD, Jun Kikuchi, MD, PhD, Hiroyuki Fukui, MD, Akinori Hashiguchi, MD, PhD, Katsuya Suzuki, MD, PhD, Yuko Kaneko, MD, PhD: Keio University School of Medicine, Tokyo, Japan; [2]Tsutomu Takeuchi, MD, PhD: Keio University School of Medicine, Tokyo, Japan and Saitama Medical University, Saitama, Japan.

Drs Hiramoto and Saito contributed equally to this work.

Additional supplementary information cited in this article can be found online in the Supporting Information section (http://onlinelibrary.wiley.com/doi/10.1002/art.43017).

Author disclosures are available at https://onlinelibrary.wiley.com/doi/10.1002/art.43017.

Address correspondence via email to Yuko Kaneko, MD, PhD, at ykaneko.z6@keio.jp.

Submitted for publication December 5, 2023; accepted in revised form September 19, 2024.

approaches have been used to identify serum and urine proteins as unbiased screening biomarkers in LN.[10–13] However, all these studies identified urinary biomarkers by comparing patients with active LN and healthy controls. Hence, these studies did not consider the various differences in histologic characteristics between active and chronic lesions in LN. Recently, the Accelerating Medicines Partnership study reported urine biomarkers associated with each renal histologic finding, according to the NIH activity and chronicity index.[14,15] However, biomarkers that can predict the progression of individual lesions remain unidentified. This study aimed to identify the pathogenic signal pathway in LN and elucidate urinary biomarkers for predicting the presence or severity of histologic findings of LN by precisely evaluating renal histology.

PATIENTS AND METHODS

Patients and sample preparation. Consecutive patients with biopsy-proven class III/IV, III/IV+V, or V LN were recruited from Keio University Hospital. Samples from two cohorts were used: (1) a discovery cohort for screening, including patients with LN (n = 24) and diabetic nephropathy (n = 3) diagnosed by renal biopsy, and (2) a validation cohort for enzyme-linked immunosorbent assay (ELISA) validation, including patients with LN (n = 24). Serum and urine samples were collected within one week before renal biopsy and treatment intensification. Clean-catch midstream urine samples were collected in sterile containers and refrigerated within one hour after collecting the samples. Blood samples were collected, and the serum was immediately separated by centrifugation. The samples were then aliquoted and stored at –80°C. The clinical data at the time of sample collection were recorded. Informed consent was obtained from all patients, and the study was approved by the Ethics Committee of our institution (Keio University School Hospital, approval number 20140093).

Aptamer-based screening. Serum and urine samples obtained from patients in the discovery cohort were analyzed by screening with a slow off-rate modified DNA aptamer–based capture array (SOMAscan; SomaLogic), which is a comprehensive high-throughput proteomic assay using an Agilent microarray readout that measures 1,305 proteins.[16] This assay is based on interactions between the aptamers and proteins in a sample. First, aptamer-coated streptavidin beads were added to the sample to allow the aptamers to bind to the proteins. Next, the bound proteins were tagged with biotin, and the aptamer–protein complexes were released from the streptavidin beads. These aptamer–protein complexes were then recaptured on a second set of streptavidin beads, and aptamers were released from these proteins. Finally, the aptamers were hybridized to complementary sequences on a microarray chip and quantified by fluorescence. Concentrations were measured for 1,305 proteins, and the results were calculated as relative fluorescent units (RFU). RFU is related to the amount of protein in the original sample. These RFU values were standardized by urinary creatinine concentration.

Histologic scoring system. We evaluated renal histologic findings more quantitatively than the ISN/RPS lesion definitions and classification of renal involvement or the NIH activity and chronicity index by developing the original scoring system.[17,18] The scoring system included a total of 20 renal histologic findings, including 16 glomerular lesions and 4 tubulointerstitial lesions (Supplementary Tables 1 and 2). The renal histology was evaluated using a light microscope. Light microscopy specimens were embedded in paraffin, sectioned, and stained with hematoxylin-eosin, periodic acid-Schiff, periodic acid-silver methenamine, and Masson's trichrome reagent. Each glomerular histologic finding was scored using two methods. (1) For endocapillary hypercellularity and subendothelial deposits, the percentage of lesions in the total glomerular capillary tuft was calculated in the range of 0% to 100%, and the percentage was defined as the score of one glomerulus. The average score of all glomeruli was used as the histologic score of each case. (2) For histologic findings of glomeruli other than those described previously, the presence or absence of lesions was evaluated. The percentage of glomeruli with lesions was calculated in the range of 0% to 100%, and this percentage was used as the histologic score of each case. For tubulointerstitial lesions, the percentage of lesions relative to the whole area of the tubulointerstitium was calculated in the range of 0% to 100%, and the percentage was used as the score of each case. For glomerular lesions, a score was calculated for each glomerulus, and the average of the scores of all glomeruli was used as the histologic score of the case. Histologic scores were assigned by two skilled raters (KH and SS) supervised by a pathologist (AH), and the mean of the two was used for correlation analysis. This scoring system can quantify the diversity and expansion of renal histologic features in LN more precisely than the ISN/RPS classification or the NIH activity and chronicity index because it includes the same or more items as the existing evaluation systems.

Validation studies using ELISA. ELISA tests were performed on candidate urinary proteins that correlated with specific histologic scores in the discovery cohort. The correlation between the ELISA test results and renal histologic scores in the validation cohort was then confirmed. The concentrations of urinary proteins, including calgranulin B (Cloud-Clone), S100A12 (R&D Systems), high mobility group N1 (HMGN1) (Cloud-Clone), interleukin-8 (IL-8) (R&D Systems), allograft inflammatory factor 1 (AIF-1) (Cloud-Clone), superoxide dismutase 1 (SOD1) (RayBiotech), monocyte chemotactic protein 1 (MCP-1) (R&D Systems), FSTL3 (R&D Systems), and insulin-like growth factor binding protein 5 (IGFBP-5) (R&D Systems), were measured

using ELISA. Absolute urinary protein levels were determined using standard curves run on each ELISA plate and standardized by the urinary creatinine concentration.

Immunohistochemistry. Immunohistochemical staining of the renal tissues was performed using a Leica BOND MAX Immunostainer (Leica Biosystems) for calgranulin B, MCP-1, and IGFBP-5. After deparaffinization, the renal tissues were stained with BOND Epitope Retrieval Solution 1 (AR9961, Leica Biosystems) for calgranulin B and BOND Epitope Retrieval Solution 2 for MCP-1 and IGFBP-5 (AR9640, Leica Biosystems). For immunohistochemical staining, the renal tissues were incubated with 1:2,000 diluted mouse monoclonal anti–calgranulin B (TA804091S, OriGene Technologies), 1:100 diluted mouse monoclonal anti–MCP-1 (MAB 679, R&D Systems), and 1:50 diluted mouse monoclonal anti–IGFBP-5 (MAB875, R&D Systems) antibodies. BOND Polymer Refine Detection (DS9800; Leica Biosystems) was used as the secondary antibody.

Data analysis. The JMP software version 15 (SAS Institute) was used for statistical analysis. Group comparisons were performed using the Wilcoxon rank sum test. Receiver operating characteristic (ROC) curve analysis was performed to analyze the sensitivity, specificity, and cutoff values of the biomarkers for renal histopathological findings. From the data of the aptamer-based screening assay and histologic scores, a heatmap of the correlation coefficients was created, and cluster analysis was performed using the Python 3.9 (Python Seaborn package) programming. Spearman's rank correlation and Pearson's correlation coefficients were used for correlation related to aptamer-based screening–measured and ELISA-measured data, respectively. There were two reasons for using Spearman's correlation in the screening phase of this study: (1) The measurements by SOMAscan themselves may not reflect precise concentrations and could show considerable variability in results, and (2) ranking was necessary when extracting specific clusters of urinary proteins during cluster analysis. Euclidean distance was used for the distance matrix, and Ward's method was used for hierarchical clustering.

The Enrichr web tool (open source available from https://amp.pharm.mssm.edu/Enrichr) was used to determine the cellular origin of the proteins that correlated with individual clusters of renal lesions. Ingenuity pathway analysis (IPA) was used to ascertain which known pathways were enriched by proteins that were highly correlated with individual clusters of renal lesions. Data were analyzed using IPA (QIAGEN Inc, https://www.qiagen.com/us). Protein–protein interaction (PPI) analysis was performed to identify interactions between individual clusters of renal lesions and highly correlated proteins. The PPI database STRING (available from https://string-db.org/) was used, and clustering was performed with the k-means method. All data relevant to the study are included in the article or uploaded as online supplementary information.

RESULTS

Cluster analysis with histologic score and aptamer-based protein screening. Urine and blood samples from 24 patients with LN (class III/IV = 14, III/IV+V = 6, V = 4) were used in the discovery cohort, and urine samples from 24 patients with LN (class III/IV = 10, III/IV+V = 6, V = 8) were used in the validation cohort. The clinical characteristics and renal histologic scores of the discovery, validation, and diabetic nephropathy groups are presented in Supplementary Tables 3 and 4, respectively. The LN classification based on the renal pathology score completely matched the ISN/RPS classification, which was assessed by a pathologist. The two raters have shown good interrater reliability for histologic assessments in the discovery and validation cohorts (κ values of 0.62 to 0.95 for the presence or absence of 20 renal histologic findings).

We first performed a cluster analysis on 20 pathology items according to the correlation between each item and the histologic score. Cluster analysis of the 20 renal histologic findings identified five clusters (Figure 1A). Cluster 1 (extracapillary lesions) included cellular or fibrocellular crescents, fibrinoid necrosis, adhesions, and fibrous crescents. Cluster 2 (endocapillary lesions) included only active lesions within the glomerular tuft, including endocapillary hypercellularity, neutrophil infiltration, subendothelial deposits, and karyorrhexis. Cluster 3 (membranous and mesangial lesions) included basement membrane and mesangial lesions. Cluster 4 (tubulointerstitial lesions) contained all tubulointerstitial lesions but not glomerular lesions. Cluster 5 (other lesions) included two minor lesions: podocyte hypertrophy and collapsed glomeruli.

Subsequently, the correlation between the histologic scores and 1,305 urinary proteins was evaluated via cluster analysis for each of the five histologic clusters. For each protein, we calculated the sum of the ranks of correlation coefficients with each histologic score included in the histologic clusters. Then the mean ranks of the correlation coefficients of the proteins for each urinary protein subgroup (UG) were compared, and the UGs with the highest ranks were identified. In clusters 1, 2, and 4, UGs (UG1, 2, and 4, respectively) with high correlation coefficients for each histologic score were identified (Figure 1B and C). UG1, 2, and 4 contained 119, 59, and 85 urinary proteins, respectively (Figure 1D). These UGs shared the same proteins with each other to some extent, although the number of common proteins was less than that of each noncluster overlapping protein between UG1 and UG4 or UG2 and UG4. Notably, UG1 shared more than half of the same proteins with UG2. No urinary protein cluster with high correlation coefficients was extracted in clusters 3 and 5. Hence, we focused on UG1, 2, and 4 in our subsequent analyses. Representative renal histologic findings from clusters

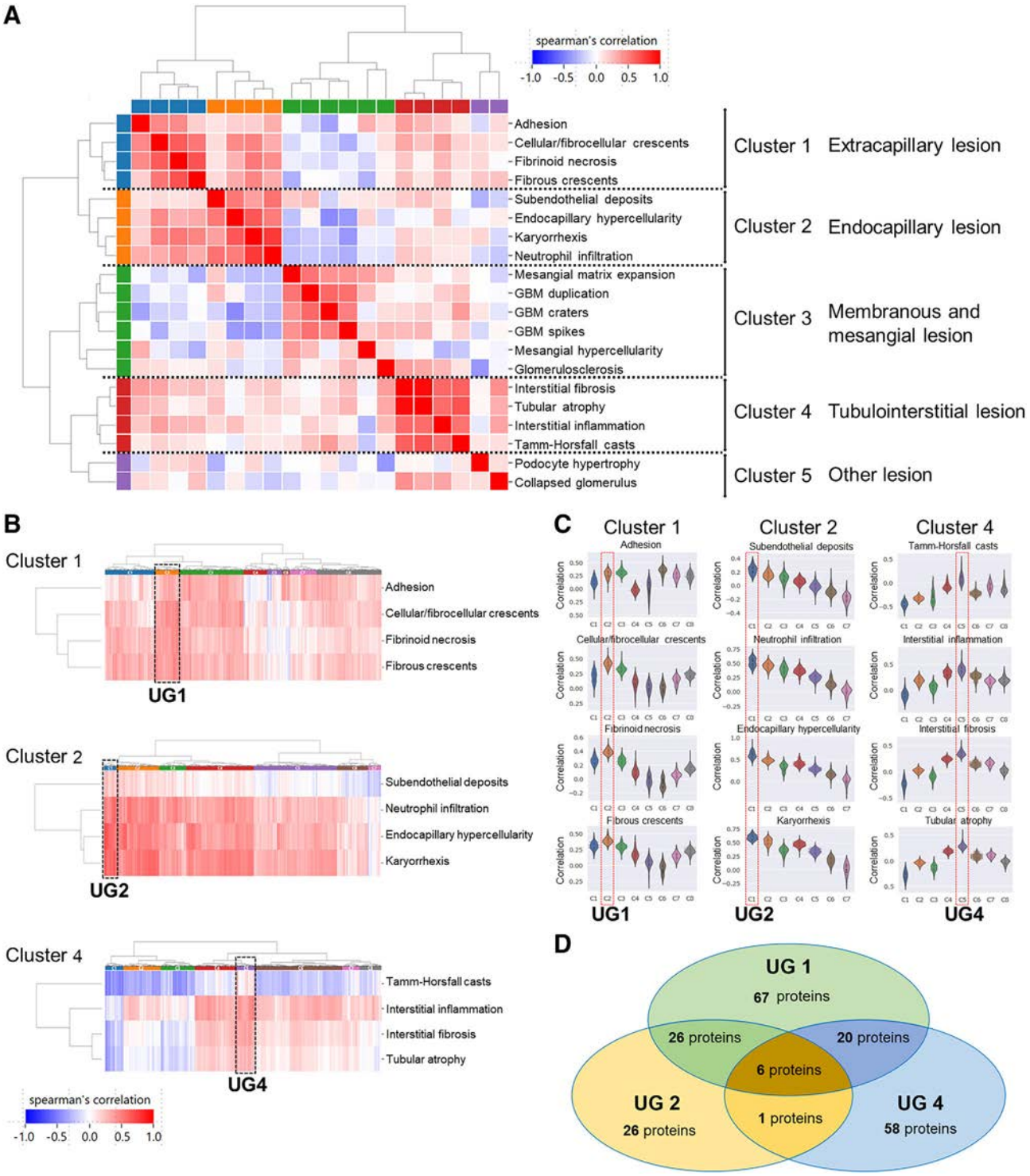

Figure 1. Cluster analysis with histologic score and aptamer-based protein screening. (A) Cluster analysis performed on 20 pathology items according to the correlation among each histologic score. (B and C) Extracted UGs with high correlation coefficients for each histologic score in clusters 1, 2, and 4 (UG1, 2, and 4, respectively). (D) Venn diagram of urinary protein numbers in UG1, 2, and 4. GBM, glomerular basement membrane; UG, urinary protein subgroup.

1, 2, and 4 are shown in Supplementary Figure 1. We also created heatmaps of correlation coefficients among each protein group (UG1, 2, and 4) and 20 histologic findings as a supplementary analysis (Supplementary Figure 2).

Cell-type enrichment analysis. Cell-type enrichment analysis revealed that different cell types were associated with urinary protein molecules in each subgroup (Figure 2A). UG1 was characterized by an abundance of proteins derived from

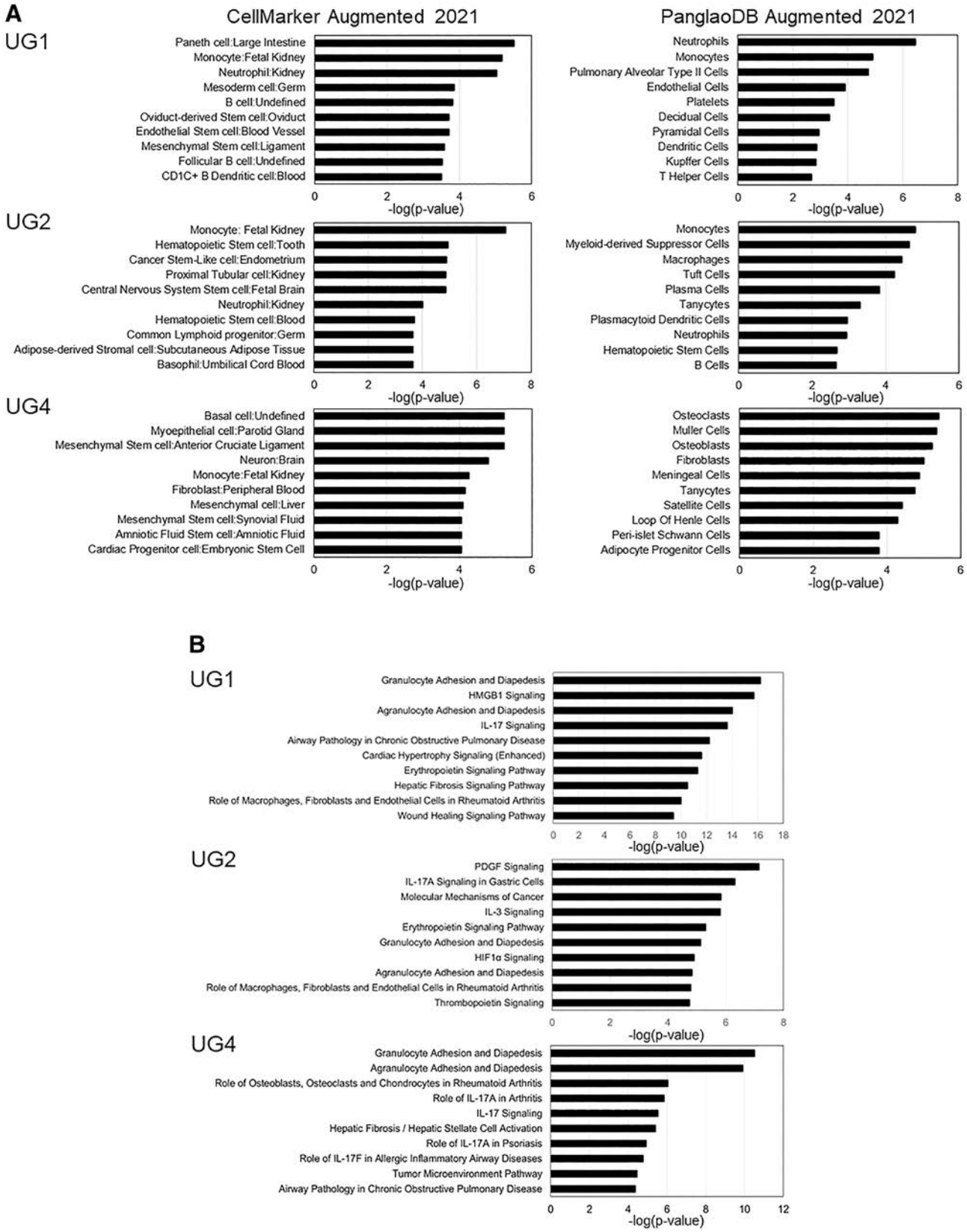

Figure 2. Cell-type enrichment analysis and canonical pathways by IPA in each subgroup. (A) Cell-type enrichment analysis is performed using the CellMarker and PanglaoDB databases on the Enrichr platform. (B) The top 10 canonical pathways determined by IPA were up-regulated in each subgroup. HIF-1α, hypoxia-inducible factor 1α; HMGB1, high mobility group protein B1; IL, interleukin; IPA, ingenuity pathways analysis; PDGF, platelet-derived growth factor; UG, urinary protein subgroup.

the vascular endothelial cells and platelets, in addition to monocytes and neutrophils. In general, UG2 proteins are derived from cells involved in innate and acquired immunity, such as monocytes, neutrophils, plasma cells, and plasmacytoid dendritic cells. In contrast, UG4 contained many proteins derived from the mesenchymal stem cell lineages involved in fibrosis pathology, in addition to the expected appearance of monocytes.

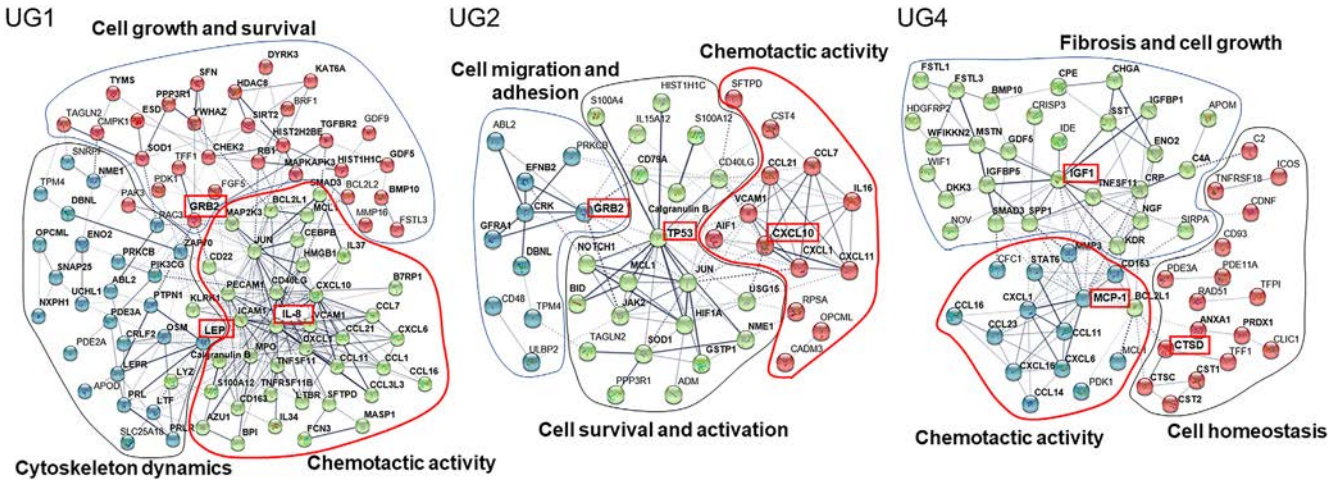

Figure 3. PPI analysis in each subgroup. The PPI networks are partitioned into three clusters based on the k-means clustering algorithm. PPI, protein–protein interaction; UG, urinary protein subgroup, TAGLN2; transgelin-2, TYMS; thymidylate synthase, CMPK1; CMP kinase, ESD; S-formylglutathione hydrolase 1, SOD1; superoxide dismutase 1, PDK1; pyruvate dehydrogenase kinase isozyme 1, GRB2; growth factor receptor-bound protein 2, PPP3R1; calcineurin subunit B type 1, YWHAZ; 14-3-3 protein zeta/delta, CHEK2; serine/threonine-protein kinase Chk2, FGF5; fibroblast growth factor 5, SFN; 14-3-3 protein sigma, HDAC8; histone deacetylase 8, SIRT2; NAD-dependent protein deacetylase sirtuin-2, HIST2H2BE; histone H2B type 2-E, RB1; retinoblastoma-associated protein 1, DYRK3; dual specificity tyrosine-phosphorylation-regulated kinase 3, MAPKAPK3; MAP kinase-activated protein kinase 3, KAT6A; histone acetyltransferase KAT6A, BRF1; transcription factor IIIB 90 kDa subunit, TGFBR2; TGF-beta receptor type-2, HIST1H1C; histone H1.2, BCL2L2; Bcl-2-like protein 2, MMP16; matrix metalloproteinase-16, GDF9; growth/differentiation factor 9, BMP10; bone morphogenetic protein 10, FSTL3; follistatin-related protein 3, SNRPF; small nuclear ribonucleoprotein F, NME1; nucleoside diphosphate kinase A, PAK3; serine/threonine-protein kinase PAK 3, RAC3; ras-related C3 botulinum toxin substrate 3, ZAP70; tyrosine-protein kinase ZAP-70, TPM4; tropomyosin alpha-4 chain, DBNL; drebrin-like protein, OPCML; opioid-binding protein/cell adhesion molecule, ENO2; gamma-enolase, PRKCB; protein kinase C beta type, PIK3CG; phosphatidylinositol 4,5-bisphosphate 3-kinase catalytic subunit gamma isoform, SNAP25; synaptosomal-associated protein 25, ABL2; abelson tyrosine-protein kinase 2, PTPN1; tyrosine-protein phosphatase non-receptor type 1, KLRK1; NKG2-D type II integral membrane protein, LEP; leptin, NXPH1; neurexophilin-1, UCHL1; ubiquitin carboxyl-terminal hydrolase isozyme L1, PDE3A; cGMP-inhibited 3',5'-cyclic phosphodiesterase A, OSM; oncostatin-M, CRLF2; cytokine receptor-like factor 2, PDE2A; cGMP-dependent 3',5'-cyclic phosphodiesterase, LEPR; leptin receptor, LYZ; lysozyme C, APOD; apolipoprotein D, PRL; prolactin, LTF; lactotransferrin, PRLR; prolactin receptor, SLC25A18; mitochondrial glutamate carrier 2, MAP2K3; dual specificity mitogen-activated protein kinase kinase 3, BCL2L1; Bcl-2-like protein 1, SMAD3; mothers against decapentaplegic homolog 3, MCL1; induced myeloid leukemia cell differentiation protein Mcl-1, JUN; transcription factor AP-1, CEBPB; CCAAT/enhancer-binding protein beta, IL37; interleukin-37, HMGB1; high mobility group protein B1, PECAM1; platelet endothelial cell adhesion molecule, CD40LG; CD40 ligand, CXCL10; C-X-C motif chemokine 10, B7RP1; ICOS ligand, ICAM1; intercellular adhesion molecule 1, IL-8; interleukin-8, VCAM1; vascular cell adhesion protein 1, CCL7; C-C motif chemokine 7, MPO; myeloperoxidase, CXCL1; C-X-C motif chemokine 1, CCL21; C-C motif chemokine 21, CXCL6; C-X-C motif chemokine 6, TNFSF11; tumor necrosis factor ligand superfamily member 11, CCL11; C-C motif chemokine 11, CCL1; C-C motif chemokine 1, CCL16; C-C motif chemokine 16, TNFSF11; tumor necrosis factor receptor superfamily member 11B, LTBR; lymphotoxin Beta Receptor, SFTPD; pulmonary surfactant-associated protein D, CCL3L3; C-C motif chemokine 3-like 3, AZU1; azurocidin, BPI; bactericidal permeability-increasing protein, IL34; interleukin-34, FCN3; ficolin-3, MASP1; mannan-binding lectin serine protease 1, EFNB2; ephrin-B2, GFRA1; GDNF family receptor alpha-1, ULBP2; UL16 binding protein 2, Calgranulin B; S100A9, TP53; cellular tumor antigen p53, NOTCH1; neurogenic locus notch homolog protein 1, JAK2; Janus kinase 2, AIF1; allograft inflammatory factor 1, HIF1A; hypoxia-inducible factor 1-alpha, ADM; adrenomedullin, GSTP1; glutathione S-transferase P, FSTL1; follistatin-related protein 1, CPE; carboxypeptidase E, CHGA; chromogranin-A, IGFBP1; insulin-like growth factor-binding protein 1, APOM; apolipoprotein M, HDGFRP2; hepatoma-derived growth factor-related protein 2, WFIKKN2; WAP, Kazal, immunoglobulin, Kunitz and NTR domain-containing protein 2, MSTN; growth/differentiation factor 11/8, GDF5; growth/differentiation factor 5, IDE; insulin-degrading enzyme, IGFBP5; insulin-like growth factor-binding protein 5, CRP; C-reactive protein, NGF; beta-nerve growth factor, SPP1; osteopontin, KDR; vascular endothelial growth factor receptor 2, STAT3; signal transducer and activator of transcription 3, MCP-1; monocyte chemotactic protein 1, ICOS; inducible T-cell costimulator, CDNF; cerebral dopamine neurotrophic factor, PDE11A; dual 3',5'-cyclic-AMP and -GMP phosphodiesterase 11A, RAD51; DNA repair protein RAD51 homolog 1, TFPI; tissue factor pathway inhibitor, ANXA1; annexin A1, PRDX1; peroxiredoxin-1, CTSD; cathepsin D, CTSC; dipeptidyl peptidase 1, CST1; cystatin-SN, TFF1; trefoil factor 1, CLIC1; chloride intracellular channel protein 1, CST2; cystatin-SA. Color figure can be viewed in the online issue, which is available at http://onlinelibrary.wiley.com/doi/10.1002/art.43017/abstract.

Table 1. The top 30 proteins of UG1, 2, and 4 with high correlation coefficients between histological score and urinary protein concentration*

UG1					UG2					UG4				
Molecule	C/FC crescents	Fibrinoid necrosis	Fibrous crescents	Adhesion	Molecule	Endocapillary hypercellularity	Karyorrhexis	Neutrophil infiltration	Subendothelial deposits	Molecule	Interstitial fibrosis	Tubular atrophy	Interstitial inflammation	Tamm-Horsfall casts
S100A12	**0.634**	**0.446**	0.399	0.354	AIF1	**0.891**	**0.635**	**0.529**	0.369	FSTL3[a]	**0.561**	**0.489**	**0.691**	0.368
Calgranulin B[b]	**0.618**	**0.459**	0.374	0.296	SOD	**0.742**	**0.691**	**0.512**	0.204	MCP-1	**0.548**	**0.551**	**0.716**	**0.421**
Calcineurin B a	**0.565**	**0.434**	**0.424**	0.223	6Ckine[a]	**0.732**	**0.616**	**0.628**	0.370	CRIS3	**0.485**	0.385	**0.427**	0.332
CEBPB	**0.534**	**0.401**	0.386	0.341	MCP-3	**0.725**	**0.642**	**0.573**	0.262	AN32B	**0.451**	**0.436**	**0.462**	0.383
HMGN1	**0.528**	**0.440**	**0.418**	0.290	HMGN1	**0.724**	**0.698**	**0.686**	0.358	Somatostatin-28	**0.451**	**0.401**	0.338	0.176
cGS-PDE	**0.527**	0.396	0.386	0.234	Tropomyosin 4	**0.718**	**0.575**	**0.455**	0.299	b-NGF[a]	**0.450**	0.358	**0.485**	0.121
Apo D	**0.508**	0.384	0.352	0.282	SP-D	**0.710**	**0.693**	**0.553**	0.340	VEGF sR2[a]	**0.442**	0.345	**0.450**	−0.006
PKC-B-II	**0.499**	**0.404**	**0.416**	0.188	EFNB2	**0.709**	**0.601**	**0.573**	0.292	ARMEL[a]	**0.430**	0.365	0.396	−0.004
B7-H2	**0.498**	0.360	0.346	0.130	GSTP1	**0.698**	**0.565**	**0.453**	0.315	PDK1	**0.429**	0.353	**0.415**	0.130
Soggy-1	**0.496**	**0.414**	0.389	0.296	VCAM-1	**0.692**	**0.613**	**0.464**	0.273	CSRP3[a]	**0.425**	0.332	**0.446**	0.161
HDGR2	**0.495**	**0.440**	**0.418**	0.284	IgM[a]	**0.690**	**0.505**	**0.452**	0.274	STAT6	**0.424**	0.311	**0.456**	0.154
PSME1	**0.494**	**0.402**	0.380	0.134	IP-10	**0.683**	**0.629**	**0.558**	0.208	IGFBP-5[a]	**0.407**	0.326	0.292	0.152
Azurocidin	**0.493**	0.346	0.327	0.300	S100A12	**0.683**	**0.613**	**0.473**	0.287	NSE	**0.405**	0.305	**0.523**	0.092
Transgelin-2	**0.489**	**0.418**	0.386	0.266	PLXC1	**0.682**	**0.557**	**0.471**	0.324	C2[a]	0.400	0.361	0.295	0.196
IL-8	**0.487**	**0.421**	0.316	0.212	Transgelin-2	**0.665**	**0.625**	**0.489**	0.267	NovH[a]	0.394	0.321	0.354	0.076
Kallikrein 14	**0.485**	**0.414**	0.389	0.270	S100A4	**0.656**	**0.560**	**0.462**	0.264	NCC27[a]	0.392	0.365	**0.411**	0.051
ABL2	**0.484**	**0.419**	0.351	0.348	PKC-B-II	**0.649**	**0.694**	**0.507**	0.239	WFKN2[a]	0.391	0.288	0.375	−0.023
Histone H1.2	**0.482**	**0.404**	0.362	0.219	cGS-PDE	**0.649**	**0.642**	**0.427**	0.266	GHC2	0.388	0.278	**0.413**	0.010
BMP10	**0.481**	**0.464**	**0.494**	0.312	40S RPSA	**0.648**	**0.558**	0.376	0.221	CFC1	0.388	0.249	0.356	0.189
IP-10	**0.477**	**0.425**	**0.500**	0.345	CD5L[a]	**0.642**	**0.607**	**0.506**	0.255	FAM107B[a]	0.387	0.294	**0.459**	0.185
OPG	**0.476**	**0.418**	0.386	0.216	UCRP	**0.637**	**0.575**	**0.487**	0.189	SPINT2[a]	0.384	0.272	**0.484**	0.448
Rb	**0.470**	0.383	**0.404**	0.337	PSME1	**0.634**	**0.506**	**0.452**	0.116	Calpastatin	0.381	0.303	0.321	0.039
PDE3A	**0.468**	0.399	0.387	0.329	GFRa-1	**0.619**	**0.564**	0.375	0.110	ApoM	0.377	0.297	0.304	0.087
HPLN1	**0.467**	**0.470**	**0.430**	0.238	IgA	**0.616**	**0.577**	0.381	0.238	HDGR2	0.377	0.287	**0.423**	0.064
LD78-β	**0.462**	**0.401**	0.369	0.253	CD48[a]	**0.603**	**0.582**	**0.518**	0.228	BCL2-like 1 protein[a]	0.374	0.310	**0.464**	0.023
DYRK3	**0.461**	0.395	0.371	0.304	Calgranulin B[b]	**0.603**	**0.597**	0.381	0.143	COLEC12[a]	0.374	0.245	**0.439**	0.085
Leptin[a]	**0.459**	**0.433**	**0.455**	0.321	Histone H1.2	**0.592**	**0.570**	**0.544**	0.158	MPIF-1[a]	0.374	0.306	0.271	0.083
TFF1	**0.459**	0.369	**0.416**	0.323	ABL2	**0.586**	**0.656**	**0.522**	0.276	Eotaxin	0.373	0.241	**0.484**	0.196
Ficolin-3	**0.457**	**0.440**	**0.464**	0.307	Nectin-like protein 1	**0.585**	**0.546**	**0.435**	0.184	PDE3A	0.368	0.271	**0.419**	−0.008
MASP3	**0.453**	0.395	0.371	0.355	NDKA	**0.581**	**0.618**	**0.452**	0.153	MMP-16[a]	0.366	0.270	**0.424**	−0.037

* Spearman correlation coefficients are indicated in bold and if they showed statistical significance ($P < 0.05$). AIF1, allograft inflammatory factor 1; b-NGF, β-nerve growth factor; C/FC crescents, cellular/fibrocellular crescents; CFC, colony-forming cell; HMGN1, high mobility group nucleosome binding domain 1; SOD, superoxide dismutase.

[a] The urine proteins are shown with an indication of statistical significance if their urinary concentrations were significantly higher in patients with diabetic nephropathy than in those with LN ($P < 0.05$).

[b] The urine proteins are shown with an indication of statistical significance if their urinary concentrations were significantly higher in patients with LN than in those with diabetic nephropathy ($P < 0.05$).

IPA. IPA generated common and distinct pathways among the top 10 pathways in each subgroup (Figure 2B). Leukocyte adhesion–associated signals were activated in all three subgroups. In UG1, high mobility group protein B-cell receptor CD221 signaling was significantly activated compared to that in the other subgroups. Inflammation-related pathways such as IL-3 and hypoxia-inducible factor 1α signaling are dominant in UG2. In UG4, various kinds of IL-17–related signals and fibrosis-related pathways, such as fibrosis signaling pathways and pathology in chronic obstructive pulmonary disease, are prevalent. In addition, in the integrated IPA of UG1, 2, and 4, it was confirmed that signaling pathways related to inflammatory cytokines and granulocyte or monocyte function were highly activated (Supplementary Figure 3).

PPI analysis. In UG1, the proteins contributing to chemotactic activity, cell growth and survival, and cytoskeletal dynamics were confirmed. In UG2, the associated proteins contributing to chemotactic activity, cell migration and adhesion, and cell survival and differentiation were identified. In UG4, proteins contributing to chemotactic activity, fibrosis, and cellular homeostasis were identified (Figure 3).

Identification of urinary biomarker protein correlated with individual histologic score. We attempted to identify urinary protein markers specific to the renal histologic findings in each cluster among the proteins included in the three subgroups. Table 1 shows the top 30 proteins of UG1, 2, and 4 with high correlation coefficients between the histologic score and urinary protein concentration. The top 30 proteins are listed according to the most prevalent renal histologic findings in clusters 1, 2, and 4. The top 20 proteins with high correlation coefficients for all 20 pathologic findings are listed in Supplementary Table 5.

The number of correlated candidate urinary proteins varied according to the renal histology. For active glomerular lesions resulting mainly from inflammatory mechanisms, urine proteins with a correlation of $\rho > 0.4$ were frequently detected in glomerular lesions, including cellular or fibrocellular crescents in cluster 1 and endocapillary hypercellularity in cluster 2. Meanwhile, no urinary protein was correlated with subendothelial deposition in cluster 2. There were also no positive correlations among urinary proteins that could be detected in basement membrane lesions in cluster 3.

In the analysis of UG1 and UG2, a comparison with diabetic nephropathy was made to exclude proteins that were not specifically increased in the urine, even in nonnephritis pathologies of the glomerulus. Because the scores of interstitial inflammation and interstitial fibrosis correlated with each other ($\rho = 0.59$, $P < 0.01$), we focused on proteins that correlated with only one of the histologic scores in the analysis of UG4. To increase the detection rate of ELISA, proteins with an average intensity of <1,000 RFU in 24 cases were excluded. Under these conditions, the top 15 proteins with high correlation coefficients in the most prevalent renal histologic findings in UG1, 2, and 4 were selected as candidate proteins (Supplementary Table 6). Among the urinary proteins in UG1 and UG2, only calgranulin B levels were significantly higher in the LN group than in the diabetic nephropathy group ($P = 0.02$). In addition to calgranulin B, S100A12, HMGN1, and IL-8 were selected in UG1 and AIF-1, SOD1, S100A12, and HMGN1 were selected in UG2 as candidate proteins that did not significantly increase but tended to increase in urinary concentrations in patients with LN compared to those with diabetic nephropathy. In UG4, MCP-1 ($\rho = 0.72$, $P < 0.001$) and FSTL3 ($\rho = 0.69$, $P < 0.001$) were selected as candidate proteins correlated with interstitial inflammation scores. Only IGFBP-5 was extracted as a candidate protein that correlated solely with interstitial fibrosis scores ($\rho = 0.41$, $P = 0.048$) and not with interstitial inflammation scores. No protein correlated only with the interstitial inflammation scores.

The urinary concentrations of these nine candidate proteins were measured using ELISA and reanalyzed for correlation with the histologic scores. The results for S100A12, HMGN1, IL-8, AIF-1, SOD1, and FSTL3 were less sensitive or did not correlate with the results of the aptamer-based screening (Supplementary Table 7). High correlations were found among the results obtained by ELISA and aptamer-based screening for calgranulin B, MCP-1, and IGFBP-5 ($r > 0.7$; Figure 4A). The proteins, measured by ELISA, were then analyzed for correlation with the histologic scores. Urinary calgranulin B levels correlated with the histologic scores of cellular or fibrocellular crescents ($r = 0.65$, $P < 0.001$) and endocapillary hypercellularity ($r = 0.72$, $P < 0.001$), representative of clusters 1 and 2 (Figure 4B). Urinary calgranulin B levels also correlated with the histologic scores of neutrophil infiltration ($r = 0.58$, $P = 0.003$), karyorrhexis ($r = 0.68$, $P < 0.001$), and fibrinoid necrosis ($r = 0.56$, $P = 0.005$) in cluster 2 (data not shown). MCP-1 and IGFBP-5 urinary levels correlated with interstitial inflammation ($r = 0.65$, $P < 0.001$) and fibrosis scores ($r = 0.47$, $P = 0.018$), respectively, in the 24 patients with LN (Figure 4B). In addition, a stronger correlation was observed for IGFBP-5 when three cases of diabetic nephropathy with significant interstitial fibrosis were included ($r = 0.83$, $P < 0.001$) (data not shown). The correlation between each serum protein concentration detected by aptamer-based screening and the renal histologic score was also analyzed in the discovery cohort; however, serum calgranulin and cellular or fibrocellular crescents ($\rho = 0.26$, $P = 0.22$), endocapillary hypercellularity ($\rho = 0.22$, $P = 0.29$), neutrophil infiltration ($\rho = 0.07$, $P = 0.73$), karyorrhexis ($\rho = 0.03$, $P = 0.89$) or fibrinoid necrosis ($\rho = 0.02$, $P = 0.93$), serum MCP-1 and interstitial inflammation scores ($\rho = 0.23$, $P = 0.27$), and serum IGFBP-5 and interstitial fibrosis scores ($\rho = 0.25$, $P = 0.24$) showed no significant correlation with each other (Supplementary File).

Validation of the three urinary proteins associated with the individual histologic score in the validation

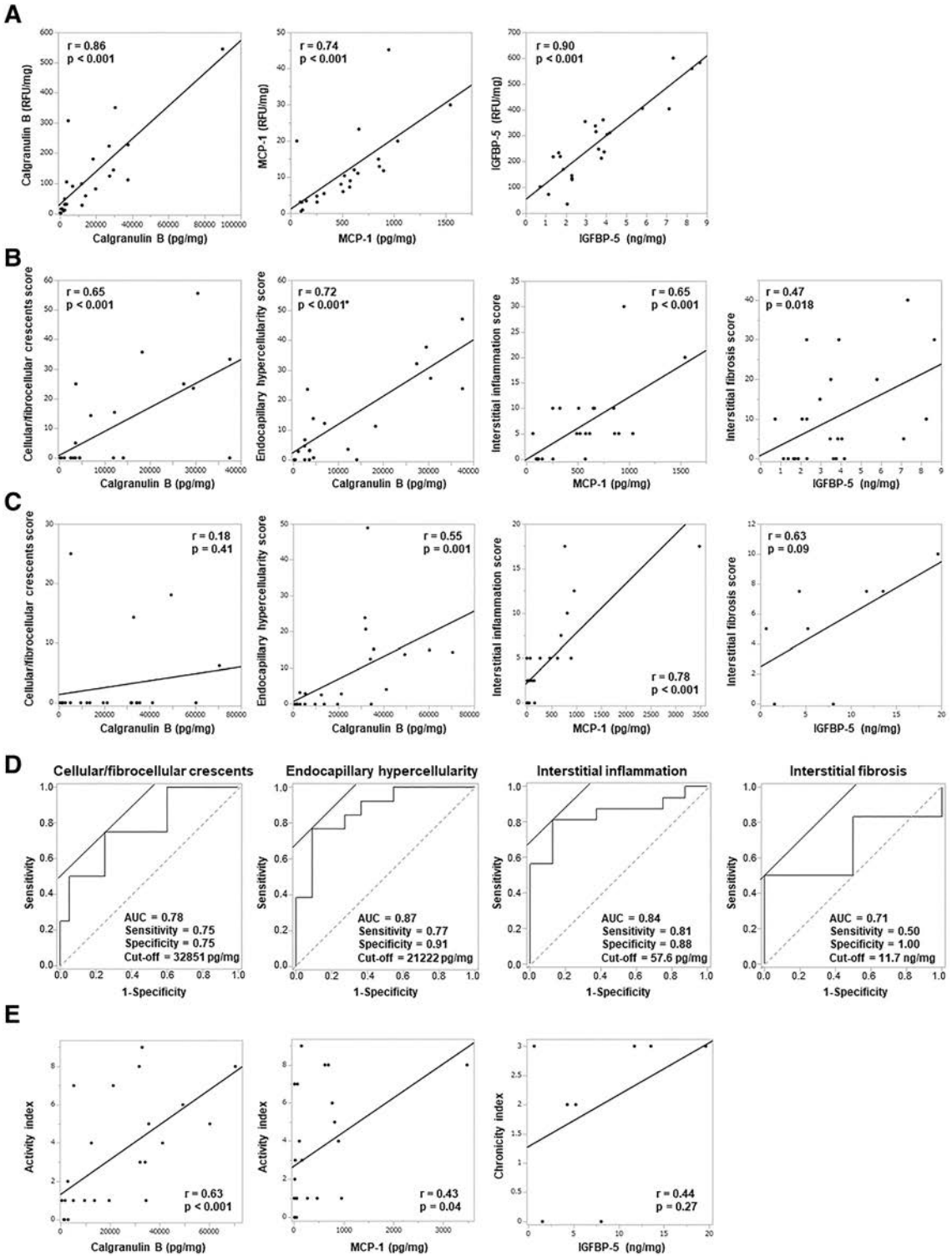

Figure 4. ELISA validation of urinary calgranulin B, MCP-1, and IGFBP-5 levels in the discovery and validation cohort. (A) Correlation between aptamer screening and ELISA results of urine samples from 24 patients with LN. (B and C) Correlation among urinary calgranulin B, MCP-1, and IGFBP-5 levels and the histologic scores of cellular or fibrocellular crescents and endocapillary hypercellularity, interstitial inflammation, and interstitial fibrosis, respectively, in the discovery (B) and validation (C) cohorts. (D) Receiver operating characteristic curves for the presence of cellular or fibrocellular crescents and endocapillary hypercellularity using urinary calgranulin B level, interstitial inflammation using urinary MCP-1 level, and interstitial fibrosis using urinary IGFBP-5 level in the validation cohort. (E) Correlation among urinary calgranulin B and MCP-1 levels and activity index and IGFBP-5 level and chronicity index in the validation cohort. The plots show the concentrations of each urinary protein. Urinary protein concentrations are standardized using urinary creatinine levels. AUC, area under curve; ELISA, enzyme-linked immunosorbent assay; IGFBP, insulin-like growth factor binding protein; MCP, membrane cofactor protein; RFU, relative fluorescence units.

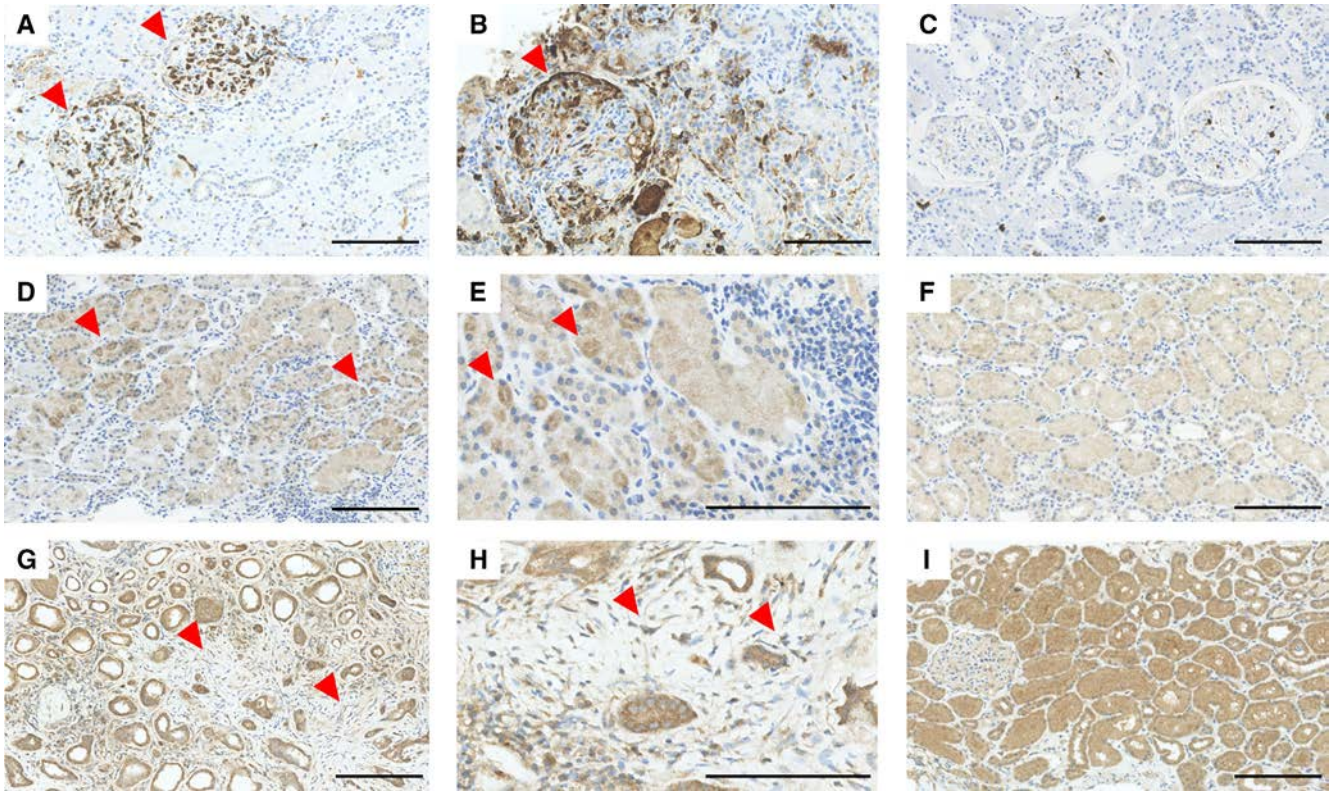

Figure 5. Immunohistochemical staining of the renal tissues from the patients with LN. (A and B) Localization of calgranulin B proteins in cells infiltrating the glomerulus with (A) endocapillary hypercellularity (LN class IV) and (B) cellular or fibrocellular crescents (LN class IV) (arrowheads). (C) Little expression of calgranulin B in the glomeruli without active lesions, such as endocapillary hypercellularity or cellular or fibrocellular crescents (LN class V). (D and E) Localization of MCP-1 proteins in the tubular epithelial cells in renal tissues with high histologic scores for interstitial inflammation (arrowheads). (F) Absence of MCP-1 expression in the tubular epithelial cells without high histologic scores for interstitial inflammation. (G and H) Localization of IGFBP-5 in the spindle-shaped fibroblasts at sites of interstitial fibrosis (arrowheads). (I) Localization of IGFBP-5 proteins in the normal tubular epithelial cell. Bar = 100 μm. IGFBP, insulin-like growth factor binding protein; LN, lupus nephritis; MCP, membrane cofactor protein. Color figure can be viewed in the online issue, which is available at http://onlinelibrary.wiley.com/doi/10.1002/art.43017/abstract.

cohort. The correlation between ELISA-measured urinary protein concentrations and each histologic score was confirmed in the validation cohort for calgranulin B, MCP-1, and IGFBP-5. Urinary calgranulin B levels correlated with the histologic scores of endocapillary hypercellularity (r = 0.55, $P = 0.001$) (Figure 4C). However, the validation cohort had fewer cases of cellular or fibrocellular crescents (Supplementary Table 3). Therefore, we could not confirm a significant correlation between the urinary calgranulin B levels and histologic scores (r = 0.41, $P = 0.18$) (Figure 4C). The urinary MCP-1 levels correlated with the histologic scores of interstitial inflammation (r = 0.78, $P < 0.001$) (Figure 4C). In the eight cases in which measurement of the urinary IGFBP-5 levels was possible, there was a tendency to correlate with the histologic scores of interstitial fibrosis, but no significant difference was observed (r = 0.63, $P = 0.09$) (Figure 4C). The correlation coefficients among all histologic scores of clusters 1, 2, and 4 and ELISA results of these three urinary protein concentrations in the discovery cohort, validation cohort, and diabetic nephropathy were shown in a heatmap (Supplementary Figure 4).

Using the results of the validation cohort, ROC analysis was performed to determine whether urinary calgranulin B, MCP-1, and IGFBP-5 levels could discriminate the presence or absence of each histologic finding (Figure 4D). These three urinary proteins exhibited moderate accuracy: calgranulin B with areas under the curve (AUCs) of 0.78 for cellular or fibrocellular crescents and 0.87 for endocapillary hypercellularity, MCP-1 with an AUC of 0.84 for interstitial inflammation, and IGFBP-5 with an AUC of 0.71 for interstitial fibrosis. In addition, it was confirmed in the validation cohort that urinary calgranulin B levels showed a strong correlation with activity index (r = 0.63, $P < 0.001$), but urinary MCP-1 levels did not (r = 0.43, $P = 0.04$). Urinary IGFBP-5 levels were not significantly correlated with chronicity index (r = 0.44, $P = 0.27$) (Figure 4E).

Immunohistochemical staining of the renal tissues. Immunohistochemical staining of the renal tissues was performed to clarify the localization of calgranulin B, MCP-1, and IGFBP-5. Calgranulin B proteins were localized to the cells infiltrating the glomerulus with endocapillary hypercellularity and cellular or fibrocellular crescents but not to the cells in tubulointerstitial lesions. In addition, glomeruli without these active lesions showed little expression of calgranulin B (Figure 5A–C). In the renal tissues with

high histologic scores for interstitial inflammation, MCP-1 proteins were localized on the tubular epithelial cells but not on the cells infiltrating tubulointerstitial lesions (Figure 5D–F). IGFBP-5 proteins were localized on the spindle-shaped fibroblasts present at sites of interstitial fibrosis and normal tubular epithelial cells (Figure 5G–I). Neither MCP-1 nor IGFBP-5 was localized in the glomeruli.

DISCUSSION

The previously reported proteome analyses aimed at comparing patients with LN and healthy controls or those with active and inactive LN to identify biomarkers that could distinguish them from each other.[9–11] The present study is novel in that, via a proteomic analysis, we identified urinary biomarkers in patients with LN that correlate with a renal histologic scoring system to precisely reflect the characteristics and progression of individual active and chronic lesions. In this study, pathway analyses revealed the protein and cell-to-cell relationships associated with each renal histologic finding. Neutrophils and monocytes are the dominant immune cell type in LN and have been implicated in its pathogenesis.[19,20] This study corroborates previous findings by demonstrating that the activation of granulocytes and monocytes is involved in both glomerular and tubulointerstitial lesions. Furthermore, a stronger association of proteins related to neutrophils and monocytes is observed in active endocapillary and extracapillary lesions (ie, S100A12, calgranulin B, IL-8, and azurocidin). This finding is consistent with previous reports in LN with active glomerulonephritis.[19] In contrast, an enhancement of various kinds of IL-17–related signals was observed in tubulointerstitial lesions. In lupus model mice, IL-17 increased the expression of molecules such as MCP-1 in renal tubular epithelial cells (RTECs), thereby promoting the renal infiltration of macrophages.[21] Furthermore, IL-17 stimulation of RTECs increased messenger RNA expression of other chemokines, such as Cxcl1, Cxcl2, and Cxcl8, which attract monocytes and neutrophils.[22] Consequently, under IL-17 stimulation, RTECs produce mediators that recruit dendritic cells and macrophages, which are crucial sources of transforming growth factor β that promote renal fibrosis,[23] establishing IL-17 as a key driver of RTEC-mediated immunopathogenesis in LN. Thus, these findings support the results obtained from pathway analyses of interstitial inflammation, tubular atrophy, and interstitial fibrosis in this study.

Calgranulin B (S100A9) belongs to the S100 family of proteins and exists as a heterodimer of S100A8 in vivo. S100A8/A9 are mainly expressed in the cytoplasm of neutrophils, monocytes, plasmacytoid dendritic cells, and endothelial cells and play a pro-inflammatory role in various autoimmune diseases.[24,25] Serum and urinary S100A8/A9 concentrations are known to increase in patients with active LN.[26–28] The present study newly showed a correlation between urinary calgranulin B levels and quantified active intraglomerular lesions in the LN. In addition, immunohistochemical staining of the renal tissues from patients with high urinary calgranulin B concentrations showed the localization of calgranulin B in cells infiltrating the glomerulus. These results suggest that urinary calgranulin B levels may reflect local renal pathology, making it more important to measure urinary calgranulin B concentrations.

MCP-1 (CCL2) is a chemokine secreted by monocytes, macrophages, fibroblasts, and vascular endothelial cells that contributes to monocyte activation and migration via CCR2.[29] MCP-1 is a useful urinary biomarker for predicting disease activity and renal prognosis in patients with LN.[30,31] Urinary MCP-1 has also been reported as a biomarker that can predict inflammatory cell infiltration of the tubulointerstitium in patients with LN.[32] The present study demonstrated a correlation between quantified interstitial inflammation and urinary MCP-1 concentration, indicating its potential as a detailed predictor of the severity of interstitial inflammation in patients with LN. MCP-1 was strongly expressed in the tubular epithelial cells in the renal tissues, where interstitial inflammation was more prominent. This indicates that MCP-1 expression in the tubular epithelial cells promotes inflammatory cell infiltration into the renal interstitium. However, urinary MCP-1 levels did not significantly correlate with the severity of active glomerular lesions in the present study. This result reinforces the possibility that urinary MCP-1 levels can specifically predict the severity of interstitial inflammation.

IGFBP-5 belongs to the IGFBP family and contributes to the regulation of insulin-like growth factor signaling. It has been reported to be involved in renal diseases, particularly chronic kidney disease (CKD), after its expression was discovered in the renal interstitium of patients with CKD using single-cell analysis.[33,34] IGFBP-5 has also been reported to promote lung tissue fibrosis and participate in tissue remodeling.[35] We newly reported that urinary IGFBP-5 levels can predict the severity of interstitial fibrosis in the renal tissues. Immunohistochemical staining showed IGFBP-5 staining in the cells that appeared to be fibroblasts in lesions with interstitial fibrosis, suggesting that it is associated with the pathogenesis of fibrosis.

Some urinary proteins, such as vascular cell adhesion molecule 1 and activated leukocyte cell adhesion molecule, have been reported to correlate with activity index in patients with active LN.[36,37] Urinary calgranulin B also predicted activity index with as strong a correlation as these proteins in our study. In contrast, urinary levels of MCP-1 and IGFBP-5 did not show a strong correlation with activity or chronicity index. This is probably explained by the finding that urinary MCP-1 and IGFBP-5 were associated with only one histologic finding of all components in activity or chronicity index, whereas urinary calgranulin B was associated with the major components of histologic findings in activity index.

This study had some limitations. First, our scoring system was not clinically validated, although it comprehensively included

histologic findings based on the ISN/RPS classification and the NIH index. Second, the validation failed to confirm the significance of the correlation between urinary calgranulin B levels and the histologic scores of cellular or fibrocellular crescents or urinary IGFBP-5 levels and the histologic scores of interstitial fibrosis. The former occurred because fewer patients in the validation cohort presented with cellular or fibrocellular crescents. The latter was due to the small number of cases in which IGFBP-5 levels could be measured. Further validation using urine samples from a larger sample is required. Third, we did not perform analyses of urinary proteins associated with the histologic findings included in the clusters of membranous and mesangial lesions and other lesions. Fourth, the clinical usefulness of urinary calgranulin B, MCP-1, and IGFBP-5 levels was not demonstrated. A longitudinal study is warranted to investigate the relationship between these three urinary proteins and disease progression or improvement over time. Fifth, the present study could not include sufficient samples of diabetic nephropathy because renal biopsies are not commonly performed in patients with diabetic nephropathy. The limited samples of diabetic nephropathy could affect the accuracy of candidate protein extraction.

In conclusion, various urinary proteins that correlate with certain renal histologic findings may reflect the different pathogeneses involved in each renal lesion. The extraction and identification of these urinary proteins may enhance clinical management and are expected to be useful in precision medicine.

ACKNOWLEDGMENTS

We thank Ms. Harumi Kondo for assistance with collecting clinical data. IPA data were provided to the authors with explicit permission from QIAGEN, Inc. We would like to thank Editage (www.editage.jp) for English language editing. We also thank Ryo Takano (former employee of Mitsubishi Tanabe Pharma Corporation), Shinji Kojima, and Fumihiko Miyoshi (Mitsubishi Tanabe Pharma Corporation) for bioinformatics analysis.

AUTHOR CONTRIBUTIONS

All authors were involved in drafting the article or revising it critically for important intellectual content, and all authors approved the final version to be published. Dr Kaneko had full access to all of the data in the study and takes responsibility for the integrity of the data and the accuracy of the data analysis.

Study conception and design. Hiramoto, Saito, Hanaoka, Hashiguchi, Suzuki, Takeuchi, Kaneko.

Acquisition of data. Hiramoto, Saito, Hanaoka, Kikuchi, Fukui, Hashiguchi.

Analysis and interpretation of data. Hiramoto, Saito, Hashiguchi.

ROLE OF THE STUDY SPONSOR

Mitsubishi Tanabe Pharma Corporation had no role in the study design or in the collection or interpretation of the data, the writing of the manuscript, or the decision to submit the manuscript for publication. Publication of this article was not contingent upon approval by Mitsubishi Tanabe Pharma Corporation.

REFERENCES

1. Dörner T, Furie R. Novel paradigms in systemic lupus erythematosus. Lancet 2019;393(10188):2344–2358.
2. Cameron JS. Lupus nephritis. J Am Soc Nephrol 1999;10(2):413–424.
3. Borchers AT, Leibushor N, Naguwa SM, et al. Lupus nephritis: a critical review. Autoimmun Rev 2012;12(2):174–194.
4. Azoicăi T, Belibou IM, Lozneanu L, et al. Large variability of the activity and chronicity indexes within and between histological classes of lupus nephritis. Rom J Morphol Embryol 2017;58(1):73–78.
5. Bajema IM, Wilhelmus S, Alpers CE, et al. Revision of the International Society of Nephrology/Renal Pathology Society classification for lupus nephritis: clarification of definitions, and modified National Institutes of Health activity and chronicity indices. Kidney Int 2018;93(4):789–796.
6. Rijnink EC, Teng YKO, Wilhelmus S, et al. Clinical and histopathologic characteristics associated with renal outcomes in lupus nephritis. Clin J Am Soc Nephrol 2017;12(5):734–743.
7. Yu F, Wu LH, Tan Y, et al. Tubulointerstitial lesions of patients with lupus nephritis classified by the 2003 International Society of Nephrology and Renal Pathology Society system. Kidney Int 2010;77(9):820–829.
8. Giannico G, Fogo AB. Lupus nephritis: is the kidney biopsy currently necessary in the management of lupus nephritis? Clin J Am Soc Nephrol 2013;8(1):138–145.
9. Aragón CC, Tafúr RA, Suárez-Avellaneda A, et al. Urinary biomarkers in lupus nephritis. J Transl Autoimmun 2020;3:100042.
10. Zhang X, Jin M, Wu H, et al. Biomarkers of lupus nephritis determined by serial urine proteomics. Kidney Int 2008;74(6):799–807.
11. Somparn P, Hirankarn N, Leelahavanichkul A, et al. Urinary proteomics revealed prostaglandin H(2)D-isomerase, not Zn-α2-glycoprotein, as a biomarker for active lupus nephritis. J Proteomics 2012;75(11):3240–3247.
12. Stanley S, Vanarsa K, Soliman S, et al. Comprehensive aptamer-based screening identifies a spectrum of urinary biomarkers of lupus nephritis across ethnicities. Nat Commun 2020;11(1):2197.
13. Vanarsa K, Soomro S, Zhang T, et al. Quantitative planar array screen of 1000 proteins uncovers novel urinary protein biomarkers of lupus nephritis. Ann Rheum Dis 2020;79(10):1349–1361.
14. Fava A, Rao DA, Mohan C, et al; Accelerating Medicines Partnership in Rheumatoid Arthritis and Systemic Lupus Erythematosus Network. Urine proteomics and renal single-cell transcriptomics implicate interleukin-16 in lupus nephritis. Arthritis Rheumatol 2022;74(5):829–839.
15. Fava A, Buyon J, Magder L, et al; Accelerating Medicines Partnership in RA/SLE network. Urine proteomic signatures of histological class, activity, chronicity, and treatment response in lupus nephritis. JCI Insight 2024;9(2):e172569.
16. SomaLogic. *SOMAscan Proteomic Assay Technical White Paper*. SomaLogic, Inc; 2015.
17. Weening JJ, D'Agati VD, Schwartz MM, et al; International Society of Nephrology Working Group on the Classification of Lupus Nephritis; Renal Pathology Society Working Group on the Classification of Lupus Nephritis. The classification of glomerulonephritis in systemic lupus erythematosus revisited. Kidney Int 2004;65(2):521–530.
18. Austin HA III, Muenz LR, Joyce KM, et al. Diffuse proliferative lupus nephritis: identification of specific pathologic features affecting renal outcome. Kidney Int 1984;25(4):689–695.
19. Banchereau R, Hong S, Cantarel B, et al. Personalized immunomonitoring uncovers molecular networks that stratify lupus patients. Cell 2016;165(3):551–565.

20. Olmes G, Büttner-Herold M, Ferrazzi F, et al. CD163+ M2c-like macrophages predominate in renal biopsies from patients with lupus nephritis. Arthritis Res Ther 2016;18(1):90.
21. Ramani K, Biswas PS. Interleukin 17 signaling drives type I interferon induced proliferative crescentic glomerulonephritis in lupus-prone mice. Clin Immunol 2016;162:31–36.
22. Ramani K, Pawaria S, Maers K, et al. An essential role of interleukin-17 receptor signaling in the development of autoimmune glomerulonephritis. J Leukoc Biol 2014;96(3):463–472.
23. Kassianos AJ, Wang X, Sampangi S, et al. Increased tubulointerstitial recruitment of human CD141(hi) CLEC9A(+) and CD1c(+) myeloid dendritic cell subsets in renal fibrosis and chronic kidney disease. Am J Physiol Renal Physiol 2013;305(10):F1391–F1401.
24. Sedaghat F, Notopoulos A. S100 protein family and its application in clinical practice. Hippokratia 2008;12(4):198–204.
25. Wang S, Song R, Wang Z, et al. S100A8/A9 in Inflammation. Front Immunol 2018;9:1298.
26. Turnier JL, Fall N, Thornton S, et al. Urine S100 proteins as potential biomarkers of lupus nephritis activity. Arthritis Res Ther 2017; 19(1):242.
27. Davies JC, Midgley A, Carlsson E, et al. Urine and serum S100A8/A9 and S100A12 associate with active lupus nephritis and may predict response to rituximab treatment. RMD Open 2020;6(2):e001257.
28. Tantivitayakul P, Benjachat T, Somparn P, et al. Elevated expressions of myeloid-related proteins-8 and -14 are danger biomarkers for lupus nephritis. Lupus 2016;25(1):38–45.
29. Singh S, Anshita D, Ravichandiran V. MCP-1: Function, regulation, and involvement in disease. Int Immunopharmacol 2021;101(Pt B): 107598.
30. Rovin BH, Song H, Birmingham DJ, et al. Urine chemokines as biomarkers of human systemic lupus erythematosus activity. J Am Soc Nephrol 2005;16(2):467–473.
31. Gulati G, Bennett MR, Abulaban K, et al. Prospective validation of a novel renal activity index of lupus nephritis. Lupus 2017;26(9): 927–936.
32. Zhang X, Nagaraja HN, Nadasdy T, et al. A composite urine biomarker reflects interstitial inflammation in lupus nephritis kidney biopsies. Kidney Int 2012;81(4):401–406.
33. Wang S, Chi K, Wu D, et al. Insulin-like growth factor binding proteins in kidney disease. Front Pharmacol 2021;12:807119.
34. Park J, Shrestha R, Qiu C, et al. Single-cell transcriptomics of the mouse kidney reveals potential cellular targets of kidney disease. Science 2018;360(6390):758–763.
35. Nguyen XX, Muhammad L, Nietert PJ, et al. IGFBP-5 promotes fibrosis via increasing its own expression and that of other pro-fibrotic mediators. Front Endocrinol (Lausanne) 2018;9:601.
36. Singh S, Wu T, Xie C, et al. Urine VCAM-1 as a marker of renal pathology activity index in lupus nephritis. Arthritis Res Ther 2012;14(4): R164.
37. Ding H, Lin C, Cai J, et al. Urinary activated leukocyte cell adhesion molecule as a novel biomarker of lupus nephritis histology. Arthritis Res Ther 2020;22(1):122.

Arthritis & Rheumatology
Vol. 77, No. 3, March 2025, pp 311–321
DOI 10.1002/art.43018

American College of Rheumatology
Empowering Rheumatology Professionals

Impact of IgG Fc Glycosylation on Disease Dynamics in Patients With Primary Sjögren Disease

Helena Achten,[1] Leander Meuris,[2] Liselotte Deroo,[3] Matthias Jarlborg,[4] Tine Decruy,[4] Joke Deprez,[4] Emilie Dumas,[4] Kristel De Boeck,[5] Eva Genbrugge,[5] Wouter Bauters,[5] Frederick Dochy,[5] David Creytens,[3] Dimitri Roels,[5] Nico Callewaert,[2] Dirk Elewaut,[1] and Isabelle Peene[6]

Objective. Glycans attached to the Fc region of IgG antibodies influence their pro- or anti-inflammatory effector function. We aimed to explore the interrelation of the Fc glycosylation profile and disease transition, disease activity, and outcome in patients with suspected and confirmed primary Sjögren disease (SjD).

Methods. IgG Fc sialylation and IgG Fc galactosylation serum levels were determined in 300 patients from the Belgian Sjögren's Syndrome Transition Trial. This cohort includes both suspected and confirmed patients with SjD meeting the 2016 American College of Rheumatology/EULAR criteria. Salivary gland involvement was evaluated through ultrasonography (Hocevar score 0–48) and histopathology (focus score). The relative amount of sialylated and galactosylated IgG was determined by capillary electrophoresis after using the endoglycosidase S-based assay.

Results. Patients with SjD exhibited significantly lower sialylation and galactosylation levels versus asymptomatic carriers of anti-SSA and patients with sicca. Lower sialylation and galactosylation levels were significantly associated with an increase in B cell activation markers and distinct autoantibody profiles, particularly with multiple autoantibody reactivities. They were also linked to histopathological salivary gland alterations, higher Hocevar scores, and, importantly, risk factors for non-Hodgkin lymphoma (NHL) development. In contrast, patients with SjD who were mono-anti-Ro60 positive and those who were anti-SSA negative had normal IgG Fc glycosylation.

Conclusion. This study points to a novel role of IgG Fc glycosylation in patients with SjD in predicting disease transition, monitoring disease activity, and stratifying risk of NHL development.

INTRODUCTION

Primary Sjögren disease (SjD) refers to a prototypic autoimmune disease characterized by oral and ocular dryness, known as sicca. Additionally, SjD often presents a broad range of extraglandular manifestations and carries a substantial risk for development of lymphoma. Hence, around 5% of patients with SjD evolve into having non-Hodgkin lymphoma (NHL).[1] The clinical heterogeneity of SjD poses challenges for both medical practitioners and researchers because required management and prognosis may vary substantially.[2] The underlying pathophysiology driving SjD is believed to be multifactorial, involving an interplay between salivary gland epithelial cells and both arms of the innate and adaptive immune system.[3] The contribution of the latter is illustrated by the presence of IgG autoantibodies against SSA (Ro52/Ro60) and SSB (La), which constitute hallmark features of the disease.[3,4]

These autoantibodies may precede clinical onset of disease for more than two decades.[5,6] The exact temporal relationship of their presence, disease induction, and subsequent clinical

The Belgian Sjögren's Syndrome Transition Trial cohort was supported by the Fund for Scientific Research on Rheumatology (grant 2018-J5820590-210858). Dr Achten's work was supported by the Research Foundation – Flanders (grant 11J6923N). These financial resources have been used to support data collection and management. There was no involvement of any kind in the study conduction. The corresponding author has full access to all the data and takes the final responsibility for the decision to submit for publication.

[1]Helena Achten, MD, Dirk Elewaut, MD, PhD: Ghent University Hospital and Gent University, Ghent, Belgium, and VIB-UGent Inflammation Research Center, Zwijnaarde, Belgium; [2]Leander Meuris, PhD, Nico Callewaert, PhD: VIB-UGent Center for Medical Biotechnology, Ghent, Belgium; [3]Liselotte Deroo, MD, PhD, David Creytens, MD, PhD: Ghent University Hospital and Gent University, Ghent, Belgium; [4]Matthias Jarlborg, MD, PhD, Tine Decruy, Joke Deprez, PhD, Emilie Dumas, PhD: VIB-UGent Inflammation Research Center, Zwijnaarde, Belgium; [5]Kristel De Boeck, Eva Genbrugge, MD, Wouter Bauters, MD, Frederick Dochy, MD, Dimitri Roels, MD: Ghent University Hospital, Ghent, Belgium; [6]Isabelle Peene, MD, PhD: Ghent University Hospital and Gent University, Ghent, Belgium, VIB-UGent Inflammation Research Center, Zwijnaarde, Belgium, and AZ Sint-Jan Brugge AV, Bruges, Belgium.

Drs Elewaut and Peene contributed equally to this work.

Additional supplementary information cited in this article can be found online in the Supporting Information section (https://acrjournals.onlinelibrary.wiley.com/doi/10.1002/art.43018).

Author disclosures and graphical abstract are available at https://onlinelibrary.wiley.com/doi/10.1002/art.43018.

Address correspondence via email to Isabelle Peene, MD, PhD, at Isabelle.Peene@UZGent.be.

Submitted for publication February 2, 2024; accepted in revised form September 3, 2024.

presentation is still elusive. What is known, however, is that antibodies exhibit both anti-inflammatory and proinflammatory effector functions. A crucial regulator of antibody effector function is the N-glycosylation of the Fc domains of IgG, which influences the conformation and thereby the antibody's affinity for Fcγ receptors (FcγRs).[7] IgG Fc glycosylation is a posttranslational modification process in which oligosaccharides are covalently bound to asparagine 297, a conserved binding site on each of the two IgG Fc regions. The attached glycans comprise a variable amount of sialic acid, galactose, fucose, and bisecting N-acetylglucosamine moieties on a heptasaccharide core structure.[8] Sialic acid residues play a dual role in modulating the antibody's function. First, they impair the proinflammatory capacity of antibodies by reducing their binding to activating type I FcγRs. Second, they are immunosuppressive by increasing antibody binding to inhibitory type II FcγRs.[7,9] Another prominent glycan alteration in autoimmune diseases, associated with inflammation and disease progression, is the decrease in the IgG Fc galactosylation level.[7,9–11] The underlying mechanism is still debated, but increased binding to activating type I FcγRs has been proposed.[9,12,13]

The presence of autoantibodies in asymptomatic carriers suggests an initial breakdown of immune tolerance,[5,6] but the mechanism(s) driving conversion into disease are still enigmatic and suggest the need for an additional, secondary factor.[11] In this context, a shift in the Fc glycosylation profile from an anti- to proinflammatory state may serve as switch-instigating progression into SjD.[7] Therefore, we examined the Fc glycosylation profile in a cohort representing the entire SjD disease spectrum, ranging from asymptomatic carriers of anti-SSA (those at risk of SjD) to individuals with fully blown SjD. This enabled us to seek associations of Fc glycosylation, disease transition, and correlations with disease activity and outcome.

PATIENTS AND METHODS

The Belgian Sjögren's Syndrome Transition Trial (BeSSTT) is a prospective, observational, longitudinal cohort including both patients with SjD, according to the 2016 American College of Rheumatology (ACR)/EULAR classification criteria,[4] and patients with suspected SjD, characterized by the presence of at least one criterion, either objective sicca or the presence of one immunologic criterion. The immunologic criterion is fulfilled when patients have anti-SSA antibodies (Ro52 and/or Ro60) or a positive salivary gland biopsy with a focus score (FS) ≥1.[14] Patients from the BeSSTT cohort follow a standardized prospective yearly follow-up.

A standardized clinical set of metadata including demographics, clinical data, and laboratory parameters were collected from all patients. Ocular staining score was assessed using the Sjögren's International Collaborative Clinical Alliance scheme.[15] Schirmer's test and unstimulated salivary flow rate were performed according to the guidelines of the ACR/EULAR classification criteria.[4] The EULAR Sjögren's Syndrome Disease Activity Index (ESSDAI) was applied to measure systemic disease activity.[16] Ultrasonographic abnormalities were assessed by two dedicated radiologists using the Hocevar score, similar as previously reported.[17] Here, a good alignment was observed between both assessors with an interclass correlation coefficient for an interrater reliability of 0.85. The intrarater reliabilities were 0.85 and 0.92.[18] Three categories of Hocevar scores were made: negative (0–14), moderate (15–26), and high (27–48).[19] Results of labial salivary gland biopsies were recorded when available, and FS was determined.[20] Immunohistochemistry characterized T cells (CD3), B cells (CD20), plasma cells (CD138), and follicular dendritic cells (FDCs; CD21).[21] Histopathological results were available in 148 patients; 120 were evaluated at the pathology department of the Ghent University Hospital (David Creytens). Autoimmune serology was determined using a symphony screen (14-5671-01; Thermo Fisher Scientific) allowing screening of a mixture of nuclear and cytoplasmic antigens. Positive samples were further investigated using an antiextractable nuclear antigen line blot (1590-1601-5 G; Euroimmun) to separately detect antibodies to SSA (Ro52 and/or Ro60) and SSB/La. All data, except for the salivary gland biopsy, were obtained at baseline between October 2019 and June 2022. The Ghent University Hospital Ethics Committee granted approval for this project (BeSSTT: EC 2019/0452), and all participants provided written informed consent in accordance with the principles outlined in the Declaration of Helsinki.

Serum was collected in BD Vacutainer SST2, aliquoted, and stored at −80°C. IgG Fc glycosylation was determined in serum from 300 consecutively included patients using endoglycosidase S (endoS) to specifically release IgG Fc N-glycans followed by fluorescent labeling and analysis on capillary electrophoresis as previously described by Vanderschaeghe et al.[22] Briefly, 2.5 μL of serum was incubated with 25 U of endoS for one hour at 37°C in 150 mmol/L NaCl and 50 mmol/L Tris-HCl (pH 8.5). Released glycans were fluorescently labeled with aRisk minopyrene trisulfonic acid, analyzed by capillary electrophoresis (3500 Genetic Analyzer), and quantified using GeneMapper version 3.7. The relative levels of sialylation and galactosylation were calculated based on relative peak heights.

Statistical analysis. Study data were collected and managed using REDCap electronic data capture tools hosted at the Ghent University Hospital.[23,24] Statistical analyses were performed using R (R core 2021, version 4.1.2). Kruskal–Wallis, Mann–Whitney U, and Pearson chi-square tests were applied. Post hoc analyses were adjusted using the Bonferroni correction. Simple linear and multiple regression models were applied. $P \leq 0.05$ was considered statistically significant.

RESULTS

Patient features and IgG Fc glycosylation in relation to disease state. Hallmarks of SjD include sicca, anti-SSA antibodies, and salivary gland involvement even though histopathological assessment is not indispensable to diagnose SjD. To investigate the interrelation between IgG glycosylation and different domains of SjD (sicca, antibodies, and glandular involvement), we therefore analyzed data of 288 patients that were categorized into four well-defined disease states (patients with sicca complaint, those with sicca, those at risk of SjD, and those with SjD). Fc glycosylation profiles, demographic data, laboratory parameters, and results on salivary gland involvement for each disease state are provided in Table 1. Seven patients were not assigned to a disease state due to the unavailability of the anti-SSA/Ro status at baseline. Five patients with FS ≥1 without fulfillment of any other ACR-EULAR classification criterion were not categorized.[4] Supplementary Figure 1 provides precise numerical details for each analysis.

The relative levels of sialylation and galactosylation were significantly lower in patients with SjD compared to patients with sicca and sicca complaint and compared to patients who were at risk of SjD ($P < 0.001$; Figure 1A). When applying multilinear regression with age as the covariate, we observed a significant negative association between the SjD state and the relative levels of sialylation and galactosylation. Additionally, the analysis was repeated in a subset of patients for whom FS was available (n = 139), yielding similar results: the relative levels of sialylation and galactosylation were found to be the lowest in patients with SjD and differed significantly from patients with sicca and sicca complaint ($P \leq 0.001$). The latter did not show significant differences from patients who were at risk of SjD (Figure 1B).

Figure 1 clearly indicates that galactosylation levels below 40% separate patients with SjD from those without. A galactosylation level below 40% yielded a very high specificity and positive predictive value of 97.3% and 93.8%, respectively, for SjD classification in patients with suspicion of SjD. A galactosylation lower than 55% had a positive predictive value of 75% for SjD classification and a sensitivity of 76.8%. Sialylation and galactosylation levels were highly correlated with each other (Spearman Correlation Coefficient [Rs] = 0.93, $P < 0.001$). In line with this, we noticed that a sialylation level below 5% could also distinguish patients with SjD from those without. This corresponds to a high specificity and positive predictive value of 97.3% and 93.0%, respectively (Table 1).

IgG Fc glycosylation in relation to disease activity markers, autoantibody profile, and prognosis. We next evaluated the Fc glycosylation levels in relation to the various ESSDAI domains. Here, associations were found solely with the biologic and hematologic domains (ie, lymphocytes).[25] As shown in Table 2, patients with normal lymphocyte levels had significantly higher levels of sialylation and galactosylation versus those with mild lymphopenia ($P < 0.05$) and those with severe lymphopenia ($P < 0.001$). Quite striking was the observation that this is accompanied with a gradual and progressive loss because patients with mild lymphopenia had significantly higher sialylated and galactosylated IgG levels than those with a severe lymphopenia ($P < 0.05$). Second, the serum levels of sialylated and galactosylated IgG levels were inversely linked with rheumatoid factor (RF; $P < 0.001$); increased RF levels were accompanied with reduced levels of sialylated and galactosylated IgG. Finally, indicators of enhanced B cell activation such as IgG, IgA, β2-microglobulin, and hypergammaglobulinemia were linked to lower levels of sialylated and galactosylated IgG. Taken together, these results pointed to a significant association between B cell activity and sialylated and galactosylated IgG levels.

We next evaluated the putative association with surrogate indicators of glandular involvement such as salivary gland ultrasonography (SGUS). Here, patients with the highest Hocevar scores (27–48) exhibited significantly lower levels of sialylated and galactosylated IgG versus those with moderate (15–26) or negative (0–14) scores ($P \leq 0.001$; Figure 2). The relationship between sialylated and galactosylated IgG and salivary gland involvement was further supported by immunohistochemistry, which revealed lower levels of sialylation ($P < 0.05$) and galactosylation ($P < 0.01$) in patients with an FS ≥1 compared to those with an FS <1 (Figure 3). In addition, sialylation and galactosylation levels tend to inversely correlate with the CD20 to CD3 ratio in salivary glands. Remarkably, in the presence of FDCs in salivary glands, significantly lower sialylation and galactosylation levels were seen ($P \leq 0.05$). Results are given in Table 2. Thus, serum sialylation and galactosylation levels are linked to salivary gland involvement and are reduced in relation to germinal center reaction.

Six distinct autoantibody profiles were identified in the BeSSTT: anti-SSA negativity (anti-SSA$^-$), mono-anti-Ro60 reactivity, mono-anti-Ro52 reactivity, reactivity against both Ro52 and Ro60 (double anti-Ro52$^+$Ro60$^+$), reactivity against SSB and both Ro52 and Ro60 (triple anti-Ro52$^+$Ro60$^+$ SSB$^+$), and reactivity against SSB in addition to monoreactivity against Ro52 or Ro60 (anti-Ro52$^+$/60$^+$ SSB$^+$). The latter group (n = 6) was not included in the analysis given the small number, with five patients who were anti-Ro60$^+$SSB$^+$ and one patient who was anti-Ro52$^+$SSB$^+$. As depicted in Figure 4, in the whole cohort, the median percentages of sialylated and galactosylated IgG differed significantly between the autoantibody profiles ($P \leq 0.001$). Triple anti-Ro52$^+$Ro60$^+$ SSB$^+$ had the lowest median percentage of sialylated and galactosylated IgG, followed by patients with mono-anti-Ro52$^+$ and double anti-Ro52$^+$Ro60$^+$. In contrast to patients with mono-anti-Ro52$^+$, patients with mono-anti-Ro60$^+$ had higher levels of sialylated and galactosylated IgG like patients with anti-SSA$^-$. Within patients with SjD, similar results were obtained; patients with anti-Ro60$^+$ SjD had the highest sialylation and galactosylation levels, followed by patients with anti-SSA-negative SjD;

Table 1. Classification of disease states in patients with primary SjD: correlating IgG Fc glycosylation profiles with distinct clinical phenotypes*

Disease state	Patients with sicca complaint (n = 22)	Patients with sicca (n = 53)	Patients who were at risk of SjD (n = 36)	Patients with SjD (n = 177)	*P* value (α = 0.05)
ACR/EULAR classification criteria for patients with SjD					
Objective sicca	0 (0)	53 (100)	0 (0)	168 (95)	<0.001
Anti-SSA positivity	0 (0)	0 (0)	36 (100)	166 (94)	<0.001
FS ≥ 1, n/total available biopsies (%)	0/11 (0)	0/37 (0)	0/10 (0)	57/81 (70)	<0.001
IgG Fc glycosylation					
Sialylated IgG, median (IQR), %	9.6 (1.7)	8.2 (2.7)	9.0 (3.4)	6.8 (3.0)	<0.001
Sia ≤ 5%	0 (0)	2 (4)	1 (3)	40 (23)	–
5% < Sia < 8.5%	5 (23)	26 (49)	13 (36)	98 (55)	–
Sia ≥ 8.5%	17 (77)	25 (47)	22 (61)	39 (22)	–
Galactosylated IgG, median (IQR), %	59.9 (8.9)	55.2 (13.0)	58.4 (14.0)	47.2 (15.0)	<0.001
Gal < 40%	0 (0)	2 (4)	1 (3)	46 (26)	–
40% ≤ Gal < 55%	5 (23)	24 (45)	13 (36)	90 (51)	–
Gal ≥ 55%	17 (77)	27 (51)	22 (61)	41 (23)	–
Demographics					
Age, mean (±SD), y	45 (±10)	51 (±12)	43 (±13)	53 (±15)	<0.001
Female	19 (86)	50 (94)	33 (92)	158 (89)	0.64
B cell activity markers					
Hypergammaglobulinemia	0 (0)	3 (6)	4 (11)	55 (31)	<0.001
IgG (g/L), mean (±SD)	10.4 (±2.0)	10.7 (±2.7)	12.3 (±2.8)	14.8 (±5.8)	<0.001
RF negative (<11.4 U/mL)	21 (96)	53 (100)	31 (86)	108 (61)	–
RF weakly positive (11.4–40.0 U/mL)	1 (4)	0 (0)	4 (11)	32 (18)	–
RF strongly positive (>40 U/mL)	0 (0)	0 (0)	1 (3)	37 (21)	–
Lymphopenia	1 (4)	2 (4)	6 (17)	43 (24)	<0.01
Lymphoma prevalence	0 (0)	0 (0)	0 (0)	4 (2)	0.48
Ultrasonography					
Hocevar score, mean (±SD)	12 (±8)	9 (±9)	13 (±12)	23 (±14)	<0.001
Negative Hocevar score (0–14)	13 (59)	43 (81)	22 (61)	60 (34)	–
Low positive Hocevar score (15–26)	9 (41)	8 (15)	6 (17)	47 (27)	–
High positive Hocevar score (27–48)	0 (0)	2 (4)	8 (22)	70 (39)	–
Autoantibody profile					
Anti-SSA$^-$	22 (100)	53 (100)	0 (0)	16 (9)	–
Anti-Ro52$^+$	0 (0)	0 (0)	7 (19)	17 (10)	–
Anti-Ro60$^+$	0 (0)	0 (0)	13 (36)	17 (10)	–
Anti-Ro52$^+$Ro60$^+$	0 (0)	0 (0)	11 (31)	66 (37)	–
Anti-Ro52$^+$Ro60$^+$SSB$^+$	0 (0)	0 (0)	4 (11)	56 (32)	–
Anti-Ro52$^+$SSB$^+$/ anti-Ro60$^+$SSB$^+$	0 (0)	0 (0)	1 (3)	5 (3)	–
Total ESSDAI score, median (IQR)	0 (2)	0 (2)	1 (2)	2 (4)	<0.001

* All values are n (%) unless otherwise indicated. Objective sicca is defined by the presence of at least one of the following results: Schirmer test ≤5 mm per five minutes, ocular staining score ≥5 in at least one eye, salivary flow rate ≤0.1 mL per minute. Lymphopenia defined as lymphocytes <1,000/μL. *P* values refer to comparison based on Kruskal–Wallis or Pearson chi-square tests. ACR, American College of Rheumatology; ESSDAI, EULAR Sjögren's Syndrome Disease Activity Index; FS, focus score; Gal, IgG Fc galactosylation level; IQR, interquartile range; RF, rheumatoid factor; Sia, IgG Fc sialylation level; SjD, Sjögren disease.

meanwhile, patients with triple-positive SjD had the lowest median percentages of sialylated and galactosylated IgG. Patients with Anti-Ro60$^+$ and triple-positive SjD differed significantly from each other ($P < 0.01$; Supplementary Figure 2). Remarkably, within patients who were at risk of SjD, there were

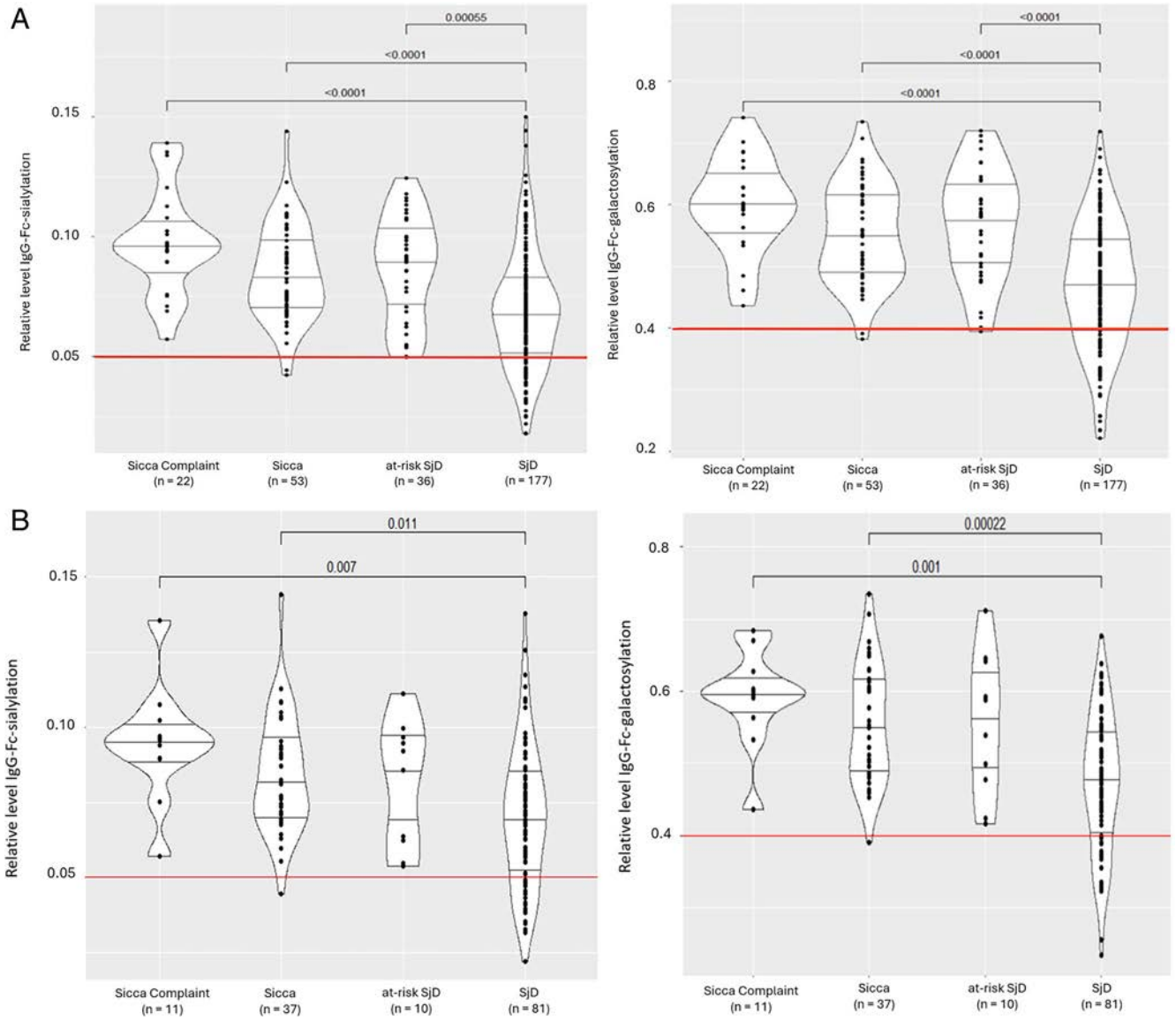

Figure 1. Relative levels of IgG Fc sialylation and galactosylation in relation to disease state. (A) All patients, irrespective of focus score (n = 288). (B) Only patients with an available focus score (n = 139). Sialylation/galactoyslation levels under this treshold are highly specific for SjD patients (red line). SjD, Sjögren disease.

no significant differences between different autoantibody profiles (Supplementary Figure 3).

Using the risk assessment tool developed by Fragkioudaki et al,[1] we estimated the risk of developing NHL in the entire cohort of 289 patients. Out of these, 257 patients (89%) exhibited zero to two risk factors and were classified as low risk, whereas 32 individuals (11%) presented with three to six risk factors, designating them as high risk for NHL.[1] Significantly, those classified as high risk showed markedly lower levels of sialylation and galactosylation compared to those in the group who were low risk ($P < 0.05$). When considering zero to one risk factors as low risk and two or more as high risk, an even more pronounced difference in Fc glycosylation between low and high risk was observed ($P < 0.001$). We assessed the positive and negative predictive value of galactosylated IgG levels to identify individuals at risk for NHL development.

Among the 49 patients with galactosylation levels below 40%, only a small subset of 8 patients presented with a high risk (three to six risk factors), resulting in a sensitivity of only 25% and a positive predictive value of 16% for the galactosylation threshold of 40% in predicting high NHL risk. Conversely, among the 240 patients with high galactosylation levels, only 24 patients had a high risk, yielding a high specificity and negative predictive value of 84% and 90%, respectively. Hence, it is evident that within patients with lower galactosylation levels, a higher proportion is at risk for NHL. Conversely, patients with SjD with unaffected galactosylated IgG levels have a low probability of having

Table 2. Relative levels of IgG Fc sialylation and galactosylation in relation to B cell activity markers, salivary gland involvement, autoantibody profile, and risk for non-Hodgkin lymphoma*

Characteristic	n or n (%)	Sialylated IgG, median (IQR), %[a]	Galactosylated IgG, median (IQR), %[a]
Lymphocytes in PB	297	$P < 0.001$	$P < 0.001$
No lymphopenia (>1,500/μL)	140 (47.1)	7.8 (3.0)	54.1 (12.6)
Mild lymphopenia (1,000–1,500/μL)	105 (35.4)	7.1 (3.3)	50.2 (12.0)
Strong lymphopenia (<1,000/μL)	52 (17.5)	6.1 (2.8)	43.7 (14.5)
Gamma globulins in PB, %[b]	300	$P < 0.001$	$P < 0.001$
Hypogammaglobulinemia	16 (5.3)	7.8 (1.8)	52.4 (8.4)
Normal percentage of gamma globulins	222 (74.0)	7.7 (3.2)	52.8 (13.7)
Hypergammaglobulinemia	62 (20.7)	5.5 (3.1)	42.3 (15.1)
IgG in PB	300	$P < 0.001$	$P < 0.001$
Low IgG (<7.0 g/L)	9 (3.0)	9.0 (3.4)	54.9 (3.0)
Normal IgG (7.0 g/L ≤ IgG ≤ 16 g/L)	225 (75.0)	7.7 (3.2)	52.0 (13.6)
High IgG (>16 g/L)	66 (22.0)	6.1 (3.5)	43.3 (16.9)
IgA in PB	300	$P < 0.01$	$P < 0.001$
Low IgA (<0.71 g/L)	6 (2.0)	5.6 (1.9)	39.9 (6.2)
Normal IgA (0.71 g/L ≤ IgA ≤ 3.65 g/L)	258 (86.0)	7.5 (3.2)	51.7 (13.7)
High IgA (>3.65 g/L)	36 (12.0)	6.5 (3.6)	44.1 (16.7)
β2 microglobulin	283	$P < 0.001$	$P < 0.001$
Normal β2 microglobulin (≤2.53 mg/L)	233 (82.3)	7.8 (3.01)	53.9 (13.1)
High β2 microglobulin (>2.53 mg/L)	50 (17.7)	5.1 (2.7)	37.8 (15.6)
RF, U/mL	300	$P < 0.001$	$P < 0.001$
Negative RF (≤11.40 U/mL)	225 (75.0)	7.7 (3.0)	53.3 (14.0)
Weakly positive RF (11.40 < RF ≤ 40U/mL)	37 (12.3)	7.1 (2.8)	48.7 (18.0)
Strongly positive RF (>40 U/mL)	38 (12.7)	5.3 (2.4)	39.8 (14.2)
Autoantibody profile	288	$P < 0.001$	$P < 0.001$
Anti-SSA$^-$	97 (33.7)	8.6 (2.7)	55.3 (12.9)
Mono-anti-Ro52$^+$	24 (8.3)	6.7 (2.6)	48.4 (15.1)
Mono-anti-Ro60$^+$	30 (10.4)	8.6 (3.7)	57.1 (13.3)
Double anti-Ro52$^+$Ro60$^+$	77 (26.7)	7.1 (3.6)	48.1 (13.6)
Triple anti-Ro52$^+$Ro60$^+$ SSB$^+$	60 (20.8)	6.4 (2.8)	46.0 (13.7)
SGUS Hocevar score	300	$P < 0.001$	$P < 0.001$
Negative Hocevar score (0–14)	149 (49.6)	7.7 (3.3)	53.9 (14.3)
Low positive Hocevar score (15–26)	71 (23.7)	8.1 (2.6)	53.9 (11.4)
High positive Hocevar score (27–48)	80 (26.7)	6.1 (2.6)	43.9 (14.5)
Histopathology FS	120	$P < 0.05$	$P < 0.01$
FS < 1	77 (64.1)	8.2 (2.6)	54.9 (12.1)
FS ≥ 1	43 (35.8)	7.0 (3.4)	48.1 (12.2)
Immunohistochemistry			
CD3$^+$	117 (99.1)	7.72 (3.1)	51.8 (14.0)
CD3$^-$	1 (0.9)	4.16	33.0
CD20$^+$	106 (89.8)	7.7 (3.9)	51.8 (15.7)
CD20$^-$	12 (10.2)	7.6 (2.7)	50.2 (13.9)
CD21$^+$	38 (32.5)	6.9 (3.9)	47.5 (0.1)
CD21$^-$	79 (67.5)	8.2 (2.1)	53.5 (9.3)
CD138$^+$	107 (93.0)	7.6 (3.2)	51.7 (10.3)
CD138$^-$	8 (7.0)	7.4 (1.8)	53.2 (1.8)
CD3/CD20 > 1	46 (42.9)	8.2 (2.7)	55.2 (13.4)
CD3/CD20 = 1	43 (40.2)	7.7 (2.8)	49.9 (12.6)
CD3/CD20 < 1	18 (16.8)	7.1 (4.3)	48.8 (13.2)
Risk of non-Hodgkin lymphoma[1]	289	$P = 0.06$	$P < 0.05$
Zero to two risk factors	257 (88.9)	7.5 (3.5)	51.1 (15.0)
Three to six risk factors	32 (11.1)	6.8 (3.6)	48.1 (15.4)
Risk of non-Hodgkin lymp	289	$P < 0.001$	$P < 0.001$
Zero to one risk factors	174 (60.2)	8.0 (3.2)	54.1 (9.3)
Two risk factors	83 (28.7)	6.2 (3.0)	45.3 (10.7)
Three to six risk factors	32 (11.1)	6.8 (3.6)	46.4 (10.5)

* *P* values refer to comparison based on Kruskal–Wallis tests or Mann–Whitney U tests (α = 0.05). FS, focus score; IQR, interquartile range; PB, peripheral blood; RF, rheumatoid factor; SGUS, salivary gland ultrasonography.
[a] *P* values of all significant differences are shown. No significant differences were found between positive or negative immunohistochemistry results, except for CD21 ($P \leq 0.05$).
[b] The threshold values for the percentage of gamma globulins evolved over time due to a change in the measuring method in our hospital clinical chemistry laboratory. In the initial 215 samples, the threshold values ranged from 8.7% to 17.7%, whereas in the last 85 samples, these values shifted to 11.1% to 18.8%.

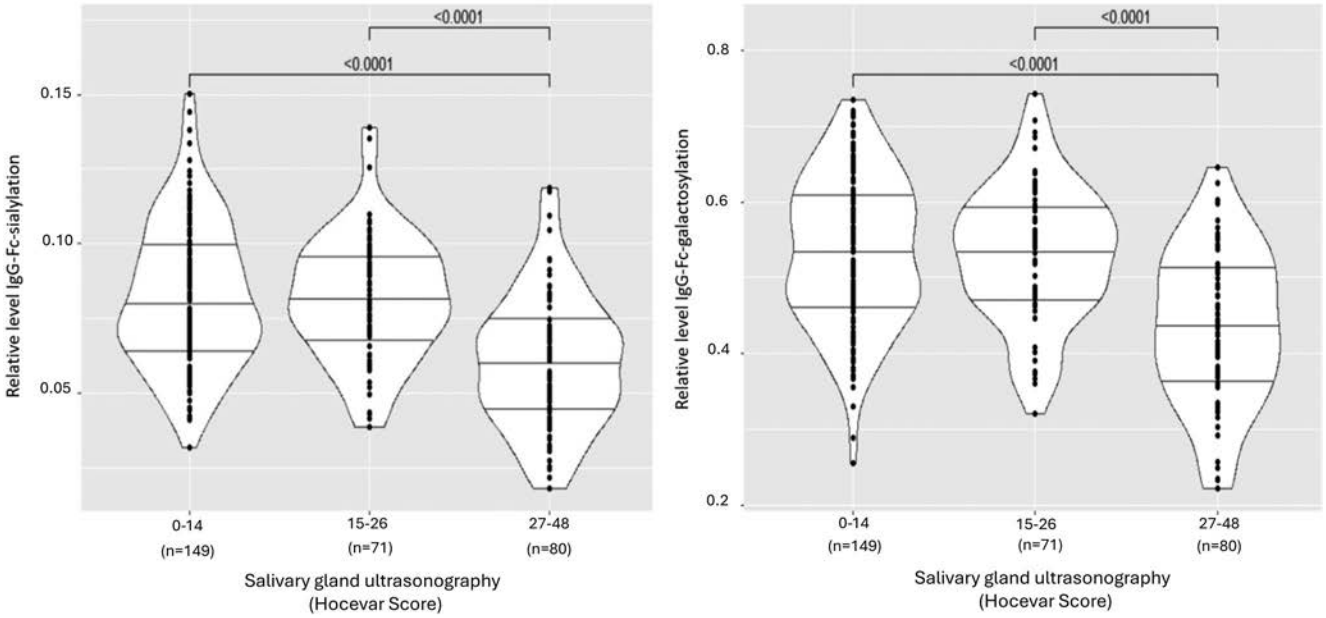

Figure 2. Relative levels of IgG Fc sialylation and galactosylation in function of salivary gland involvement assessed by ultrasonography.

NHL. Nevertheless, galactosylation or sialylation levels alone are not clear indicators of NHL risk. Therefore, we investigated what distinguishes patients who were high risk with low levels from patients who were high risk with preserved glycosylation levels.

Patients who were high risk with low galactosylation or sialylation appeared to more often exhibit RF positivity, mono-anti-Ro52/triple reactivity, and monoclonal gammopathy of undetermined significance (MGUS). In contrast, those with high sialylation and galactosylation levels more frequently manifested Raynaud phenomenon besides anti-SSA positivity. Thus, the Fc glycosylation profile was significantly associated with RF levels, the presence of MGUS, and anti-SSA positivity, three of the four laboratory risk factors ($P < 0.05$).[1] Consistent with this, sialylation and galactosylation levels correlated inversely with the total number of laboratory risk factors for NHL (anti-SSA, RF, C4, MGUS; $P < 0.001$).[1] Collectively, these data clearly indicate that Fc glycosylation changes in patients with SjD represent an important risk factor for disease transition, severity, and outcome.

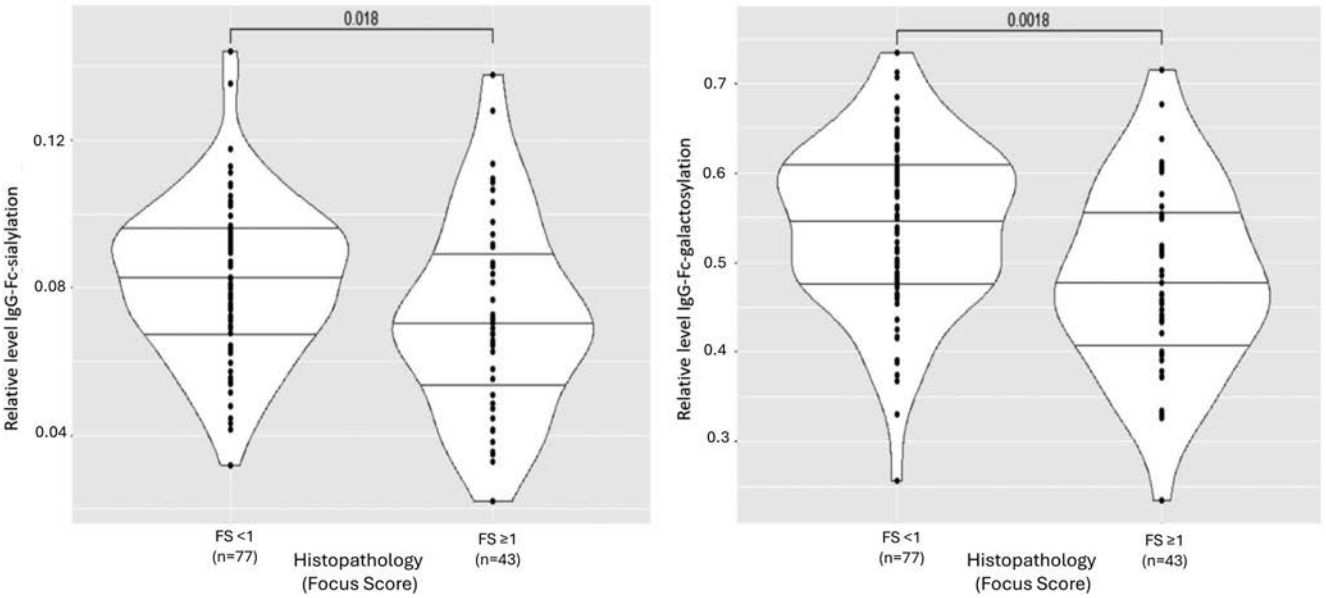

Figure 3. Relative levels of IgG Fc sialylation and galactosylation in function of salivary gland involvement assessed by histopathology. FS, focus score.

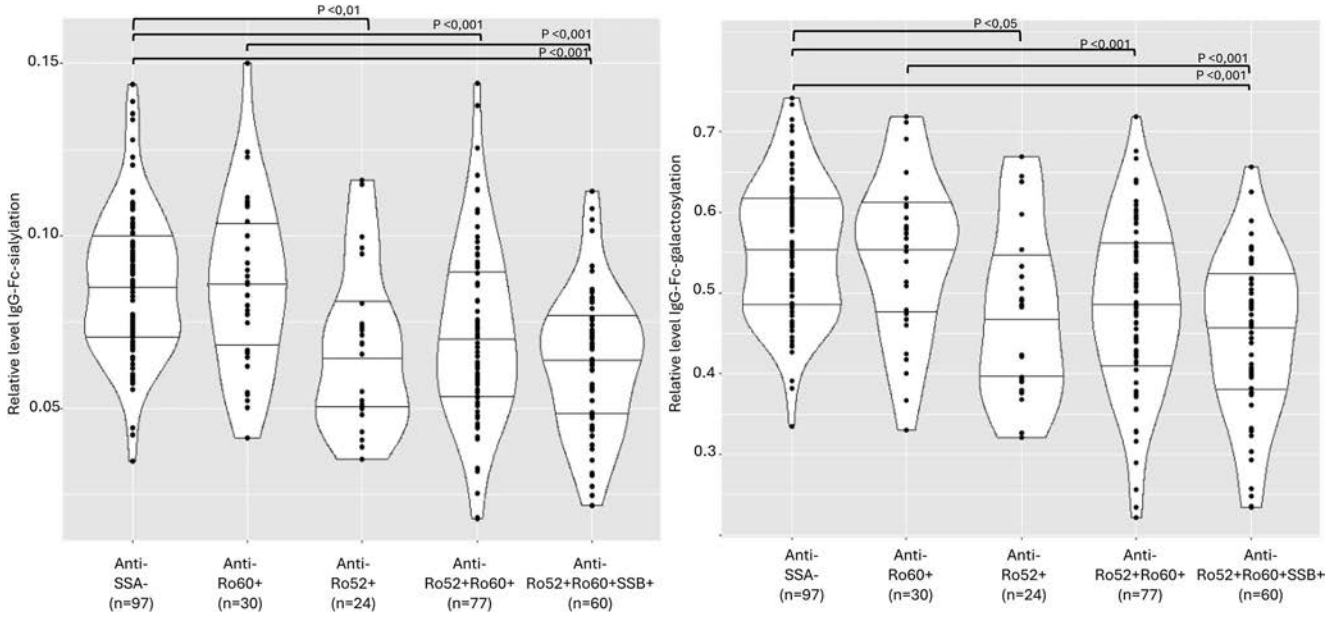

Figure 4. Relative levels of IgG Fc sialylation and galactosylation in function of autoantibody profile.

DISCUSSION

This is the first study investigating the link among IgG Fc glycosylation, disease transition, and activity in an observational cohort of patients with suspected or confirmed SjD. The strength of this cohort is the availability of asymptomatic individuals with anti-SSA antibodies, which we have referred to as "patients who were at risk of SjD" because they are at risk to develop SjD in the future.[5] Our results yielded several exciting findings. First, we observed a stepwise loss in sialylated IgG and galactosylated IgG levels when comparing patients who were at risk of SjD to patients with SjD. This potentially reflects a more anti-inflammatory profile in patients who were at risk of SjD versus the more proinflammatory properties[8] that have been generally ascribed to reduced sialylated and galactosylated IgG levels in patients with SjD. Importantly, these observations were observed regardless of age because adjustment for age revealed independent significant associations between disease state and sialylation and galactosylation levels. This is of great importance because sialylation and galactosylation levels typically decrease with age.[26] However, in patients with SjD, the effect of age is overridden by the impact on disease stage and activity. Second, loss in sialylated and galactosylated serum IgG levels appear to be most confined to the subset with the highest degree of autoantibody reactivity, as indicated by anti-Ro52-60 and anti-SSB. Third, serum levels of sialylated and galactosylated IgG were found to correlate with histopathological alterations in the salivary gland and with signs of B cell activation and germinal center reaction. Finally, normal levels of sialylated and galactosylated IgG were linked to low risk for NHL development, whereas reduced levels enrich patients at risk, albeit that sensitivity was only moderate.

Similar to anti-cyclic citrullinated peptide (anti-CCP) antibodies preceding disease onset in patients with rheumatoid arthritis,[27] our findings suggest that Fc glycosylation could potentially serve as a biomarker predicting the transition to SjD. Notably, significant differences were found between diagnosed patients with SjD versus patients who were at risk of SjD, patients with sicca, or patients with sicca complaints. Early detection of disease transition could offer a crucial window for timely immune intervention, potentially curbing irreversible damage to salivary glands. As a potential diagnostic biomarker for SjD, we discovered that in patients with suspected SjD, a galactosylation level below 40% proved to be highly specific for identifying patients with SjD, even in the absence of other parameters. However, a significant proportion of patients meeting the ACR/EULAR classification criteria[4] still exceeds this threshold, which pinpoints a substantial variation in Fc glycosylation profiles among patients with SjD. This diversity reflects that patients with SjD, despite meeting these criteria, still exhibit substantial heterogeneity that may compromise the composition of homogeneous populations for clinical trials.[2] In this context, the presence of distinct endotypes has scrutinized the development of effective treatments throughout the entire SjD spectrum. Therefore, we investigated the association between the Fc glycosylation, autoantibody profile, and disease activity in patients with SjD to evaluate if sialylation and galactosylation IgG measurements could be of help.

Triple (anti-Ro52-60-SSB) reactivity had the lowest sialylation and galactosylation levels, followed by patients with anti-

Ro52 and who were double positive. We previously uncovered that patients who were triple positive represent the most affected subgroup within those with SjD.[28] However, it remains uncertain if the observed lowest sialylation and galactosylation levels in individuals who were triple positive are the cause or consequence of higher disease activity. Additionally, it is unclear whether these Fc glycosylation changes occur in response to local inflammation in the salivary glands and whether these Fc glycosylation changes are restricted to autoantibodies. In this context, autoantibody-restricted IgG glycosylation alterations have only been described in some rheumatic diseases such as rheumatoid arthritis and anti-neutrophil cytoplasmic antibody associated vasculitis. Here, anti-CCP antibodies and anti-proteinase-3 antibodies were found to have even lower galactosylation levels than the levels reported for the total IgG.[9,27,29] In patients with MGUS and multiple myeloma, monoclonal antibodies showed lower sialylation levels than the coexisting polyclonal antibodies, suggesting B cell–dependent, antigen-specific glycosylation patterns.[30] In line with a putative role for antigen-specific glycosylation is our observation of higher sialylation and galactosylation levels in patients with anti-SSA–negative SjD. However, a formal proof for antigen-specific glycosylation in the context of SjD is still lacking but would need analysis of the glycosylation profile of anti-SSA (Ro52/Ro60) and anti-SSB (La), including subclass specific profiling.[31] This, however, was beyond the scope of the current study. Curiously, Fc glycosylation status in serum IgG was found to correlate very well with presence or absence of salivary gland involvement. Hence, we showed an inverse correlation to both local salivary gland involvement by histopathology and signs of B cell activation and presence of FDCs. The former is marked by clearly lower sialylation and galactosylation levels in patients showing a high degree of abnormalities on SGUS and/or a positive FS compared to those with less SGUS abnormalities and a negative FS, respectively. Moreover, the lowest sialylation and galactosylation levels were observed in B cell predominance over T cells on salivary gland biopsies and in the presence of FDCs. This is of conceptual interest because FDCs are tightly associated with B cells and critical for germinal center formation, thereby facilitating B cell activation and affinity maturation.[32] In this context, it is important to note that FDCs are reported to produce interleukin (IL)-6[33,34] because lower sialylation and galactosylation levels were shown by IL-6–inducing adjuvants.[35] Therefore, it can be anticipated that the production of IL-6 by FDCs in ectopic germinal centers may contribute to the lower sialylation and galactosylation levels found. Bartsch et al[35] also showed that IL-6 induced follicular T helper (Th) cells and Th17 cells by the IL-23 pathway.[32] Importantly, the IL-23–Th17 axis was previously reported to down-regulate the expression of beta-galactoside alpha-2,6-sialyltransferase 1, an enzyme responsible for adding sialic acid, in newly developing plasmablasts and plasma cells.[36] Thus, the glycosylation profile of serum IgG outlined here might reflect local B cell activation and affinity maturation within ectopic germinal centers. The clear association between B cell activity and loss of IgG sialic acid and galactose is in alignment with a recent proof of concept study by Morel et al[37] that indicated changes in B cells and their subsets from patients with SjD and systemic lupus erythematosus carrying altered glycosylation profiles. This in turn may be linked to heightened B cell activity due to the loss of B cell suppression. More precisely, sialic acid–terminated glycans play a role in immune modulation by binding to CD22 (siglec 2), an inhibitory coreceptor of the B cell.[29,37] These interactions contribute to maintaining peripheral tolerance by suppressing the B cell receptor signaling.[38] Sialic acid glycans also bind CD23 on B cells, thereby inducing inhibitory FcγRIIb and elevating the threshold for B cell activation.[39] Furthermore, they have lower affinity for proinflammatory type I FcγRs and C1q. Hence, the loss of sialic acid as seen in patients with the most active SjD might shift the immune response to proinflammatory and higher B cell activity.[29,40] However, this study does not allow to draw conclusions on the functional implications of the changes in Fc glycosylation profiles. The role of agalactosylated glycans, which are generally considered proinflammatory, is less well studied.[13] Within our study, a subgroup with remarkably low sialylation and galactosylation levels exhibited a significant degree of local and systemic involvement. These observations suggest that Fc glycosylation may be a valuable tool for identifying and prioritizing patients with SjD who require more intensive follow-up and personalized clinical management.[41]

A major concern in patients with SjD is an enhanced risk for development of NHL. Indeed, 5% of patients with SjD develop NHL, mostly a mucosa-associated lymphoid tissue lymphoma (MALT).[1] The precise mechanisms underlying the transformation from benign B cell proliferation to malignancy are not yet fully understood, but uncontrolled B cell activation plays a critical role.[42] Several key indicators (eg, production of autoantibodies, hypocomplementemia, and vasculitis by precipitation of immune complexes) are considered independent risk factors for NHL among individuals with SjD.[1,43] Fragkioudaki et al[1] developed a tool incorporating seven risk factors in patients with SjD with a cumulative total score that serves as an indicator of an individual's risk for developing NHL. Given that the Fc glycosylation profile is known to influence B cell responses, we reasoned this may play a role in NHL development. However, given the low prevalence of patients with NHL associated with SjD in our cross-sectional study (n = 4), we could not directly explore the association between Fc glycosylation and NHL prevalence/incidence. As an alternative strategy, we applied the tool by Fragkioudaki et al[1] to assess the interrelation between Fc glycosylation and risk of NHL development.[1] Galactosylated IgG levels were found to be lower in patients with an increased risk score for NHL (eg, presence of three to six risk factors). Although sensitivity and positive predictive value were modest, specificity and negative predictive value were high. Thus, when galactosylation levels of IgG are unaffected, the probability of having a high-risk profile for NHL development is low.

We also evaluated associations with individual prognostic factors and noted a significant association between sialylation and galactosylation levels and RFs. Bende et al[44] previously reported that at least 75% of salivary gland MALT lymphomas in patients with SjD expressed RFs. RFs are well recognized to form immune complexes: IgM-RF form complement activating immune complexes with IgG-containing antigen–antibody complexes. In this context, the association between different sialylation and galactosylation IgG levels are indicative of a broader array of B cell activation. Along the same lines, also in patients with MGUS, which is known to represent a substantial risk for developing NHL (IgM MGUS) and multiple myeloma (IgG and IgA MGUS),[45] lower sialylation and galactosylation Ig levels have been reported.[45]

Furthermore, the significantly reduced sialylation and galactosylation levels in the presence of an increasing total number of laboratory risk factors suggests potential of Fc glycosylation as a biomarker for assessing the NHL risk. Nevertheless, to ascertain whether Fc glycosylation independently predicts NHL risk beyond established risk factors, rigorous multivariate analysis in larger cohorts is necessary. Besides, profiling of other glycoforms as Fc fucosylation may be essential to gain a comprehensive understanding of their diverse influences on the antibody's effector function.[46]

Our study has several strengths because it covers the entire disease spectrum within SjD, which permits comparisons across different patient groups accounting for different stages (patients with sicca, patients who were at risk of SjD, and patients with SjD). To address age and sex influence on Fc glycosylation, age-matched and sex-matched healthy controls need to be incorporated. By using a group only with sicca with comparable demographics, we believe we effectively mitigated this issue. Even though it could be perceived that disease categorization into various subsets is somehow artificial, confident classification of 139 patients based on histopathological data was achieved. Analysis of the entire cohort confirmed consistent trends in laboratory markers and SGUS findings, reinforcing reliability. Although this study revealed significant associations between glycosylation profiles and various disease states, it cannot establish causality or determine their functional implications. Nonetheless, our findings strongly suggest the potential of Fc glycosylation as a biomarker for SjD activity. The longitudinal data from our yearly follow-up will enable us to evaluate its effectiveness in predicting disease progression, specifically the transition from asymptomatic carriers of anti-SSA to patients with SjD or other autoimmune diseases.[47] Furthermore, our results indicate that Fc glycosylation was associated both with local and systemic B cell disease activity and with established risk factors for NHL development.[1] Given advancements in cost-effective, high-throughput techniques, it might be feasible to perform Fc glycosylation measurement in daily clinical practice, maybe even in saliva.[22,48] As such, it could aid in tackling the challenges of early diagnosis, clinical heterogeneity, stratification for inclusion, and prognosis and potentially even be used as surrogate endpoint in clinical trials.[29,49]

AUTHOR CONTRIBUTIONS

All authors were involved in drafting the article or revising it critically for important intellectual content, and all authors approved the final version to be published. Dr Peene had full access to all of the data in the study and takes responsibility for the integrity of the data and the accuracy of the data analysis.

Study conception and design. Achten, Meuris, Jarlborg, Decruy, Deprez, Dumas, Callewaert, Elewaut, Peene.

Acquisition of data. Achten, Meuris, Deroo, Jarlborg, Decruy, Deprez, Dumas, De Boeck, Genbrugge, Bauters, Dochy, Creytens, Roels, Callewaert, Elewaut, Peene.

Analysis and interpretation of data. Achten, Meuris, Deroo, Jarlborg, Decruy, Deprez, Dumas, Elewaut, Peene.

REFERENCES

1. Fragkioudaki S, Mavragani CP, Moutsopoulos HM. Predicting the risk for lymphoma development in Sjogren syndrome: an easy tool for clinical use. Medicine (Baltimore) 2016;95(25):e3766.
2. Arends S, de Wolff L, Deroo L, et al. Selection of study endpoints and patients for clinical trials in primary Sjögren's syndrome. Clin Exp Rheumatol 2022;40(12):2225–2232.
3. Nocturne G, Mariette X. Advances in understanding the pathogenesis of primary Sjögren's syndrome. Nat Rev Rheumatol 2013;9(9):544–556.
4. Shiboski CH, Shiboski SC, Seror R, et al. 2016 American College of Rheumatology/European League Against Rheumatism classification criteria for primary Sjögren's syndrome: a consensus and data-driven methodology involving three international patient cohorts. Ann Rheum Dis 2017;76(1):9–16.
5. Theander E, Jonsson R, Sjöström B, et al. Prediction of Sjögren's syndrome years before diagnosis and identification of patients with early onset and severe disease course by autoantibody profiling. Arthritis Rheumatol 2015;67(9):2427–2436.
6. Rivera TL, Izmirly PM, Birnbaum BK, et al. Disease progression in mothers of children enrolled in the Research Registry for Neonatal Lupus. Ann Rheum Dis 2009;68(6):828–835.
7. Seeling M, Bruckner C, Nimmerjahn F. Differential antibody glycosylation in autoimmunity: sweet biomarker or modulator of disease activity? Nat Rev Rheumatol 2017;13(10):621–630.
8. Goulabchand R, Vincent T, Batteux F, et al. Impact of autoantibody glycosylation in autoimmune diseases. Autoimmun Rev 2014;13(7):742–750.
9. Kissel T, Toes REM, Huizinga TWJ, et al. Glycobiology of rheumatic diseases. Nat Rev Rheumatol 2023;19(1):28–43.
10. Basset C, Dueymes M, Devauchelle V, et al. Changes in glycosylation of immunoglobulins in primary Sjögren's syndrome. Ann Med Interne (Paris) 1998;149(1):42–44.
11. Buhre JS, Becker M, Ehlers M. IgG subclass and Fc glycosylation shifts are linked to the transition from pre- to inflammatory autoimmune conditions. Front Immunol 2022;13:1006939.
12. Irvine EB, Alter G. Understanding the role of antibody glycosylation through the lens of severe viral and bacterial diseases. Glycobiology 2020;30(4):241–253.
13. Radovani B, Gudelj I. N-glycosylation and inflammation; the not-so-sweet relation. Front Immunol 2022;13:893365.
14. Greenspan JS, Daniels TE, Talal N, et al. The histopathology of Sjögren's syndrome in labial salivary gland biopsies. Oral Surg Oral Med Oral Pathol 1974;37(2):217–229.

15. Whitcher JP, Shiboski CH, Shiboski SC, et al. A simplified quantitative method for assessing keratoconjunctivitis sicca from the Sjögren's syndrome international registry. Am J Ophthalmol 2010;149(3): 405–415.
16. Seror R, Bowman SJ, Brito-Zeron P, et al. EULAR Sjögren's Syndrome Disease Activity Index (ESSDAI): a user guide. RMD Open 2015;1(1):e000022.
17. Hocevar A, Ambrozic A, Rozman B, et al. Ultrasonographic changes of major salivary glands in primary Sjogren's syndrome. Diagnostic value of a novel scoring system. Rheumatology (Oxford) 2005;44(6):768–772.
18. Deroo L, Achten H, De Boeck K, et al. Discriminative power of salivary gland ultrasound in relation to symptom-based endotypes in suspected and definite primary Sjogren's syndrome. Semin Arthritis Rheum 2022;56:152075.
19. Mossel E, van Nimwegen JF, Stel AJ, et al. Clinical phenotyping of primary Sjögren syndrome patients using salivary gland ultrasonography: data from the RESULT cohort. J Rheumatol 2021;48(5): 717–727.
20. Daniels TE, Cox D, Shiboski CH, et al. Associations between salivary gland histopathologic diagnoses and phenotypic features of Sjögren's syndrome among 1,726 registry participants. Arthritis Rheum 2011;63(7):2021–2030.
21. Fisher BA, Jonsson R, Daniels T, et al. Standardisation of labial salivary gland histopathology in clinical trials in primary Sjögren's syndrome. Ann Rheum Dis 2017;76(7):1161–1168.
22. Vanderschaeghe D, Meuris L, Raes T, et al. Endoglycosidase S enables a highly simplified clinical chemistry procedure for direct assessment of serum IgG undergalactosylation in chronic inflammatory disease. Mol Cell Proteomics 2018;17(12):2508–2517.
23. Harris PA, Taylor R, Minor BL, et al. The REDCap consortium: building an international community of software platform partners. J Biomed Inform 2019;95:103208.
24. Harris PA, Taylor R, Thielke R, et al. Research electronic data capture (REDCap)–a metadata-driven methodology and workflow process for providing translational research informatics support. J Biomed Inform 2009;42(2):377–381.
25. Seror R, Ravaud P, Mariette X, et al. EULAR Sjogren's Syndrome Patient Reported Index (ESSPRI): development of a consensus patient index for primary Sjogren's syndrome. Ann Rheum Dis 2011; 70(6):968–972.
26. Dall'Olio F. Glycobiology of aging. Subcell Biochem 2018;90: 505–526.
27. Rombouts Y, Ewing E, van de Stadt LA, et al. Anti-citrullinated protein antibodies acquire a pro-inflammatory Fc glycosylation phenotype prior to the onset of rheumatoid arthritis. Ann Rheum Dis 2015;74(1): 234–241.
28. Deroo L, Achten H, De Boeck K, et al. The value of separate detection of anti-Ro52, anti-Ro60 and anti-SSB/La reactivities in relation to diagnosis and phenotypes in primary Sjögren's syndrome. Clin Exp Rheumatol 2022;40(12):2310–2317.
29. Li D, Lou Y, Zhang Y, et al. Sialylated immunoglobulin G: a promising diagnostic and therapeutic strategy for autoimmune diseases. Theranostics 2021;11(11):5430–5446.
30. Bosseboeuf A, Allain-Maillet S, Mennesson N, et al. Pro-inflammatory state in monoclonal gammopathy of undetermined significance and in multiple myeloma is characterized by low sialylation of pathogen-specific and other monoclonal immunoglobulins. Front Immunol 2017;8:1347.
31. Plomp R, Ruhaak LR, Uh HW, et al. Subclass-specific IgG glycosylation is associated with markers of inflammation and metabolic health. Sci Rep 2017;7(1):12325.
32. Kranich J, Krautler NJ. How follicular dendritic cells shape the b-cell antigenome. Front Immunol 2016;7:225.
33. Wu Y, El Shikh ME, El Sayed RM, et al. IL-6 produced by immune complex-activated follicular dendritic cells promotes germinal center reactions, IgG responses and somatic hypermutation. Int Immunol 2009;21(6):745–756.
34. McHugh J. Systemic lupus erythematosus: B cell-derived IL-6 promotes disease. Nat Rev Rheumatol 2017;13(11):633.
35. Bartsch YC, Eschweiler S, Leliavski A, et al. IgG Fc sialylation is regulated during the germinal center reaction following immunization with different adjuvants. J Allergy Clin Immunol 2020;146(3):652–666.e11.
36. Pfeifle R, Rothe T, Ipseiz N, et al. Regulation of autoantibody activity by the IL-23-T(H)17 axis determines the onset of autoimmune disease. Nat Immunol 2017;18(1):104–113.
37. Morel M, Pochard P, Echchih W, et al. Abnormal B cell glycosylation in autoimmunity: a new potential treatment strategy. Front Immunol 2022;13:975963.
38. Müller J, Nitschke L. The role of CD22 and siglec-G in B-cell tolerance and autoimmune disease. Nat Rev Rheumatol 2014;10(7):422–428.
39. Smith KG, Clatworthy MR. FcgammaRIIB in autoimmunity and infection: evolutionary and therapeutic implications. Nat Rev Immunol 2010;10(5):328–343.
40. Wang TT, Maamary J, Tan GS, et al. Anti-HA glycoforms drive B cell affinity selection and determine influenza vaccine efficacy. Cell 2015; 162(1):160–169.
41. Verhelst X, Dias AM, Colombel JF, et al. Protein glycosylation as a diagnostic and prognostic marker of chronic inflammatory gastrointestinal and liver diseases. Gastroenterology 2020;158(1):95–110.
42. Nocturne G, Pontarini E, Bombardieri M, et al. Lymphomas complicating primary Sjögren's syndrome: from autoimmunity to lymphoma. Rheumatology (Oxford) 2021;60(8):3513–3521.
43. Quartuccio L, Isola M, Baldini C, et al. Biomarkers of lymphoma in Sjögren's syndrome and evaluation of the lymphoma risk in prelymphomatous conditions: results of a multicenter study. J Autoimmun 2014;51:75–80.
44. Bende RJ, Janssen J, Beentjes A, et al. Salivary gland mucosa-associated lymphoid tissue-type lymphoma from Sjögren's syndrome patients in the majority express rheumatoid factors affinity-selected for IgG. Arthritis Rheumatol 2020;72(8):1330–1340.
45. Tomi AL, Belkhir R, Nocturne G, et al. Brief report: monoclonal gammopathy and risk of lymphoma and multiple myeloma in patients with primary Sjögren's syndrome. Arthritis Rheumatol 2016;68(5):1245–1250.
46. Dekkers G, Treffers L, Plomp R, et al. Decoding the human immunoglobulin G-glycan repertoire reveals a spectrum of Fc-receptor- and complement-mediated-effector activities. Front Immunol 2017;8:877.
47. Chan EKL. Anti-Ro52 Autoantibody is common in systemic autoimmune rheumatic diseases and correlating with worse outcome when associated with interstitial lung disease in systemic sclerosis and autoimmune myositis. Clin Rev Allergy Immunol 2022;63(2):178–193.
48. Longobardi S, Lopez-Davis C, Khatri B, et al. Autoantibodies identify primary Sjögren's syndrome in patients lacking serum IgG specific for Ro/SS-A and La/SS-B. Ann Rheum Dis 2023;82:1181–1190.
49. Engdahl C, Bondt A, Harre U, et al. Estrogen induces St6gal1 expression and increases IgG sialylation in mice and patients with rheumatoid arthritis: a potential explanation for the increased risk of rheumatoid arthritis in postmenopausal women. Arthritis Res Ther 2018;20(1):84.

Arthritis & Rheumatology
Vol. 77, No. 3, March 2025, pp 322–334
DOI 10.1002/art.43029

American College of Rheumatology
Empowering Rheumatology Professionals

Systemic Sclerosis Dermal Fibroblast Exosomes Trigger Type 1 Interferon Responses in Keratinocytes via a TBK/JAK/STAT Signaling Axis

Jessica Bryon,[1] Christopher W. Wasson,[1] Katja Koeppen,[2] Francesca Chandler,[1] Leon F. Willis,[1] Stefano Di Donato,[3] Elliott Klein,[2] Elton Zeqiraj,[1] Rebecca L. Ross,[1] and Francesco Del Galdo[3]

Objective. Activation of type I interferon (IFN) response has been shown to correlate with disease activity in systemic sclerosis (SSc). It is currently unknown whether the tissue-specific type I IFN activation is a consequence of the response observed in blood or rather its source. Exosomes from SSc fibroblasts were recently shown to activate macrophages in vitro. Here, we aimed to determine the source of type I IFN signature in SSc skin biopsies and the potential role of exosomes from SSc dermal fibroblasts in the process.

Methods. Skin biopsies were obtained from the forearms of healthy patients and of those with SSc and processed for dermal fibroblasts and keratinocytes. Exosomes were isolated from healthy and SSc dermal fibroblast supernatants by ultracentrifugation and added to human skin keratinocytes. Keratinocyte transcriptome was analyzed by RNA sequencing (RNA-seq) analysis. TANK-binding kinase (TBK) and JAK were inhibited using a small molecule inhibitor (GSK8612) and tofacitinib, respectively.

Results. SSc skin biopsies showed the highest levels of type I IFN response in the epidermal layer. RNA-seq analysis of keratinocytes transcriptome following exposure to dermal fibroblast exosomes showed strong up-regulation of IFN signature genes induced by SSc exosomes compared to healthy control. Inhibition of TBK or JAK activity suppressed the up-regulation of the IFN signature induced by SSc exosomes.

Conclusion. IFN activation of SSc keratinocytes is dependent on their crosstalk with dermal fibroblasts and inducible by extracellular exosomes. Our data indicate that SSc fibroblast exosomes contribute to the type I IFN activation in SSc skin through activation of pattern recognition receptors upstream of TBK.

INTRODUCTION

Systemic sclerosis (SSc) is a connective tissue disease driven by tissue and vascular fibrosis of the skin and internal organs. Myofibroblasts have been widely characterized as the key cellular elements of tissue fibrosis for more than two decades. In this context, the key role of profibrotic pathways such as transforming growth factor β and Wnt has been dissected in fine detail. More recently, the activation of type I interferon (IFN) pathway has been associated with markers of disease activity and progression in both skin and lung manifestations, but its relationship with fibroblast activation is less clear.[1-3]

Immunohistochemistry analysis of SSc skin biopsies has revealed that, although there is a clear sign of type I IFN activation in SSc dermal fibroblasts, the epidermal layer is the major producer of type I IFN response.[2] The trigger for the response in the epidermis is still unclear. Previous studies have shown cancer-associated fibroblast (CAF) exosomes can induce IFN-stimulated

Supported by a Boehringer Ingelheim opn2EXPERTS funding call (to Drs Wasson and Del Galdo). Dr Bryon's work was funded by a National Institute for Health and Care Research (NIHR) Biomedical Research Centre (BRC) PhD studentship (Scleroderma workstream) to Dr Del Galdo. Dr Chandler's work was supported by a Wellcome Trust PhD studentship (219997/Z/19/Z). Dr Zeqiraj's work was supported by a Wellcome Senior Research Fellowship (grant 222531/Z/21/Z). Dr Del Galdo's work was funded by the national institute for health and care research (NIHR) Leeds biomedical research centre (BRC) (NIHR203331).

[1]Jessica Bryon, PhD, Christopher W. Wasson, PhD, Francesca Chandler, PhD, Leon F. Willis, PhD, Elton Zeqiraj, PhD, Rebecca L. Ross, PhD: University of Leeds, Leeds, United Kingdom; [2]Katja Koeppen, PhD, Elliott Klein, PhD: Boehringer Ingelheim, Ridgefield, Connecticut; [3]Stefano Di Donato, MD, Francesco Del Galdo, MD: University of Leeds and the National Institute for Health and Care Research Leeds Musculoskeletal Biomedical Research Centre, Leeds, United Kingdom.

Drs. Bryon and Wasson are co-first authors and contributed equally to this work.

Additional supplementary information cited in this article can be found online in the Supporting Information section (https://acrjournals.onlinelibrary.wiley.com/doi/10.1002/art.43029).

Author disclosures are available at https://onlinelibrary.wiley.com/doi/10.1002/art.43029.

Address correspondence via email to Francesco Del Galdo, MD, at f.delgaldo@leeds.ac.uk.

Submitted for publication January 10, 2024; accepted in revised form August 15, 2024.

gene (ISG) expression in associated epithelial cells.[4] In particular, CAF exosomes were shown to trigger type I IFN activation through uncapped RNA-dependent activation of retinoic acid–inducible gene I (RIG-I) in the epithelial cells, which in turn was dependent on increased activity of RNA polymerase III (Pol III).[5] These findings are particularly relevant as SSc fibroblasts share a number of similarities with CAFs,[6,7] and autoantibodies against RNA Pol III are one of the SSc-specific antinuclear antibodies carrying poor prognostic value for disease progression.[8] Consistent with these findings, while our studies were in progress, Bhandari et al showed that SSc dermal fibroblast exosomes are able to trigger the activation of macrophages in vitro.[9] These recent data support the previously observed role of dermal fibroblasts in participating in the pathogenesis of SSc beyond tissue fibrosis[10] and possibly in a direct activation of the immune events participating to tissue damage.

In this context, we set out to determine whether SSc dermal fibroblasts could participate in the type I IFN response observed in SSc skin, particularly through extracellular vesicles. Here we show for the first time that the type I IFN activation shown by keratinocytes in vivo can be driven by SSc fibroblast exosomes. Furthermore, we show that exosomes induced type I IFN signaling in keratinocytes is dependent upon the exosome RNA induced activation of the TANK-binding kinase (TBK)1/JAK/STAT signaling cascade.

MATERIALS AND METHODS

Patient cell lines. Full thickness skin biopsies were surgically obtained from the forearms of four adult healthy controls and five adult patients with recent onset SSc, defined as a disease duration of less than 18 months from the appearance of clinically detectable skin induration. All patients satisfied the 2013 American College of Rheumatology/EULAR criteria for the classification of SSc[29]. All participants provided written informed consent to participate in the study. Informed consent procedures were approved by NRES-011NE to author FDG. Fibroblasts were isolated and established as previously described. SSc keratinocytes were grown from dissected skin biopsies and grown in keratinocyte grown media (Promega). Primary cells were immortalized using human telomerase reverse transcriptase (hTERT) to produce healthy control hTERT and SSc hTERT.

Cell culture. The immortalized keratinocyte cell line HaCaTs were maintained in Dulbecco's modified Eagle medium (DMEM) (Gibco) supplemented with 10% fetal bovine serum (FBS) (Sigma) and penicillin-streptomycin (Sigma). HaCaTs were stimulated with 1% total volume of healthy and SSc fibroblasts exosomes for 48 hours. TBK1 was inhibited with GSK8612 (10 μM) and JAK1 inhibitor tofacitinib (10 μM) for 48 hrs.

Transwell assay. Fibroblasts were seeded onto 0.4-micron pore polyethylene terephthalate transmembranes (Corning). An equal number of HaCaTs were seeded into a separate cell-culture plate. Upon confluency, the pore was inserted into the well and incubated for 48 hours. The HaCaTs were harvested for RNA and protein analysis. The fibroblasts were stained with DAPI and counted to ensure equal amounts of fibroblasts were used in the experiment.

Exosome isolation. Fibroblast cell cultures were grown as discussed above with exosome-depleted FBS. Exosomes were isolated from media collected after 48 to 72 hours by ultracentrifugation (42,000 revolutions per minute for 2 hours). The pelleted exosomes were isolated using the total exosome isolation reagent (Invitrogen) and resuspended in phosphate buffered saline (PBS). RNA was then extracted and purified using the Total Exosome RNA & Protein Isolate Kit (Invitrogen), according to the manufactures protocol.

Exosomal RNA transfections. Exosomal RNA (50 ng) isolated from healthy or SSc fibroblast exosomes was transfected into HaCaTs using Lipofectamine 2000 (Invitrogen) and incubated for 48 hours. In addition, the exosome RNA was pretreated with RNase A for 2 hours at 37°C, after which the RNase A was inhibited with RNase inhibitor before transfection. Lipofectamine 2000 in the absence of RNA was added to the mock control cells.

Immunolabeling and visualization of fibroblast-derived exosomes internalization in human epidermal keratinocytes. Isolated fibroblast exosomes were stained Vybrant DiO cell-labeling solution (Invitrogen) and added to HaCaT culture media. Exosomes were added at 3, 6, 10, 24, and 48 hours, over a time course. The HaCaTs were imaged on an LMS700 confocal scanning inverted microscope. The images were processed in Image J and Zen 3.1 (blue edition) software.

CD63 enzyme-linked immunosorbent assay. Exosome abundance was measured using the ExoELISA-ULTRA CD63 enzyme-linked immunosorbent assay (ELISA) (System Biosciences). The ELISA plate is precoated with an anti-CD63 primary antibody, which recognizes the tetraspanin CD63 on the exosome surface. The secondary antibody contains a horseradish peroxidase enzyme used for signal amplification. The colorimetric substrate 3,3′,5,5′-tetramethylbenzidine is used for the assay read out. The results are read on a Thermo Scientific Multiskan EX spectrophotometer at a wavelength of 450 nm.

Dynamic light scattering. Exosomes were diluted in sterile PBS to a concentration of 100 nM. The samples were injected (150 μL, per sample) into a Wyatt miniDawn Treos system (equipped with an additional dynamic light scattering [DLS] detector). The raw data were analyzed using the ASTRA 6.0.3 software

supplied by the instrument, with the regularization algorithm used to generate the size-distribution histograms. The histograms of signal intensity versus hydrodynamic radius were then plotted in OriginLab.

Western blotting. Total proteins were extracted from fibroblasts in radioimmunoprecipitation assay buffer and resolved by sodium dodecyl sulfate–polyacrylamide gel electrophoresis (10%–15% Tris-Glycine). Proteins were transferred onto Hybond nitrocellulose membranes (Amersham) and probed with antibodies specific for pSTAT1, total STAT1 (Cell Signaling Technology), CD63 (Abcam), TSG101(Abcam), histone 3 (Cell Signaling Technology), pIRF3 (Abcam), IRF3 (Cell Signaling Technology), and β-Actin (Sigma). Immunoblots were visualized with species-specific horseradish peroxidase (HRP)-conjugated secondary antibodies (Sigma) and enhanced chemiluminescence (Thermo Scientific/Pierce) on a Bio-Rad ChemiDoc imaging system.

RNA sequencing. Quality control of fastq files was performed with FastQC version 0.11.9. Reads were aligned to the human reference genome version GRCh38.84 using STAR aligner version 2.5.2b.[13] MultiQC version 1.11[14] was used to perform quality control on the alignment and generate an overall quality control report. Downstream analyses and visualizations were performed using R version 4.1.2 (https://www.R-project.org/). BAM alignment files generated by STAR were transformed into count tables using Rsubread version 2.8.1[15].The R package edgeR version 3.36.0[16] was used for differential gene expression analysis. Gene set enrichment analysis for gene ontology biologic processes was performed using WebGestalt[27,28].

Quantitative reverse transcription–polymerase chain reaction. RNA was extracted from cells using commercial RNA extraction kits (Zymo Research). RNA (1 μg) was reverse transcribed using complementary DNA synthesis kits (ThermoFisher Scientific). Quantitative reverse transcription–polymerase chain reactions (qRT-PCRs) were performed using SyBr Green PCR kits on a Thermocycler with primers specific for MX1 (forward: CGACACGAGTTCCACAAATG reverse: AAGCC TGGCAGCTCTCTACC), CXCL10 (forward; GGTGAGAAGAGA TGTCTGAATCC reverse; GTCCATCCTTGGAAGCACTGCA), CXCL11 (forward; TCCCCCATGTTCAAAAGAGGAC reverse; ATATCTGCCACTTTCACTGCTTTTAC), OAS1 (forward; CGGAC CCTACAGGAAACTTG reverse; GAAGCAGGAGGTCTCACCAG), IFIT1 (forward; GACTGGCAGAAGCCCAGACT reverse; GCGGAA GGGATTTGAAAGCT) and GAPDH (forward; ACCCACTCCTCCA CCTTTGA reverse; CTGTTGCTGTAGCCAAATTCGT). Data were analyzed using the ΔΔ Ct method. GAPDH served as a housekeeping gene. Type I IFN superarray was performed using manufacturer protocol (Qiagen).

Transmission electron microscopy. Healthy and SSc exosomes were loaded onto carbon-coated copper grids (Formvar/Carbon, 300 mesh Cu, Agar Scientific). Grids were glow discharged for 30 seconds at 0.39 mBar pressure and 10 mA (PELCO easiGlow, Ted Pella). Grids were incubated for 1 minute with a 7-μL sample, washed three times with ddH_2O, and stained with 2% (weight/volume) uranyl acetate. Data were collected using a Tecnai F20 transmission electron microscope (FEI) at 200 KeV, fitted with a Ceta CMOS CCD camera (FEI). Micrographs were collected at 40,000× magnification with a pixel size of 3.51 Å. Image J was used to add a scale bar and quantify the size of the vesicles.

Immunohistochemistry. Immunohistochemistry was performed as previously described.[2] Sections were stained with a pSTAT1 (Cell Signaling Technology 1/200), MX1 (Abcam 1/100), and CXCL10 antibody (Abcam 1/200), visualized using an HRP-conjugated mouse secondary, and counterstained with hematoxylin.

Statistical analysis. Data are presented as the mean ± SE. Statistical analysis was performed using a two-tailed, paired Student's *t*-test for singular analysis and analysis of variance tests for multicomparison analysis.

Ethics approval and consent to participate. The study was approved by National Research Ethics service (NRES) committee North East-Newcastle & North Tyneside: REC Ref: 15/NE/0211 to FDG. All participants provided written informed consent to participate in this study. Informed consent procedure was approved by NRES-011NE to FDG by the University of Leeds.

RESULTS

Loss of SSc keratinocyte expression of type 1 IFN signature in vitro and induction by SSc dermal fibroblast coculture. Previous studies, including our own, have shown that keratinocytes in SSc skin are a major source of ISG expression.[2] Consistent with these findings, we observed high levels of pSTAT1, CXCL10, and MX1 in the epidermis of SSc skin compared to healthy control biopsies (Figure 1A). We then set out to determine whether SSc keratinocytes could maintain the ISG response when isolated from the skin, similarly to what has been repeatedly observed for the profibrotic activation of dermal fibroblasts.[17] SSc keratinocytes isolated from the same biopsies shown in Figure 1A did not display elevated MX1, CXCL10, or CXCL11 transcript levels or pSTAT1 protein levels (Figure 1B–E), compared to healthy control keratinocytes, when cultured in vitro. Interestingly, these isolated SSc keratinocytes were still able to induce ISG expression upon stimulation with

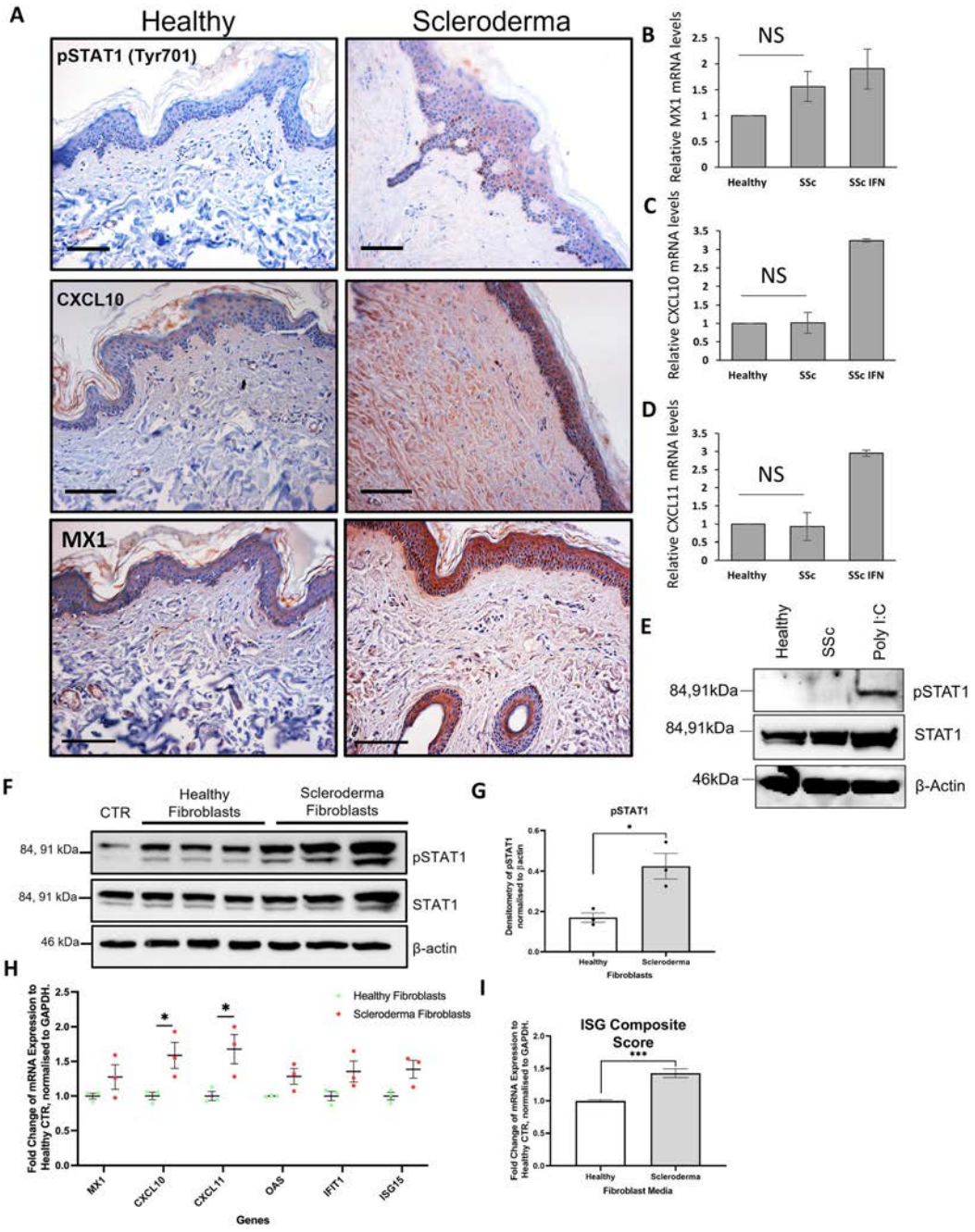

Figure 1. Scleroderma dermal fibroblasts induce type I IFN signaling in keratinocytes. (A) Healthy (N = 5) and SSc (N = 5) skin sections obtained from patient forearms were stained with antibodies specific for phosphorylated STAT1, CXCL10, and MX1. Scale bars represent 50 μm. (B–D) SSc skin keratinocytes were isolated from skin biopsies and passaged three times; RNA was then isolated. SSc keratinocytes were stimulated with IFN-α (2 ng/mL) for 2.5 hours. (B) MX1, (C) CXCL10, and (D) CXCL11 transcript levels were assessed by qRT-qPCR. Graphs represent fold change relative to healthy control. (E) Protein was isolated from SSc keratinocytes (n = 3) and healthy (n = 3) control keratinocytes. Lysates from healthy keratinocytes stimulated with POLY I:C (24 hours 10 μg/mL) was used as a positive control. pSTAT1 and total STAT1 protein levels were assessed by Western blot. β-actin was used as a loading control. (F and G) Healthy (n = 3) and scleroderma (n = 3) fibroblasts were cocultured in cell-culture inserts with human epidermal keratinocytes (HaCaTs) for 48 hours in serum-free DMEM. (F) pSTAT1 (Tyr701) and STAT1 protein levels were assessed by Western blot. β-actin was used as a loading control. (G) Protein expression of pSTAT1 was quantified by densitometry and normalized to β-actin levels. (H) Fold change of mRNA transcript expression of ISGs (MX1, CXCL10, CXCL11, OAS, IFIT1, and ISG15) in HaCaTs cocultured with healthy fibroblasts, compared to SSc. (I) Fold change of mRNA transcript expression of an ISG composite score of the six genes described in H genes, normalized to GAPDH and ribosomal protein as a housekeeping gene, relative to mean healthy exosome-treated HaCaTs. *$P < 0.05$; ***$P < 0.001$. CTR, Control; DMEM, Dulbecco's modified Eagle medium; IFN, interferon; ISG, IFN-stimulated gene; mRNA, messenger RNA; NS, not significant; RT-qPCR, quantitative reverse transcription–polymerase chain reaction; SSc, systemic sclerosis.

IFN-α (Figure 1C and D), suggesting the type I IFN signaling pathway is still functional in the SSc keratinocytes in culture.

Next, we assessed whether SSc fibroblasts could trigger type I IFN response in keratinocytes. To focus our study on the role of the fibroblasts we cocultured the skin keratinocyte cell line HaCaTs with three different healthy and SSc fibroblasts in a transwell assay (Figure 1F). We observed that both healthy and SSc dermal fibroblasts triggered STAT1 phosphorylation in HaCaTs compared to the control, with a significantly greater induction in the HaCaTs cultured with SSc dermal fibroblasts (Figure 1G). Accordingly, SSc dermal fibroblasts induced greater levels of messenger RNA (mRNA) expression of ISGs (MX1, CXCL10, CXCL11, OAS1, IFIT1, and ISG15) compared to healthy control (Figure 1H; Supplementary Figure 1). Combining the ISG analyzed in a composite score as previously described,[2] we observed an overall 1.5-fold increase of ISG induction in the HaCaTs cocultured with SSc fibroblasts compared to healthy control (Figure 1I).

Characteristics of healthy and SSc fibroblast exosomes. To determine whether fibroblast exosomes could contribute to the induction of type I IFN in keratinocytes, we isolated exosomes from healthy and SSc fibroblast supernatants. Firstly, we observed that healthy and SSc fibroblasts secreted similar amounts of exosomes as shown by similar levels of exosome marker expression (TSG101 and CD63) in the isolated exosomes (Figure 2A). This was confirmed via CD63 ELISA whereby we quantified that both healthy and SSc fibroblasts secreted exosomes in the order of 1×10^{10} (from 20 million fibroblasts) (Figure 2B). Furthermore, electron microscopy analysis and DLS indicated that the exosomes secreted from healthy and SSc fibroblasts were of similar size and distribution (Figure 2C and D). Finally, we set out to determine the cell entry kinetics of both sets of exosomes as assessed by membrane-specific dye staining followed by immunofluorescence analysis. As shown in Figure 2E, we observed no apparent difference in timing and intracellular localization of fibroblast exosomes from SSc or healthy control dermal fibroblasts, with a time-dependent increase in exosome uptake continuing to rise up to the 48 hours in both sets (Figure 2F).

Proinflammatory effect of SSc fibroblast exosomes on keratinocytes compared with healthy control fibroblast exosomes. To determine the global effects of the SSc fibroblast exosomes on skin keratinocytes, we performed RNA sequencing (RNA-seq) of HaCaTs following a 48-hour culture in exosome conditioned media (1% total volume) (Figure 3A). Hierarchical clustering of differentially expressed genes (DEGs) showed a clear separation of the transcriptomic response induced by exosomes compared to mock and a separation between SSc and healthy exosomes (Figure 3B). The RNA-seq analysis revealed there were 1,097 DEGs ($P < 0.05$ and abs (log2 FC) > 1) between HaCaTs stimulated with healthy fibroblast exosomes compared to control HaCaTs, 881 DEGs in HaCaTs stimulated with SSc fibroblast exosomes compared to control HaCaTs, and 60 DEGs in HaCaTs stimulated with SSc fibroblast exosomes compared to HaCaTs stimulated with healthy fibroblasts exosomes. Within the 60 SSc-specific DEGs found, 39 were up-regulated (Figure 3C) and 21 were down-regulated (Figure 3D) in keratinocytes stimulated with SSc fibroblast exosomes compared to healthy control. In addition, Supplementary Table 1 contains a list of the top 60 DEGs (fold change) found in HaCaTs stimulated with SSc fibroblast exosomes compared to healthy fibroblast exosomes.

Gene ontology enrichment analysis using the fold changes for all detected genes revealed that several pathways involved in immune signaling (responses to type 1 IFN, responses to IFN-γ, humoral immune responses, and response to chemokines) were up-regulated in HaCaTs stimulated with SSc fibroblast exosomes compared to healthy fibroblast exosomes (Figure 4A). Analysis of individual genes showed a number of ISGs were differentially up-regulated in HaCaTs stimulated with SSc fibroblast exosomes, as shown in the volcano plot (Figure 4B). A list of the 25 most significant DEGs is shown in Figure 4C. The list includes a number of ISGs. Further analysis of type I IFN signaling in HaCaTs stimulated with healthy and SSc dermal fibroblast exosomes compared to the mock control revealed that the healthy dermal fibroblast exosomes impart an anti-inflammatory response on the keratinocytes as shown by reduced expression of a number of ISGs. Expression levels of interleukin (IL)-7, CXCL6, CXCL1, GBP1, MMP7, TREM2, and CTSS were significantly reduced in HaCaTs stimulated with healthy fibroblast exosomes compared to unexposed HaCaTs (Figure 4D). Expression levels of these ISGs were also significantly reduced in HaCaTs stimulated with healthy control fibroblasts compared to HaCaTs stimulated with SSc fibroblasts and not significantly different between HaCaTs stimulated with SSc dermal fibroblast exosomes and unexposed control HaCaTs (Supplemental Figure 2). Collectively, these data suggest that an important function of exosomes in healthy skin is to dampen proinflammatory IFN signaling in keratinocytes, thus contributing to homeostasis, and that the lack of this anti-inflammatory effect of exosomes secreted by SSc fibroblasts on keratinocytes may lead to loss of homeostasis and contribute to a more proinflammatory state in patients with SSc.

Previous studies have shown SSc fibroblast[9] and CAF exosomes[4,5] actively stimulate macrophages and epithelial cells compared to healthy control fibroblast exosomes. Here we show healthy dermal fibroblast exosomes negatively regulate type I IFN signaling and this ability is lost in SSc fibroblasts, causing an increase type I IFN signature in HaCaTs relative to healthy control exosomes. To validate this finding, we performed a qRT-PCR–based superarray to assess 79 type I IFN–dependent ISGs on RNA isolated from HaCaTs treated with healthy and SSc dermal

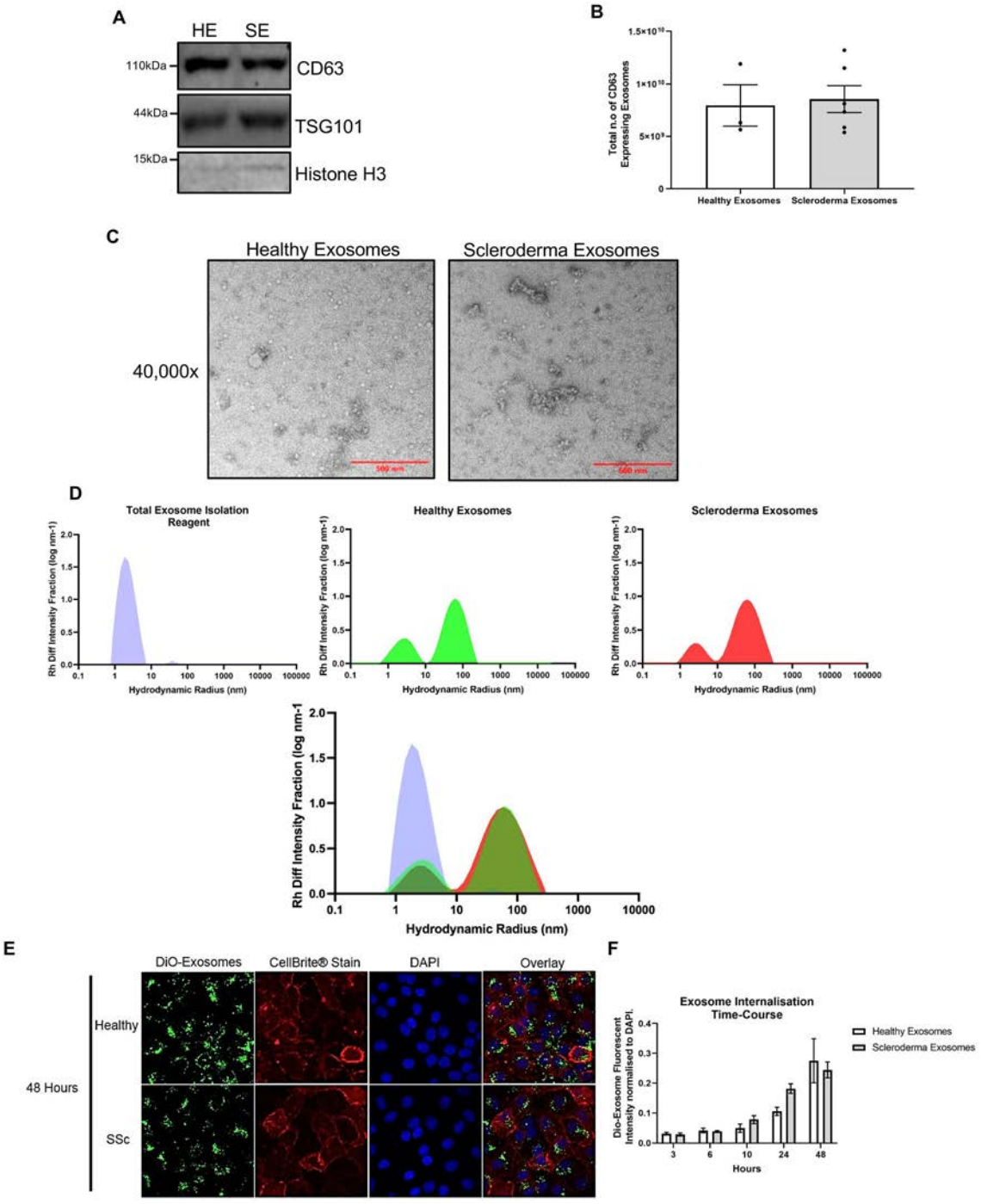

Figure 2. Characterization of exosomes from healthy SSc dermal fibroblasts. Exosomes were isolated from healthy (n = 3) and SSc (n = 6) fibroblast media. (A) Isolated exosomes were probed for TSG101, CD63, and histone H3 by Western blot. (B) CD63 ELISA quantification of exosomes from healthy (n = 3) and SSc (n = 5) patient fibroblasts. (C) Representative transmission electron microscopy images of healthy and scleroderma exosomes at 40,000× magnification. (D) Representative size-distribution histograms of diluted total exosome isolate buffer, healthy (n = 3) and SSc (n = 3) exosomes, from regularization analysis of dynamic light scattering data. (E) Healthy and SSc fibroblast exosomes were stained with DiO-lipid dye and added to HaCaTs at 3, 6, 10, 24, and 48 hours. (F) Bar charts illustrates the green, fluorescent intensity per image, normalized to include a DAPI intensity, per three images over a time course (3, 6, 10, 24, and 48 hours). ELISA, enzyme-linked immunosorbent assay; HE, healthy exome; Rh diff Hydrodynamic Radius; SSc, systemic sclerosis; SE, SSc exome.

fibroblast exosomes. Volcano plot analysis on three independent experiments showed 16 ISGs up-regulated by SSc exosomes compared to healthy exosomes (Figure 5A and B; Supplementary Figure 3). Altogether, the qRT-PCR–based IFN array validated the RNA-seq data, indicating a strong type I IFN response in HaCaTs stimulated with SSc fibroblast exosomes compared to healthy

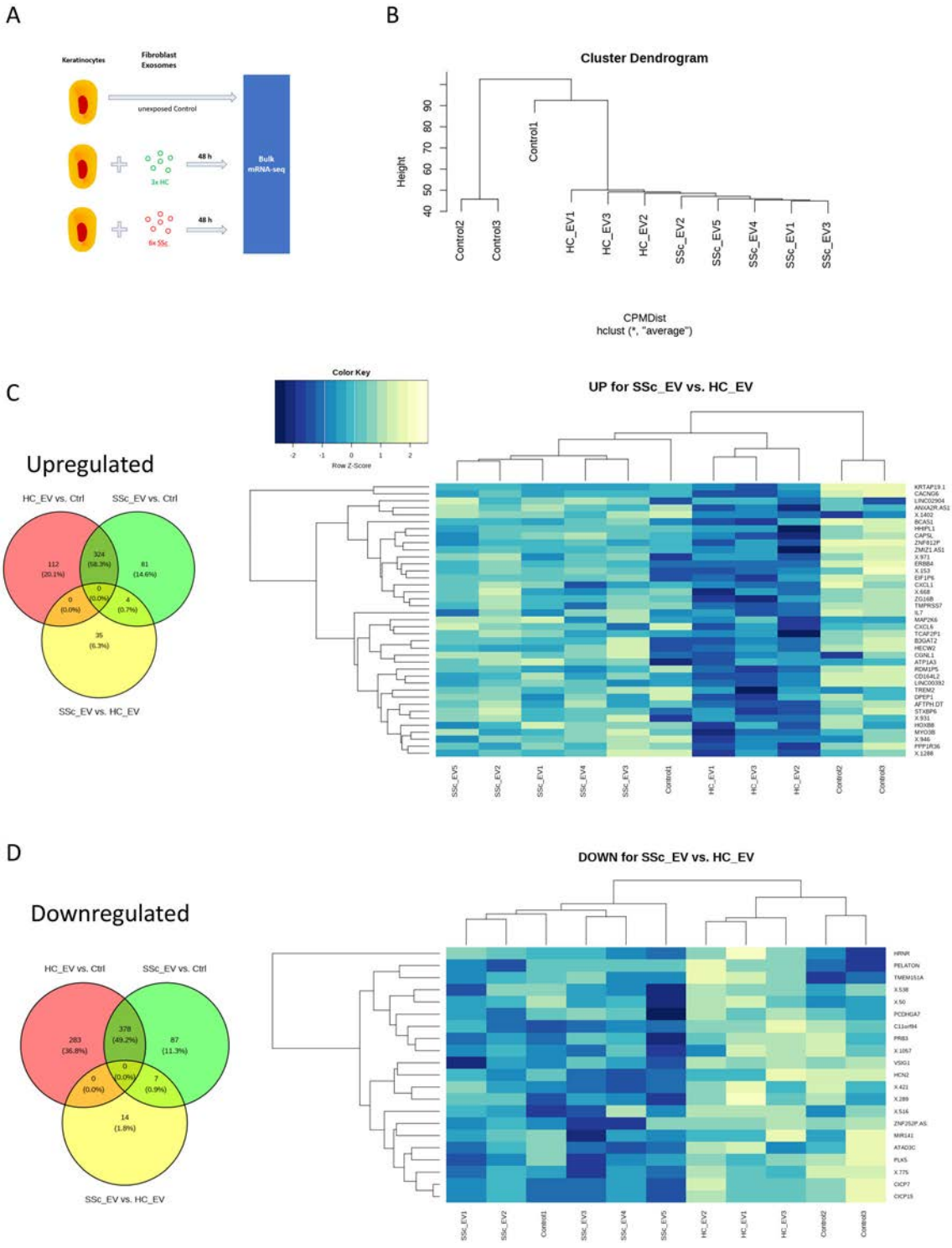

Figure 3. Global gene analysis of keratinocytes stimulated with healthy and SSc dermal fibroblast exosomes. (A) Schematic representation of experimental approach for the RNA-seq analysis. HaCaT keratinocytes were stimulated with healthy (n = 3) and SSc (n = 5) fibroblast exosomes for 48 hours. RNA was isolated from the stimulated HaCaTs, and RNA-seq analysis was performed. (B) Cluster dendrogram clustering of the responses of healthy and SSc in HaCaTs compared to control. Venn diagram and heatmaps of differential expression genes with a fold change greater than 1.5-fold scaled by row for (C) genes up-regulated and (D) genes down-regulated in HaCaTs stimulated with SSc fibroblast exosomes compared to healthy fibroblast exosomes. The heat map illustrates significantly ($P < 0.05$) differentially expressed genes and the color scale represents the row Z-score, with dark blue representing low gene expression levels and light yellow indicating high expression relative to other samples in the same row. ctrl, control; EV, Extracellular Vesicles; HC, healthy control; mRNA-seq, messenger RNA sequencing; RNA-seq, RNA sequencing; SSc, systemic sclerosis.

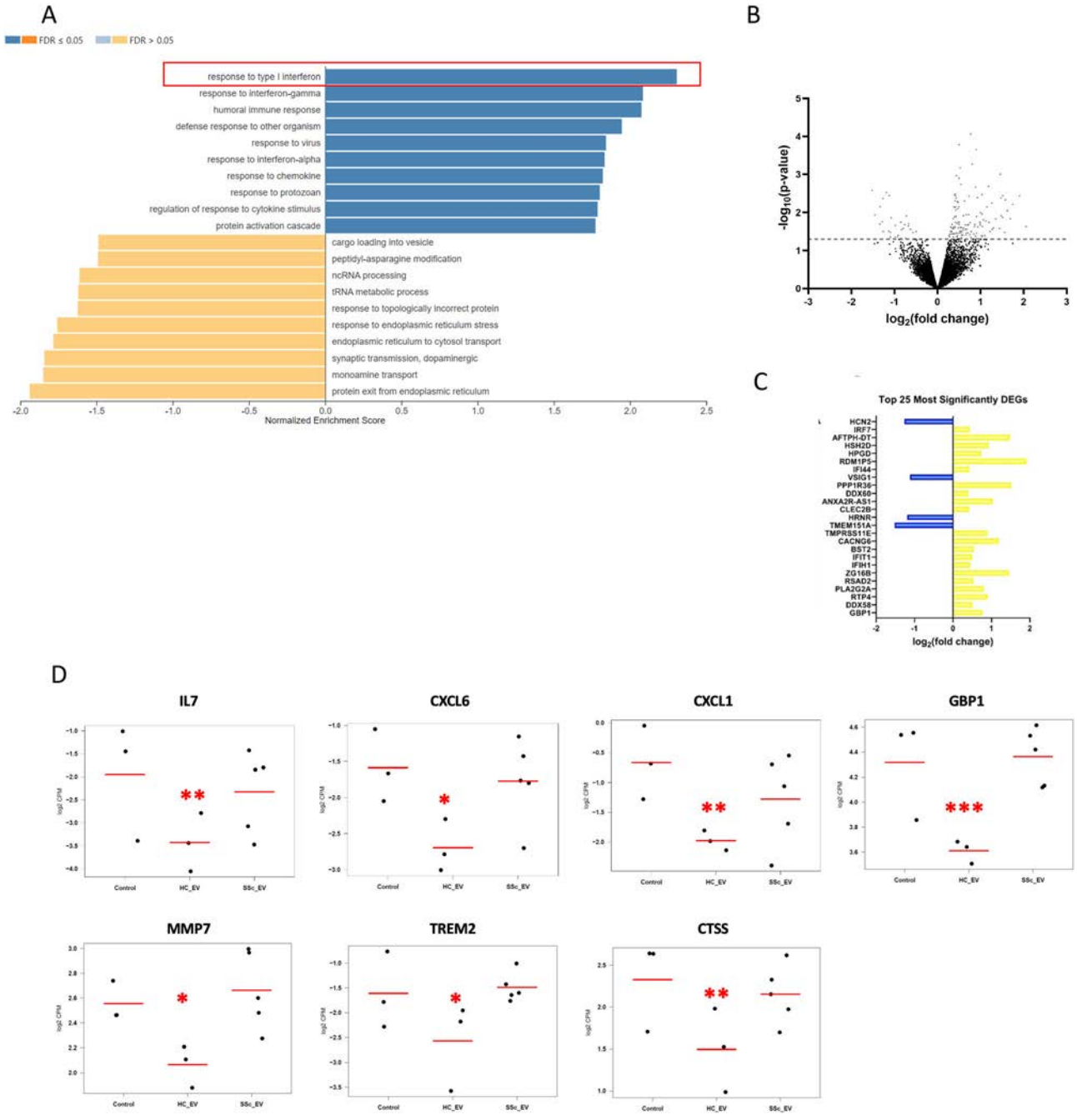

Figure 4. SSc fibroblast exosomes impart a proinflammatory effect on keratinocytes compared to healthy control fibroblast exosomes. (A) Gene ontology enrichment analysis of biologic processes associated with DEGs, in HaCaTs treated with SSc exosomes compared to healthy control exosomes. Dark blue or orange = FDR < 0.05; light blue or orange FDR > 0.05. (B) Volcano plot of log2 fold change against-log10 *P* value for each DEG in HaCaTs stimulated with SSc fibroblast-derived exosomes, when compared against healthy exosomes. Red = significant DEGs. Blue = significant DEGs associated with interferon signaling. (C) A list of the 25 most significant DEG from the analysis. (D) Gene expression levels of selected ISGs (IL-7, CXCL6, CXCL1, GBP1, MMP7, TREM2, and CTSS). Comparisons made between control HaCaTs and HaCaTs stimulated with healthy and SSc dermal fibroblast exosomes. **P* < 0.05; ***P* < 0.01; ****P* < 0.001. DEG, differentially expressed gene; FDR, false discovery rate; IL, interleukin; ISG, interferon-stimulated gene; ncRNA, noncoding RNA; SSc, systemic sclerosis; tRNA, transfer RNA.

control exosomes. At the protein level, whole-cell protein lysates from the HaCaTs in the same experimental conditions showed a time-dependent increase in pSTAT1 levels (Figure 5C and D), consistent with the RNA findings (Figure 5A–B) and the kinetics of exosome internalization (Figure 2E). Accordingly, the ISG composite score showed a similar increment over time, becoming significantly induced by SSc exosomes at 24 and 48 hours (Figure 5E).

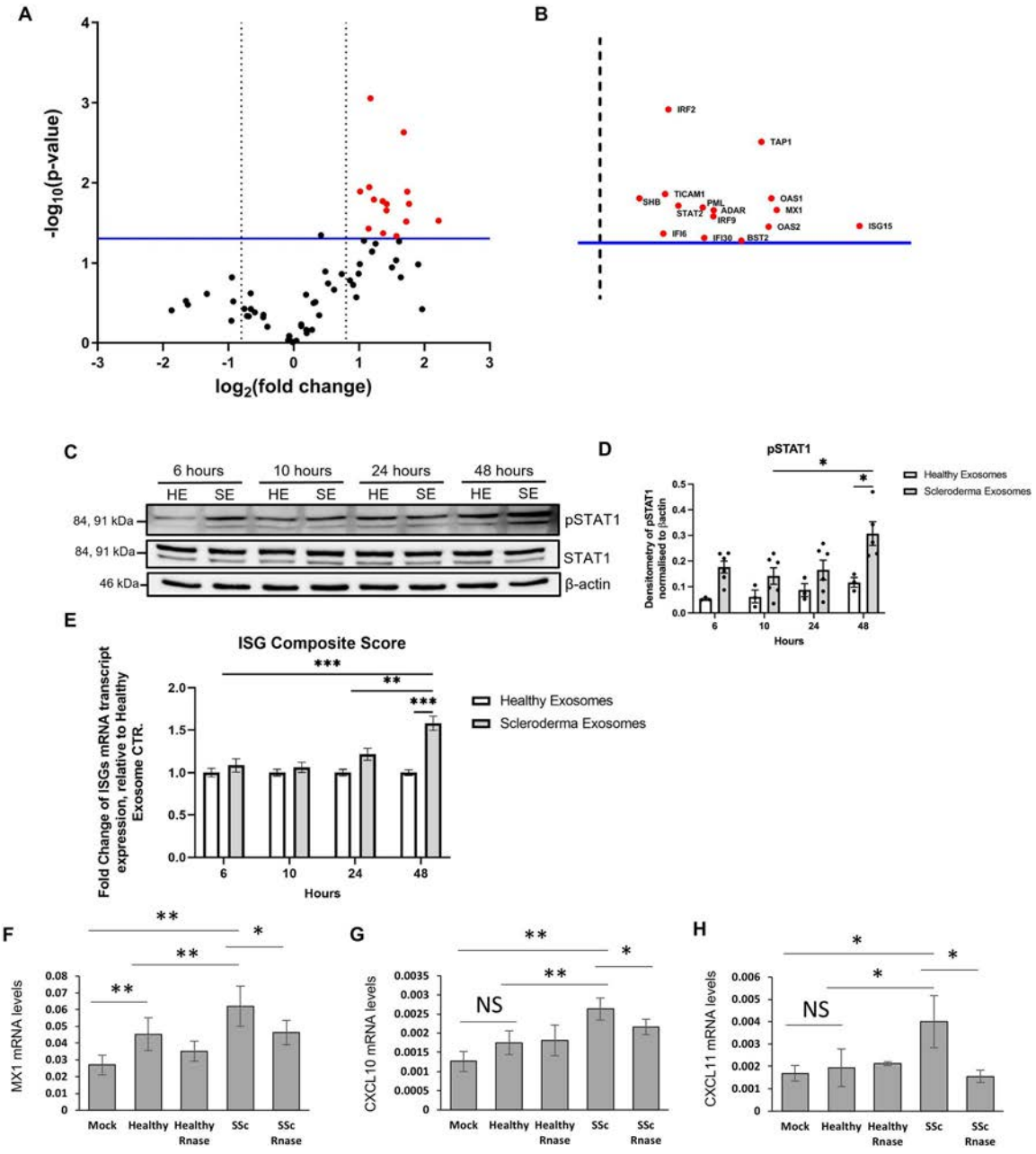

Figure 5. Scleroderma dermal fibroblast exosomes induce type 1 IFN signaling in keratinocytes through their RNA content. HaCaT keratinocytes were stimulated with healthy and SSc fibroblast exosomes for 48 hours. RNA was extracted from the stimulated HaCaTs. A type 1 IFN superarray was performed. (A) Volcano plot which shows the fold change of gene expression of IFN type 1–stimulated genes in HaCaTs stimulated with SSc exosomes relative to HaCaTs stimulated with healthy exosomes. (B) An enlarged version of the volcano plot in illustrating the identifiers of the genes significantly up-regulated in SSc versus healthy exosome-treated HaCaTs. HaCaT keratinocytes were stimulated with healthy and SSc fibroblast exosomes for 6 to 48 hours. Protein and RNA were isolated from stimulated HaCaTs. (C) pSTAT1 (Tyr701) and STAT1 protein levels were assessed by Western blot. β-actin was used as a loading control. (D) Bar chart illustrates quantification of protein expression by densitometry and normalized to β-actin levels. Data represent means ± SE. Data were checked for normality and statistically analyzed using a two-way multiple comparison ANOVA, normalized by Tukey. (E) Bar chart illustrates the fold change of mRNA transcript expression of an ISG composite score of multiple IFN-related genes normalized to GAPDH, relative to healthy exosome stimulations, over a time course. ISG composite score included 6 ISGs: MX1, CXCL10, CXCL11, OAS, IFIT1, and ISG1. Data represent means ± SE. Data were checked for normality and statistically analyzed using a two-way multiple comparison ANOVA, normalized by Tukey. RNA was extracted from healthy and SSc fibroblast exosomes and transfected into HaCaT cells for 48 hours. In addition, the RNA was pretreated with RNase before transfection. (F) MX1, (G) CXCL10, and (H) CXCL11 transcript levels were assessed by RT-qPCR. *$P < 0.05$; **$P < 0.01$; ***$P < 0.001$. ANOVA, analysis of variance; CTR, Control; IFN, interferon; ISG, IFN-stimulated gene; mRNA, messenger RNA; NS, not significant; RT-qPCR, quantitative reverse transcription–polymerase chain reaction; SSc, systemic sclerosis.

Type 1 IFN signaling in keratinocytes from SSc fibroblast exosomes through a TBK1/JAK-dependent response to their RNA cargo. Previous studies have shown that specific uncapped RNA transcripts within CAF exosomes can trigger type I IFN signaling in epithelial cells[5,9]. Therefore, we wanted to determine if the RNA contained within the SSc fibroblast exosomes contributed to the type I IFN stimulation observed in keratinocytes. RNA was extracted from healthy and SSc dermal fibroblast exosomes and transfected into HaCaT cells (50 ng RNA). Healthy fibroblast exosome RNA had minimal effects on MX1, CXCL10, and CXCL11 expression in HaCaTs compared to control cells. SSc fibroblast exosome RNA induced a 2.5-fold increase in MX1 ($P = 0.002$), 2-fold increase in CXCL10 ($P = 0.0015$), and 3-fold increase in CXCL11 ($P = 0.016$) expression in HaCaTs (Figure 5F–H). Pretreatment of exosome extracts with RNase significantly suppressed the up-regulation of MX1, CXCL10 and CXCL11, although with variable efficiency (Figure 5F–H). This suggests that the RNA within the exosomes directly contributed to type I IFN response of HaCaT, in vitro.

There are a number of ways RNA cargo could induce a type I IFN response, such as a microRNA (miRNA)-induced up-regulation of type I IFN or a direct stimulation of RNA sensors, as has been described for CAF-derived exosomes.[4,5] Most RNA pattern recognition receptors (TLR-7, RIG-I, and MDA5) signal through TBK1. Therefore, we used the specific TBK1 inhibitor GSK8612 to interrogate the pathway in response to exosome stimulation. The observed increased STAT1 activation by SSc fibroblast exosomes was completely abolished with the TBK1 inhibitor (Figure 6A and B). Accordingly, TBK1 inhibition also suppressed the induction of ISG expression in the HaCaTs (Figure 6C). Taken together, this suggests the SSc fibroblast exosomes induce type I IFN signaling in HaCaTs through TBK1. TBK1 is known to activate STAT1 through IRF3/7 in response to viral infections.[18] Interestingly, the SSc fibroblast exosomes did not activate IRF3 in keratinocytes (Supplementary Figure 4). This suggests that TBK1 activates STAT1 through an alternative pathway. This was further highlighted in the type 1 IFN array and RNA-seq data in which IFN-α/β expression was not induced by the SSc fibroblast exosomes.

To determine whether the TBK1 induced activation of STAT was JAK dependent, we used the JAK1 inhibitor tofacitinib in the same experimental conditions of Figure 6A and B. Similar to TBK inhibition, tofacitinib completely blocked the SSc fibroblast exosome–mediated STAT1 activation in HaCaTs (Figure 6D and E) as well as ISG expression (Figure 6F), suggesting that the observed type I IFN response is mediated by activation of JAK. Neither GSK8612 nor tofacitinib affected total STAT1 levels in unstimulated HaCaTs (Supplementary Figure 5). In addition, we observed undetectable levels of pSTAT1 in the unstimulated HaCaTs. Taken together with the data in Figure 6, it suggests that healthy fibroblasts exosomes can induce pSTAT1 levels compared to unstimulated HaCaTs but that SSc fibroblast exosomes further enhance this induction of pSTAT1 in the HaCaTs.

Analysis of mRNA content between healthy and SSc fibroblast exosomes. In the data above we have shown that SSc dermal fibroblast exosomes can induce a type 1 IFN response in keratinocytes through the TBK1/JAK signaling axis. Further analysis showed that the RNA within the exosomes can induce the type 1 IFN response (Figure 5F–H). We next wanted to identify potential RNA transcripts within the SSc fibroblast exosomes that induce the response. We extracted RNA from healthy and SSc fibroblast exosomes and performed RNA-seq analysis to assess differential mRNA abundance in SSc compared to healthy control exosomes. Hierarchical clustering of 253 genes that were significantly up-regulated in the SSc fibroblast exosomes compared to the healthy control showed a clear separation between groups (Supplementary Figure 6A). Individual plots for the eight most highly up-regulated abundant transcripts (>5 counts per minute) are shown in Supplementary Figure 6B. Pathway analysis of the DEGs did not identify any IFN-related pathways, but AFF3 and H19, which are two of the most significant DEGs, have tentatively been implicated in immune responses in other autoimmune conditions including rheumatoid arthritis.[19,20]

DISCUSSION

In this study we have shown the type I IFN response observed in SSc skin is mainly driven by keratinocytes. Importantly, we also show that keratinocytes are "responding" to a primary trigger in their microenvironment as they lose any sign of type I IFN activation once cultured in vitro. Parallel to this evidence, coculture experiments clearly indicate that SSc dermal fibroblasts are able to induce type I IFN activation in keratinocytes, which can be induced by isolated exosomes. These data suggest that dermal fibroblasts may participate to the pathogenesis of SSc not only for their profibrotic activation but also in triggering and/or sustaining the type I IFN response observed in the tissue. Furthermore, these data also suggest that the increase in type I IFN–inducible chemokines observed in peripheral blood may be a consequence of a tissue driven type I IFN response rather than its source. Similar data have been suggested in the pathogenesis of systemic lupus erythematosus.[21] This interpretation would also be consistent with the observation that serum proteome correlated with skin transcriptome better than peripheral blood transcriptome in SSc.[22] The transfection of exosome cargo RNA in human keratinocytes suggested that the RNA contained within SSc exosomes is contributing to, if not driving, the type I IFN response. Finally, we interrogated the signaling pathway behind this response with small molecule inhibitors. Although a fine dissection of the pathway(s) fell outside the scope of this study, we were able to demonstrate that SSc fibroblast exosomes induce ISG expression through a TBK1/JAK/STAT1 signaling cascade (Figure 6G).

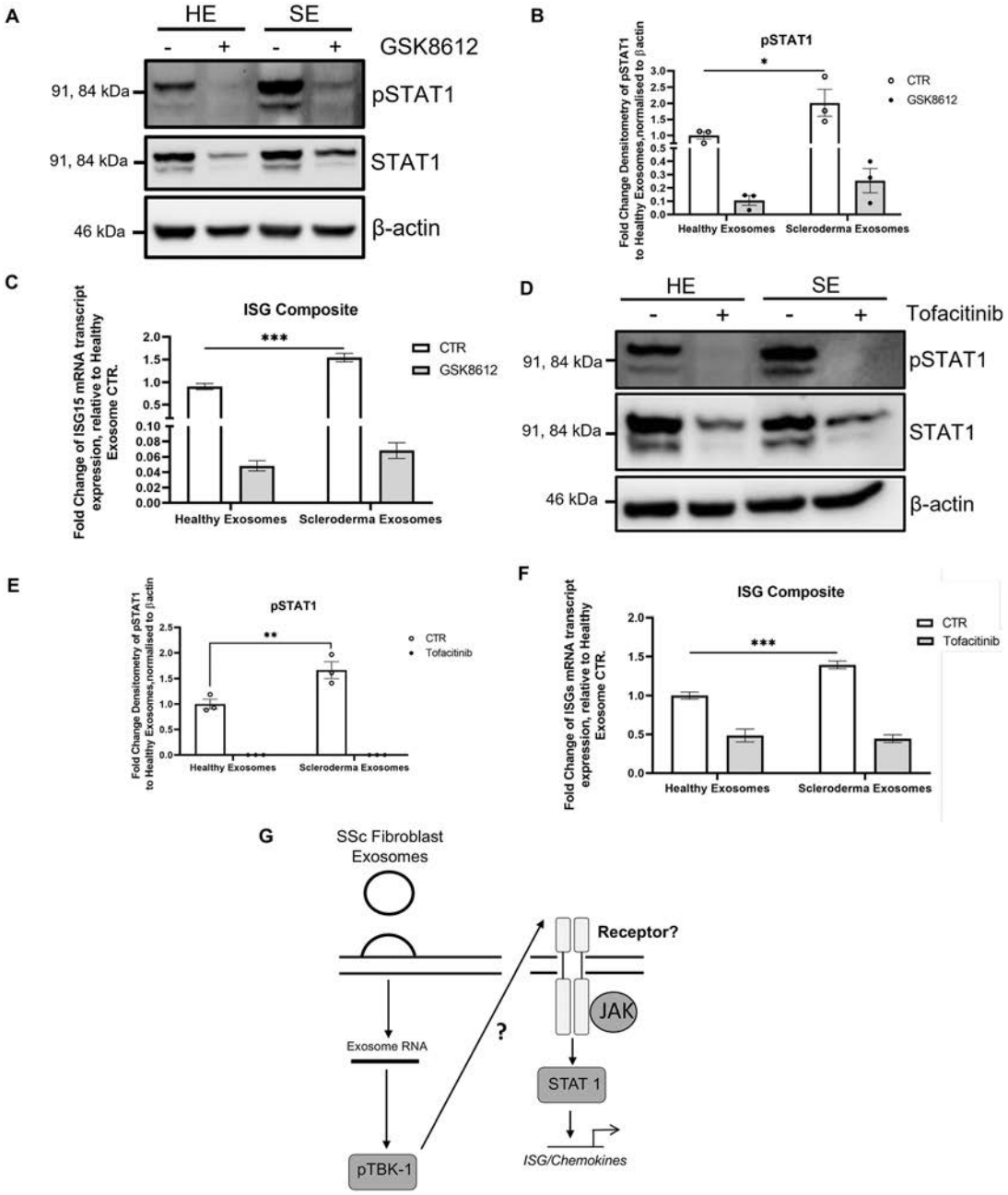

Figure 6. Inhibition of TANK-binding kinase and JAK-STAT blocks SSc fibroblast exosome–mediated type I IFN signaling in HaCaTs. (A) HaCaTs were stimulated with healthy and SSc fibroblast exosomes for 48 hours. In addition, the HaCaTs were treated with 10 μM GSK8612, one hour before stimulation. pSTAT1 and STAT1 protein levels were assessed by Western blot. β-actin was used as a loading control. (B) The bar chart illustrates densitometry analysis of pSTAT1. Data represent means ± SE from three biologic repeats. (C) Fold change of mRNA transcript expression of multiple IFN-related genes, normalized by housing keeping gene GAPDH, and relative to untreated healthy exosome-treated HaCaTs. Data represent means ± SE from three biologic repeats (healthy) and four biologic repeats (SSc). ISG composite score included 6 ISGs: MX1, CXCL10, CXCL11, OAS, IFIT1, and ISG15. Statistical analysis was performed using a multiple comparison two-way ANOVA, normalized to Tukey. (D) HaCaTs were stimulated with healthy and SSc exosomes for 48 hours. In addition, the HaCaTs were treated with 20 μM tofacitinib one hour before stimulation. pSTAT1 and STAT1 protein levels were assessed by Western blot. β-actin was used as a loading control. (E) The bar chart illustrates densitometry analysis of pSTAT1. Data represent means ± SE from three biologic repeats. (F) Fold change of mRNA transcript expression of multiple IFN-related genes, normalized by housing keeping gene GAPDH, and relative to untreated healthy exosome-treated HaCaTs. Data represent means ± SE. ISG composite score included six ISGs: MX1, CXCL10, CXCL11, OAS, IFIT1, and ISG15. Statistical analysis was performed using a multiple comparison two-way ANOVA, normalized to Tukey. (G) Schematic representation of the mechanism behind SSc fibroblast exosome induction of type I IFN signaling. $^{*}P < 0.05$; $^{**}P < 0.01$; $^{***}P < 0.001$. ANOVA, analysis of variance; CTR, Control; HE, healthy exome; IFN, interferon; ISG, IFN-stimulated gene; mRNA, messenger RNA; SE, SSc exome; SSc, systemic sclerosis.

We believe that these data contribute to identifying the source of type I IFN activation in SSc skin, but we also acknowledge that there are still a number of unanswered questions regarding this phenomenon. Specifically, we still do not have a clear understanding of the factors downstream of TBK1. One standout candidate is IRF3/7. TBK1 has been shown to phosphorylate and activate IRF3/7 in response to viral and bacterial infections, which in turn drives a type I IFN response.[18] Interestingly, we have shown that SSc fibroblasts exosomes do not activate IRF3 (Supplementary Figure 4). This suggests TBK1 induces ISG expression through alternative downstream targets. One possible target is NF-κB, which is known to be a downstream target of TBK1.[23] This hypothesis will be explored in future studies.

The specific exosome cargo that triggers the type I IFN response in the keratinocytes is not fully understood. We have shown that exosome RNA can induce ISG expression in the keratinocytes, but this does not rule out the possibility that proteins or other second messengers in the cargo could also play a role. The exosomes may contain cytokines, which upon exosome uptake could trigger the signaling cascade we have described in the results. Analysis of mRNA content between healthy and SSc fibroblast exosomes revealed few target mRNA differentially expressed in the SSc fibroblast exosomes that may contribute to the IFN response (Supplementary Figure 6). AFF3 and H19 transcript levels were elevated in SSc fibroblast exosomes compared to healthy control fibroblasts. AFF3 is an immunoglobulin class switch factor that has been shown to be a susceptibility factor for rheumatoid arthritis,[19] and H19 has been shown to regulate ISG expression in macrophages in response to lipopolysaccharide stimulation.[20] These two factors may contribute to the type 1 IFN response in the keratinocytes, but it is more likely that the exosomes could contain unshielded/uncapped RNA as described in the CAF work.[4,5] In this regard, the uncapped RNA (RN7SL1) has been shown to be directly linked to Notch/c-Myc/RNA Pol III function. We have shown Notch signaling is enhanced in SSc,[24,25] and RNA Pol III has been implicated previously.[26] This suggests the exosome RNA from SSc fibroblasts may lead to the activation of the type I IFN pathway in the keratinocytes through recognition of uncapped RNA structures. Therefore, future work will focus on proteomic and RNA-seq analysis of SSc fibroblast exosome cargo to determine if cytokines or the specific RNA transcript RN7SL1 are present in the exosomes. Exosomes are known carriers of miRNA, and a number of miRNA are known to regulate type I IFN responses. Furthermore, a number of differentially expressed long noncoding RNAs in SSc have been implicated in regulating IFN responses.[11] Therefore, it is possible that a number of miRNA or long noncoding RNA within the exosomes may regulate the responses we have observed in the keratinocytes.

Interestingly, the RNA-seq data revealed that healthy fibroblast exosomes have an anti-inflammatory effect on HaCaTs that is lost in SSc fibroblast exosomes, which have a counteractive effect. This sheds a new light on the possible role of healthy fibroblasts exosomes in regulating the immune response to maintain skin homeostasis, whereas this homeostatic regulation is disrupted with SSc fibroblast exosomes. When healthy fibroblast exosomal RNA was isolated and transfected into keratinocytes, the RNA did not impart an anti-inflammatory effect (Figure 5F–H) as observed in the RNA-seq analysis (Figure 3) This suggests proteins within the healthy fibroblast exosomes may impart the anti-inflammatory response, but the RNA from SSc fibroblast exosomes reverses this effect.

The ability of the JAK inhibitor tofacitinib to prevent SSc fibroblast exosome–mediated ISG expression is intriguing. These data suggest exosome-mediated ISG expression is triggered by cytokine receptor–mediated activation of STAT1. The precise cytokine receptor involved is still unknown (Figure 6). There are a number of receptors that may play a role including the IL-6 and IFN-1 receptor. Future work will involve testing the supernatants of exosome stimulated keratinocytes for candidate stimulatory cytokines.

An exciting element of the tofacitinib data is that this drug is approved in the clinic for rheumatoid and psoriatic arthritis. Early clinical trials in SSc have had promising outcomes.[12] Tofacitinib blocked ISG signatures in both fibroblasts and keratinocytes. Our data follow those produced in the trial and add an extra layer of mechanistic data by suggesting the compound is blocking the effects of the ISG signature driven through the crosstalk between these cells.

Bhandari et al showed that SSc fibroblast exosomes can induce macrophage activation.[9] This observation is complementary to our data showing the same exosomes can induce a type 1 IFN response in keratinocytes. It remains to be determined what factor(s) within the exosomes lead to the activation of the macrophages and keratinocytes. Therefore, it would be interesting to investigate if the RNA contained within the exosomes can induce the response in macrophages. In addition, it would be interesting to investigate if the supernatant from the exosome stimulated macrophages could induce a response in the keratinocytes and vice versa. This could result in an immune signaling cascade in patient skin with the fibroblast exosomes as the culprit of this cascade. Bhandari et al showed the supernatant from exosome stimulated macrophages could induce myofibroblast activation in naïve fibroblasts. This suggests the exosomes induce a potent response in the macrophages. Unfortunately, from the study we were unable to conclude if the healthy dermal fibroblast exosomes imparted an anti-inflammatory response in the macrophages (similar to the keratinocytes), as the authors did not show a comparison between unstimulated macrophages and macrophages stimulated with healthy fibroblast exosomes.

In conclusion, we have proposed a mechanism behind the type 1 IFN response found is SSc skin keratinocytes, and our experimental data suggest that tissue fibroblasts may be at least one of the sources of type I IFN activation observed in SSc.

ACKNOWLEDGMENTS

We thank Prof Sheena Radford (Leeds) for access to the DLS machine, funded by the Medical Research Council (G0900958).

AUTHOR CONTRIBUTIONS

All authors contributed to at least one of the following manuscript preparation roles: conceptualization AND/OR methodology, software, investigation, formal analysis, data curation, visualization, and validation AND drafting or reviewing/editing the final draft. As corresponding author, Dr Del Galdo confirms that all authors have provided the final approval of the version to be published, and takes responsibility for the affirmations regarding article submission (eg, not under consideration by another journal), the integrity of the data presented, and the statements regarding compliance with institutional review board/Declaration of Helsinki requirements.

ROLE OF THE STUDY SPONSOR

Boehringer Ingelheim colleagues had a role in the study design or in the collection, analysis, or interpretation of the data, the writing of the manuscript, or the decision to submit the manuscript for publication. Publication of this article was contingent upon approval by Boehringer Ingelheim.

REFERENCES

1. Kakkar V, Assassi S, Allanore Y, et al. Type 1 interferon activation in systemic sclerosis: a biomarker, a target or the culprit. Curr Opin Rheumatol 2022;34(6):357–364.
2. Ross RL, Corinaldesi C, Migneco G, et al. Targeting human plasmacytoid dendritic cells through BDCA2 prevents skin inflammation and fibrosis in a novel xenotransplant mouse model of scleroderma. Ann Rheum Dis 2021;80(7):920–929.
3. Liu X, Mayes MD, Tan FK, et al. Correlation of interferon-inducible chemokine plasma levels with disease severity in systemic sclerosis. Arthritis Rheum 2013;65(1):226–235.
4. Boelens MC, Wu TJ, Nabet BY, et al. Exosome transfer from stromal to breast cancer cells regulates therapy resistance pathways. Cell 2014;159(3):499–513.
5. Nabet BY, Qiu Y, Shabason JE, et al. Exosome RNA unshielding couples stromal activation to pattern recognition receptor signalling in cancer. Cell 2017;170(2):352–366.e13.
6. Del Galdo F, Sotgia F, de Almeida CJ, et al. Decreased expression of caveolin 1 in patients with systemic sclerosis: crucial role in the pathogenesis of tissue fibrosis. Arthritis Rheum 2008;58(9):2854–2865.
7. Wasson CW, Ross RL, Morton R, et al. The intracellular chloride channel 4 (CLIC4) activates systemic sclerosis fibroblasts. Rheumatology (Oxford) 2021;60(9):4395–4400.
8. Wielosz E, Dryglewska M, Majdan M. Clinical consequences of the presence of anti-RNA Pol III antibodies in systemic sclerosis. Postepy Dermatol Alergol 2020;37(6):909–914.
9. Bhandari R, Yang H, Kosarek NN, et al. Human dermal fibroblast-derived exosomes induce macrophage activation in systemic sclerosis. Rheumatology (Oxford) 2023;62(SI):SI114–SI124.
10. Liakouli V, Elies J, El-Sherbiny YM, et al. Scleroderma fibroblasts suppress angiogenesis via TGF-β/caveolin-1 dependent secretion of pigment epithelium-derived factor. Ann Rheum Dis 2018;77(3):431–440.
11. Mariotti B, Servaas NH, Rossato M, et al. The long non-coding RNA NRIR drives IFN-response in monocytes: implication for systemic sclerosis. Front Immunol 2019;10:100.
12. Khanna D, Padilla C, Tsoi LC, et al. Tofacitinib blocks IFN-regulated biomarker genes in skin fibroblasts and keratinocytes in a systemic sclerosis trial. JCI Insight 2022;7(17):E159566.
13. Dobin A, Davis CA, Schlesinger F, et al. STAR: ultrafast universal RNA-seq aligner. Bioinformatics 2013;29(1):15–21.
14. Ewels P, Magnusson M, Lundin S, et al. MultiQC: summarize analysis results for multiple tools and samples in a single report. Bioinformatics 2016;32(19):3047–3048.
15. Liao Y, Smyth GK, Shi W. The R package Rsubread is easier, faster, cheaper and better for alignment and quantification of RNA sequencing reads. Nucleic Acids Res 2019;47(8):e47.
16. Robinson MD, McCarthy DJ, Smyth GK. edgeR: a Bioconductor package for differential expression analysis of digital gene expression data. Bioinformatics 2010;26(1):139–140.
17. Chadli L, Sotthewes B, Li K, et al. Identification of regulators of the myofibroblast phenotype of primary dermal fibroblasts from early diffuse systemic sclerosis patients. Sci Rep 2019;9(1):4521.
18. Perry AK, Chow EK, Goodnough JB, et al. Differential requirement for TANK-binding kinase-1 in type I interferon responses to toll-like receptor activation and viral infection. J Exp Med 2004;199(12):1651–1658.
19. Tsukumo SI, Subramani PG, Seija N, et al. AFF3, a susceptibility factor for autoimmune diseases, is a molecular facilitator of immunoglobulin class switch recombination. Sci Adv 2022;8(34):eabq0008.
20. Zhu X, Zhu Y, Ding C, et al. LncRNA H19 regulates macrophage polarization and promotes Freund's complete adjuvant-induced arthritis by upregulating KDM6A. Int Immunopharmacol 2021;93:107402.
21. Psarras A, Alase A, Antanaviciute A, et al. Functionally impaired plasmacytoid dendritic cells and non-haematopoietic sources of type I interferon characterize human autoimmunity. Nat Commun 2020;11(1):6149.
22. Farutin V, Kurtagic E, Pradines JR, et al. Multiomic study of skin, peripheral blood, and serum: is serum proteome a reflection of disease process at the end-organ level in systemic sclerosis? Arthritis Res Ther 2021;23(1):259.
23. Möser CV, Stephan H, Altenrath K, et al. TANK-binding kinase 1 (TBK1) modulates inflammatory hyperalgesia by regulating MAP kinases and NF-κB dependent genes. J Neuroinflammation 2015;12(1):100.
24. Wasson CW, Abignano G, Hermes H, et al. Long non-coding RNA HOTAIR drives EZH2-dependent myofibroblast activation in systemic sclerosis through miRNA 34a-dependent activation of NOTCH. Ann Rheum Dis 2020;79(4):507–517.
25. Wasson CW, Ross RL, Wells R, et al. Long non-coding RNA HOTAIR induces GLI2 expression through Notch signalling in systemic sclerosis dermal fibroblasts. Arthritis Res Ther 2020;22(1):286.
26. Cavazzana I, Ceribelli A, Airo' P, et al. Anti-RNA polymerase III antibodies: a marker of systemic sclerosis with rapid onset and skin thickening progression. Autoimmun Rev 2009;8(7):580–584.
27. Zhang B, Kirov S, Snoddy J. WebGestalt: an integrated system for exploring gene sets in various biological contexts. Nucleic Acids Res 2005;33(Web Server issue):W741–W748.
28. Liao Y, Wang J, Jaehnig EJ, et al. WebGestalt 2019: gene set analysis toolkit with revamped UIs and APIs. Nucleic Acids Res 2019;47(W1):W199–W205.
29. van den Hoogen F, Khanna D, Fransen J, et al. 2013 classification criteria for systemic sclerosis: an American college of rheumatology/European league against rheumatism collaborative initiative. Ann Rheum Dis. 2013;72(11):1747–1755. https://doi.org/10.1136/annrheumdis-2013-204424

Arthritis & Rheumatology
Vol. 77, No. 3, March 2025, pp 335–345
DOI 10.1002/art.42996

American College of Rheumatology
Empowering Rheumatology Professionals

Weight Loss After Receiving Anti-Obesity Medications and Gout Among Individuals With Overweight and Obese: A Population-Based Cohort Study

Jie Wei,[1] Yilun Wang,[2] Nicola Dalbeth,[3] Junqing Xie,[4] Jing Wu,[5] Chao Zeng,[6] Guanghua Lei,[6] and Yuqing Zhang[7]

Objective. Weight loss is conditionally recommended for gout management; however, its impact on incident gout and recurrent gout flares among individuals who were overweight and obese remains unknown. We investigate the relationship between weight loss rate following treatment with anti-obesity medications and the risk of incident gout and recurrent gout flares among individuals who were overweight or obese.

Methods. Using data from the Health Improvement Network, we selected individuals aged 18 and older who were overweight or obese and started anti-obesity medication. We emulated a target trial to examine the association of different weight loss rates, slow (2%–5%), moderate (5%–10%), or fast (≥10%), within the first year of treatment with incident gout and recurrent gout flares during a 5 year follow-up period.

Results. Among 131,000 participants without gout being treated with orlistat, the 5-year risk of incident gout was 1.6% for those with weight gain or stability, compared with 1.5%, 1.3%, and 1.2% for those with slow, moderate, and fast weight loss, respectively. Compared with the group with weight gain or stability, the hazard ratios were 0.91 (95% confidence interval [CI] 0.81–1.01), 0.82 (95% CI 0.72–0.92), and 0.73 (95% CI 0.62–0.86) for those with a slow, moderate, and fast rate of weight loss, respectively. Similar results were observed for the recurrent gout flares among 3,847 individuals with overweight or obese with gout treated with orlistat.

Conclusion. A higher rate of weight loss after receiving treatment with orlistat within 1 year was associated with lower risks of incident gout and lower rates of recurrent gout flares among overweight or obese people.

INTRODUCTION

Gout, the most common form of inflammatory arthritis, is typified by recurring intensely painful flares and associated disability.[1] In recent decades, both the incidence and prevalence of gout have increased, likely due to population aging and prevalent overweight and obese.[2] Gout is strongly associated with cardiometabolic comorbidities and their sequelae, including all-cause

Supported by the National Key Research and Development Plan (grant 2022YFC2505500 to Dr Zeng and grant 2022YFC3601900 to Dr Lei), the National Natural Science Foundation of China (grant 82302771 to Dr Wang, grants 82072502 and 82372474 to Dr Zeng, and grants 81930071 and U21A20352 to Dr Lei), the Project Program of National Clinical Research Center for Geriatric Disorders (grant 2021LNJJ06 to Dr Wei and grant 2022LNJJ07 to Dr Zeng), the Natural Science Foundation of Hunan Province (grant 2022JJ20100 to Dr Wei), the Central South University Innovation-Driven Research Program (grant 2023CXQD031 to Dr Zeng), the Science and Technology Innovation Program of Hunan Province (2022RC1009 to Dr Wei and 2022RC3075 to Dr Zeng) and the Scientific Research Program of the Education Department of Hunan Province (grant 296840 to Dr Wang).

[1]Jie Wei, PhD: Xiangya Hospital, Central South University, the Hunan Key Laboratory of Joint Degeneration and Injury, the Key Laboratory of Aging-Related Bone and Joint Diseases Prevention and Treatment, Ministry of Education, Xiangya Hospital, Central South University, and the Xiangya School of Public Health, Central South University, Changsha, China; [2]Yilun Wang, MD, PhD: Xiangya Hospital, Central South University, the Hunan Key Laboratory of Joint Degeneration and Injury, and the Key Laboratory of Aging-Related Bone and Joint Diseases Prevention and Treatment, Ministry of Education, Xiangya Hospital, Central South University, Changsha, China; [3]Nicola Dalbeth, MD: University of Auckland, Auckland, New Zealand; [4]Junqing Xie, PhD: University of Oxford, Oxford, United Kingdom; [5]Jing Wu, MS: The Hunan Key Laboratory of Joint Degeneration and Injury and Key Laboratory of Aging-Related Bone and Joint Diseases Prevention and Treatment, Ministry of Education, Xiangya Hospital, Central South University, Changsha, China; [6]Chao Zeng, MD, PhD; Guanghua Lei, MD, PhD: Xiangya Hospital, Central South University, the Hunan Key Laboratory of Joint Degeneration and Injury, the Key Laboratory of Aging-Related Bone and Joint Diseases Prevention and Treatment, Ministry of Education, Xiangya Hospital, Central South University, and the National Clinical Research Center for Geriatric Disorders, Xiangya Hospital, Central South University, Changsha, China; [7]Yuqing Zhang, DSc: The Mongan Institute, Massachusetts General Hospital, Harvard Medical School, Boston.

Drs Wei and Wang are co-first authors and contributed equally to this work.

Although we are unable to share the datasets, code lists are available on request. Applications to access data can be made via https://www.the-health-improvement-network.com.

Additional supplementary information cited in this article can be found online in the Supporting Information section (https://acrjournals.onlinelibrary.wiley.com/doi/10.1002/art.42996).

Author disclosures and graphical abstract are available at https://onlinelibrary.wiley.com/doi/10.1002/art.42996.

Address correspondence via email to Chao Zeng, MD, PhD, at zengchao@csu.edu.cn; to Guanghua Lei, MD, PhD, at lei_guanghua@csu.edu.cn; or to Yuqing Zhang, DSc, at yzhang108@mgh.harvard.edu.

Submitted for publication April 23, 2024; accepted in revised form September 10, 2024.

death.[3,4] Thus, identifying modifiable risk factors for gout occurrence and its recurrent flares in people with established gout could guide the development of a targeted strategy to reduce its impact on society.

Overweight and obese are key risk factors for gout and play a major role in its rising incidence and prevalence.[1] Purposeful weight loss has been shown to positively impact serum urate levels, prevent the onset of gout, and reduce the frequency of gout flares;[5–7] however, the totality of the evidence of intentional weight loss on the incident gout and its recurrent flares is lacking, mainly because most adult participants tend not to experience weight loss with aging in the observational studies.[8] Weight loss from exercise, calorie restriction, or their combination may benefit the management of gout; however, their short-term effect seems small, and the long term effect on the clinical course of gout is uncertain.[9,10] Orlistat, a lipase inhibitor that decreases dietary fat absorption by approximately 30% in the stomach and pancreas,[11,12] is used in obesity management. Research indicates that orlistat-induced weight loss can modestly improve cardiovascular risk factors while also lowering the risk of diabetes progression in high-risk individuals.[11,13] Moreover, it is regarded as a safe treatment with rare serious adverse events.[14,15] To date, limited evidence exists on the relationship between weight loss after receiving anti-obesity medication, for example, orlistat, to either incident gout or gout flares in the population with overweight or obese.

We conducted population-based cohort studies designed to emulate randomized controlled trials (RCTs) to investigate how weight loss rate within the first year of receiving anti-obesity medications impacts the risk of incident gout in individuals with overweight or obese without a history of gout, and the recurrence of gout flares in individuals with overweight or obese with existing gout.

METHODS

Data source. We utilized data from the Health Improvement Network (THIN), a part of the IQVIA Medical Research Database, which compiles electronic health records from general practitioners (GPs) in the United Kingdom. The database includes sociodemographic information, anthropometric measurements, lifestyle factors, and details of GP visits such as prescriptions, specialist diagnoses, hospital admissions, and laboratory results. Diagnoses are coded using the Read classification system, and medications are coded with a Multilex-based dictionary. This study was approved by the IQVIA Medical Research Database's scientific review committee and Xiangya Hospital's Institutional Review Board, with a waiver of informed consent. Reporting followed the Strengthening the Reporting of Observational Studies in Epidemiology guidelines for observational studies in epidemiology.[16]

Study design and cohort definition. Eligible participants were aged 18 or older, had received orlistat, and maintained continuous GP enrollment for at least 1 year before entering the study between January 1, 2000, and June 30, 2023. The date of the first orlistat prescription was designated as the index date for each participant. Individuals were excluded if they had a history of cancer, underwent bariatric surgery, had received other anti-obesity medications (ie, sibutramine, rimonabant, and glucagon-like peptide-1 receptor agonists [GLP-1 RA] including exenatide, liraglutide, lixisenatide, albiglutide, dulaglutide, and semaglutide) before the index date, had no body mass index (BMI) measurement, or had most recent BMI before the index date was less than 25. For the study of the incident gout, eligible participants should not have gout or had not received any antigout treatment (ie, allopurinol, colchicine, probenecid, febuxostat, or sulfinpyrazone) before the index date. For the study of the recurrent gout flares, eligible participants had a diagnosis of gout before the index date. Gout was defined using Read codes, based on methods from previous studies utilizing THIN.[17]

We modeled analyses of a hypothetical target trial using a cloning, censoring, and weighting approach to evaluate the rate of weight loss within 1 year after receiving orlistat on the risk of incident gout and gout flares, respectively.[18] We created four copies for each initiator at baseline and assigned the four replicates to one of the following weight loss intervention arms: weight gain or stable (weight loss < 2% or weight gain), slow (2% ≤ weight loss < 5%), moderate (5% ≤ weight loss < 10%), or fast (weight loss ≥ 10%) within the first year of receiving orlistat.[19,20] The weight loss rate was calculated by subtracting baseline weight from the weight at or near the end of the year, and then dividing the difference by the baseline weight. The study design is illustrated in Figure 1A, and the key protocol details are provided in Supplementary Tables 1 and 2.

This study received approval from the medical ethical committee of Xiangya Hospital (2018091077), with a waiver of informed consent. This study was approved by the IQVIA Medical Research Database Scientific Review Committee (23SRC030).

Assessment of outcomes. The primary outcome was incident gout during the 5 year follow-up after starting orlistat. Incident gout was defined as either receiving any antigout treatment (ie, allopurinol, colchicine, probenecid, febuxostat, or sulfinpyrazone) within 90 days of the first recorded Read code for gout or having a recorded gout diagnosis on the same date as a prescription for nonsteroidal anti-inflammatory drugs (NSAIDs). This approach has been previously employed in a study,[17] and the gout definition has demonstrated a positive predictive value of 90% in the General Practice Research Database in the United Kingdom,[21] in which 60% of patients overlapped with THIN. The secondary outcome was recurrent gout flares over 5 years after receiving orlistat, defined as either a recorded Read code for gout

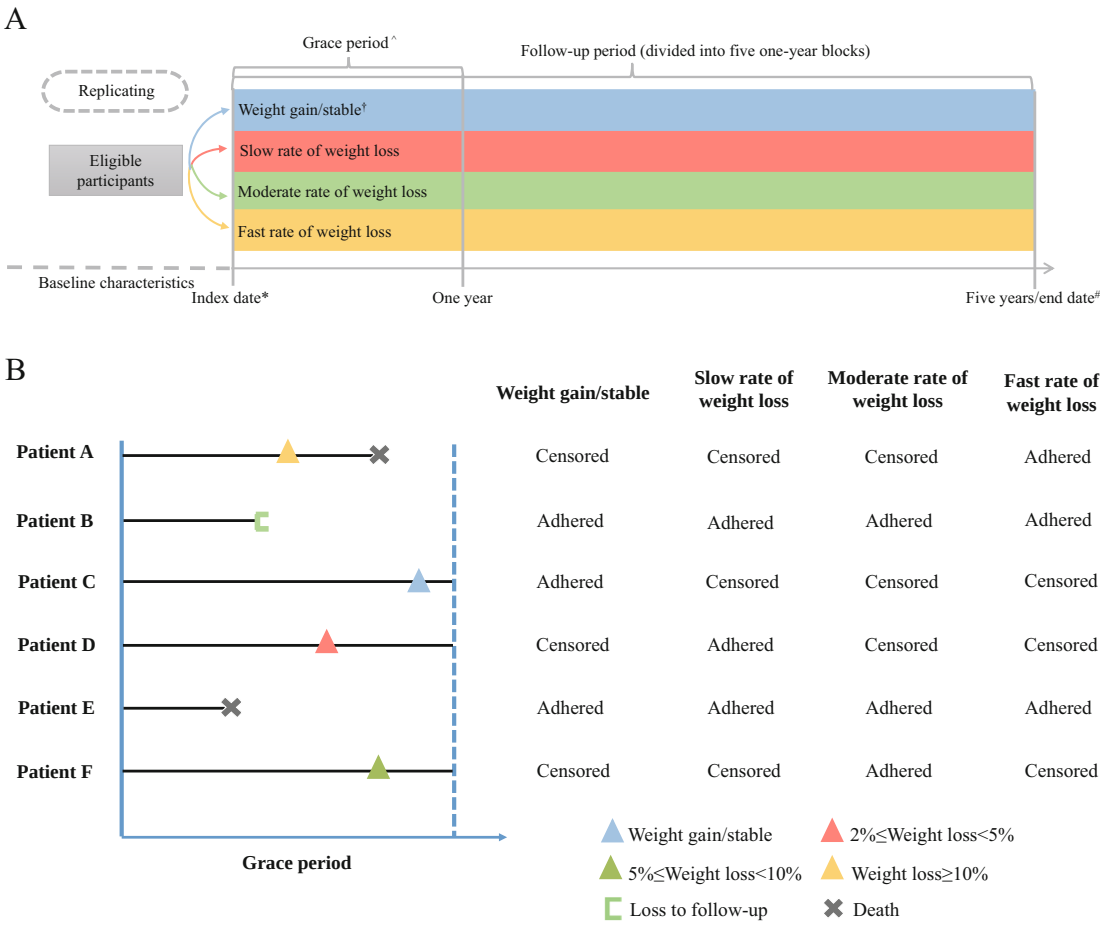

Figure 1. (A) Study design of a hypothetical randomized controlled trial (target trial) on which we modeled our observational data analysis, and (B) cloning and censoring in six hypothetical patients. GP, general practitioner; THIN, the Health Improvement Network. *Index date was defined as the first date of orlistat reception. #The end date was defined by the date of incident gout, death, disenrollment from a GP practice participating in THIN, 5 years of follow-up, or the end of the study (June 30, 2023), whichever occurred first. †Weight change = (weight$_{\text{last record during grace period}}$ − weight$_{\text{baseline}}$)/weight$_{\text{baseline}}$×100%. We used the following cut points to assign categories of weight change: weight gain/stable (<2% weight loss or weight gain), slow (≥2 and <5% loss), moderate (≥5 and <10% loss) or fast (≥10%) rate of weight loss. ^Participants were given 1 year to reduce their weight after receiving with the orlistat. Replicates would be censored if they deviated from their assigned treatment at the end of the grace period (eg, replicate in the group with a fast rate of weight loss (≥10% loss) would be censored if the participant's weight loss <10% or weight gain).

flare or a Read code for gout accompanied by a prescription for NSAIDs, glucocorticoids, or colchicine on the same date.[4]

Assessment of covariates. Data on sociodemographics (ie, sex, age and socioeconomic deprivation index score), anthropometrics (ie, BMI and weight), serum urate (SU), lifestyle factors (drinking and smoking status), and comorbidities (ie, diabetes, hypertension, myocardial infarction, depression, chronic obstructive pulmonary disease, osteoporosis, hyperlipidemia, pneumonia or infection, fracture, rheumatoid arthritis, osteoarthritis, fall, heart failure, liver disease, stroke, and chronic kidney disease) before the index date were extracted from THIN. Health care usage (including hospitalizations, GP visits, and specialist referrals) and medication use (antihypertensives, antidiabetic, statins, anticoagulants, aspirin, NSAIDs, opioids, glucocorticoids, estrogen, loop diuretics, thiazide diuretics, thiazide-like diuretics) in the year leading up to the index date were also recorded. Urate-lowering therapy and colchicine treatment were assessed during the year before the index date for recurrent flares. Participants with missing data on socioeconomic deprivation index score, smoking status, and drinking status were included and were considered as a separate category for covariates in all analyses. Baseline SU levels were only considered in the sensitivity analyses, with participants having missing SU values being excluded. Additionally, time-varying covariates, such as lifestyle factors, medication treatment, and health care usage, were collected from the index date until censoring.

Statistical analysis. For the primary outcome, participants were observed until they experienced incident gout, died, disenrolled from a GP in THIN, completed 5 years of follow-up, or reached the study end date (June 30, 2023), whichever occurred

first. Follow-up was divided into five 1-year intervals starting from the initiation of orlistat. A 1-year grace period was allowed for participants to achieve their assigned rate of weight loss after starting orlistat.[22] Participants were censored if they deviated from their assigned group during the grace period (Figure 1B). Those who developed gout, were lost to follow-up, or died before reaching the weight loss target were considered adherent to their assignment and contributed to the outcome in each arm. To address potential selection bias from censoring, we applied inverse probability weighting (IPW).[18] The denominator of the IPW was calculated using logistic regression, incorporating baseline covariates and time-varying factors (eg, lifestyle, medication use, health care usage) from the index date to censoring. To account for the competing risk of death, we conducted a cross-sectional pooling analysis, comparing gout risk across the four weighted groups by adjusting for the rate of weight loss, year of follow-up (linear and quadratic terms), and baseline confounders.[23] Robust standard errors were employed to calculate 95% confidence intervals (CIs) for hazard ratio estimates. The absolute risk difference of incident gout over 5 years was estimated using pooled logistic models with interaction terms for rate of weight loss and follow-up year. A nonparametric bootstrap analysis with 20 samples was conducted to compute 95% CIs for absolute estimates.

We took a similar approach to assess the relation of the weight loss after receiving orlistat to the risk of recurrent gout flares. Considering that the number of gout flares comprises non-negative integers, displaying a positively skewed distribution and overdispersion with an excess of zeros, we performed zero-inflated negative binomial regression to estimate the rate ratio (RR) and corresponding 95% CI for comparing the rate of recurrent gout flares among four comparison groups.[24] This statistical approach addresses overdispersion and zero inflation by assuming the population can be divided into two groups: one in which individuals always experience zero counts and another in which individuals have zero or more counts. The likelihood of being in the group with always zero counts is modeled using a logit specification (zero inflation model), whereas counts in the group with zero or more counts are modeled using a negative binomial specification (count model). The first model included only the intercept term, whereas the second model included an indicator for the rate of weight loss, adjusted for the year of follow-up (including linear and quadratic terms) and baseline confounders.

We performed five sensitivity analyses to test the reliability of the study results. First, we conducted several subgroup analyses by stratifying the participants according to sex (male or female), BMI (BMI ≥ 30 or 25 ≤ BMI < 30), and baseline SU levels (no baseline SU values, baseline SU levels ≤ 404 μmol/L, or baseline SU levels > 404 μmol/L). Second, we analyzed participants receiving any anti-obesity medications (eg, orlistat, sibutramine, rimonabant, and GLP-1 RA including exenatide, liraglutide, lixisenatide, dulaglutide and semaglutide).[15,25] Third, among participants who had baseline SU levels, we further adjusted for baseline SU levels. Fourth, we censored the participants at the end of the 1-year grace period if they did not have an updated weight measurement. Fifth, we allowed a 6-month grace period for replicates to reach their target rate of weight loss after starting orlistat. Replicates were censored if they deviated from their assigned treatment during this period. All analyses were performed using SAS software (version 9.4, SAS Institute Inc.), with a two-sided *P* value of <0.05 considered statistically significant for all tests.

RESULTS

Relation of weight loss to the risk of incident gout. We identified 131,000 eligible participants for the incident gout analysis (Figure 2). The baseline characteristics of the participants are shown in Table 1. The mean age was 45.0 years and 77.3% were women. The mean BMI was 37, and the mean weight was 102.8 kg. Both baseline covariates and time-varied covariates during the grace period were well balanced between the four comparison groups after IPW (Table 1 and Supplementary Table 3). The mean treatment duration of orlistat was 46.3 days for the group with weight gain or stability, 97.4 days for the group with a slow rate of weight loss, 132.0 days for the group with a moderate rate of weight loss, and 156.7 days for the group with a fast rate of weight loss.

As shown in Table 2 and Figure 3, the risk of incident gout was the lowest in the group with a fast rate of weight loss (1.2%), followed by the group with a moderate rate of weight loss (1.3%), the group with a slow rate of weight loss (1.5%), and the group with weight gain or stability (1.6%). Compared with the group with weight gain stability, the 5-year risk differences of incident gout were –0.1% (95% CI –0.2% to 0.0%) for the group with a slow rate of weight loss, –0.3% (95% CI –0.3% to –0.1%) for the group with a moderate rate of weight loss, and –0.4% (95% CI –0.5% to –0.2%) for the group with a fast rate of weight loss. The corresponding hazard ratios for incident gout were 0.91 (95% CI 0.81–1.01), 0.82 (95% CI 0.72–0.92), and 0.73 (95% CI 0.62–0.86), respectively. Results from the subgroup analysis stratifying by sex showed a similar inverse association between the rate of weight loss and the risk of incident gout (Supplementary Table 4). Moreover, consistent findings were obtained when restricting the analysis to participants without a baseline SU value, those with baseline SU levels greater than 404 μmol/L, obese, those receiving any anti-obesity medications, or further adjustment for baseline SU (Table 2 and Supplementary Table 4). Additionally, results remained consistent when censoring participants who did not have an updated weight measurement at the end of the 1-year grace period or those who did not adhere to their treatment assignment during the 6-month grace period (Table 2). We did not observe significant associations between the rate of weight loss and the risk of incident gout

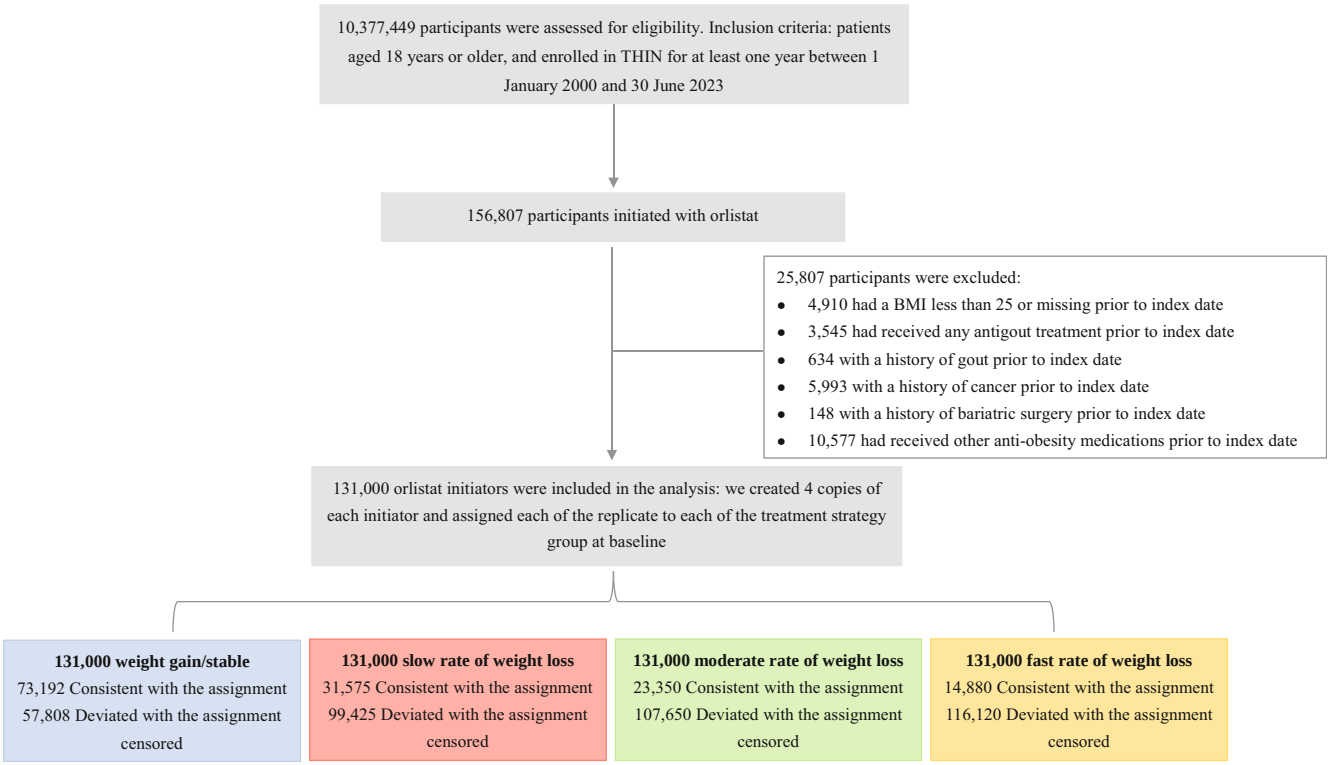

Figure 2. Selection process of the included participants in assessing the relation of rate of weight loss over a 1-year grace period after receiving orlistat to the risk of incident gout. BMI, body mass index; THIN, the Health Improvement Network. Color figure can be viewed in the online issue, which is available at http://onlinelibrary.wiley.com/doi/10.1002/art.42996/abstract.

among participants with overweight or those with baseline SU levels ≤ 404 μmol/L (Supplementary Table 4).

Relation of weight loss to the risk of recurrent gout flares. We identified eligible 3,847 patients with gout for the analysis of the recurrent gout flares (Supplementary Figure 1). The baseline characteristics of the patients are shown in Supplementary Table 5. The mean age was 56.6 years, with 29.4% being women. The mean BMI was 38.5, and the average weight was 114.0 kg. Both baseline covariates and time-varied covariates during the grace period showed comparable distribution between the four comparison groups after IPW (Supplementary Tables 5 and 6). The mean treatment duration of orlistat was 57.3 days for the group with weight gain or stability, 110.7 days for the group with a slow rate of weight loss, 152.6 days for the group with a moderate rate of weight loss, and 189.1 days for the group with a fast rate of weight loss.

As shown in Table 3, the rates of recurrent flares were the lowest in the group with a fast rate of weight loss (26.4%), followed by the group with a moderate rate of weight loss (28.9%), the group with a slow rate of weight loss (31.3%), and the group with weight gain or stability (33.1%). Compared with the group with weight gain or stability, the RRs of the recurrent gout flares were 0.93 (95% CI 0.80–1.08), 0.83 (95% CI 0.71–0.96) and 0.71 (95% CI 0.60–0.84) for the group with a slow rate of weight loss, group with a moderate rate of weight loss, and group with a fast rate of weight loss, respectively. The results from sensitivity analyses, which included only men, patients with obese, those receiving any anti-obesity medications, and those further adjusted for baseline SU, as well as those who were censored for not having an updated weight measurement at the end of the 1-year grace period or those for not adhering to their treatment assignment during the 6-month grace period, showed no material change (Supplementary Table 7 and Table 3). However, we observed a significant association between the rate of weight loss and recurrent gout flares only among patients with gout with baseline SU levels greater than 404 μmol/L (Supplementary Table 7). Because of the limited sample size, we did not analyze the relation between weight loss rate and recurrent gout flares in individuals with overweight (n = 155).

DISCUSSION

In this extensive UK GP electronic health records database, we found inverse dose–response associations of weight loss rate within 1 year after receiving orlistat, one of the most common anti-obesity medications, with both incident gout and recurrent gout flares, especially among the population with obese or those with high baseline SU levels. Several studies have explored the link between purposeful weight loss and the risk of incident gout. In the Health Professionals Follow-Up Study, losing more than 10 pounds was linked to a reduced risk of incident gout over

Table 1. Baseline characteristics of population with overweight or obese receiving orlistat*

Characteristics	Weight gain/ stable[a]	Slow rate of weight loss[a]	Moderate rate of weight loss[a]	Fast rate of weight loss[a]	SMD before weighting	Weight gain/ stable[a]	Slow rate of weight loss[a]	Moderate rate of weight loss[a]	Fast rate of weight loss[a]	SMD after weighting
Demographics										
Age, mean (SD), y	43.7 (13.5)	46.1 (13.8)	46.1 (14.0)	45.2 (14.0)	0.099	45.1 (13.7)	45.7 (13.6)	45.9 (13.8)	46.1 (13.8)	0.039
Socioeconomic deprivation index, %[b]					0.027					0.029
1	13.4	14.2	14.2	13.7		13.8	14.1	14.4	14.4	
2	14.5	15.2	15.2	15.2		15.0	15.1	15.3	15.8	
3	19.2	19.1	18.9	19.3		19.2	19.2	19.0	19.7	
4	21.9	21.6	21.6	21.5		21.9	21.8	22.0	21.4	
5	21.2	20.3	20.1	20.1		20.8	20.9	20.8	20.0	
Missing	9.8	9.6	10.0	10.2		9.4	8.8	8.4	8.7	
Female, %	77.4	76.0	77.2	78.6	0.031	77.3	77.0	77.4	78.6	0.020
BMI, mean (SD)	37.0 (6.2)	37.3 (6.0)	37.5 (6.1)	38.2 (6.4)	0.102	37.2 (6.4)	37.2 (6.0)	37.2 (6.0)	37.7 (6.0)	0.037
Weight, mean (SD), kg	102.4 (21.0)	103.1 (20.1)	103.3 (20.5)	105.4 (21.3)	0.074	102.9 (21.2)	102.7 (20.0)	102.6 (20.2)	103.6 (20.4)	0.026
SU, mean (SD), μmol/L[c]	321.6 (87.9)	329.1 (89.7)	326.2 (90.2)	331.9 (94.5)	0.062	323.0 (87.8)	321.6 (86.3)	319.6 (87.1)	320.4 (90.4)	0.021
Lifestyle factors										
Drinking (%)					0.051					0.012
None	21.5	21.3	21.5	21.6		21.3	21.0	20.8	20.8	
Past	2.5	2.8	2.9	3.0		2.6	2.6	2.6	2.6	
Current	62.0	64.6	64.3	63.0		63.3	64.2	64.3	64.2	
Missing	14.0	11.3	11.4	12.4		12.7	12.3	12.4	12.4	
Smoking, %					0.056					0.015
None	50.0	50.6	49.8	50.0		50.1	50.2	50.0	50.2	
Past	24.9	27.9	27.5	26.0		26.3	26.8	26.8	26.7	
Current	23.0	19.8	21.1	22.0		21.6	21.0	21.1	20.9	
Missing	2.1	1.7	1.6	2.0		2.0	2.0	2.1	2.2	
Comorbidity, %										
Diabetes	13.1	18.3	16.3	13.4	0.085	15.2	16.1	15.7	14.4	0.026
Hypertension	24.2	29.7	29.1	27.8	0.066	27.3	28.5	28.7	29.2	0.023
Myocardial infarction	1.9	2.5	2.3	1.7	0.032	2.1	2.2	2.2	1.9	0.014
Stroke	1.0	1.1	1.2	1.0	0.006	1.1	1.1	1.1	1.1	0.003
Heart failure	0.9	1.2	1.1	1.1	0.014	1.0	1.0	1.0	1.0	0.002
Hyperlipidemia	7.2	8.9	8.4	7.3	0.040	7.9	8.3	8.3	7.9	0.010
Depression	21.8	22.0	21.9	21.8	0.003	21.9	21.8	21.7	21.7	0.003
Chronic obstructive pulmonary disease	2.0	2.4	2.4	2.5	0.017	2.3	2.3	2.3	2.4	0.005
Fall	6.3	7.3	7.0	6.5	0.023	6.8	6.9	6.9	6.8	0.004
Osteoporosis	1.0	1.1	1.2	1.1	0.013	1.1	1.1	1.1	1.1	0.003
Pneumonia or infection	6.0	6.3	6.3	5.7	0.014	6.1	6.2	6.3	6.0	0.006
Fracture	19.4	19.1	19.3	19.5	0.005	19.2	19.2	19.2	19.3	0.002
Chronic kidney disease	1.8	2.5	2.4	2.2	0.026	2.1	2.1	2.1	2.0	0.004
Rheumatoid arthritis	0.9	1.0	0.9	0.9	0.003	0.9	0.9	0.9	1.0	0.004
Osteoarthritis	11.0	13.6	14.2	13.8	0.049	12.8	13.2	13.6	14.3	0.024
Liver disease	1.9	2.3	2.2	2.1	0.014	2.1	2.1	2.0	2.0	0.003

(Continued)

Table 1. (*Cont'd*)

Characteristics	Weight gain/ stable[a]	Slow rate of weight loss[a]	Moderate rate of weight loss[a]	Fast rate of weight loss[a]	SMD before weighting	Weight gain/ stable[a]	Slow rate of weight loss[a]	Moderate rate of weight loss[a]	Fast rate of weight loss[a]	SMD after weighting
Medication, %[d]										
Antihypertensive	32.2	37.8	37.4	35.8	0.065	35.3	36.5	36.7	37.1	0.019
Antidiabetics	10.8	14.9	13.1	10.5	0.078	12.4	13.1	12.8	11.5	0.025
Statins	16.7	22.2	20.9	17.5	0.083	19.2	20.3	20.2	19.2	0.018
Anticoagulants	1.4	1.6	1.6	1.5	0.011	1.5	1.5	1.5	1.4	0.006
Aspirin	9.9	13.2	12.4	10.6	0.060	11.5	12.3	12.2	11.7	0.015
NSAIDs	41.2	42.5	43.0	41.6	0.021	42.2	42.5	42.8	42.6	0.006
Opioids	14.3	15.3	15.1	15.6	0.018	14.8	14.9	14.6	14.9	0.004
Glucocorticoids	6.9	7.3	7.4	7.8	0.019	7.1	7.0	7.0	7.3	0.006
Estrogen	14.1	13.6	13.6	13.5	0.008	13.9	13.9	14.0	14.0	0.001
Loop diuretics	6.6	7.5	7.5	7.7	0.022	7.2	7.4	7.4	7.6	0.008
Thiazide diuretics	10.6	13.0	13.2	12.5	0.042	12.2	12.8	13.0	13.6	0.022
Thiazide-like diuretics	1.4	1.6	1.6	1.6	0.008	1.5	1.5	1.5	1.5	0.001
Health care usage, mean (SD)[d]										
Hospitalizations	0.3 (0.9)	0.3 (0.9)	0.3 (0.9)	0.3 (1.0)	0.012	0.3 (0.9)	0.3 (0.8)	0.3 (0.9)	0.3 (0.9)	0.016
General practice visits	6.3 (5.9)	6.9 (6.0)	6.7 (6.0)	6.5 (6.0)	0.054	6.6 (6.4)	6.6 (5.7)	6.5 (5.8)	6.4 (5.7)	0.026
Specialist referrals	0.5 (0.9)	0.6 (1.0)	0.5 (1.0)	0.5 (1.0)	0.026	0.5 (1.0)	0.5 (0.9)	0.5 (0.9)	0.5 (0.9)	0.020

* BMI, body mass index; NSAID, nonsteroidal anti-inflammatory drug. SMD, standardized mean difference; SU, serum urate.
[a] The groups were defined as the following: weight gain/stable, weight loss <2% or weight gain; slow rate of weight loss, ≥2% and <5%; moderate rate of weight loss, ≥5% and <10%; and fast rate of weight loss, weight loss ≥10%.
[b] The socioeconomic deprivation index was measured by the Townsend Deprivation Index, which was grouped into quintiles from 1 (least deprived) to 5 (most deprived).
[c] The SMD was calculated among participants whose SU values were available.
[d] Frequency during the 1 year before the index date.

Table 2. Associations between the rate of weight loss after receiving orlistat within the 1-year grace period and incident gout in the population with overweight or obese*

Characteristics	Weight gain/stable[a] (n = 131,000)	Slow rate of weight loss[a] (n = 131,000)	Moderate rate of weight loss[a] (n = 131,000)	Fast rate of weight loss[a] (n = 131,000)
Weighted incident gout, n	1,629	1,605	1,384	1,044
Weighted risk over 5 years, %	1.6	1.5	1.3	1.2
Weighted risk difference, % (95% CI)	0.0 (ref)	−0.1 (−0.2 to 0.0)	−0.3 (−0.3 to −0.1)	−0.4 (−0.5 to −0.2)
Weighted HR, HR (95% CI)	1.00 (ref)	0.91 (0.81–1.01)	0.82 (0.72–0.92)	0.73 (0.62–0.86)
Sensitivity analysis				
Treatment with any anti-obesity medications, HR (95% CI)[b]	1.00 (ref)	0.90 (0.82–0.99)	0.83 (0.74–0.92)	0.75 (0.65–0.86)
Adjusted the baseline SU, HR (95% CI)	1.00 (ref)	0.80 (0.63–1.01)	0.71 (0.53–0.94)	0.72 (0.52–0.99)
Additional censoring,[b] HR (95% CI)	1.00 (ref)	0.87 (0.78–0.97)	0.78 (0.69–0.88)	0.70 (0.60–0.82)
6-month grace period,[b] HR (95% CI)	1.00 (ref)	0.97 (0.87–1.08)	0.89 (0.79–1.01)	0.77 (0.63–0.93)

* CI, confidence interval; HR, hazard ratio; ref, reference; SU, serum urate.
[a] The groups were defined as the following: weight gain/stable, weight loss <2% or weight gain; slow rate of weight loss, ≥2% and <5%; moderate rate of weight loss, ≥5% and <10%; and fast rate of weight loss, weight loss ≥10%.
[b] Anti-obesity medications included orlistat (n = 131,000), sibutramine (n = 17,326), rimonabant (n = 2,027), and glucagon-like peptide-1 receptor agonists including exenatide (n = 4,535), liraglutide (n = 6,400), lixisenatide (n = 734), dulaglutide (n = 3,375) and semaglutide (n = 1,339); additional censoring was defined as participants who did not have an updated weight measurement at the end of 1-year grace period were censored; 6-month grace period means participants who did not adhere with their treatment assignment during the 6-month grace period.

12 years of follow-up.[8] However, the cause of the weight change was not specified. One study reported a 34% reduction in gout incidence following bariatric surgery, with a follow-up extending up to 26 years.[5] In that study, patients who received conventional nonsurgical obesity treatment served as the comparison cohort who received either advanced lifestyle modification or no treatment at all. Therefore, it remains unclear if the lower risk of incident gout was due to weight loss or to other confounders.

Other studies showed beneficial effects of weight loss through diet, lifestyle factors, physical activity, or a combination on gout flares. For example, a pilot study that included 13 patients showed that diet-induced weight loss was associated with decreased frequency of gout flares.[26] However, the study did not have a comparator, making it difficult to claim if such an effect was due to weight loss. Two studies reported a rise in the immediate postoperative period and a subsequent decline in SU levels

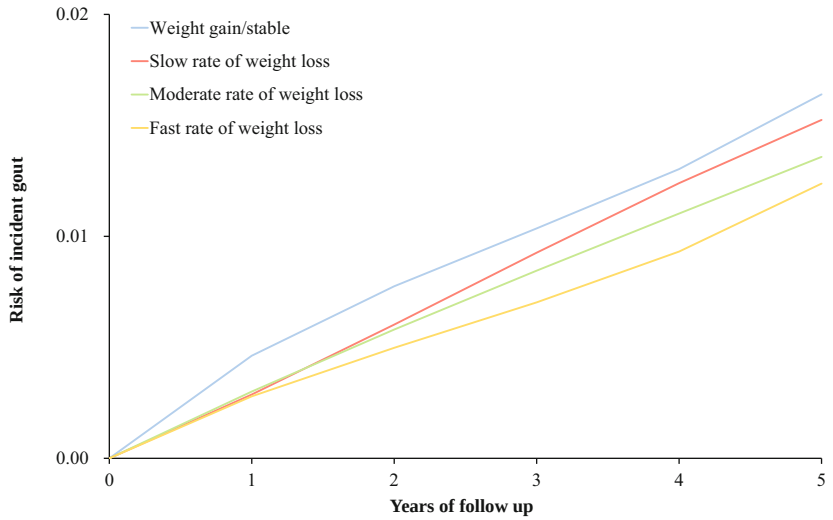

Number at risk

Weight gain/stable	131000	67197	61696	56645	51688	46751
Slow rate of weight loss	131000	26186	24253	22425	20570	18706
Moderate rate of weight loss	131000	18564	17228	15925	14670	13337
Fast rate of weight loss	131000	10564	9829	9090	8369	7612

Figure 3. Five-year risk of incident gout among populations with overweight or obese in groups with weight gain/stable, slow rate of weight loss, moderate rate of weight loss, and fast rate of weight loss receiving orlistat. Color figure can be viewed in the online issue, which is available at http://onlinelibrary.wiley.com/doi/10.1002/art.42996/abstract.

Table 3. Associations between the rate of weight loss after receiving orlistat within the 1-year grace period and recurrent gout flares in the population with overweight or obese with gout*

Characteristics	Weight gain/stable[a] (n = 3,847)	Slow rate of weight loss[a] (n = 3,847)	Moderate rate of weight loss[a] (n = 3,847)	Fast rate of weight loss[a] (n = 3,847)
Weighted number of gout flares	1,410	1,266	1,096	918
Unweighted number of recurrent flares	690	609	497	434
1	385	318	279	248
2	94	68	54	45
3	24	25	17	15
4	8	12	11	9
≥5	2	5	3	3
Weighted rate over 5 years,[b] %	33.1	31.3	28.9	26.4
Weighted rate difference, % (95% CI)	0.0 (ref)	−1.8 (−7.1 to 2.3)	−4.2 (−7.6 to −0.3)	−6.7 (−11.3 to −2.4)
Weighted RR, RR (95% CI)	1.00 (ref)	0.93 (0.80–1.08)	0.83 (0.71–0.96)	0.71 (0.60–0.84)
Sensitivity analysis				
Patients with obese, RR (95% CI)	1.00 (ref)	0.91 (0.78–1.06)	0.81 (0.70–0.95)	0.70 (0.59–0.83)
Treatment with any anti-obesity medications, RR (95% CI)[c]	1.00 (ref)	0.99 (0.86–1.13)	0.85 (0.74–0.98)	0.78 (0.67–0.90)
Adjusted the baseline SU, RR (95% CI)	1.00 (ref)	0.77 (0.63–0.93)	0.66 (0.54–0.81)	0.61 (0.49–0.76)
Additional censoring,[c] HR (95% CI)	1.00 (ref)	0.99 (0.90–1.09)	0.98 (0.88–1.08)	0.84 (0.75–0.94)
6-month grace period,[c] HR (95% CI)	1.00 (ref)	0.98 (0.89–1.08)	0.95 (0.86–1.05)	0.86 (0.77–0.96)

* CI, confidence interval; HR, hazard ratio; ref, reference; RR, rate ratio; SU, serum urate.
[a] The groups were defined as the following: weight gain/stable, weight loss <2% or weight gain; slow rate of weight loss, ≥2% and <5%; moderate rate of weight loss, ≥5% and <10%; and fast rate of weight loss, weight loss ≥10%.
[b] The weighted rate of recurrent flares was calculated by dividing the weighted number of recurrent flares over 5 years of follow-up by the total number of the participants.
[c] Anti-obesity medications included orlistat (n = 3,847), sibutramine (n = 343), rimonabant (n = 114), and glucagon-like peptide-1 receptor agonists, including exenatide (n = 293), liraglutide (n = 505), lixisenatide (n = 54), dulaglutide (n = 288) and semaglutide (n = 117); additional censoring was defined as participants who did not have an updated weight measurement at the end of 1-year grace period were censored; 6-month grace period means participants who did not adhere with their treatment assignment during the 6-month grace period.

and gout flare among patients undergoing bariatric surgery.[6,27] Two post hoc analyses of the Multiple Risk Factor Intervention Trial (MRFIT) observed a dose–response relationship of weight change with the frequent recurrent gout flares and the therapeutic target SU level.[28,29] However, weight loss in MRFIT was induced by a combination of several interventions consisting of smoking cessation, dietary modification, increased physical activity, and antihypertensive treatment.[30]

Nonspecific intervention strategy for weight change makes it challenging to implement in the real world setting. Two recent RCTs also evaluated the effect of intentional weight loss (ie, intensive dietary intervention or orlistat use) on recurrent flares among patients with gout.[31,32] One study did not find statistically significant effects of intensive dietary intervention on gout flares, possibly because of its small sample size (29 vs 32 participants) and short-term intervention period.[31] In contrast, the other study demonstrated that orlistat reduced the rate of recurrent gout flares compared with placebo in patients with gout.[32] Our study evaluated the association between the rate of weight loss following orlistat initiation and the risk of incident gout and recurrent gout flares. We observed inverse dose–response relationships, with higher rates of weight loss after receiving orlistat being linked to a reduced risk of incident gout and recurrent flares.

Various biologic mechanisms linking weight loss to the risk of gout have been proposed. Elevated SU is the prerequisite for gout development and the decrease in SU is a central goal in the management of people with gout. Studies have consistently shown that weight control plays an important role in controlling SU levels,[28] through its effect on improvement in renal function[6] and insulin resistance,[33] the decrease in serum triglyceride levels,[34] and possibly even diet changes.[26] Previous studies also suggested that the long term effect of weight loss on reducing the risk of recurrent gout flares is not solely attributed to the decrease in SU levels. It is also linked to reversing or ameliorating several risk factors, including insulin resistance and the pro-inflammatory state.[6,27] These factors are known to trigger flares in patients with gout and are commonly found in people with obese.[35]

Our study has several strengths. First, although we can theoretically design an RCT to examine the effect of different rates of weight loss within 1 year after receiving orlistat on the risk of incident gout and recurrent gout flares, several methodologic and logistic difficulties make an RCT challenging to conduct. Most importantly, the cost of such an RCT (eg, including 166,767 participants in each of the four comparison groups and following them for 5 years in the current study) would be formidable, which is also the case for the RCT of the recurrent flares. Using data from the observational study, we emulated an RCT. We adhered to several clinical trial principles, including a well-defined intervention strategy, that is, four arms of weight loss (<2%, 2–5%, 5–10%, and >10%) over a 1-year treatment with the anti-obesity medication

(ie, orlistat), a clearly-defined target population (ie, participants with overweight or obese with or without gout), and well-defined study outcomes (ie, incident gout and recurrent gout flares). Second, follow-up began at the start of orlistat treatment to prevent immortal time bias. Finally, we adjusted for potential confounders and employed IPW to address loss to follow-up. These measures collectively strengthened the internal validity of our study.

Our study has potential limitations that should be acknowledged. First, despite our rigorous efforts to control for confounders, some variables, such as disease severity, exercise levels, and diet, might not be fully captured by the data available in THIN. Therefore, residual confounding cannot be entirely ruled out. For instance, aside from alcohol intake, the consumption of purine-rich foods can directly influence SU levels and potentially increase the risk of gout flares.[9,10] If baseline dietary intake habits were unevenly distributed between comparison groups or changed following the index date, our study findings could be biased. Second, THIN lacks hospitalization data, so some patients experiencing recurrent gout flares might not consult their GPs. Third, using a pragmatic approach to identify gout flares may lead to misclassification, potentially underestimating the risk of recurrent flares. However, gout flares in this study were identified based on documented codes for gout or a gout code coupled with a prescription for NSAIDs, glucocorticoids, or colchicine on the same date, suggesting these medications were likely used to treat gout flares. If misclassification occurred, it is anticipated to be nondifferential and would likely bias results toward the null. Fourth, among the included participants, 25.5%, 15.5%, 15.1%, and 18.1% had their weight measured during the 9 to 12 months, 6 to 9 months, 3 to 6 months, and within 3 months after receiving orlistat, respectively. More participants who achieved the target of the group with a fast rate of weight loss had their updated weight measured during the 9 to 12 months after receiving orlistat (44%) compared with other exposure groups (32% for the group with a moderate rate of weight loss, 22% for the group with a slow rate of weight loss, and 17% for the group with weight stability, respectively). Additionally, 25.9% of participants did not have their weight measured after receiving orlistat, so their baseline weight was used as a substitute. Therefore, potential exposure misclassification due to the timing of the weight measurement and the missing updated weight data may introduce bias in the current study. Future studies incorporating more frequent and consistent weight measurements across all participants may be necessary to verify our findings. Finally, because SU measurement may not be routinely performed for the target population, 93.9% of participants in the incident gout analysis and 47.5% in the recurrent gout flares analysis had missing baseline SU values. Furthermore, only 7% of participants in the incident gout analysis and 54.9% in the recurrent gout flare analysis had updated SU levels measured after achieving the target rate of weight loss. This limitation restricts our ability to thoroughly investigate and substantiate the biologic mechanisms linking weight loss to the risk of incident gout or gout flares.

The 2020 American College of Rheumatology gout clinical practice guideline conditionally recommended weight loss for individuals with obese or overweight with gout, regardless of disease activity.[36] However, the preferred method and the optimal magnitude of weight loss remained undetermined. Although intensive lifestyle interventions, such as reducing caloric intake and increasing physical activity, offer significant benefits, long term adherence to these changes can be challenging, limiting their effectiveness.[37] Pharmacologic treatments, such as orlistat, present an alternative strategy for managing overweight and obese. Our study provides empirical evidence of a dose–response effect of weight loss after receiving orlistat within 1 year lowers the risk of incident gout and recurrent gout flares. If future research confirms these results, they could inform policy and enhance strategies for preventing gout and recurrent flares in the population with overweight or obese. In summary, weight loss after receiving orlistat within 1 year was associated with a lower risk of incident gout and recurrent gout flares, especially among the population with obese or those with high SU levels.

AUTHOR CONTRIBUTIONS

All authors contributed to at least one of the following manuscript preparation roles: conceptualization AND/OR methodology, software, investigation, formal analysis, data curation, visualization, and validation AND drafting or reviewing/editing the final draft. As corresponding authors, Drs Zeng, Lei, and Zhang confirm that all authors have provided the final approval of the version to be published, and take responsibility for the affirmations regarding article submission (eg, not under consideration by another journal), the integrity of the data presented, and the statements regarding compliance with institutional review board/Declaration of Helsinki requirements.

REFERENCES

1. Dehlin M, Jacobsson L, Roddy E. Global epidemiology of gout: prevalence, incidence, treatment patterns and risk factors. Nat Rev Rheumatol 2020;16(7):380–390.
2. Safiri S, Kolahi AA, Cross M, et al. Prevalence, incidence, and years lived with disability due to gout and its attributable risk factors for 195 countries and territories 1990–2017: a systematic analysis of the Global Burden of Disease study 2017. Arthritis Rheumatol 2020; 72(11):1916–1927.
3. Perez-Ruiz F, Martínez-Indart L, Carmona L, et al. Tophaceous gout and high level of hyperuricaemia are both associated with increased risk of mortality in patients with gout. Ann Rheum Dis. 2014;73(1): 177–182.
4. Cipolletta E, Tata LJ, Nakafero G, et al. Association between gout flare and subsequent cardiovascular events among patients with gout. JAMA 2022;328(5):440–450.
5. Maglio C, Peltonen M, Neovius M, et al. Effects of bariatric surgery on gout incidence in the Swedish Obese Subjects study: a non-randomised, prospective, controlled intervention trial. Ann Rheum Dis 2017;76(4):688–693.
6. Dalbeth N, Chen P, White M, et al. Impact of bariatric surgery on serum urate targets in people with morbid obesity and diabetes: a prospective longitudinal study. Ann Rheum Dis 2014;73(5):797–802.

7. Dessein PH, Shipton EA, Stanwix AE, et al. Beneficial effects of weight loss associated with moderate calorie/carbohydrate restriction, and increased proportional intake of protein and unsaturated fat on serum urate and lipoprotein levels in gout: a pilot study. Ann Rheum Dis 2000;59(7):539–543.
8. Choi HK, Atkinson K, Karlson EW, et al. Obesity, weight change, hypertension, diuretic use, and risk of gout in men: the Health Professionals Follow-Up Study. Arch Intern Med 2005;165(7):742–748.
9. Danve A, Sehra ST, Neogi T. Role of diet in hyperuricemia and gout. Best Pract Res Clin Rheumatol 2021;35(4):101723.
10. Yokose C, McCormick N, Choi HK. Dietary and lifestyle-centered approach in gout care and prevention. Curr Rheumatol Rep 2021; 23(7):51.
11. Sumithran P, Proietto J. Benefit-risk assessment of orlistat in the treatment of obesity. Drug Saf 2014;37(8):597–608.
12. Padwal RS, Majumdar SR. Drug treatments for obesity: orlistat, sibutramine, and rimonabant. Lancet 2007;369(9555):71–77.
13. McNeely W, Benfield P. Orlistat. Drugs 1998;56(2):241–249.
14. Hong JL, Meier CR, Sandler RS, et al. Risk of colorectal cancer after initiation of orlistat: matched cohort study. BMJ 2013;347:f5039.
15. Rucker D, Padwal R, Li SK, et al. Long term pharmacotherapy for obesity and overweight: updated meta-analysis. BMJ 2007; 335(7631):1194–1199.
16. Lewis JD, Schinnar R, Bilker WB, et al. Validation studies of the Health Improvement Network (THIN) database for pharmacoepidemiology research. Pharmacoepidemiol Drug Saf 2007;16(4):393–401.
17. Zhang Y, Peloquin CE, Dubreuil M, et al. Sleep apnea and the risk of incident gout: a population-based, body mass index-matched cohort study. Arthritis Rheumatol 2015;67(12):3298–3302.
18. Hernán MA. How to estimate the effect of treatment duration on survival outcomes using observational data. BMJ. 2018;360:k182.
19. Gregg E, Jakicic J, Blackburn G, et al; Look AHEAD Research Group. Association of the magnitude of weight loss and changes in physical fitness with long-term cardiovascular disease outcomes in overweight or obese people with type 2 diabetes: a post-hoc analysis of the Look AHEAD randomised clinical trial. Lancet Diabetes Endocrinol 2016; 4(11):913–921.
20. Wing RR, Lang W, Wadden TA, et al; Look AHEAD Research Group. Benefits of modest weight loss in improving cardiovascular risk factors in overweight and obese individuals with type 2 diabetes. Diabetes Care 2011;34(7):1481–1486.
21. Meier CR, Jick H. Omeprazole, other antiulcer drugs and newly diagnosed gout. Br J Clin Pharmacol 1997;44(2):175–178.
22. Chanoine JP, Hampl S, Jensen C, et al. Effect of orlistat on weight and body composition in obese adolescents: a randomized controlled trial. JAMA 2005;293(23):2873–2883.
23. Hernán MA, Brumback B, Robins JM. Marginal structural models to estimate the causal effect of zidovudine on the survival of HIV-positive men. Epidemiology 2000;11(5):561–570.
24. Yau KKW, Wang K, Lee AH. Zero-inflated negative binomial mixed regression modeling of over-dispersed count data with extra zeros. Biom J 2003;45(4):437–452.
25. Müller TD, Blüher M, Tschöp MH, et al. Anti-obesity drug discovery: advances and challenges. Nat Rev Drug Discov 2022;21(3): 201–223.
26. Dessein PH, Shipton EA, Stanwix AE, et al. Beneficial effects of weight loss associated with moderate calorie/carbohydrate restriction, and increased proportional intake of protein and unsaturated fat on serum urate and lipoprotein levels in gout: a pilot study. Ann Rheum Dis 2000;59(7):539–543.
27. Romero-Talamás H, Daigle CR, Aminian A, et al. The effect of bariatric surgery on gout: a comparative study. Surg Obes Relat Dis 2014; 10(6):1161–1165.
28. Zhu Y, Zhang Y, Choi HK. The serum urate-lowering impact of weight loss among men with a high cardiovascular risk profile: the Multiple Risk Factor Intervention Trial. Rheumatology (Oxford) 2010;49(12): 2391–2399.
29. Nguyen UD, Zhang Y, Louie-Gao Q, et al. Obesity paradox in recurrent attacks of gout in observational studies: clarification and remedy. Arthritis Care Res (Hoboken) 2017;69(4):561–566.
30. Benfari RC. The multiple risk factor intervention trial (MRFIT). III. The model for intervention. Prev Med 1981;10(4):426–442.
31. Christensen R, Zobbe K, Nielsen SM, et al. Weight loss for patients with gout and concomitant obesity: a proof-of-concept randomized trial. Arthritis Rheumatol 2024;76(5):806–812.
32. Liu S, Lin X, Tao M, et al. Efficacy and safety of orlistat in male patients with overweight/obesity and hyperuricemia: results of a randomized, double-blind, placebo-controlled trial. Lipids Health Dis 2024; 23(1):77.
33. Facchini F, Chen YD, Hollenbeck CB, et al. Relationship between resistance to insulin-mediated glucose uptake, urinary uric acid clearance, and plasma uric acid concentration. JAMA 1991;266(21): 3008–3011.
34. Richette P, Poitou C, Manivet P, et al. Weight loss, xanthine oxidase, and serum urate levels: a prospective longitudinal study of obese patients. Arthritis Care Res (Hoboken) 2016;68(7):1036–1042.
35. Chen SY, Chen CL, Shen ML. Manifestations of metabolic syndrome associated with male gout in different age strata. Clin Rheumatol 2007;26(9):1453–1457.
36. FitzGerald JD, Dalbeth N, Mikuls T, et al. 2020 American College of Rheumatology guideline for the management of gout. Arthritis Care Res (Hoboken) 2020;72(6):744–760.
37. Laine C, Wee CC. Overweight and obesity: current clinical challenges. Ann Intern Med 2023;176(5):699–700.

American College of Rheumatology
Empowering Rheumatology Professionals

Arthritis & Rheumatology
Vol. 77, No. 3, March 2025, pp 346–355
DOI 10.1002/art.43027

Weight Reduction and Target Serum Urate Level: A Longitudinal Study of Annual Medical Examination

Sho Fukui,[1] Masato Okada,[2] Tomohiro Shinozaki,[3] Takahiro Suzuki,[2] Takehiro Nakai,[2] Hiroki Ozawa,[2] Hiromichi Tamaki,[2] Mitsumasa Kishimoto,[4] Hiroshi Hasegawa,[5] Takeaki Matsuda,[5] Javier Marrugo,[6] Sara K. Tedeschi,[6] Hyon K. Choi,[7] and Daniel H. Solomon[6]

Objective. Our objective was to evaluate associations of weight reduction with serum urate (SU) changes and achieving an SU level <6 mg/dL in the real-world setting, outside of specific weight reduction interventions.

Methods. We analyzed systematically collected data of annual medical examination participants from October 2012 to October 2022. Exposure was weight change (increase or decrease) between two consecutive visits, categorized as minimal (≤0.9 kg, reference), small (1.0–4.9 kg), moderate (5.0–9.9 kg), and large (≥10 kg). Outcomes included SU changes between two consecutive visits and achieving an SU level <6 mg/dL in participants with hyperuricemia (SU level ≥7 mg/dL at the previous visit).

Results. We identified 58,630 eligible participants (median age 46 years, 51.3% female, 19.4% with overweight, median SU level 5.3 mg/dL, and 5.6% with a history of gout and/or hyperuricemia) with 336,814 visits over a median of 5.3 years. After adjustment for relevant covariates, linear general estimating equations estimated mean SU changes based on observed weight reductions (vs minimal changes) were as follows: small, −0.10 mg/dL (95% confidence interval [CI] −0.10 to −0.09 mg/dL); moderate, −0.34 mg/dL (95% CI −0.36 to −0.32 mg/dL); and large, −0.64 (95% CI −0.70 to −0.58 mg/dL). In participants with hyperuricemia, adjusted relative risks for achieving an SU level <6 mg/dL by modified Poisson regression were 1.25 (95% CI 1.15–1.37) in small weight reductions, 2.82 (95% CI 2.43–3.27) in moderate weight reductions, and 5.27 (95% CI 4.15–6.70) in large weight reductions, with corresponding numbers needed to treat of 61.1 for small weight reductions, 8.5 for moderate weight reductions, and 3.6 for large weight reductions.

Conclusion. Small weight reductions were associated with only small SU changes. Some participants with hyperuricemia can achieve the target SU level with moderate to large weight reductions.

INTRODUCTION

Hyperuricemia, often defined by a serum urate (SU) level of ≥6.8 mg/dL (the saturation point for monosodium urate crystallization in the body), is becoming increasingly common.[1–3] Elevated SU levels is a strong risk factor for gout,[4–6] the most frequent instance of inflammatory arthritis[7] that leads to acute or chronic joint pain and impaired quality of life.[8,9] Although genetics is a key driver of gout risk, lifestyle represents an important and modifiable risk factor for gout and hyperuricemia.[10–12] Obesity is associated with gout[13] and hyperuricemia,[14] and may be a more important risk factor for elevated SU levels than specific dietary components.[15] Obesity appears to have a direct relationship with high SU levels via insulin resistance, and insulin resistance reduces uric acid clearance from the kidneys.[16–18]

Obesity has been considered a potential treatment target to improve SU levels and prevent gout. Current guidelines conditionally recommend weight loss in patients with gout, whereas the

Dr Solomon's work was supported by the NIH (grant AR-P3-0072577).

[1]Sho Fukui, MD, MPH: Brigham and Women's Hospital and Harvard Medical School, Boston, Massachusetts, St. Luke's International Hospital, Tokyo, Japan, Kyorin University School of Medicine, Tokyo, Japan; [2]Masato Okada, MD, Takahiro Suzuki, MD, MPH, Takehiro Nakai, MD, Hiroki Ozawa, MD, Hiromichi Tamaki, MD: St. Luke's International Hospital, Tokyo, Japan; [3]Tomohiro Shinozaki, MPH, PhD: Tokyo University of Science, Tokyo, Japan; [4]Mitsumasa Kishimoto, MD, PhD: St. Luke's International Hospital and Kyorin University School of Medicine, Tokyo, Japan; [5]Hiroshi Hasegawa, MD, PhD, Takeaki Matsuda, MD, PhD: Kyorin University School of Medicine, Tokyo, Japan; [6]Javier Marrugo, MD, Sara K. Tedeschi, MD, MPH, Daniel H. Solomon, MD, MPH: Brigham and Women's Hospital and Harvard Medical School, Boston, Massachusetts; [7]Hyon K. Choi, MD, DrPH: Massachusetts General Hospital and Harvard Medical School, Boston.

Additional supplementary information cited in this article can be found online in the Supporting Information section (http://onlinelibrary.wiley.com/doi/10.1002/art.43027).

Author disclosures and graphical abstract are available at https://onlinelibrary.wiley.com/doi/10.1002/art.43027.

Address correspondence via email to Sho Fukui, MD, MPH, at sfukui@bwh.harvard.edu.

Submitted for publication May 21, 2024; accepted in revised form September 26, 2024.

certainty of the evidence is very low.[3,19] Massive weight loss, approximately 30 kg, through bariatric surgery consistently improves SU levels.[20,21] However, a systematic review and several interventional studies demonstrated conflicting evidence about the effect of smaller weight reductions on SU levels.[21–28] Previous studies had different interventions for weight reduction.[25–28] In addition, many previous studies were interventional studies with strict lifestyle modification,[25–27] and studies mainly targeted patients with obesity whose body mass index (BMI) was often ≥30 from US[20,23,28] or European populations.[27] There have been very limited real-world data about the direct effect of various weight reductions on SU level improvement.

Hence, this study investigated the association between weight change and SU level change in a real-world Japanese population using a large annual medical examination database. This study focuses on whether weight reduction contributes to achieving a target SU level (<6.0 mg/dL) in patients with hyperuricemia.

MATERIALS AND METHODS

Study design and setting. Longitudinal analyses were performed using St. Luke's Health Checkup Database (SLHCD) from October 2012 to October 2022. SLHCD is a systematically collected large database of annual medical examinations at a preventive medicine center, St. Luke's International Hospital, a tertiary care center in Tokyo, Japan. In Japan, all full-time employees are mandated to participate in annual medical examinations.[29] As previously described,[30,31] SLHCD includes patient demographics, medical history of various diseases with treatment status, lifestyle questionnaire results, and results of examinations (eg, height, weight, vital signs, laboratory tests, electrocardiogram, chest x-ray, and several optional examinations). We conducted this study following the Declaration of Helsinki and ethical guidelines for medical research in Japan. Informed consent was obtained using an opt-out approach. This study was approved by the St. Luke's International University Institutional Review Board. The study followed the Strengthening the Reporting of Observational Studies in Epidemiology reporting guideline.

Study participants. All participants who underwent the annual medical examination twice or more times during the study period (October 2012 to October 2022) were potentially eligible. We excluded participants who refused to use their data for research and those with errors in answers to the questionnaire (eg, answers out of the possible range, <0.1% of participants). Then, to minimize the possibility of weight changes by diseases, we excluded participants with current or history of chronic kidney disease stage G4 or 5 or on dialysis, cardiovascular diseases including ischemic heart diseases, malignancies (esophageal, stomach, colon, liver, lung, breast, ovary, uterine, cervix, and prostate), and chronic infections (tuberculosis and other mycobacterial infections).

Exposure of interest and outcomes. The exposure of interest was weight change (in kilograms) between the two consecutive visits. We described the first visit of two consecutive visits as the "previous visit" and the second visit as the "concurrent visit." Staff nurses measured and recorded body weight during medical checkups. Participants wore uniforms (patient gowns) during the annual examination to reduce variations in body weight by clothing and shoes. Weight changes, increases and decreases, were considered as a continuous variable. Then, they were categorized as follows based on the previous research[23]: minimal change (–0.9 to 0.9 kg, a reference category), small (1.0–4.9 kg), moderate (5.0–9.9 kg), and large (≥10 kg) increase or decrease.

The primary outcome was change in SU level between two consecutive visits. The SU level change was calculated by subtracting the SU level at the concurrent visit from the previous visit. SU was routinely measured at every visit in the examination by uricase oxidization method (Clinical Chemistry Analyzers, JCA-BM2250/6070; JEOL Ltd). The secondary outcomes included achievement of target SU levels (<6.0 mg/dL) at concurrent visits and SU level decrease by ≥1.0 mg/dL or ≥0.5 mg/dL. Analyses for these secondary outcomes were performed only in participants with an SU level ≥7.0 mg/dL at the previous visits.

Covariates. We simultaneously included covariates measured at the previous visit and changes in covariates between two visits into models. Covariates at the previous visit included age; sex; BMI; estimated glomerular filtration rate (eGFR) based on Japanese-specific formula;[32] SU level (at the previous visit); history of gout or hyperuricemia; medication administration for gout and/or hyperuricemia, hypertension, diabetes, and dyslipidemia (yes or no); current smoking (yes or no); alcohol intake (drinks per day); and categorical frequency of diets (carbohydrate, meat and eggs, seafood, soy, milk and dairy products, vegetables, fruits, sweets, and fatty diet) in the dietary questionnaire.

In addition to covariates at the previous visit, we included change variables between two consecutive visits, including dietary changes, changes in smoking status (initiated, discontinued, or remained the same status), alcohol intake changes (drinks per day, one drink included 10 g of ethanol), eGFR changes (mL/min/1.73m^2), and changes in medication status (initiated, discontinued, or remained the same status), which were also included in the model. For dietary change, we calculated semiquantitative changes in dietary consumption for each dietary category. Because diet consumptions were recoded as ordinal variables, we assigned integers to those variables sequentially. Then, we calculated semiquantitative changes by subtracting the diet consumption at one visit from that in the previous visit.

Statistical analyses and ethical approval. We described participant characteristics at baseline using summary statistics, including numbers with percentages and medians with

interquartile ranges (IQRs). Scatter plots helped visualize the crude association of weight changes with continuous SU changes with simple linear prediction; histograms were used for categorical weight changes. Then, considering intrapersonal correlations, we applied multivariable linear general estimating equations (GEEs) with robust variance to evaluate the β coefficients for the association of continuous weight changes to SU changes. Additionally, we used restricted cubic splines with six fixed knots (−10, −5, −1, +1, +5, and +10 kg) in weight change to flexibly evaluate the form of the association between continuous weight change and SU level change. To reduce the influence of minor variations in weight, associations of categorized weight changes with SU level changes were assessed using the linear GEE. Stratified subgroup analyses were performed by sex (male or female), history of gout or hyperuricemia (yes or no), previous SU levels (<7, 7–8, and ≥8 mg/dL), BMI at previous visits (<25, 25–30, and ≥30), and their combination (SU level ≥7 mg/dL and BMI >25 or not). Then, we supplementarily summarized the association of SU changes with alcohol and dietary changes, in comparison to categorical weight changes. In this analysis, alcohol changes were categorized (no change, <2, 2–4, and >4 drink increase or decrease) for intelligible comparison. R^2 of the fully adjusted model and partial R^2 of univariate models of weight change and each dietary change were calculated. Finally, to reduce the influence of medications on SU level, we performed sensitivity analyses that excluded participants who took medications for gout or hyperuricemia, hypertension, diabetes, and dyslipidemia during the study period.

In participants with hyperuricemia (SU level ≥7 mg/dL at the previous visit), modified Poisson regression with patient-clustered robust variance estimated the adjusted relative risk (RR) of categorical weight changes (vs minimal change) for achieving target SU level (<6.0 mg/dL), SU level decrease by ≥1.0 mg/dL, or SU level decrease by ≥0.5 mg/dL. The numbers needed to treat (NNTs) were calculated based on the adjusted RR. Subgroup analyses were performed in participants with gout and/or hyperuricemia diagnosis. Stratified analyses by previous SU levels (7–8 or ≥8 mg/dL) and BMI (<25 or ≥25) were also conducted.

All multivariable analyses adjusted for covariates at the previous visit included the following: age, sex, BMI, eGFR, SU level, history of gout or hyperuricemia, relevant medication administration (medications for gout or hyperuricemia, hypertension, diabetes, and dyslipidemia), smoking status, alcohol intake, and relevant dietary consumptions. To reduce the direct effect of other changes in the lifestyles or conditions, change variables between two visits, including dietary changes, changes in smoking status, alcohol intake changes, eGFR changes, and changes in medication administration, were also included in the models.

We performed complete-case analyses because only a small amount of data were missing; 489 (0.83%) participants had one or more missing values. Point estimates and 95% confidence intervals (CI) without *P* values were reported, considering the observational nature of this study. We conducted all statistical analyses with Stata (version 17.1; StataCorp). The St Luke's International University Institutional Review Board approved this study (22-R105). Data are not publicly available due to our institution's regulations. The transcripts for Stata software (version 17.1, StataCorp) in this study are available on reasonable request to the corresponding author (SF). SF had full access to all the data in the study and was responsible for the integrity and accuracy of analyses.

RESULTS

Characteristics of study participants. Among 67,467 participants who had annual examinations twice or more times during the follow-up, we identified 58,630 eligible participants with 336,814 visits for the analyses. The most common reason for exclusion was a history of malignancies (n = 8,369) (Supplemental Figure 1). At baseline, the median age of the participants was 46 years (IQR 38.0–55.0 years), and 51.3% were female. The median BMI was 22.0 (IQR 19.9–24.3), 16.5% (n = 9,660) had overweight (BMI 25–30), and 2.9% (n = 1,691) had obesity (BMI ≥30). The median SU level was 5.3 mg/dL (IQR 4.4–6.4 mg/dL), and 5.6% (n = 3,291) had a current or previous diagnosis of gout or hyperuricemia. In 15.5% (n = 9,094) of participants, we found a baseline SU ≥7.0 mg/dL (Table 1). A total of

Table 1. Characteristics of medical checkup participants at baseline*

Characteristic	Total (N = 58,630)
Age, median (interquartile range)	46.0 (38.0–55.0)
Sex, n (%)	
Male	28,540 (48.7)
Female	30,090 (51.3)
Body mass index, median (interquartile range)	22.0 (19.9–24.3)
Normoweight (body mass index <25), n (%)	47,275 (80.6)
Overweight (body mass index from 25 to 30), n (%)	9,660 (16.5)
Obese (body mass index ≥30), n (%)	1,691 (2.9)
Estimated glomerular filtration rate, median (interquartile range), mL/min/1.73m^2	77.9 (67.9–88.9)
Serum urate, median (interquartile range), mg/dL	5.3 (4.4–6.4)
<6.0, n (%), mg/dL	37,795 (64.5)
6 to 7, n (%), mg/dL	11,669 (19.9)
7 to 8, n (%), mg/dL	6,586 (11.2)
≥8, n (%), mg/dL	2,508 (4.3)
Current or history of gout or hyperuricemia, n (%)	3,291 (5.6)
Receiving pharmacological treatment for gout or hyperuricemia	1,718 (2.9)
Medication use for conditions below, n (%)	8,058 (13.7)
Hypertension	5,209 (8.9)
Diabetes	1,184 (2.0)
Dyslipidemia	3,746 (6.4)

* Continuous variables are presented as median (interquartile range) based on their distribution.

60.5% (n = 35,488) participants were regular alcohol drinkers, with a median alcohol intake of 1.4 drinks per day at baseline (Supplemental Table 1). The questionnaire results showed a good distribution of participants in each category of diet frequency at baseline. During the study period, the median total number of visits for each participant was 5.0 times (IQR 3.0–9.0 times) over a median follow-up of 5.3 years (IQR 2.5–8.7 years), and a median visit interval was 1.0 year (IQR 1.0–1.2 years).

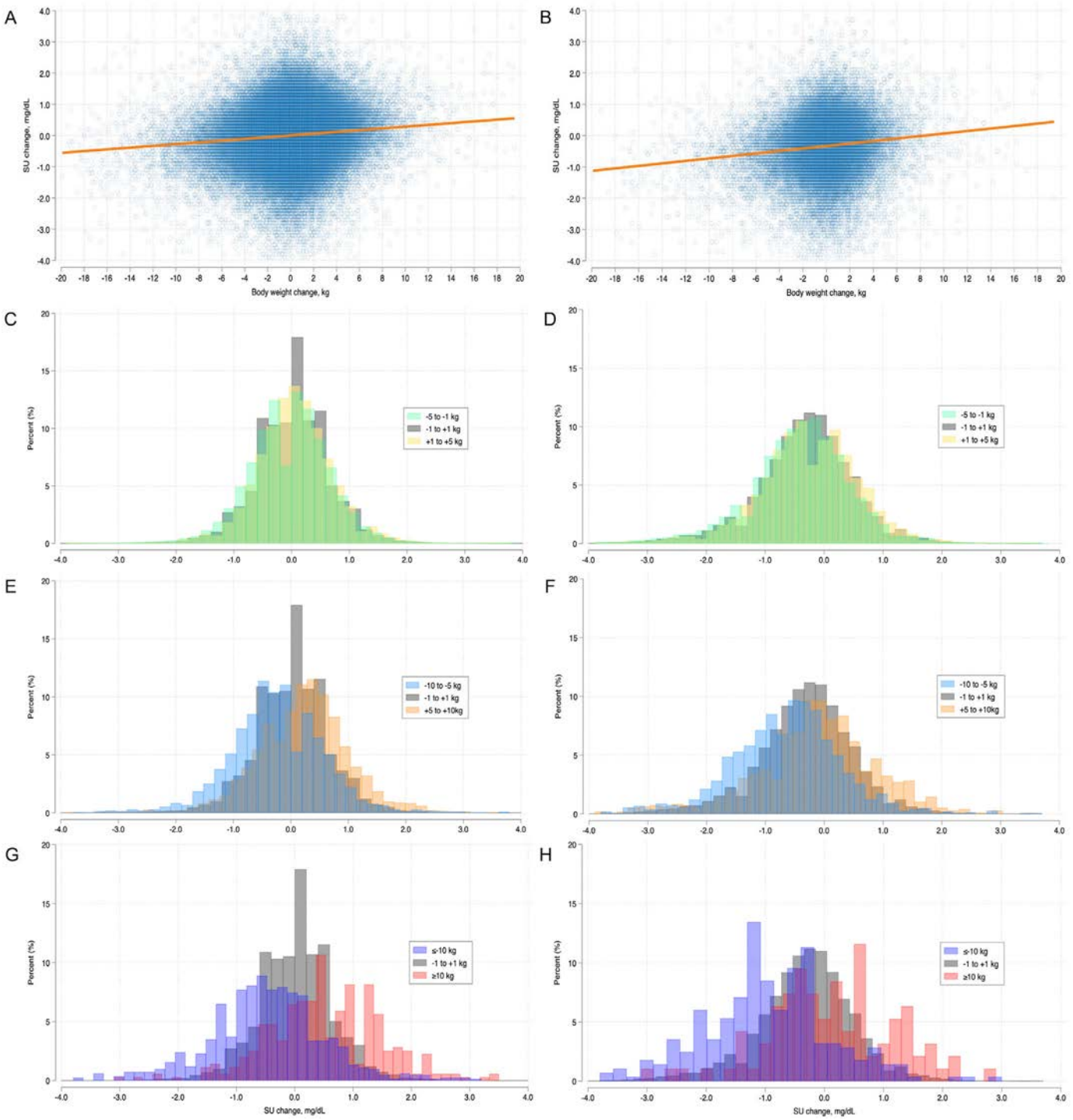

Figure 1. Body weight change and SU level changes in total participants or participants with hyperuricemia. Scatter plots of SU change against body weight change with (A) simple linear prediction and histograms of SU change by (C) small, (E) moderate, and (G) large weight change in total participants. (B, D, F, H) The same figures are shown in participants with hyperuricemia (SU levels ≥7 mg/dL at the previous visits). SU, serum urate.

Baseline characteristics and questionnaire results in patients with a diagnosis of gout and/or hyperuricemia are summarized in Supplemental Tables 2 and 3.

Continuous weight changes and changes in SU levels. We observed a positive unadjusted association between weight change and SU level change (Figure 1). When adjusted for covariates, weight loss of 1 kg was associated with a mean SU level decrease of 0.044 mg/dL (95% CI 0.042–0.046 mg/dL) in the overall study population and 0.052 mg/dL (95% CI 0.049–0.056 mg/dL) in participants with SU levels of ≥7.0 mg/dL at the previous visit. The restricted cubic splines showed that the adjusted relationships between changes in weight and SU level changes were generally linear in the overall population and in participants with hyperuricemia (see Figure 2).

Categorical weight changes and changes in SU levels. Treating minimal weight change as the reference category, the adjusted mean changes in SU levels were –0.10 mg/dL (95% CI –0.10 to –0.09 mg/dL) for small weight reduction, –0.34 mg/dL (95% CI –0.36 to –0.32 mg/dL) for moderate weight reduction, and –0.64 mg/dL (95% CI –0.70 to –0.58 mg/dL) for large weight reduction (Figure 3). The positive associations between weight changes and SU level changes were consistent across the subgroups. In participants with higher SU levels and higher BMIs at the previous visit, weight reductions were associated with larger decreases in SU levels (see Figure 3). Weight changes had larger associations with SU, compared to alcohol and dietary changes (Supplemental Figure 2). The R^2 of the fully adjusted model was 22%, and the partial R^2 of categorical weight change was approximately 1% (Supplemental Table 4). Sensitivity analyses in participants without relevant medication administration found similar results (Supplemental Table 5).

Achievement of target SU level or relevant SU improvement by weight reduction in patients with hyperuricemia. SU levels of ≥7.0 mg/dL were observed at 42,913 visits among 14,760 participants. Distributions of SU levels before and after weight reductions in this population were visualized by weight reduction groups in Supplemental Figure 3. The larger weight reduction group tended to have higher SU levels at the previous visit, but more participants achieved the target SU level at concurrent visits (Table 2). Adjusted RRs for achieving the target SU level (<6.0 mg/dL) were 1.25 (95% CI 1.15–1.37) for

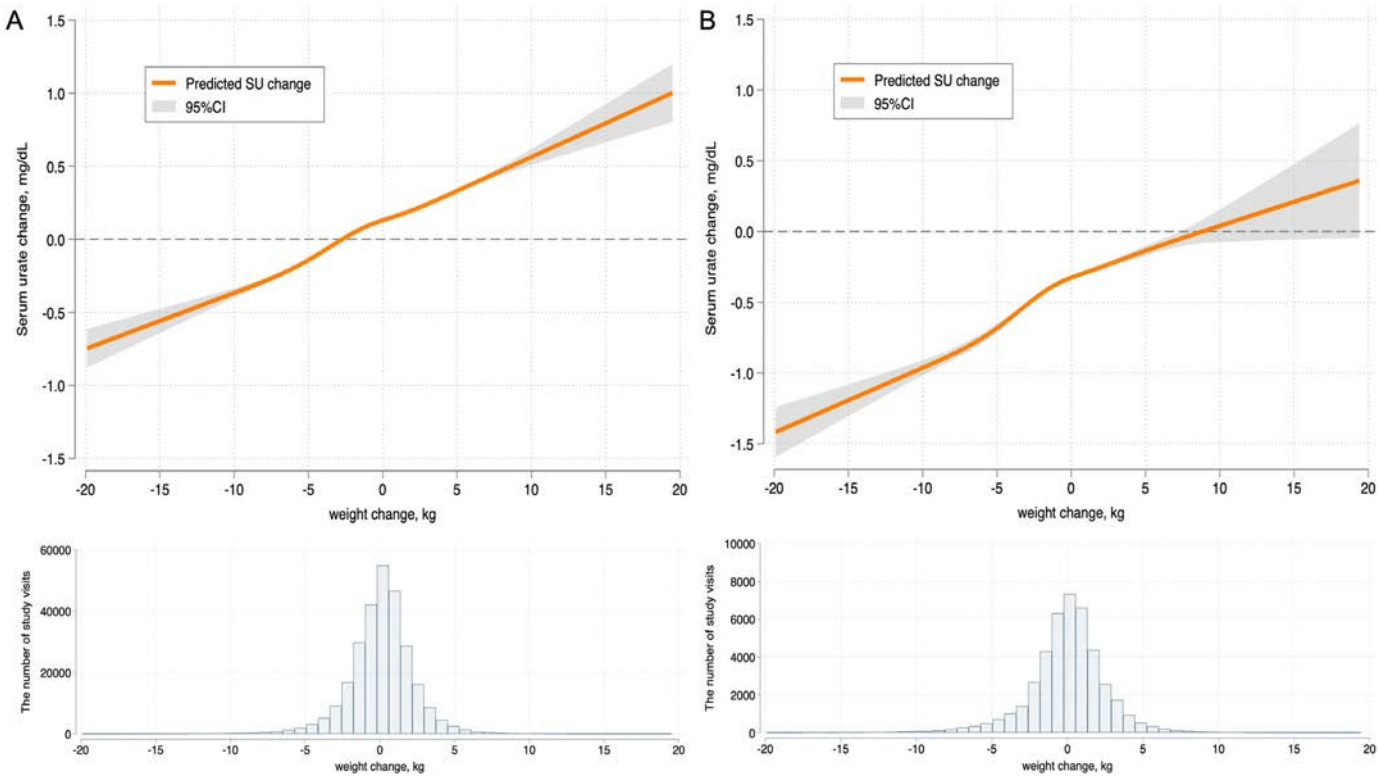

Figure 2. Restricted cubic splines of adjusted association between continuous weight changes and SU level changes in (A) total participants and (B) participants with hyperuricemia (SU levels ≥7 mg/dL). Six fixed knots of weight change (–10, –5, –1, +1, +5, and +10) were used for the spline in averaged participants. The model was adjusted for covariates at previous visits (age, sex, body mass index, estimated glomerular filtration rate, SU, history of hyperuricemia or gout, relevant medication administration, smoking status, alcohol intake, and relevant dietary consumption). Change variables between two visits were also included in the model (dietary changes, changes in smoking status, alcohol intake changes, estimated glomerular filtration rate changes, and changes in relevant medications). CI, confidence interval; SU, serum urate. Color figure can be viewed in the online issue, which is available at http://onlinelibrary.wiley.com/doi/10.1002/art.43027/abstract.

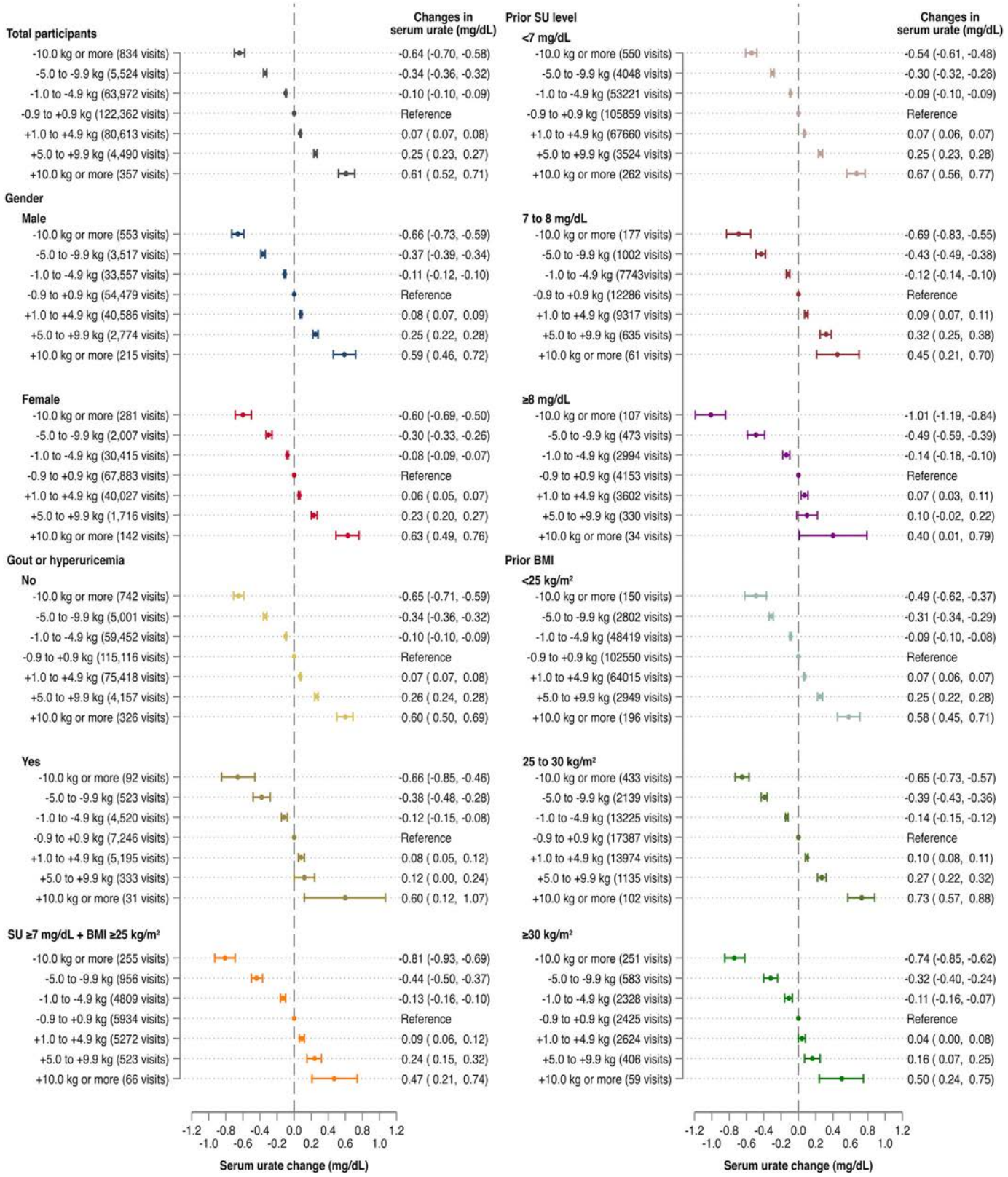

Figure 3. Categorical body weight change and SU level changes in total participants and in subgroups. Points and bars are point estimates and 95% confidence intervals. Results were adjusted for covariates at previous visits (age, sex, BMI, estimated glomerular filtration rate, SU, history of gout or hyperuricemia, relevant medication administration, smoking status, alcohol intake, and relevant dietary consumption). Change variables between two visits were also included in the model (dietary changes, changes in smoking status, alcohol intake changes, estimated glomerular filtration rate changes, and changes in relevant medication). The stratified subgroup analyses excluded stratified variables from the models. BMI, body mass index; SU, serum urate. Color figure can be viewed in the online issue, which is available at http://onlinelibrary.wiley.com/doi/10.1002/art.43027/abstract.

small (vs minimal) weight reduction, 2.82 (95% CI 2.43–3.27) for moderate weight reduction, and 5.27 (95% CI 4.15–6.70) for large weight reduction. The corresponding NNTs based on adjusted RRs were 61.1 (95% CI 42.1–104.4) for small weight reduction, 8.5 (95% CI 6.9–10.9) for moderate weight reduction, and 3.6 (95% CI 2.6–4.4) for large weight reduction (Table 2). Similar dose-response associations were observed between weight changes and SU level decreases by ≥1.0 or by ≥0.5 mg/dL (Table 2). The results were similar in the subgroup analyses, which included participants with gout and/or hyperuricemia diagnoses (8,704 visits among 2,514 participants) (see Supplemental Table 6). In stratified analyses, the NNT for achieving target SU level was smaller in participants with previous SU levels of 7–8 mg/dL compared to those with previous SU levels of ≥8 mg/dL (Supplemental Table 7).

DISCUSSION

In this large longitudinal study of 58,630 participants, we found robust and positive linear associations between weight changes and SU level changes. A small amount of weight loss was associated with a small decrease in SU levels. In contrast, moderate to large weight reduction was associated with a reasonable proportion of patients with hyperuricemia achieving relevant SU improvement and/or target SU levels. These results were consistent across the subgroups, including gout and/or hyperuricemia populations.

In contrast to previous studies, this is a real-world study without known imposed lifestyle interventions. Nevertheless, the extent of associations between weight change and SU level change in this study was very similar to a previous analysis of the Multiple Risk Factor Intervention Trial in high cardiovascular risk men in the United States[23]; both studies found similar dose-response associations. We applied restricted cubic splines and found that weight and SU level change have an approximately linear association. Compared to some previous studies,[25,26] the SU decrease for the same weight reduction was smaller in this study. This is probably due to the absence of a specific dietary intervention[26] and lower baseline SU levels.[25] Patients with high SU levels should have larger declines in SU levels due to regression to the mean.[33] Several interventions in previous studies, such as dietary modification, coach-directed weight loss, and metformin administration, did not show improvement in SU levels.[21,27,28] However, the lack of association may have been due to small relative weight reductions[21,28] and a small sample size.[27]

The current study found that small weight reductions (~5 kg) were associated with only small SU level improvement (–0.1 mg/dL) and were unlikely to help patients with hyperuricemia achieve target SU levels. In contrast, some participants with moderate or large weight reduction achieved the target SU levels (<6.0 mg/dL); compared with minimal weight change, the NNTs were 8.5 in the moderate weight reduction group and 3.6 in large weight reduction group. Weight reduction appeared to be more effective in participants with mild hyperuricemia (SU 7–8 mg/dL), as indicated by the smaller NNTs compared to those with SU levels ≥8 mg/dL. The association was maintained in the gout and/or hyperuricemia subgroup. Weight reduction may be an effective strategy to improve SU levels in patients with gout. In patients with obesity, weight reduction is reasonable because of its larger association with SU improvement and reduced cardiovascular risks.[34,35] Urate-lowering therapy should be appropriately initiated to achieve target SU because only a portion (13.9–19.4%) of participants with hyperuricemia with moderate to large weight reductions would achieve the target SU levels.

A large number of participants and repeatedly measured weight and SU data enabled us to perform the longitudinal and subgroup analyses, including the gout and/or hyperuricemia subpopulation. The study database included comprehensive covariates and only a small amount of missing data. Our database lacks the details of medications affecting SU levels (eg, aspirin, diuretics, antihypertensives, sodium-glucose cotransporter-2 inhibitors, statins, and antituberculosis agents).[36] However, this study excluded patients with cardiovascular diseases, chronic kidney disease, and chronic mycobacterium infections, which are often treated with these medications. In addition, results were consistent in the sensitivity analyses in participants without medication administration for gout and/or hyperuricemia and other comorbidities. This study evaluated only SU levels without incident gout, but SU is an established target in gout management. We had no data on the reason for weight reductions, but we excluded participants with conditions that may cause weight changes. Bariatric surgery is very rare in Japan.[37] We might underestimate the association between weight reduction and SU level improvement when participants had fluid depletion, which caused both weight loss and SU level increase.[38] However, the annual medical examination typically included participants without acute diseases. The results of dietary change on SU level change should be carefully interpreted. The questionnaire lacks details of food items in each food category, and results shown are after adjustment for weight changes. To evaluate semiquantitative changes in dietary consumption, we assumed the association of one categorical frequency change with SU level change was the same across all categories. This assumption may cause residual confounding, but adjusting for dietary changes contributed to evaluating the direct association between weight change and SU level change. SU level measurement has diurnal variations and relatively large random errors,[39,40] which typically lead to underestimation of the association. Our analyses did not consider the timing of the day in the measurement of SU, but the large sample size of this study may reduce the influence of random errors. Finally, most participants in this study were relatively healthy Japanese people with infrequent comorbidities and rare obesity, which may limit the generalizability of the findings.

Table 2. Categorical body weight change and achieving target SU level (<6.0 mg/dL) or relevant SU decrease in participants with hyperuricemia (SU ≥7.0 mg/dL) at a previous visit*

	Weight change categories						
	Large decrease (−10.0 kg or more)	Moderate decrease (−9.9 to −5.0 kg)	Small decrease (−4.9 to −1.0 kg)	Minimal change (−0.9 to +0.9 kg)	Small increase (+1.0 to +4.9 kg)	Moderate increase (+5.0 to +9.9 kg)	Large increase (+10.0 kg or more)
Total number of visits(number of patients)	284 (278)	1,475 (1,383)	10,737 (7,456)	16,438 (9,050)	12,919 (8,169)	965 (872)	95 (91)
The number of visits achieving the target SU level (<6.0 mg/dL), n (%) (number of patients)	55 (19.4) (55)	205 (13.9) (203)	788 (7.3) (779)	1,055 (6.4) (1,022)	691 (5.4) (678)	51 (5.3) (50)	3 (3.2) (3)
Crude RR (95% CI)[a]	3.02 (2.36–3.85)	2.17 (1.88–2.49)	1.14 (1.05–1.25)	Reference	0.83 (0.76–0.92)	0.82 (0.62–1.09)	0.49 (0.16–1.50)
Adjusted RR (95% CI)[b]	5.27 (4.15–6.70)	2.82 (2.43–3.27)	1.25 (1.15–1.37)	Reference	0.80 (0.73–0.88)	0.78 (0.59–1.03)	0.48 (0.15–1.52)
NNT based on adjusted RR (95% CI)[c]	3.6 (2.7–4.9)	8.5 (6.9–10.9)	61.1 (42.1–104.4)	Reference	NA	NA	NA
Number of visits achieving the SU decrease by ≥1.0 mg/dL, n (%) (number of patients)	142 (50) (140)	499 (33.8) (488)	2,482 (23.1) (2,321)	3,152 (19.2) (2,899)	2,338 (18.1) (2,186)	186 (19.3) (184)	12 (12.6) (12)
Crude RR (95% CI)[a]	2.61 (2.31–2.94)	1.76 (1.63–1.91)	1.21 (1.15–1.26)	Reference	0.94 (0.90–0.99)	1.01 (0.88–1.15)	0.66 (0.39–1.12)
Adjusted RR (95% CI)[b]	3.05 (2.67–3.49)	1.9 (1.75–2.06)	1.23 (1.17–1.29)	Reference	0.87 (0.84–0.92)	0.79 (0.70–0.90)	0.56 (0.34–0.94)
NNT based on adjusted RR (95% CI)[c]	2.5 (2.1–3.1)	5.8 (4.9–7.0)	22.7 (18.2–29.8)	Reference	NA	NA	NA
The number of visits achieving the SU decrease by ≥0.5 mg/dL, n (%) (number of patients)	199 (70.1) (195)	864 (58.6) (838)	4,932 (45.9) (4,339)	6,701 (40.8) (5,515)	4,970 (38.5) (4,322)	318 (33) (309)	30 (31.6) (30)
Crude RR (95% CI)[a]	1.72 (1.59–1.86)	1.44 (1.37–1.51)	1.13 (1.1–1.16)	Reference	0.94 (0.92–0.97)	0.81 (0.74–0.89)	0.77 (0.58–1.03)
Adjusted RR (95% CI)[b]	2.02 (1.85–2.2)	1.57 (1.49–1.65)	1.17 (1.14–1.20)	Reference	0.91 (0.88–0.93)	0.72 (0.66–0.79)	0.72 (0.54–0.96)
NNT based on adjusted RR (95% CI)[c]	2.4 (2.0–2.9)	4.3 (3.8–5.0)	14.7 (12.3–18.0)	Reference	NA	NA	NA

* CI, confidence interval; NA, not applicable; NNT, number needed to treat; RR, relative risk; SU, serum urate.
[a] Modified Poisson regression with cluster robust variance estimated 95% CIs.
[b] Results were adjusted for covariates at previous visits (age, sex, body mass index, estimated glomerular filtration rate, SU, history of gout or hyperuricemia, relevant medication administration, smoking status, alcohol intake, and dietary consumption). Change variables between two visits were also included in the model (dietary changes, changes in smoking status, alcohol intake changes, estimated glomerular filtration rate changes, and changes in relevant medication).
[c] NNT was derived from adjusted RR and the observed event proportion in participants with minimal weight change group (−0.9 to +0.9 kg).

In conclusion, this large longitudinal study found a robust positive association between weight changes and SU level changes. Small amounts of weight reduction were associated with only small changes in SU levels. Some patients with hyperuricemia may achieve the target SU level by moderate to large weight reduction. These results were consistent in the gout and/or hyperuricemia subpopulation. Moderate to large weight reduction would be a reasonable treatment option to control SU levels in patients with overweight and gout.

ACKNOWLEDGMENTS

We express our deepest gratitude to the physicians and other staff who contributed to annual medical checkups in our institution. We greatly appreciate the support from Dr Kimura in SLHCD. We sincerely thank Mr Nakajima and the Information System Unit in St. Luke's International Hospital for supporting data collection.

AUTHOR CONTRIBUTIONS

All authors contributed to at least one of the following manuscript preparation roles: conceptualization AND/OR methodology, software, investigation, formal analysis, data curation, visualization, and validation AND drafting or reviewing/editing the final draft. As corresponding author, Dr Fukui confirms that all authors have provided the final approval of the version to be published, and takes responsibility for the affirmations regarding article submission (eg, not under consideration by another journal), the integrity of the data presented, and the statements regarding compliance with institutional review board/Declaration of Helsinki requirements.

REFERENCES

1. Dehlin M, Jacobsson L, Roddy E. Global epidemiology of gout: prevalence, incidence, treatment patterns and risk factors. Nat Rev Rheumatol 2020;16(7):380–390.
2. Chen-Xu M, Yokose C, Rai SK, et al. Contemporary prevalence of gout and hyperuricemia in the United States and decadal trends: the National Health and Nutrition Examination Survey, 2007-2016. Arthritis Rheumatol 2019;71(6):991–999.
3. FitzGerald JD, Dalbeth N, Mikuls T, et al. 2020 American College of Rheumatology guideline for the management of gout. Arthritis Care Res (Hoboken) 2020;72(6):744–760.
4. Dalbeth N, Phipps-Green A, Frampton C, et al. Relationship between serum urate concentration and clinically evident incident gout: an individual participant data analysis. Ann Rheum Dis 2018;77(7):1048–1052.
5. Perez-Ruiz F, Herrero-Beites AM, Carmona L. A two-stage approach to the treatment of hyperuricemia in gout: the "dirty dish" hypothesis. Arthritis Rheum 2011;63(12):4002–4006.
6. McCormick N, Yokose C, Challener GJ, et al. Serum urate and recurrent gout. JAMA 2024;331(5):417–424.
7. Zhu Y, Pandya BJ, Choi HK. Prevalence of gout and hyperuricemia in the US general population: the National Health and Nutrition Examination Survey 2007-2008. Arthritis Rheum 2011;63(10):3136–3141.
8. Dalbeth N, Gosling AL, Gaffo A, et al. Gout. Lancet 2021;397(10287):1843–1855.
9. Kyu HH, Abate D, Abate KH, et al; GBD 2017 DALYs and HALE Collaborators. Global, regional, and national disability-adjusted life-years (DALYs) for 359 diseases and injuries and healthy life expectancy (HALE) for 195 countries and territories, 1990-2017: a systematic analysis for the Global Burden of Disease Study 2017. Lancet 2018;392(10159):1859–1922.
10. McCormick N, Rai SK, Lu N, et al. Estimation of primary prevention of gout in men through modification of obesity and other key lifestyle factors. JAMA Network Open 2020;3(11):e2027421–e2027421.
11. Choi HK, McCormick N, Lu N, et al. Population impact attributable to modifiable risk factors for hyperuricemia. Arthritis Rheumatol 2020;72(1):157–165.
12. Major TJ, Topless RK, Dalbeth N, et al. Evaluation of the diet wide contribution to serum urate levels: meta-analysis of population based cohorts. BMJ 2018;363:k3951.
13. Choi HK, Atkinson K, Karlson EW, et al. Obesity, weight change, hypertension, diuretic use, and risk of gout in men: the health professionals follow-up study. Arch Intern Med 2005;165(7):742–748.
14. Shirasawa T, Ochiai H, Yoshimoto T, et al. Cross-sectional study of associations between normal body weight with central obesity and hyperuricemia in Japan. BMC Endocr Disord 2020;20(1):2.
15. Wang J, Chen S, Zhao J, et al. Association between nutrient patterns and hyperuricemia: mediation analysis involving obesity indicators in the NHANES. BMC Public Health 2022;22(1):1981.
16. Yamashita S, Matsuzawa Y, Tokunaga K, et al. Studies on the impaired metabolism of uric acid in obese subjects: marked reduction of renal urate excretion and its improvement by a low-calorie diet. Int J Obes 1986;10(4):255–264.
17. Ter Maaten JC, Voorburg A, Heine RJ, et al. Renal handling of urate and sodium during acute physiologic hyperinsulinaemia in healthy subjects. Clin Sci (Lond) 1997;92(1):51–58.
18. Facchini F, Chen YD, Hollenbeck CB, et al. Relationship between resistance to insulin-mediated glucose uptake, urinary uric acid clearance, and plasma uric acid concentration. JAMA 1991;266(21):3008–3011.
19. Hisatome I, Ichida K, Mineo I, et al. Japanese Society of Gout and Uric & Nucleic Acids 2019 Guidelines for Management of Hyperuricemia and Gout 3rd edition. Gout and Uric & Nucleic Acids. 2020;44-(Supplement):sp-1–sp-40.
20. Romero-Talamás H, Daigle CR, Aminian A, et al. The effect of bariatric surgery on gout: a comparative study. Surg Obes Relat Dis 2014;10(6):1161–1165.
21. Dalbeth N, Chen P, White M, et al. Impact of bariatric surgery on serum urate targets in people with morbid obesity and diabetes: a prospective longitudinal study. Ann Rheum Dis 2014;73(5):797–802.
22. Nielsen SM, Bartels EM, Henriksen M, et al. Weight loss for overweight and obese individuals with gout: a systematic review of longitudinal studies. Ann Rheum Dis 2017;76(11):1870–1882.
23. Zhu Y, Zhang Y, Choi HK. The serum urate-lowering impact of weight loss among men with a high cardiovascular risk profile: the Multiple Risk Factor Intervention Trial. Rheumatology (Oxford) 2010;49(12):2391–2399.
24. Barskova VG, Eliseev MS, Kudaeva FM, et al. [Effect of metformin on the clinical course of gout and insulin resistance]. Klin Med (Mosk) 2009;87(7):41–46.
25. Dessein PH, Shipton EA, Stanwix AE, et al. Beneficial effects of weight loss associated with moderate calorie/carbohydrate restriction, and increased proportional intake of protein and unsaturated fat on serum urate and lipoprotein levels in gout: a pilot study. Ann Rheum Dis 2000;59(7):539–543.
26. Yokose C, McCormick N, Rai SK, et al. Effects of low-fat, mediterranean, or low-carbohydrate weight loss diets on serum urate and cardiometabolic risk factors: a secondary analysis of the Dietary Intervention Randomized Controlled Trial (DIRECT). Diabetes Care 2020;43(11):2812–2820.

27. Christensen R, Zobbe K, Nielsen SM, et al. Weight loss for patients with gout and concomitant obesity: a proof-of-concept randomized trial. Arthritis Rheumatol 2024;76(5):806–812.
28. Hu JR, Yeh HC, Mueller NT, et al. Effects of a behavioral weight loss intervention and metformin treatment on serum urate: results from a randomized clinical trial. Nutrients 2021;13(8):2673.
29. OECD. OECD Reviews of Public Health: Japan: A Healthier Tomorrow. OECD Reviews of Public Health. 2019. https://doi.org/10.1787/9789264311602-en.
30. Fukui S, Okada M, Rahman M, et al. Differences in the association between alcoholic beverage type and serum urate levels using standardized ethanol content. JAMA Netw Open 2023;6(3):e233398–e233398.
31. Fukui S, Okada M, Shinozaki T, et al. Changes in alcohol intake and serum urate changes: longitudinal analyses of annual medical examination database. Ann Rheum Dis 2024:83(8):1072–1081.
32. Matsuo S, Imai E, Horio M, et al. Revised equations for estimated GFR from serum creatinine in Japan. Am J Kidney Dis 2009;53(6):982–992.
33. Barnett AG, van der Pols JC, Dobson AJ. Regression to the mean: what it is and how to deal with it. Int J Epidemiol 2004;34(1):215–220.
34. Powell-Wiley TM, Poirier P, Burke LE, et al; American Heart Association Council on Lifestyle and Cardiometabolic Health; Council on Cardiovascular and Stroke Nursing; Council on Clinical Cardiology; Council on Epidemiology and Prevention; and Stroke Council. Obesity and Cardiovascular Disease: a scientific statement from the American Heart Association. Circulation 2021;143(21):e984–e1010.
35. Wing RR, Lang W, Wadden TA, et al; Look AHEAD Research Group. Benefits of modest weight loss in improving cardiovascular risk factors in overweight and obese individuals with type 2 diabetes. Diabetes Care 2011;34(7):1481–1486.
36. Leung N, Yip K, Pillinger MH, et al. Lowering and raising serum urate levels: off-label effects of commonly used medications. Mayo Clin Proc 2022;97(7):1345–1362.
37. Sasaki A, Wakabayashi G, Yonei Y. Current status of bariatric surgery in Japan and effectiveness in obesity and diabetes. J Gastroenterol 2014;49(1):57–63.
38. Feinstein EI, Quion-Verde H, Kaptein EM, et al. Severe hyperuricemia in patients with volume depletion. Am J Nephrol 1984;4(2):77–80.
39. Shaffer A, Rahn E, Saag K, et al. Variation in serum urate levels in the absence of gout and urate lowering therapy. BMC Rheumatol 2021;5(1):32.
40. Devgun MS, Dhillon HS. Importance of diurnal variations on clinical value and interpretation of serum urate measurements. J Clin Pathol 1992;45(2):110–113.

Arthritis & Rheumatology
Vol. 77, No. 3, March 2025, pp 356–361
DOI 10.1002/art.43032

AMERICAN COLLEGE of RHEUMATOLOGY
Empowering Rheumatology Professionals

BRIEF REPORT

Genetic Analysis of Asymptomatic Antinuclear Antibody Production

Mehmet Hocaoğlu, Desiré Casares-Marfil, and Amr H. Sawalha

Objective. Antinuclear antibodies (ANA) are detected in up to 14% of the population, and many individuals with ANA are asymptomatic. The literature on the genetic contribution to asymptomatic ANA positivity is limited. In this study, we aimed to perform a genome-wide association study of asymptomatic ANA positivity in multiple populations.

Methods. Asymptomatic individuals who were either ANA positive or ANA negative from the All of Us Research Program were included in this study, selecting those with an ANA test performed by immunofluorescence and no evidence of autoimmune disease. Imputation was performed, and a multipopulation meta-analysis including approximately 6 million single-nucleotide polymorphisms (SNPs) was conducted. Genome-wide SNP-based heritability was estimated using the Genome-wide Complex Trait Analysis software. A cumulative genetic risk score for lupus was constructed using previously reported genome-wide significant loci.

Results. A total of 1,955 asymptomatic ANA positive and 3,634 asymptomatic ANA negative individuals across three populations were included. The multipopulation meta-analysis revealed SNPs with a suggestive association ($P < 1 \times 10^{-5}$) across 8 different loci, but no genome-wide significant loci were identified. A gene variant upstream of *HLA-DQB1*, (rs17211748, $P = 1.4 \times 10^{-6}$, odds ratio 0.82, 95% confidence interval 0.76–0.89), showed the most significant association. The heritability of asymptomatic ANA positivity was estimated to be 24.9%. Individuals who were asymptomatic and ANA positive did not exhibit increased cumulative genetic risk for lupus compared with individuals who were ANA negative.

Conclusion. ANA production is not associated with significant genetic risk and is primarily determined by environmental factors.

INTRODUCTION

Antinuclear antibodies (ANA) are associated with several immune-mediated diseases such as systemic lupus erythematosus (SLE), systemic sclerosis, Sjögren disease, and others.[1] The population prevalence of ANA positivity in the United States was estimated to be 13.8% (95% confidence interval [CI] 12.2%–15.5%), with evidence suggesting a rising prevalence of autoimmunity over recent decades.[2,3] However, variability in ANA test methods and titer interpretation leads to differences in reported ANA positivity prevalence across studies.[2] Environmental factors such as body mass index and parity status have been shown to be associated with ANA positivity,[2,4] but the role of genetic factors in ANA production is less defined. Only one genome-wide association study (GWAS) has been performed, showing the association of a variant near the *HLA-DRA* gene with ANA positivity in Japanese individuals.[5]

Previous research showed that ANA production precedes the onset of clinical symptoms in patients with SLE, suggesting that asymptomatic ANA positivity might be an intermediate state on the pathway to the development of clinical autoimmunity.[6] However, most individuals who are ANA positive do not develop any immune-mediated disease.[7] Because autoimmune diseases are complex conditions that arise from the interplay of genetic and environmental factors,[8] understanding the genetic factors associated with asymptomatic ANA production could provide insights into the early pathways of autoimmunity development and differentiate them from the terminal pathways that lead to

Supported by the National Institute of Allergy and Infectious Diseases, NIH (grant R01-AI-097134).

Mehmet Hocaoglu, MD, Desiré Casares-Marfil, PhD, Amr H. Sawalha, MD: University of Pittsburgh, Pittsburgh, Pennsylvania.

Additional supplementary information cited in this article can be found online in the Supporting Information section (https://acrjournals.onlinelibrary.wiley.com/doi/10.1002/art.43032).

Author disclosures and graphical abstract are available at https://onlinelibrary.wiley.com/doi/10.1002/art.43032.

Address correspondence via email to Amr H. Sawalha, MD, at asawalha@pitt.edu.

Submitted for publication August 15, 2024; accepted in revised form October 8, 2024.

clinical pathology. In this study, we aimed to assess the role of genetic susceptibility in ANA production in a large cohort across multiple populations.

PATIENTS AND METHODS

Study population and design. The All of Us Research Program is a cohort study aiming to enroll 1,000,000 participants with genomic data linked with environmental surveys and electronic health records (EHRs). As of the latest data release (version 7), All of Us included 312,925 and 245,388 individuals with genotyping and whole-genome sequencing data, respectively.[9] For the GWAS analysis, we selected participants who had genotyping data available and a positive ANA test in their EHR by immunofluorescence (IF) as defined by the performing laboratory, or if titer data are available, a titer greater than 1:80 (Supplementary List 1). We excluded individuals who had one positive ANA test but subsequently had a negative test by IF or enzyme-linked immunosorbent assay (ELISA). We did not include individuals who only had a positive ANA by ELISA in this study (n = 225). Individuals with any clinical code for autoimmune diseases or prescription for an immunosuppressive medication in their EHR from both the cohorts who were ANA positive and who were ANA negative were also excluded (Supplementary Figure 1, Supplementary List 2). We then conducted a sensitivity analysis by restricting the sample to individuals with available titer data and ANA titers greater than 1:160, to assess whether higher ANA titers are associated with genetic signals with a GWAS level of significance.

Quality controls, genetic similarity group assignment, and imputation. The individuals participating in the All of Us underwent genotyping with the Infinium Global Diversity Array-8 (Illumina). Variants with minor allele frequency (MAF) <1%, those deviated from Hardy–Weinberg equilibrium in patients and controls ($P < 1 \times 10^{-3}$), and variants with high missingness rates (≥0.03) were removed. In addition, A/T-C/G single-nucleotide polymorphisms (SNPs) with a MAF >0.4 were removed before imputation to avoid errors with the imputation process. Individuals with poor genotyping rates (<97%), cryptic relatedness as defined by their identity by descent proportion (PI-HAT >0.4) or missing sex information were excluded. Sex chromosomes were not analyzed in this study. Genetic similarity of the study participants to the 1000 Genomes Project populations was assessed by intersecting their genetic information and calculating the first 10 principal components (PCs) of the genotype-covariance matrix. Subsequently, a random forest classifier was trained to assign genetic similarity for each participant included in our study to one of the following superpopulations of the 1000 Genomes Project: European (EUR), Admixed American (AMR), East Asian (EAS), South Asian (SAS), and African (AFR).[10] Study participants with genetic similarity to the EUR, AMR, and AFR populations were referred to as EUR-like, AMR-like, and AFR-like, respectively. Because the sample size for participants with genetic similarity to EAS and SAS was limited (n = 115 and n = 52, respectively), they were excluded from further analyses. Individuals who are six SD away from their respective genetic population centroid were considered outliers and were removed from further analyses. PC analysis was performed using the R package *smartsnp*, which uses the EIGENSTRAT method.[11,12] Phasing and imputation were performed using Eagle2 and minimac4, respectively.[13,14] All populations from the 1000 Genomes Project phase 3 were used as reference panel for imputation and phasing. Imputed SNPs with an imputation quality metric RSQ <0.9 and a MAF >1% were removed from further analyses. Imputation procedures were performed for each genetic similarity group separately. Quality controls and statistical tests were performed using PLINK (version 1.9).[15] Imputation of HLA class I and II classical alleles within the expanded HLA region (chr6 28 to 34 Mb) was performed using SNP2HLA module of the HLA-TAPAS analysis pipeline[16] and Beagle version 5.4. The same quality control procedures described for the genome-wide imputation were applied, and only classical alleles with an imputation quality metric RSQ greater than 0.9 were used in subsequent analyses.

Statistical analysis. GWAS was performed through logistic regression on each genetic similarity group separately using the first five PCs as covariates, followed by a meta-analysis using the inverse variance method. Variants with no evidence of heterogeneity were considered under fixed-effects model (Cochran's Q test $P > 0.1$ and heterogeneity index < 50%), whereas the rest were considered under a random-effects model (Cochran's Q test $P \leq 0.1$; heterogeneity index ≥ 50%). Only variants studied in more than one genetic similarity group GWAS were included in the meta-analysis. The genome-wide significance level was established at $P < 5 \times 10^{-8}$, and the suggestive association threshold was set at $P < 1 \times 10^{-5}$. In addition, the most significant association identified in the meta-analysis was assessed in patients with SLE using logistic regression in individual genetic similarity groups followed by meta-analysis as described for the main GWAS. For this analysis, we selected patients with SLE in the All of Us database with genotyping data by including individuals who had at least two SLE clinical codes and at least two SLE-related medication prescriptions in their EHR (Supplementary List 3). The same GWAS workflow above was used in the subset analysis restricted to individuals who had an ANA titer greater than 1:160. These analyses were also first performed in each population separately, followed by a meta-analysis as described above.

To identify independent associations within the HLA region, an independence analysis was performed at the population level, followed by an inverse variance meta-analysis. The most significant variant in the region, rs17211748, was used as

a covariate in conditional logistic regressions for each population. These results were then pooled through meta-analysis. Pairwise conditional analysis was performed to test the independence of the associations detected in rs17211748 and *HLA-DQB1*05:01:01:01*.

Genome-wide SNP-based heritability estimation. We estimated the genome-wide SNP heritability based on the liability scale for ANA positivity using the Genome-wide Complex Trait Analysis software,[17] which utilizes a linkage disequilibrium (LD) and MAF-stratified genome-based restricted maximum likelihood approach to correct for LD bias. For liability calculations, we assumed the prevalence of asymptomatic ANA positivity in the population to be 15% and used the first five PCs as covariates. This analysis was performed only in EUR-like individuals (asymptomatic ANA positive n = 1,236; asymptomatic ANA negative n = 2,406) because the sample size required to provide reliable estimates (SD < 0.1) could only be achieved with total sample sizes >3,000 individuals.[18]

Cumulative SLE genetic risk score calculation. To assess the variability of SLE genetic risk among patients with SLE and individuals who were asymptomatic ANA positive and individuals who were asymptomatic ANA negative, a cumulative SLE genetic risk score (GRS) was calculated. For this analysis, we included individuals with available whole-genome sequencing data to extract all genetic data needed to accurately calculate a GRS (Supplementary Table 1). We calculated a GRS for SLE using 183 genetic susceptibility loci previously reported with a GWAS level of significance for patients with SLE.[19] Of the 183 SNPs described in the supplementary material of Harley and Sawalha,[19] we excluded five SNPs in sex chromosomes and one additional SNP (rs11845506) due to a MAF in patients of < 1% in the study in which it was reported, leaving 177 variants for GRS calculation (Supplementary Table 2). The GRS was estimated by multiplying the natural logarithm of the previously reported SLE association odds ratio (OR) for each SNP representing each locus by the risk allele counts of the corresponding SNPs as we previously described.[20] We compared the mean GRS of each group with the other two groups using Tukey's multiple comparison tests.

RESULTS

A total of 1,955 individuals who were asymptomatic and ANA positive and 3,634 individuals who were asymptomatic and ANA negative were studied. The mean age and sex distribution between individuals who were ANA positive and individuals who were ANA negative were similar across the three genetic similarity groups (Table 1). After quality controls and imputation, an independent GWAS was performed for each genetic similarity group. Because the age and sex distributions were similar across the groups who were ANA positive and who were ANA negative, no adjustment for sex and age was needed in the logistic regression models. No genome-wide significant loci were identified in any of the individual genetic similarity groups (Supplementary Figures 2 and 3). In the meta-analysis, 6,245,285 SNPs were included. Although no genome-wide significant associations ($P < 5 \times 10^{-8}$) were detected, we identified suggestive associations ($P < 1 \times 10^{-5}$) across 8 different loci (Figure 1, Supplementary Table 3). The most significant association was identified in the SNP rs17211748, a variant upstream of *HLA-DQB1* ($P = 1.4 \times 10^{-6}$, OR 0.82, 95% CI 0.76–0.89). The sensitivity analysis did not show any genome-wide significant association when restricted to individuals with an ANA titer greater than 1:160 in the multipopulation meta-analysis (EUR-like, n = 138; AMR-like, n = 104; AFR-like, n = 60; Supplementary Figure 4). We tested the genetic association in *HLA-DQB1*, that is, the risk allele in SNP rs17211748, in patients with SLE (EUR-like n = 672; AFR-like n = 527; AMR-like n = 345) compared with individuals who were asymptomatic and ANA negative. We detected a more significant genetic association with rs17211748 in patients with SLE ($P = 3.7 \times 10^{-7}$, OR 1.26, 95% CI 1.15–1.38) compared with individuals who were asymptomatic and ANA positive ($P = 1.4 \times 10^{-6}$, OR 1.22, 95% CI 1.12–1.32; Supplementary Figure 5).

Table 1. Demographic characteristics of individuals who were asymptomatic and ANA positive and individuals who were asymptomatic and ANA negative included in this study*

Genetic similarity group	Participants, n	Mean ± SD age, y	Female sex, n (%)
European-like	3,642		
ANApositive	1,236	61 ± 16.1	865 (70.0)
ANA negative	2,406	61 ± 15.3	1,675 (69.6)
African-like	859		
ANA positive	355	56 ± 14.3	259 (72.9)
ANA negative	504	55 ± 13.3	351 (69.6)
Admixed American–like	1,088		
ANA positive	364	52 ± 14.7	281 (77.2)
ANA negative	724	52 ± 14	556 (76.8)

* No statistically significant difference ($P < 0.05$) was observed for age or sex between groups per analysis of variance and chi-square testing, respectively. ANA, antinuclear antibody.

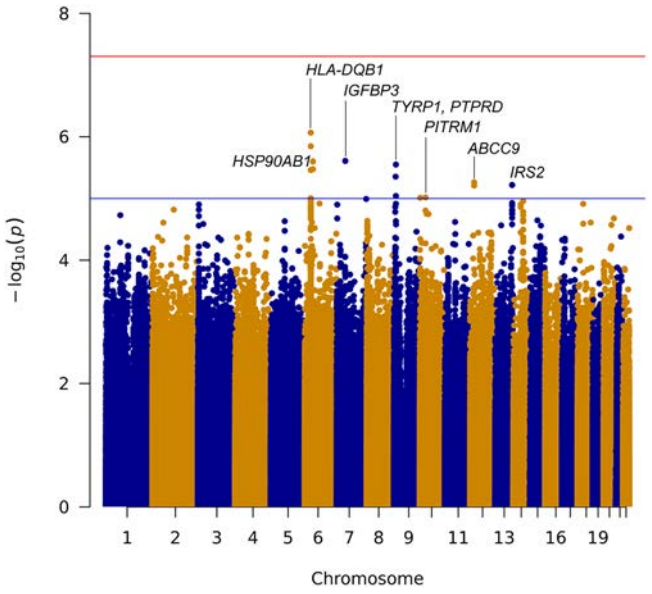

Figure 1. A Manhattan plot depicting the results from the meta-analysis across genetic similarity groups comparing individuals who were asymptomatic and ANA positive with individuals who were asymptomatic and ANA negative. The Y and X axes refer to the $-\log_{10}$ *P* values and chromosome positions, respectively. The red horizontal line represents the genome-wide association threshold ($P < 5 \times 10^{-8}$), and the blue line represents the suggestive association threshold ($P < 1 \times 10^{-5}$). Blue and orange dots represent individual SNPs. ANA, antinuclear antibody.

To assess independent genetic associations with ANA production in the HLA region, we conducted conditional genetic analysis and detected no residual genetic effects in other SNPs within this region after adjusting for rs17211748 (Supplementary Figure 6). We next imputed HLA classical alleles and examined genetic associations by comparing asymptomatic individuals who were ANA positive with asymptomatic individuals who were ANA negative across the three genetic similarity groups followed by a meta-analysis. We detected no association with any classical HLA allele that passed the threshold for suggestive significance ($P < 1 \times 10^{-5}$). The most significant association was detected with *HLA-DQB1*05:01:01:01*, which exerts a modest protective effect against ANA production ($P = 0.001$, OR 0.81). Pairwise conditional analysis showed no residual effect in *HLA-DQB1*05:01:01:01* after adjusting for rs17211748, suggesting that the classical allele modest association is driven by the effect in rs17211748 in the HLA region (Supplementary Table 4). To further assess the genetic contribution to ANA production, we calculated a genome-wide SNP-based heritability. The heritability of asymptomatic ANA positivity on the liability scale was estimated to be 24.9% (± SD 12.4%).

Finally, we estimated a total genetic risk for SLE in individuals who were asymptomatic and ANA positive compared with individuals who were asymptomatic and ANA negative and with patients with SLE. This analysis was performed separately in EUR-like, AMR-like, and AFR-like groups. There was a statistically significant difference in the mean SLE GRS between patients with SLE and both groups who were asymptomatic ANA positive and asymptomatic ANA negative across all three populations (Figure 2; Supplementary Table 5). No significant difference in SLE GRS between individuals who were asymptomatic ANA positive and individuals who were asymptomatic ANA negative was observed in any population (Figure 2).

DISCUSSION

We reported a GWAS for asymptomatic ANA positivity across three different populations and showed that individuals who were asymptomatic ANA positive are not enriched for SLE risk loci compared with individuals who were ANA negative, a consistent observation across different populations. We estimate the genome-wide SNP-based heritability of asymptomatic ANA positivity to be approximately 25%, suggesting that genetic

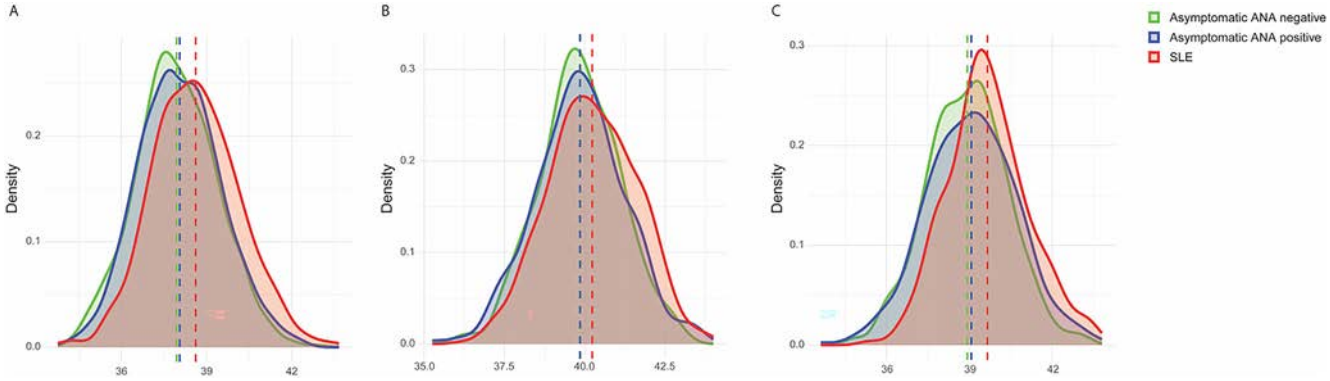

Figure 2. Comparison of cumulative genetic risk scores for SLE in individuals who were asymptomatic and ANA positive, individuals who were asymptomatic and ANA negative, and patients with SLE of (A) European genetic similarity, (B) African genetic similarity, and (C) Admixed American genetic similarity. Dashed lines represent the means of cumulative genetic risk score of each group. ANA, antinuclear antibody; SLE, systemic lupus erythematosus.

effects explain only a small fraction of the phenotypic variability due to ANA production in the population. However, it should be noted that heritability analysis was only performed in EUR-like individuals included in All of Us, and heritability estimates for ANA production might be different in different populations. We also showed that individuals who were asymptomatic ANA positive do not exhibit an increased SLE genetic risk compared with individuals who were ANA negative. These results overall suggest that the ANA positivity in the population is primarily influenced by environmental factors.

We did not detect any genetic susceptibility loci in individuals who were asymptomatic and ANA positive with GWAS level of significance. A suggestive genetic association was detected within the HLA class II region, consistent with a previous report in Japanese individuals.[5] However, it is conceivable that this genetic effect in our study reflects a small proportion of individuals who were asymptomatic ANA positive who either have an undiagnosed autoimmune disease or who could develop an autoimmune disease in the future. Indeed, the strength of the genetic association signal in rs17211748 in the *HLA-DQB1* locus, as reflected by the OR, increased when the analysis was performed in patients with SLE compared with controls who were ANA negative and healthy.

The role of asymptomatic ANA production as an early event in the pathway to autoimmunity has been well documented.[6] Our results show that asymptomatic ANA positivity is primarily driven by nongenetic factors, suggesting that ANA production as an early stage of breakdown of immune tolerance is likely driven by environmental triggers. In a small subset of individuals with sufficient genetic risk for autoimmunity, clinical disease develops. From a disease pathogenesis perspective, our data suggest that although ANA production is essential for the development of SLE, it is independent of the genetic risk for the disease. This raises the potential of developing genetic-environmental models to predict SLE risk in individuals who are asymptomatic and ANA positive. Research on environmental risk factors and gene–environment interactions is needed to build accurate risk prediction models.

This study has several strengths. We report the first GWAS in multiple populations for asymptomatic ANA production. Population-specific genetic analysis showed consistent observations across genetic similarity groups, which increases the generalizability of our results. In addition, we estimated the heritability for asymptomatic ANA positivity for the first time, which we showed to be approximately 25%, suggesting a greater role for environmental factors in ANA production.

This study has certain limitations. ANA positivity is a very heterogenous phenotype that includes various autoantibodies directed against nuclear antigens.[21] It is possible that the genetic architecture is different across different ANA patterns, titers, or specific autoantibodies. Although we did perform a sensitivity analysis for titers greater than 1:160 and found similar results, our sample sizes were small for this subgroup analysis, limited by the availability of data. Because this is a cohort established through EHR, incomplete data or misclassification bias are possible. However, we tried to mitigate this by combining evidence from both clinical codes and medication prescriptions for our case definitions and by setting a very broad definition of autoimmunity. The SNP-based heritability estimate for ANA production is based on additive genetic variance only, which does not capture all potential sources of genetic variation such as gene–gene and gene–environment interactions. In addition, the GRS calculation was based on SLE risk variants identified predominantly in EUR-like and EAS-like populations, which may limit its applicability to other populations.

In conclusion, we performed a GWAS in a large cohort of individuals who were asymptomatic and ANA positive from multiple genetic similarity groups. We provide evidence to suggest that ANA production is primarily influenced by nongenetic factors and is independent of the genetic risk for SLE. Further research is needed to characterize the environmental determinants of ANA production and the role of gene–environment interactions in the development of autoimmunity in individuals who are ANA positive.

ACKNOWLEDGMENTS

We gratefully acknowledge the All of Us participants for their contributions. We also thank the NIH All of Us Research Program for making available the data examined in this study.

AUTHOR CONTRIBUTIONS

All authors contributed to at least one of the following manuscript preparation roles: conceptualization AND/OR methodology, software, investigation, formal analysis, data curation, visualization, and validation AND drafting or reviewing/editing the final draft. As corresponding author, Dr Sawalha confirms that all authors have provided the final approval of the version to be published, and takes responsibility for the affirmations regarding article submission (eg, not under consideration by another journal), the integrity of the data presented, and the statements regarding compliance with institutional review board/Declaration of Helsinki requirements.

DATA AVAILABILITY STATEMENT

This study used data from the All of Us Research Programs Controlled Tier Dataset version 7, available to authorized users on the Researcher Workbench (https://workbench.researchallofus.org).

REFERENCES

1. Bossuyt X, De Langhe E, Borghi MO, et al. Understanding and interpreting antinuclear antibody tests in systemic rheumatic diseases. Nat Rev Rheumatol 2020;16(12):715–726.
2. Satoh M, Chan EK, Ho LA, et al. Prevalence and sociodemographic correlates of antinuclear antibodies in the United States. Arthritis Rheum 2012;64(7):2319–2327.

3. Miller FW. The increasing prevalence of autoimmunity and autoimmune diseases: an urgent call to action for improved understanding, diagnosis, treatment, and prevention. Curr Opin Immunol 2023;80:102266.
4. Parks CG, Miller FW, Satoh M, et al. Reproductive and hormonal risk factors for antinuclear antibodies (ANA) in a representative sample of U.S. women. Cancer Epidemiol Biomarkers Prev 2014;23(11):2492–2502.
5. Terao C, Ohmura K, Yamada R, et al; Nagahama Study Group. Association between antinuclear antibodies and the HLA class II locus and heterogeneous characteristics of staining patterns: the Nagahama study. Arthritis Rheumatol 2014;66(12):3395–3403.
6. Arbuckle MR, McClain MT, Rubertone MV, et al. Development of autoantibodies before the clinical onset of systemic lupus erythematosus. N Engl J Med 2003;349(16):1526–1533.
7. Tan EM, Feltkamp TE, Smolen JS, et al. Range of antinuclear antibodies in "healthy" individuals. Arthritis Rheum 1997;40(9):1601–1611.
8. Leffers HCB, Lange T, Collins C, et al. The study of interactions between genome and exposome in the development of systemic lupus erythematosus. Autoimmun Rev 2019;18(4):382–392.
9. All of Us Research Program Genomics Investigators. Genomic data in the All of Us Research Program. Nature 2024;627(8003):340–346.
10. Auton A, Brooks LD, Durbin RM, et al; 1000 Genomes Project Consortium. A global reference for human genetic variation. Nature 2015;526(7571):68–74.
11. Price AL, Patterson NJ, Plenge RM, et al. Principal components analysis corrects for stratification in genome-wide association studies. Nat Genet 2006;38(8):904–909.
12. Herrando-Pérez S, Tobler R, Huber CD. SMARTSNP, an R package for fast multivariate analyses of big genomic data. Methods Ecol Evol 2021;12(11):2084–2093. https://doi.org/10.1111/2041-210X.13684
13. Das S, Forer L, Schönherr S, et al. Next-generation genotype imputation service and methods. Nat Genet 2016;48(10):1284–1287.
14. Loh PR, Danecek P, Palamara PF, et al. Reference-based phasing using the Haplotype Reference Consortium panel. Nat Genet 2016;48(11):1443–1448.
15. Chang CC, Chow CC, Tellier LC, et al. Second-generation PLINK: rising to the challenge of larger and richer datasets. Gigascience 2015;4(1):7.
16. Luo Y, Kanai M, Choi W, et al; NHLBI Trans-Omics for Precision Medicine (TOPMed) Consortium. A high-resolution HLA reference panel capturing global population diversity enables multi-ancestry fine-mapping in HIV host response. Nat Genet 2021;53(10):1504–1516.
17. Yang J, Bakshi A, Zhu Z, et al; LifeLines Cohort Study. Genetic variance estimation with imputed variants finds negligible missing heritability for human height and body mass index. Nat Genet 2015;47(10):1114–1120.
18. Visscher PM, Hemani G, Vinkhuyzen AA, et al. Statistical power to detect genetic (co)variance of complex traits using SNP data in unrelated samples. PLoS Genet 2014;10(4):e1004269.
19. Harley ITW, Sawalha AH. Systemic lupus erythematosus as a genetic disease. Clin Immunol 2022;236:108953.
20. Hughes T, Adler A, Merrill JT, et al; BIOLUPUS Network. Analysis of autosomal genes reveals gene-sex interactions and higher total genetic risk in men with systemic lupus erythematosus. Ann Rheum Dis 2012;71(5):694–699.
21. Sawalha AH, Harley JB. Antinuclear autoantibodies in systemic lupus erythematosus. Curr Opin Rheumatol 2004;16(5):534–540.

American College of Rheumatology
Empowering Rheumatology Professionals

Arthritis & Rheumatology
Vol. 77, No. 3, March 2025, pp 362–363

LETTER

DOI 10.1002/art.43021

Fractures in patients with acute calcium pyrophosphate crystal arthritis versus matched comparators in a large cohort study: comment on the article by Tedeschi et al

To the Editor:

Calcium pyrophosphate deposition disease (CPPD) is a common and painful arthritic condition that primarily affects the elderly population. Although previous studies have shown an association between CPPD and low bone mineral density, the risk of fracture in these patients has not been thoroughly investigated.[1,2] It was with great interest that we read a recent paper by Tedeschi et al that examined the incidence of fractures in patients with acute calcium pyrophosphate (CPP) crystalline arthritis and their matched controls using a robust data set from Mass General Brigham.[3] Using machine learning algorithms and extensive electronic health record data, the authors provide important insights into the potential fracture risk associated with acute CPP crystalline arthritis. The study showed that patients with acute CPP crystalline arthritis had a significantly increased risk of fracture with an 80% increased risk of any fracture compared with matched controls. Notably, the risk of fracture was most pronounced at the wrist, a site commonly affected by both chondrocalcinosis and acute CPP crystalline arthritis. The results remained consistent even when confounding factors were excluded.

The limitations of this study should be further clarified. First, the index date for acute CPP crystal arthritis in the study was the date of the first mention of "pseudogout" in the narrative medical record or the date of the first joint crystalloid analysis that detected CPP crystals. However, the true onset of CPPD may be earlier than these records, resulting in misalignment of exposure times. This uncertainty in onset time may mask true differences in bone health. Second, although the authors corrected for a number of necessary covariates, there were still more important confounders that were overlooked, such as physical activity and alcohol consumption. Previous meta-analyses have shown a significant association between either physical activity[4] or alcohol consumption and fracture risk.[5] In addition, other covariates such as nutritional status, calcium, and vitamin D intake should not be overlooked. Finally, the study did not analyze in detail the specific effects of long-term use of different types of CPP crystal arthritis treatments (eg, nonsteroidal anti-inflammatory drugs, intra-articular injections, oral colchicine, and physical therapy) on fracture risk. Although the study performed some sensitivity analyses to rule out the effects of glucocorticoid and osteoporosis treatments, inconsistencies in the patterns of use of these medications and the duration of treatment may still have affected the results.

Despite these limitations, this important study provides a compelling rationale for further prospective studies to better understand the interaction between CPPD and fracture risk. Several avenues for future research are evident. First, detailed studies of bone turnover markers, bone mineral density assessments, and imaging studies could elucidate the extent to which CPPD affects bone integrity. Second, understanding the role of osteoprotegerin and its downstream effects in the broader population of patients with CPPD may reveal novel therapeutic targets to reduce fracture risk. Third, prospective clinical trials evaluating the impact of osteoporosis treatment in patients with CPPD may provide important insights for optimizing care and reducing fracture risk. Finally, it would be valuable to examine the impact of different CPPD treatments on fracture outcomes through mediation analyses. Given the overlap between CPPD and other diseases such as rheumatoid arthritis, a nuanced understanding of their individual and combined impact on bone health is critical. As CPPD and its associated complications continue to pose significant clinical challenges, this study is a critical step in identifying high-risk patients and developing targeted interventions to improve their outcomes.

Supported by Yunnan Province Science and Technology Department-Kunming Medical University Basic Research Joint Special Project (grant 202401AY070001–087).

Author disclosures are available at https://onlinelibrary.wiley.com/doi/10.1002/art.43021.

Bo Li and Xingxiong Jiang equally contributed to the study.

Bo Li, MB
Xingxiong Jiang, MB
Wendong Luo, MM
15887813900@163.com
Second Affiliated Hospital of Kunming Medical University
Kunming, China

1. Kleiber Balderrama C, Rosenthal AK, Lans D, et al. Calcium pyrophosphate deposition disease and associated medical comorbidities: a national cross-sectional study of US veterans. Arthritis Care Res (Hoboken) 2017;69(9):1400–1406.
2. Abhishek A, Doherty S, Maciewicz R, et al. Association between low cortical bone mineral density, soft-tissue calcification, vascular calcification and chondrocalcinosis: a case-control study. Ann Rheum Dis 2014;73(11):1997–2002.
3. Tedeschi SK, Hayashi K, Rosenthal A, et al. Fractures in patients with acute calcium pyrophosphate crystal arthritis versus matched

comparators in a large cohort study. Arthritis Rheumatol 2024;76(6):936–941.
4. Qu X, Zhang X, Zhai Z, et al. Association between physical activity and risk of fracture. J Bone Miner Res 2014;29(1):202–211.
5. Asoudeh F, Salari-Moghaddam A, Larijani B, et al. A systematic review and meta-analysis of prospective cohort studies on the association between alcohol intake and risk of fracture. Crit Rev Food Sci Nutr 2022;62(20):5623–5637.

DOI 10.1002/art.43024

Reply

To the Editor:

We agree with many of the points made by Li et al and would like to make several clarifications. We acknowledge that the date of the first episode of acute calcium pyrophosphate (CPP) crystal arthritis ("pseudogout") is likely later than the onset of calcium pyrophosphate deposition (CPPD). If differences in bone health begin at or before the time of CPPD, then assigning the date of the first episode of acute CPP crystal arthritis as the index date may magnify differences in bone health compared with patients without CPPD. For this analysis, we began follow-up after the first episode of acute CPP crystal arthritis for several reasons. First, identifying the true date of CPPD would require all patients in both cohorts to have serial joint radiographs, which are not performed in clinical care. Second, the specific manifestation of acute CPP crystal arthritis is more accurately identified than CPPD (broadly defined) in the Mass General Brigham electronic health record.[1]

Our analysis did not adjust for long-term use of treatments for CPPD disease because these may mediate the relationship between acute CPP crystal arthritis and fracture risk. We concur that formal mediation analysis would be of interest, but it was outside the scope of the present study. We fully agree that future studies investigating biomarkers of bone turnover, bone mineral density, and therapies directed at bone health have great potential to improve the health of individuals with CPPD disease—a population that will continue to grow.

Sara K. Tedeschi, MD, MPH
stedeschi1@bwh.harvard.edu
Brigham and Women's Hospital
Boston, MA

1. Tedeschi SK, Cai T, He Z, et al. Classifying pseudogout using machine learning approaches with electronic health record data. Arthritis Care Res (Hoboken) 2021;73(3):442–448.

American College of Rheumatology
Empowering Rheumatology Professionals

Arthritis & Rheumatology
Vol. 77, No. 3, March 2025, pp 364

DOI 10.1002/art.43016

Clinical Images: Erdheim-Chester disease presenting with palpitations and spondylopathy

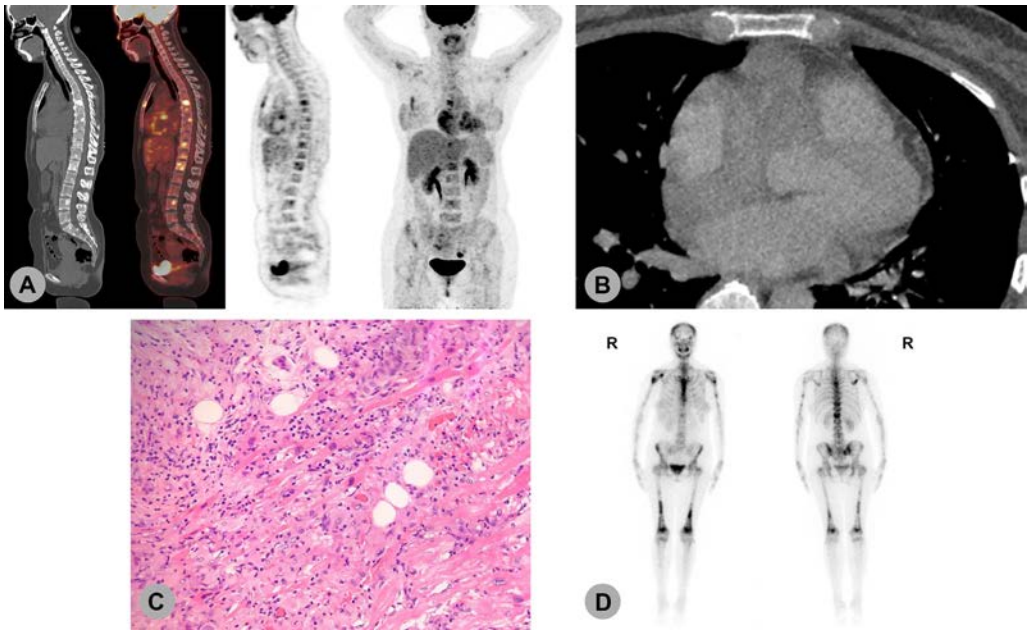

The patient, a 43-year-old woman, presented to our hospital with palpations and osteosclerotic spinal lesions disclosed by routine radiological examination. Her physical examination and laboratory results were unremarkable. ^{18}Fluorine-fluorodeoxyglucose-positron emission tomography/computed tomography (^{18}F-PET-CT) showed hypermetabolic activity on vertebrae, sternum, pelvis, scapula, humerus, and femurs and revealed mild pericardial effusion (A). The diagnosis remained ambiguous, after bone marrow smear and two consecutive bone biopsies. Preclinical POEMS syndrome was suspected owing to the osteosclerotic lesions and pericardial effusion. Therefore, the patient was followed. Six months later, her palpitations exacerbated as massive pericardial effusion developed. Cardiac computed tomography after pericardiocentesis revealed a mass invading the right atrium (B). Pathological studies after an open surgery revealed the deposition of "foamy" histocytes surrounded by inflammatory cells (C). Immunohistochemistry was positive for CD163 and CD68 and negative for Langerin and CD1a; the *BRAF*^{V600E} mutation was detected by molecular testing. Bone scintigraphy showed radioactive concentration of bilateral distal femurs (D), which is omitted by the non–whole-body ^{18}F-PET-CT. Restudy of the original images showed increased glucose metabolism on the right atrium (A). The diagnosis of Erdheim-Chester disease (ECD) was established, and the patient was introduced to a trial of *BRAF*^{V600E} inhibitor. ECD is a rare and heterogenous non-Langerhans histiocytosis whose diagnosis remains challenging. Bilateral osteosclerosis of the metadiaphysis of the lower-extremity bones is the hallmark of ECD,[1] and atypical skeletal involvement, such as the spine, pelvis, ribs, clavicles, and sternum, is common among patients.[2] It is crucial to recognize these bone lesions to unmask the underlying cause. We share the lesson learned from a case of misdiagnosis to emphasize head-to-toe workups in this multisystem disorder and call for the awareness of ECD among clinicians, radiologists, and pathologists.

Author disclosures are available at https://onlinelibrary.wiley.com/doi/10.1002/art.43016.

1. Goyal G, Heaney ML, Collin M, et al. Erdheim-Chester disease: consensus recommendations for evaluation, diagnosis, and treatment in the molecular era. Blood 2020;135:1929–1945.
2. Zhang Z, Yu W, Guan W, et al. Atypical skeletal involvement in patients with Erdheim-Chester disease: CT imaging findings. Orphanet J Rare Dis 2022;17:34.

Xiang Li
Department of Osteoporosis and Bone Diseases, Shanghai Sixth People's Hospital Affiliated to Shanghai Jiao Tong University School of Medicine, Shanghai, China

Department of Endocrinology, the Second Affiliated Hospital, Zhejiang University School of Medicine, Hangzhou, China

Chun Wang
wangchun66@sjtu.edu.cn
Department of Osteoporosis and Bone Diseases, Shanghai Sixth People's Hospital Affiliated to Shanghai Jiao Tong University School of Medicine, Shanghai, China

Arthritis & Rheumatology
Vol. 77, No. 3, March 2025, pp 365
DOI 10.1002/art.43080

American College of Rheumatology
Empowering Rheumatology Professionals

Correction to CD19 Chimeric Antigen Receptor T Cell Treatment: Unraveling the Role of B Cells in Systemic Lupus Erythematosus

Correction to "Figure 3. Key insights from CAR T cell therapy in SLE."

Arthritis & Rheumatology

Vol. 76, No. 4, April 2024, pp 497–504

DOI 10.1002/art.42784

In the middle panel of this figure, the plasma cells are identified as "CD19+CD20-" (same as the plasmablasts) – but one key point of the paper is that they are not CD19+. It should read "CD19– CD20–".

Also, in the same panel and figure, measles is misspelled as "measels."

Please see below for the corrected version of this figure.

We apologize for this error.

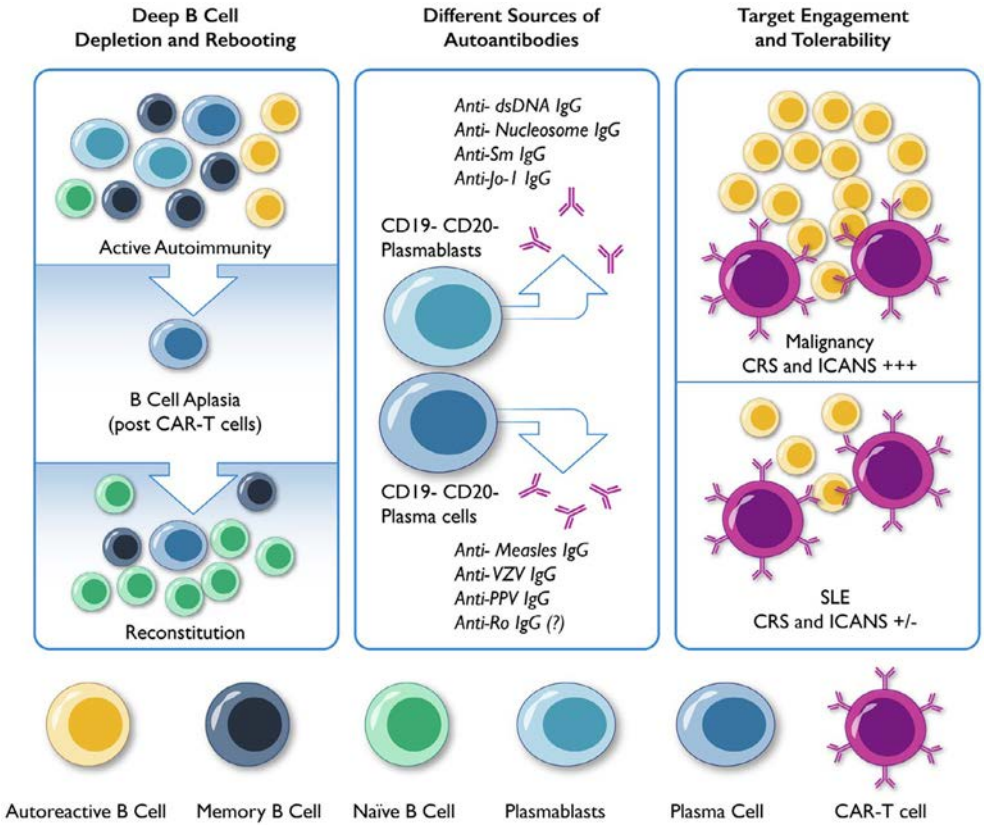

Figure 3.